

USE OF NEUTRON ABSORBERS  
FOR THE EXPERIMENTAL DETERMINATION OF  
LATTICE PARAMETERS  
IN SUBCRITICAL ASSEMBLIES

by

JOSEPH HARRINGTON III

S. B., Massachusetts Institute of Technology  
(1961)

M. S., Massachusetts Institute of Technology  
(1963)

SUBMITTED IN PARTIAL FULFILLMENT OF THE  
REQUIREMENTS FOR THE DEGREE OF  
DOCTOR OF SCIENCE

at the

MASSACHUSETTS INSTITUTE OF TECHNOLOGY

February, 1966

Signature of Author **Signature redacted**  
Department of Nuclear Engineering, February, 1966

Certified by **Signature redacted**  
Thesis Supervisor

**Signature redacted**  
Thesis Supervisor

MRL

MRL  
4/30/70

Thesis  
Nuc. Eng.  
1966  
Sc. D.

USE OF NEUTRON ABSORBERS

FOR THE EXPERIMENTAL DETERMINATION OF

LATTICE PARAMETERS

IN SUBCRITICAL ASSEMBLIES

by

JOSEPH HARRINGTON III

S. B., Massachusetts Institute of Technology  
(1961)

M. S., Massachusetts Institute of Technology  
(1963)

SUBMITTED IN PARTIAL FULFILLMENT OF THE  
REQUIREMENTS FOR THE DEGREE OF  
DOCTOR OF SCIENCE

at the

MASSACHUSETTS INSTITUTE OF TECHNOLOGY

February, 1968

Signature of Author *Joseph Harrington III*  
Department of Nuclear Engineering, February, 1968

Certified by *Joseph Kahan*  
Thesis Supervisor

*Richard P. Thompson*  
Thesis Advisor



USE OF NEUTRON ABSORBERS FOR THE  
EXPERIMENTAL DETERMINATION OF LATTICE PARAMETERS  
IN SUBCRITICAL ASSEMBLIES

by

Joseph Harrington III

Submitted to the Department of Nuclear Engineering in February, 1966, in partial fulfillment of the requirements for the degree of Doctor of Science.

ABSTRACT

A new method for measuring values of the multiplication factor for an infinite medium,  $k_{\infty}$ , has been developed; the method involves addition of neutron absorbers to subcritical assemblies. Measurements of the values of  $k_{\infty}$  for three lattices of uranium metal rods in heavy water have been made; solid copper rods were used as absorbers. Two of the lattices consisted of 0.25-inch-diameter rods of 1.143% enriched uranium on triangular spacings of 2.50 inches and 1.75 inches; a third lattice consisted of 0.75-inch-diameter rods of 0.947% enriched uranium on a triangular spacing of 2.50 inches. The values of  $k_{\infty}$  were found to be  $1.429 \pm 0.007$ ,  $1.416 \pm 0.011$ , and  $1.187 \pm 0.027$ , respectively; they were in agreement, within experimental uncertainties, with values obtained with the four-factor formula.

The method used is closely related to the Hanford (PCTR) technique for measuring  $k_{\infty}$ , which requires a critical reactor. Since it is nearly a measurement of  $(k_{\infty}-1)$ , and because the measured values are independent of a number of sources of error in the four-factor formula, the uncertainties in the measured values should be smaller than those obtained with the four-factor formula. The work shows that a 3% uncertainty in  $(k_{\infty}-1)$  may be obtained with the method, comparable with the uncertainty in PCTR measurements.

Measured values of the neutron regeneration factor,  $\eta$ , which are independent of the values of  $\nu_{25}$  and the fission cross section of the fuel, and nearly independent of the absorption cross section of the fuel, have also been determined; for the lattices of 0.25-inch rods, they are  $1.525 \pm 0.014$  and  $1.555 \pm 0.008$ , respectively; they agree well with values computed with the THERMOS code.

The results of exploratory experiments indicate that it may be possible to do the measurements in two-region subcritical assemblies.

Thesis Supervisors: Irving Kaplan

Title: Professor of Nuclear Engineering

Theos J. Thompson

Title: Professor of Nuclear Engineering

## ACKNOWLEDGEMENTS

The success of this project and of the M. I. T. Heavy Water Lattice Project as a whole has been due to the support of the U. S. Atomic Energy Commission, and to the contributions of a number of individuals. Over-all direction of the Lattice Project during the period when this research was done was shared by Professors Irving Kaplan, David Lanning, Theos Thompson, and Michael Driscoll. The author would like to thank Professor Lanning for encouragement to undertake the research reported here, and Professors Thompson, Kaplan, and Lanning for guidance at all stages of the research. Discussions with Professor Franklyn Clikeman have been helpful. Among the former members of the Lattice Project who have contributed directly to the work are Dr. Paul Brown, Dr. Philip Palmedo, Dr. Richard Simms, and Messrs. Henri Guéron, Sanford Hellman, and Cloin Robertson (see Secs. 3.6 and 3.10). Miss Barbara Kelley has helped in the weighing of foils and analysis of data. Messrs. Joseph Barch, Norman Berube, and Albert Supple have been of great assistance in the experimental work.

Staffs of the M. I. T. Reactor, Machine Shop, Electronics Shop, and Radiation Protection Office have provided assistance and advice during the experimental work. Messrs. Francis Woodworth and John Wasik gave much assistance in the fabrication of experimental equipment. Mrs. Mary Bosco has ably prepared the final manuscript of this thesis.



The patience, encouragement, and support of the author's wife and parents were instrumental to the completion of the work; his wife has also been of great assistance in the weighing of foils, analysis of data, and typing of early versions of the thesis.

The author wishes to acknowledge support from the U. S. Atomic Energy Commission through its Special Fellowship Program in Nuclear Engineering, which is administered by the Oak Ridge Institute of Nuclear Studies. All computer calculations were done at the M. I. T. Computation Center.



## TABLE OF CONTENTS

Abstract	ii
Acknowledgements	iii
List of Figures	viii
List of Tables	x
Chapter I. Introduction	1
1.1 The Neutron Multiplication Factor in an Infinite Medium ( $k_{\infty}$ )	2
1.2 The Hanford Technique	2
1.3 Objectives of the Present Work	4
1.4 Nomenclature	5
1.5 Contents of the Report	6
Chapter II. Theory of the Measurement	7
2.1 The Material Buckling, the Infinite Medium Multiplication Factor, and the Subcritical Experiment	7
2.1.1 Buckling	7
2.1.2 Relation of the Buckling to the Infinite Medium Multiplication Factor	8
2.1.3 Measurement of the Material Buckling	8
2.1.4 Use of the Four-Factor Formula for $k_{\infty}$	10
2.2 Definitions Employed	11
2.3 Relation of Factors to Measurable Quantities	14
2.3.1 Fast Fission Factor ( $\epsilon$ )	14
2.3.2 Neutron Regeneration Factor ( $\eta$ )	15
2.3.3 Thermal Utilization ( $f$ )	16
2.3.4 The Resonance Escape Probability ( $p$ )	18
2.3.5 The Ratio of Epithermal to Thermal Fissions of $U^{235}$ ( $\delta_{25}$ )	19
2.4 Experimental Determination of $k_{\infty}$ : One-Region Assembly	20
2.5 Possible Application of the Method to a Two-Region Assembly	22
2.6 Determination of Lattice Parameters Other Than $k_{\infty}$	24
2.6.1 Parameters Appearing in the Four-Factor Formula	24
2.6.2 Parameters Relating to Neutron Leakage ( $L^2, \tau$ )	24

Chapter III. Experimental Apparatus	27
3.1 Subcritical Facility and M. I. T. Reactor	27
3.2 Lattices Studied	30
3.3 Thermal Neutron Absorbers	30
3.4 Absorber Rods Used	33
3.5 Positioning and Support of Absorber Rods	34
3.6 Purpose and Method of the Experiments	51
3.7 Neutron-Detecting Foils	52
3.8 Foil Holders – Macroscopic Distribution Measurement	53
3.8.1 Radial Foil Holders	54
3.8.2 Axial Foil Holders	54
3.9 Foil Holders – Microscopic Distribution Measurement	57
3.9.1 Activation Distribution in Moderator	57
3.9.2 Activation Distribution in Rods	61
3.10 Summary of the Experiments	64
Chapter IV. Analysis of Data	69
4.1 Relative Activation Distribution and Cadmium Ratios	69
4.2 Determination of the Material Buckling	71
4.2.1 The RADFIT Code	71
4.2.2 The AXFIT Code	81
4.3 The Calculation of the Spatially-Dependent Thermal Neutron Spectrum and the Thermal Utilization	90
4.3.1 Thermal Energy Range – Unmodified Lattices	90
4.3.2 Thermal Energy Range – Modified Lattices	94
Determination of Cell Sizes	95
The Microscopic Traverses	96
4.4 Calculation of Ratio of Epithermal and Thermal Reaction Rates ( $\rho_1, \delta_{25}$ )	100
4.5 Least Squares Fitting	105
Chapter V. Results and Conclusions	108
5.1 Buckling	108
5.2 Parameters Characterizing the Thermal Energy Region	110
5.3 Parameters Characterizing the Epithermal Energy Region	113
5.4 Calculation of $k_{\infty}$	113
5.5 Discussion of Results	125
5.6 Calculation of Diffusion Area ( $L^2$ )	127



5.7	Exploratory Experiments on Two-Region Assembly	128
5.7.1	Cadmium Ratio	129
5.7.2	Buckling	134
5.8	Conclusions	136
Chapter VI.	Summary and Suggestions for the Future	138
6.1	Summary	138
6.2	Suggestions for the Future	141
6.2.1	One-Region Measurements	141
6.2.2	Two-Region Measurements	143
Appendix A.	Literature Research	145
A.1	Measurement of $k_{\infty}$ and $\eta$	145
A.2	Use of Added Absorbers in Subcritical Lattices	146
Appendix B.	Use of Added Absorbers Homogeneously Dispersed in Liquid Moderator	148
Appendix C.	Foil Counting: Procedures and Analysis of Data	151
Appendix D.	Dimensions, Densities, and Nuclear Cross Sections of Materials Used	154
D.1	Dimensions and Densities	154
D.2	Nuclear Cross Sections Used in THERMOS Calculations	155
Appendix E.	Calculation of Spectrally Averaged Parameters in a Modified Lattice with the TULIP Code	157
E.1	Calculation of Foil Activities	157
E.2	Normalization of Calculated Neutron Densities	160
E.3	Calculation of Thermal Utilization and Other Parameters	162
E.4	The TULIP Code	164
Appendix F.	Approximate Method for Calculating the Effect of Added Thermal Absorbers	182
Appendix G.	Simultaneous Experimental Determination of Diffusion Area and Fermi Age	185
Appendix H.	References	188



## LIST OF FIGURES

2.1	Neutron Life Cycle in a Thermal Neutron Reactor	13
3.1	Vertical Section of the Subcritical Assembly	28
3.2	Plan View of the Subcritical Assembly	29
3.3	Plan View of 250B1 Assembly	36
3.4	Plan View of 250A1 Assembly	37
3.5	Plan View of 250B2 Assembly	38
3.6	Plan View of 250A2 Assembly	39
3.7	Plan View of 175A1 Assembly	40
3.8	Plan View of 175A1B1 Assembly	41
3.9	Plan View of 253A2 Assembly	42
3.10	Plan View of 253A2B1(1R) Assembly	43
3.11	Plan View of 253A2B1(2R) Assembly	44
3.12	Absorber Rod Supports in 253 Assemblies	46
3.13	Top Adapter for Copper Rods	47
3.14	Absorber Rod Aligner in 250B2 Assembly	49
3.15	Ratio of Foil Activity in Off-Center Axial Traverse to Foil Activity in On-Center Traverse, as a Function of Axial Position	50
3.16	Axial Foil Holder Used in 253 Assemblies	56
3.17	The Cadmium Box Used in the Microscopic Distribution Measurement (From Ref. SI 1)	59
3.18	Foil Holder Used in Microscopic Distribution Measurement in 253 Assemblies	60
3.19	Foil Holders Used for the Measurement of the Microscopic Distribution in Fuel	62
3.20	Copper Rods Used in Microscopic Distribution Measurements (Vertical Section)	63
4.1	Relative Activation Distribution as a Function of Radial Position (R), Measured in Assembly 253A2 with Bare 0.010-Inch Gold Foils	73
4.2	Cadmium Ratio in 175A1B1 Assembly as a Function of Radial Position (Runs 25, 27)	75
4.3	Relative Activation Distribution in 250B1 Assembly as a Function of Radial Position (Run 19, Bare Foils). Radial Buckling is 2418 $\mu$ B.	77

4.4	Relative Activation Distribution in 175A1 Assembly as a Function of Radial Position (Run 33, Cadmium-Covered Foils). Radial Buckling is 2311 $\mu$ B.	78
4.5	Relative Activation Distribution in 253A2B1 Assembly as a Function of Radial Position (Run 43, Bare Foils). Radial Buckling is 2361 $\mu$ B.	79
4.6	Cadmium Ratio in 250B2 Assembly as a Function of Axial Position (Runs 16, 18)	82
4.7	Relative Activation Distribution in Four 250 Assemblies as a Function of Axial Position	86
4.8	Relative Activation Distribution in Two 175 Assemblies as a Function of Axial Position	87
4.9	Unit Cell and Smallest Repeating Cell Segment in a Lattice on a Triangular Spacing, S	91
4.10	Relative Activation Distribution Near Center Fuel Rod in 250A2 Assembly (Run 7)	98
4.11	Relative Activation Distribution Near Center Fuel Rod in 253A2 Assembly (Run 48)	99
5.1	Relative Absorption of Thermal Neutrons in Copper, $A_3$ , as a Function of Material Buckling, $B_m^2$ , for 250 Assemblies	120
5.2	Relative Absorption of Thermal Neutrons in Copper, $A_3$ , as a Function of Material Buckling, $B_m^2$ , for 175 Assemblies	121
5.3	Relative Absorption of Thermal Neutrons in Copper, $A_3$ , as a Function of Material Buckling, $B_m^2$ , for 253 Assemblies	122
5.4	Relative Absorption of Thermal Neutrons in Copper, $A_3$ , as a Function of Material Buckling, $B_m^2$ , for 250 Assemblies	123
5.5	Relative Activation Distribution in 253A2B1(2R) Assembly as a Function of Radial Position (Run 35, Bare Foils)	130
5.6	Relative Activation Distribution in 253A2B1(2R) Assembly as a Function of Radial Position (Run 37, Cadmium-Covered Foils)	131
5.7	Cadmium Ratio in 253A2B1(2R) Assembly as a Function of Radial Position	132
5.8	Cadmium Ratio in 253A2B1(2R) Assembly as a Function of Radial and Axial Position	133
E.1	Specific Activation $A^*(r)$ as a Function of Radial Position in Cell (r)	159
E.2	Moderator Subregions in 250A2 Assembly	163



## LIST OF TABLES

2.1	Constants Used	15
2.2	Index i Assigned to Materials in Cell	17
3.1	Description of Lattices Studied	31
3.2	Radiation Level as a Function of Distance from Irradiated Rod	33
3.3	Impurities Present in Copper Used in Experiments (Based on qualitative spectrographic analysis of two samples)	35
3.4	Description of Assemblies Studied	66
3.5	Number and Type of Experiments Done in Each Assembly	67
4.1	Region of Equilibrium Cadmium Ratio (Radial)	76
4.2	Radial Extrapolation Distance, $R_o - R_{lat}$	81
4.3	Region of Equilibrium Cadmium Ratio (Axial)	83
4.4	Axial Region Where Asymptotic Distribution Prevails in Each Assembly	84
4.5	Value of Extrapolated Height, $H_o$ , for Each Assembly	85
4.6	Comparison of RMS Value of Buckling Increment with S. D. of the Mean	89
4.7	Measured and Calculated Value of $\rho_{28}$	104
5.1	Measured Bucklings	109
5.2	Parameters Characterizing the Thermal Energy Region (I)	111
5.3	Parameters Characterizing the Thermal Energy Region (II)	112
5.4	Measured Parameters Characterizing the Epithermal Energy Region (I)	114
5.5	Measured Parameters Characterizing the Epithermal Energy Region (II)	115
5.6	Calculated Parameters Characterizing the Epithermal Energy Region	116
5.7	Values of $\eta$ , $\epsilon$ , $p$ , $f$ , and $1+\delta_{25}$ Based on Measured and Calculated Parameters	117
5.8	Ratios Used in the Determination of Correction Factors	118
5.9	Correction Factors for Use in Equation (2.30)	119
5.10	Values of the Multiplication Factor $k_{\infty}$	125
5.11	Measured and Calculated Values of the Diffusion Area ( $L^2$ ) for the Unmodified Lattices	128
5.12	Equilibrium Cadmium Ratio in Two-Region Assembly (253A2B1(2R))	129



5.13	Values of Radial Buckling for Two-Region Assembly (253A2B1(2R))	135
5.14	Values of Axial Buckling for Two-Region Assembly (253A2B1(2R))	135
6.1	Possible Configurations for Subcritical Two-Region Measurements of $k_{\infty}$	144
D.1	Density of Copper Samples	154
D.2	Nuclear Cross Sections of Added Absorbers	155
D.3	THERMOS Input Data: Concentrations and High Energy Cross Sections	156
E.1	Comparison of Four Methods for Normalizing Theory and Experiment: RMS Value of Percentage Residuals	161
E.2	Transport Cross Section ( $\Sigma_{tr}$ ) and Mean Free Path ( $\lambda_{tr}$ ) of Lattice Materials Based on 2200 m/sec Microscopic Cross Sections	164
E.3	Input Format for the TULIP Code	166

## CHAPTER I

### INTRODUCTION

The neutron multiplication factor for an infinite medium,  $k_{\infty}$ , is a parameter central to reactor physics and reactor analysis. Considerable effort has been expended in the past in the development of techniques for its experimental measurement and its theoretical calculation. The purpose is to determine reliable values of  $k_{\infty}$  for use in the construction of reactors for research, power, and other applications.

Although theoretical calculations, generally requiring the use of digital computers, are in wide use in the design of reactors, experimental measurements of the values of important parameters in assemblies similar, or nearly identical, to the proposed design are usually still required before construction can proceed with confidence. Because of the expense of nuclear fuels and of the experiments, it is important to obtain accurate experimental values with assemblies utilizing the minimum amount of fuel. Thus, in addition to measurements in single-region critical assemblies, a variety of alternatives have been, and are being, investigated. These include substitution measurements in critical and subcritical assemblies, single-region subcritical experiments, and measurements in miniature assemblies, and on single rods (CR 1).

The purpose of the present study is to explore another, as yet untried, approach to the problem. It is closely related to one of the critical substitution measurement methods, the technique for the measurement of  $k_{\infty}$  used at Hanford in the Physical Constants Testing Reactor (DO 2).

In the remaining sections of this chapter,  $k_{\infty}$  will be defined and formulated in terms of the familiar four factors, and the Hanford technique will be described. The objectives of the present study will then be described in detail.



## 1.1 THE NEUTRON MULTIPLICATION FACTOR IN AN INFINITE MEDIUM ( $k_{\infty}$ )

Although a number of different definitions of  $k_{\infty}$  are in use,  $k_{\infty}$  is here taken to be equal to the ratio of the total number of neutrons produced to the total number destroyed, per unit time, in an assembly so large that neutron leakage may be ignored. In terms of the neutron life cycle in an infinitely large, predominantly thermal reactor,  $k_{\infty}$  can be defined as

$$k_{\infty} = \eta\epsilon pf . \quad (1.1)$$

Here,  $\eta\epsilon$  is the total number of (fast) neutrons produced for one thermal neutron absorbed in the fuel;  $\eta$  is the number of neutrons produced by fission for one thermal neutron absorbed, and  $\epsilon$  is the total number of (fast) neutrons produced for each neutron resulting from thermal fission;  $p$  is the probability that a fast neutron escapes absorption while slowing down to thermal energies, and  $f$  is the probability that a neutron, once thermal, is captured in the fuel. It is important that the various factors be defined consistently and that each process be counted once and only once in the neutron cycle.

The multiplication factor  $k_{\infty}$  is most commonly determined by a combination of measurements and calculations which result in a value for each of the four factors on the right-hand side of Eq. (1.1), although other formulations exist (WE 2). The uncertainty in such a determination is in the neighborhood of 1% or 2%, sometimes more, generally attributable to uncertainties in the values of neutron cross sections and in the average number of neutrons produced per fission. The Hanford method, developed at the Hanford Laboratories and based on the use of the Physical Constants Testing Reactor (PCTR) (DO 2), results in considerably smaller uncertainties in the values of  $k_{\infty}$ .

## 1.2 THE HANFORD TECHNIQUE

Consider an infinite, homogeneous, neutron-multiplying medium, with  $k_{\infty}$  greater than unity. Consider also the addition, to a sample of this medium, of a quantity of a homogeneous absorber (which absorbs only thermal neutrons and causes no spectral perturbation) sufficient to reduce  $k_{\infty}$  to unity. Then Eq. (1.1) may be written:



$$1 = \eta \epsilon p f^0, \quad (1.2)$$

Under the conditions that have been defined, the thermal utilization has been changed from  $f$  to  $f^0$ , in such a way that the value of  $k_\infty$  is reduced to unity; the other factors are unchanged. If we assume, for simplicity, that the assembly is homogeneous, the thermal utilization for the two cases may be written:

$$f = \frac{\Sigma_{\text{fuel}}^a}{\Sigma_{\text{fuel}}^a + \Sigma_{\text{moderator}}^a}, \quad (1.3)$$

$$f^0 = \frac{\Sigma_{\text{fuel}}^a}{\Sigma_{\text{fuel}}^a + \Sigma_{\text{moderator}}^a + \Sigma_{\text{absorber}}^a}, \quad (1.4)$$

where  $\Sigma_i^a$  indicates the macroscopic neutron absorption cross section for material  $i$ . Then, we may write:

$$k_\infty = \frac{f}{f^0} = 1 + \frac{\Sigma_{\text{absorber}}^a}{\Sigma_{\text{fuel}}^a + \Sigma_{\text{moderator}}^a}, \quad (1.5)$$

$$k_\infty - 1 = \frac{\Sigma_{\text{absorber}}^a}{\Sigma_{\text{fuel}}^a + \Sigma_{\text{moderator}}^a}. \quad (1.6)$$

The Physical Constants Testing Reactor is a cube of graphite, 7 feet on a side, with a cavity, 2 by 2 by 7 feet, located at its center. It is made critical by enriched uranium distributed outside the boundary of the central cavity. Several cells of the lattice to be tested are placed in the cavity, together with a quantity of a distributed neutron absorber sufficient to make the reactivity of the resulting assembly the same as that of the reactor with the cavity. Such a sample is held to have a value of  $k_\infty$  equal to unity. An attempt is made to ensure that the energy spectrum of the neutrons incident on the test sample, as defined by some suitable spectral index, is the same as the spectrum that would exist in an infinitely large sample of the medium.

The Hanford technique thus consists basically of a determination of the amount of added absorber necessary for Eq. (1.2) to be satisfied.

With the amount of absorber to be used in calculating  $\Sigma_{\text{absorber}}^a$  thus determined, Eq. (1.6) may be solved for  $k_{\infty}$ , with the aid of the known cross sections. Equation (1.6) has been written for  $(k_{\infty}-1)$  rather than  $k_{\infty}$  to emphasize the major attraction of the method: the over-all uncertainty in the right-hand side due to cross-section uncertainties is proportional to the uncertainty in  $(k_{\infty}-1)$ , rather than in  $k_{\infty}$ . This result is especially important in most practical cases, where  $k_{\infty}$  is near unity. In addition, this method avoids the need for a calculated or measured value of  $\eta$ , one source of uncertainty in four-factor determinations of  $k_{\infty}$ . Finally, no particular "model" or form of reactor theory is necessary for the interpretation of the experiment. Thus, the method offers several important advantages.

### 1.3 OBJECTIVES OF THE PRESENT WORK

The first objective of the present work is to synthesize from known techniques a new method for the measurement of  $k_{\infty}$ , which retains the major advantages just ascribed to the Hanford technique, but which employs not a critical but a subcritical facility; the absorber is to be added uniformly, though not necessarily homogeneously, to the entire lattice. The amount of added absorber which reduces the measured material buckling of the assembly to zero is to be taken as the amount which exactly reduces  $k_{\infty}$  to unity.

The second objective is to explore the use of the method in heavy water moderated assemblies of slightly enriched uranium metal rods, by using it to measure  $k_{\infty}$  in three different subcritical lattices, with markedly different moderator-to-fuel ratios. The results of this work will be compared with results of activation measurements of ratios related to the factors in the four-factor formula (Eq. (1.1)), and to results of PCTR-type measurements on similar lattices.

It is possible that values of  $k_{\infty}$  can be determined by adding absorber only to a portion of the subcritical assembly. One of the objectives of this work is to conduct a limited experiment with the purpose of exploring the feasibility of this technique.

The final objective of this work is to use the data, where possible, to determine quantities related to neutron leakage, such as the Fermi age and the diffusion length.



## 1.4 NOMENCLATURE

A number of the terms here used in a specific way have alternative meanings elsewhere in the literature. They are defined as they occur, but the more important ones are here recorded for convenience.

"Lattice" is here used to mean one of the three arrangements of uranium fuel rods in heavy water to which varying amounts of neutron absorber were added. "Assembly," on the other hand, refers to a particular assembly of fuel, heavy water, and neutron absorber. These are also referred to as "mixed" or "modified" lattices. Two or more assemblies, each having a different amount of added neutron absorber, have been investigated in the course of the work on each lattice.

In the discussion so far, the term often used for extraneous absorbers introduced into neutron-multiplying assemblies — "poison" — has been avoided. The term "absorber," while less dramatic, is certainly more descriptive. Although all materials are to some extent neutron absorbers, no confusion should arise if the term "absorbers" is here considered to mean those materials temporarily introduced into a lattice, to increase its thermal neutron absorption cross section for the purpose of specific experiments.

The thermal energy region includes energies less than or equal to 0.415 ev. The epithermal energy region is divided into the resonance region, which includes energies greater than 0.415 ev but less than 1.0 Mev; the high energy region includes energies equal to or greater than 1.0 Mev.

The slowing-down areas  $L_f^2$  and  $L_r^2$ , and the diffusion area  $L_s^2$ , relate to the high, resonance, and the thermal energy regions, respectively. They are related to the nonleakage probabilities  $\ell_f$ ,  $\ell_r$ , and  $\ell_s$  by equations analogous to Eq. (2.9).

The multiplication factor  $k_\infty$ , as well as the factors generally defined in Sec. 1.1, are given precise definitions in Sec. 2.2 and related to measurable quantities in Sec. 2.3.

The capture-to-fission ratio  $\alpha_{28}$  relates to fission of  $U^{238}$  in the high energy region;  $\alpha_{25}$  relates to fission of  $U^{235}$  in the epithermal energy region. The ratio  $\bar{\alpha}$  is used only in Sec. 2.1.4 and denotes the capture-to-fission ratio in  $U^{235}$ , averaged over all energies.

A "unit cell" of a lattice (or an assembly) consists of a single fuel

rod, as well as the moderator (and added absorber) associated with it. All unit cells are identical; thus, the neutron distribution throughout an infinite lattice (or assembly) is known if the distribution in one unit cell is known. Knowledge of the neutron distribution over some segment of the unit cell is often sufficient for the specification of the distribution throughout the unit cell, from considerations of symmetry. The smallest such segment is here referred to as the "smallest repeating cell segment."

## 1.5 CONTENTS OF THE REPORT

In Chap. II, the detailed theoretical treatment of the measurement of  $k_{\infty}$  is presented; the experimental equipment and procedures are discussed in Chap. III. Chapter IV deals with the analysis of data, and Chap. V consists of the results of the work. Chapter VI summarizes and concludes the main body of this report.



## CHAPTER II

### THEORY OF THE MEASUREMENT

The theoretical basis of the method will be discussed in this chapter. The material buckling, the neutron multiplication factor in an infinite medium ( $k_\infty$ ), and the relation of the two will be discussed first; the factors comprising  $k_\infty$  will then be defined.

Next, the many modifications necessary to adapt the simplified version of the Hanford technique presented in Chap. I to cases of interest here will be discussed.

The determination of lattice parameters other than  $k_\infty$  is discussed in the final sections of this chapter.

#### 2.1 THE MATERIAL BUCKLING, THE INFINITE MEDIUM MULTIPLICATION FACTOR, AND THE SUBCRITICAL EXPERIMENT

##### 2.1.1 Buckling

The spatial distribution of the neutron flux,  $\phi(\vec{r})$ , in a bare, homogeneous, critical reactor is given by the fundamental mode solution of the Helmholtz equation,

$$\nabla^2 \phi(\vec{r}) + B^2 \phi(\vec{r}) = 0, \quad (2.1)$$

under the assumption that the flux goes to zero at the extrapolated boundaries of the system, assumed independent of neutron energy (WE 1). Here, the constant  $B^2$  may be identified with the geometric buckling ( $B_g^2$ ); it is a function only of the extrapolated dimensions of the critical reactor. Derivations of the expressions for the geometric buckling in reactors of various shapes are readily available (GL 1). For a right circular cylinder of extrapolated height  $H_0$  and extrapolated radius  $R_0$ , the buckling is:

$$B_g^2 = \left( \frac{2.4048}{R_0} \right)^2 + \left( \frac{\pi}{H_0} \right)^2. \quad (2.2)$$

The material buckling ( $B_m^2$ ) is a characteristic of a given neutron-multiplying medium; in the absence of pronounced anisotropies, such

as those caused by voids, it is a function only of the materials involved and not of the size of the assembly (CR 1). It is defined to be equal to the geometric buckling of a critical reactor composed of the given material. It may thus be measured by constructing such a reactor, determining its extrapolated boundaries, and using the appropriate expression for the geometric buckling (cf. Eq. (2.2)). Clearly, the larger the material buckling, the smaller the critical reactor. Intuitively, it may be seen that  $k_{\infty}$  and  $B_m^2$  are related, a large value of  $k_{\infty}$  implying a large value of the material buckling, and vice versa.

### 2.1.2 Relation of the Buckling to the Infinite Medium Multiplication Factor

There are a number of ways to relate  $k_{\infty}$  to  $B_m^2$  mathematically, varying from simple to relatively complex, depending on the assumptions made in representing the processes by which neutrons are produced and destroyed in the reactor. Several of these will be discussed in Sec. 2.6.2. Common to all such relationships, however, is the association of the value of unity for  $k_{\infty}$  with a zero material buckling. This follows from definitions already stated, upon noting that a reactor with a multiplication constant equal to unity is just critical by definition, since a steady-state chain reaction can then be maintained without external neutron sources. If the value of  $k_{\infty}$  for a given medium is equal to unity, a reactor composed of the medium, infinite in extent, would be just critical. The value of the geometric buckling of such a reactor would be zero, and it follows from the equivalence of geometric and material buckling for a critical reactor that the material buckling would also be zero.

### 2.1.3 Measurement of the Material Buckling

Although construction of a critical assembly is a straightforward way of measuring  $B_m^2$ , there is another way, particularly applicable in systems of relatively low buckling. It is based on the fact that the fundamental mode solution to Eq. (2.1), with  $B^2$  now associated with the material buckling, governs the spatial distribution of the neutron flux, far from sources and boundaries, in a subcritical assembly (WE 1). This holds, provided that an equilibrium neutron energy spectrum (characteristic of the critical reactor) exists throughout a



considerable volume of the assembly.

The fundamental mode spatial distribution obtained from Eq. (2.1) for positive and negative values of  $B_m^2$ , for a cylindrically symmetric assembly of extrapolated height  $H_0$  and extrapolated radius  $R_0$ , is:

$$\phi(\vec{r}) = \phi_0 J_0(\alpha r) \sinh \gamma(H_0 - z). \quad (2.3)$$

Here,  $J_0(x)$  is the zeroth order Bessel function of the first kind of  $x$ ,  $\sinh x$  is the hyperbolic sine of  $x$ ,

$$\alpha = 2.4048/R_0,$$

$r$  and  $z$  are the radial and axial position coordinates, respectively, with the origin at the center of the source plane of the assembly,

$\phi_0$  is an arbitrary constant of proportionality.

This solution holds, subject only to the requirement,

$$\alpha^2 \geq B_m^2, \quad (2.4)$$

a condition usually satisfied; the material buckling is then related to the flux distribution by the relation:

$$B_m^2 = \alpha^2 - \gamma^2. \quad (2.5)$$

The details of the development just summarized are available in basic reactor physics texts (GL 1). The various assumptions involved are also discussed in theses by Palmedo (PA 1) and Harrington (HA 1).

To measure the material buckling, it is necessary to determine the relative spatial distribution of the neutron flux within the region where the equilibrium spectrum exists, in the radial and axial directions. The values of  $\alpha$  and  $\gamma$  which yield the "best fit" of the theoretically predicted distribution to the observed distribution then are used to determine the material buckling by means of Eq. (2.5).

The material buckling (and other reactor physics parameters which characterize the critical reactor) may thus be measured in a subcritical assembly of sufficient size. The extent of the region throughout which the equilibrium spectrum holds may be determined experimentally by measuring neutron flux distributions with appropriate detectors.

The cadmium ratio  $R_{Cd}$  for a neutron detector at a given point is defined as the ratio of the observed activities, at the point in question, of detector foils without and with cadmium shields. It is a spectral index, large cadmium ratios typifying well-thermalized spectra. Constancy of the cadmium ratio over a given region of an assembly is taken as an indication that the neutron energy spectrum is invariant with position over the region.

The foregoing development, strictly speaking, applies only to large, bare, homogeneous reactors. Experiments have shown, however, that it also applies to bare, heterogeneous uranium-heavy water assemblies, among others (CO 1, PA 1). Thus, a practical and commonly-used approach to the determination of the lattice physics parameters characterizing critical reactors of this type involves the use of a subcritical assembly. With this experience in mind, extensive use of the foregoing ideas will be made here.

#### 2.1.4 Use of the Four-Factor Formula for $k_{\infty}$

As noted in the introduction, the four-factor formula is not the only one which can be used in the experimental determination of  $k_{\infty}$ . Weitzberg (WE 2) has formulated  $k_{\infty}$  directly in terms of nuclear data and experimentally measurable activation ratios:

$$k_{\infty} = \frac{\nu_{25} + (\nu_{28} - 1)\delta_{28}}{C^* + (1 + \bar{a}) + \left(\frac{1}{f} - 1\right)(1 + \bar{a})\left(\frac{1}{1 - G}\right)} \quad (2.6)$$

Here,  $C^*$  is the measured conversion ratio,  $\bar{a}$  is the average capture-to-fission ratio of  $U^{235}$ ,  $G$  is the ratio of thermal absorptions in  $U^{238}$  to thermal absorptions in the fuel, and the other quantities have their usual definitions (see Sec. 2.3).

Although independent of the four-factor or "neutron life cycle" approach to the formulation of  $k_{\infty}$ , this definition is equivalent to it, as Weitzberg has pointed out, provided that:

- 1) the basic definition of the multiplication factor is the same in each case, and
- 2) both account for the same neutron production and absorption processes.



D'Ardenne (DA 1) has evaluated  $k_{\infty}$  for three lattices similar to those studied in the present work; he used both Eqs. (1.1) and (2.6). The results obtained agreed within the uncertainties of the measurements.

There is, then, no fundamental objection to the use of the four-factor formula. For the present work, it is particularly appropriate to use this formulation because the thermal utilization is the only factor which undergoes large changes when the neutron absorbers used are introduced into the lattices. Corrections are made for changes in other parameters, but, as will be seen, they are small.

For precise work, it is vital that the factors in Eq. (1.1) be defined consistently and take into account all processes of importance in the neutron life cycle. In this connection, it should be noted that various processes in the epithermal energy range have been neglected in the simplified discussion of Chap. I. These include fission and absorption in  $U^{235}$ , as well as absorption in non-fuel materials. The definitions of  $\epsilon$ ,  $p$ ,  $\eta$ , and  $f$ , and modification of the four-factor formula to take into account the epithermal fissions in  $U^{235}$ , will be discussed in the next section.

## 2.2 DEFINITIONS EMPLOYED

The multiplication factor  $k_{\infty}$  has been defined in Chap. I as the ratio of the number of neutrons produced, per unit time in an infinitely large assembly, to the number of neutrons absorbed. Neutron leakage is not considered at this point because the assumption of infinite size automatically eliminates leakage as a neutron-removing process. The effect of leakage on measurements made in finite assemblies is considered in Sec. 2.3.

The lattices studied consisted of slightly enriched uranium metal rods, clad in aluminum and immersed in heavy water moderator. To these lattices have been added pure copper rods, clad with nickel. The neutron-producing processes to be considered are thus fission of  $U^{235}$  at thermal and epithermal energies, and fission of  $U^{238}$  at high energy. The absorption processes include absorption at all energies in uranium, copper, cladding material, and moderator. Absorption in the narrow air gap between the fuel and the cladding, in the small light water contaminant inevitably present in the moderator, and in the



nickel cladding on the copper rods, will be neglected, although all were taken into account in the detailed calculations. No loss of generality is involved.

The neutron life cycle in a typical lattice of this sort is shown schematically in Fig. 2.1. From one  $U^{235}$  fission neutron, a total of  $\epsilon$  fission neutrons from  $U^{235}$  and  $U^{238}$  slow down past the  $U^{238}$  fission threshold, here taken as 1 Mev. A fraction  $p$  of these neutrons escapes capture in the resonance energy region, here taken as the region between 0.415 ev and 1 Mev. Of the  $\epsilon p$  neutrons reaching the thermal energy region, a fraction  $f$  is absorbed at thermal energies in the fuel ( $U^{235}$  and  $U^{238}$ ). The number of  $U^{235}$  fission neutrons resulting from one thermal neutron absorbed in fuel is  $\eta$ . Thus, for one  $U^{235}$  fission neutron starting out (in the upper left-hand corner of Fig. 2.1), a total of  $\epsilon \eta p f U^{235}$  fission neutrons from thermal fission of  $U^{235}$  are created. To these must be added the fission neutrons created by epithermal fission of  $U^{235}$ . The parameter  $\delta_{25}$  is defined as the ratio of epithermal fissions in  $U^{235}$  to thermal fissions in  $U^{235}$ . The total number of  $U^{235}$  fission neutrons produced, per  $U^{235}$  fission neutron absorbed, is by definition just equal to  $k_{\infty}$ . We may therefore write:

$$k_{\infty} = (1 + \delta_{25}) \epsilon \eta p f . \quad (2.7)$$

The fast fission factor accounts for fast neutron absorption in  $U^{238}$ , as well as production of neutrons by fast fission in  $U^{238}$ . The resonance escape probability, as here defined, takes into account all epithermal absorptions in uranium and copper, whether in resonances or in the  $1/v$  component of the cross section, as well as epithermal capture in cladding or moderator.

It should be realized that the foregoing set of definitions, while complete and self-consistent, is not the only set that could be used. The most convenient definition of the factors depends, in general, on the type of assembly under investigation and the measurements to be made in it. The relation of the factors just defined to ratios which can be measured experimentally is the subject of the next section.



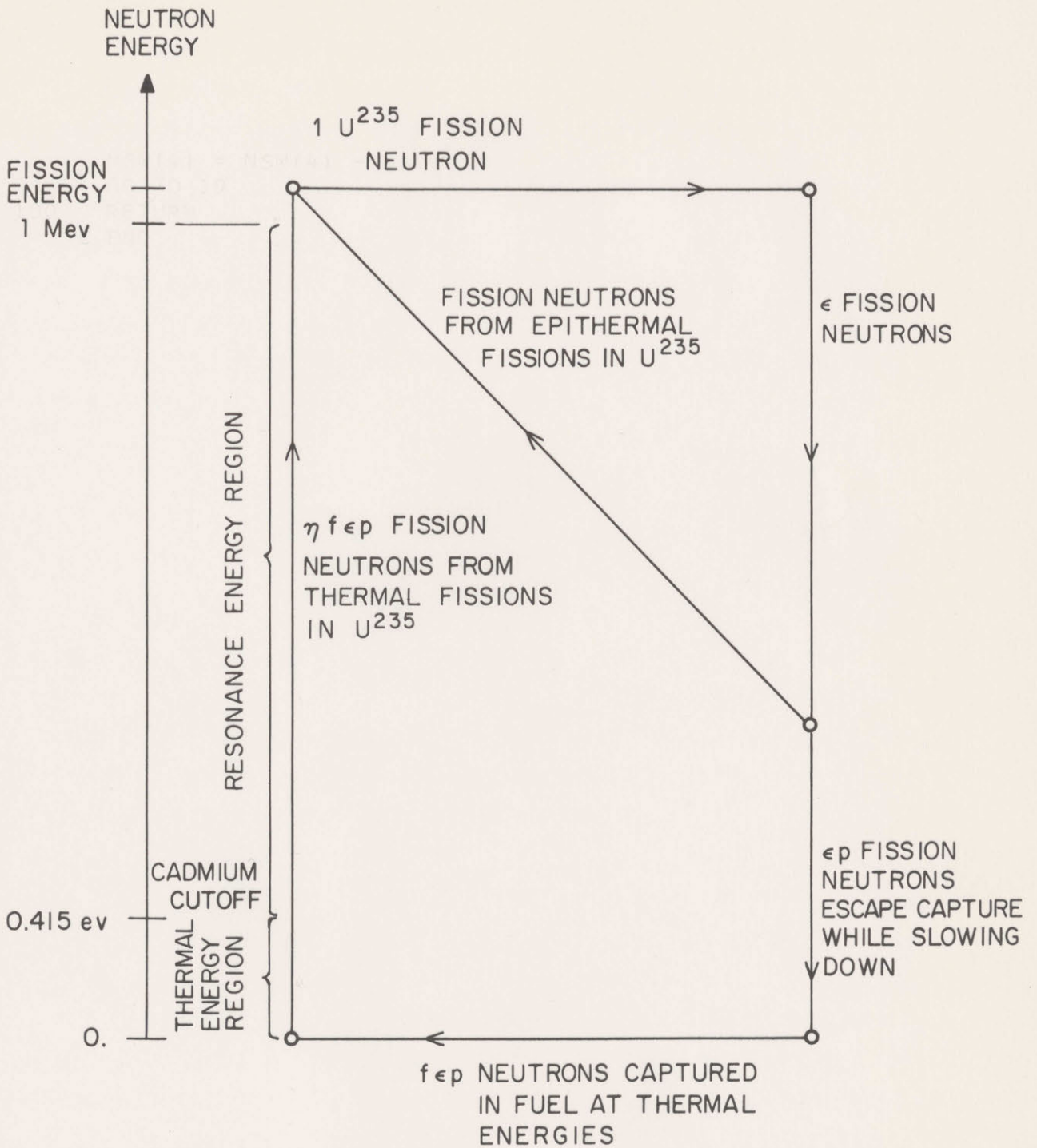


FIG. 2.1. NEUTRON LIFE CYCLE IN A THERMAL NEUTRON REACTOR

## 2.3 RELATION OF FACTORS TO MEASURABLE QUANTITIES

Much has been written on the subject of relating the several factors to experimentally observable quantities. The formulations to be used here have been selected on the basis of experience in heavy water lattice physics at M. I. T. and elsewhere.

### 2.3.1 Fast Fission Factor ( $\epsilon$ )

The experimentally measurable quantity associated with the fast fission effect is  $\delta_{28}$ , defined as the ratio of fissions in  $U^{238}$  to fissions in  $U^{235}$ , averaged over the fuel. It is related to  $\epsilon$  by the following equation (KO 1):

$$\epsilon = \frac{1 + \delta_{28} \left[ \frac{\nu_{28} - (1 + a_{28})(1 + L_f^2 B_m^2)}{\nu_{25}} \right]}{1 - \delta_{28} L_f^2 B_m^2 \frac{\nu_{28}}{\nu_{25}}}. \quad (2.8)$$

Here,  $\nu_{28}$  is the number of neutrons emitted per  $U^{238}$  fission,  $\nu_{25}$  is the same parameter for  $U^{235}$  fission,  $a_{28}$  is the capture-to-fission ratio in  $U^{238}$  above 1 Mev,  $B_m^2$  is the material buckling, and  $L_f^2$  is a parameter relating to fast neutron leakage. The nonleakage probability while slowing down to 1 Mev is taken to be:

$$l_f = \left( 1 + L_f^2 B_m^2 \right)^{-1}. \quad (2.9)$$

The values of the parameters used in the evaluation of Eq. (2.8) are given in Table 2.1.

The effect of neutron leakage from the finite assembly on the value of  $\epsilon$  is accounted for by the terms involving the buckling. In the present work, they are very small, since the material buckling in each lattice is less than  $0.0015 \text{ cm}^{-2}$ . The magnitude of the uncertainty in  $\nu_{28}$  alone renders the application of the correction factor in the numerator of Eq. (2.8) useless, and the factor is not included here.

The measurement of  $\delta_{28}$  has been treated in detail in Refs. WO 1 and BL 1.



TABLE 2.1  
Constants Used

Constant	Value	Source of Data
$\nu_{25}$	$2.43 \pm 0.02$	BO 1
$\nu_{28}$	$2.82 \pm 0.05$	SA 1
$a_{28}$	$0.107 \pm 0.010$	KO 1
$a_{25}$	$0.63 \pm 0.10$	SA 3
$L_f^2$	$7 \text{ cm}^2$	Estimate based on information in Ref. PA 2.
$L_r^2$	$113 \text{ cm}^2$	Estimate based on information in Ref. DA 1.

### 2.3.2 Neutron Regeneration Factor ( $\eta$ )

The number of neutrons liberated per  $U^{235}$  fission,  $\nu_{25}$ , is here taken to be constant as a function of incident neutron energy (see Table 2.1). The observed energy dependence of this quantity is (AN 1):

$$\nu_{25} = 2.43 + 0.145 E, \quad (2.10)$$

the units of  $E$  being Mev. Thus, only for fissions induced by neutrons with energies greater than about 0.1 Mev does the variation of  $\nu_{25}$  with energy become important. Since the lattices studied are well-moderated, and even the small amount of resonance fission occurs near or below 100 ev, constance of  $\nu_{25}$  with energy is an excellent assumption.

The factor  $\eta$  has been defined in Sec. 2.2. If  $\bar{\Sigma}_f(25)$  is taken to be the average macroscopic thermal fission cross section for  $U^{235}$ , and  $\bar{\Sigma}_a(25)$  and  $\bar{\Sigma}_a(28)$  the average macroscopic thermal absorption cross sections for  $U^{235}$  and  $U^{238}$ , respectively, then the neutron regeneration factor is defined as follows:

$$\eta = \frac{\nu_{25} \bar{\Sigma}_f(25)}{\bar{\Sigma}_a(25) + \bar{\Sigma}_a(28)}. \quad (2.11)$$

Provided that the cross sections are averaged over the thermal neutron energy spectrum which would be present in an infinitely large reactor, the value of  $\eta$  defined above is appropriate for use in the four-factor formula for  $k_{\infty}$ . This spectrum is taken to be the same as the equilibrium spectrum in the finite reactor (see Sec. 4.3.1). No corrections for leakage need be applied, since all cross sections pertain to the same energy group.

### 2.3.3 Thermal Utilization (f)

The thermal neutron absorption rate  $a_i$  in material  $i$  is:

$$a_i = \int_i \int_0^{v_c} v n(\vec{r}, v) \Sigma_i(v) dv d\vec{r}, \quad (2.12)$$

where  $n(\vec{r}, v)$  is the density of neutrons with speeds between  $v$  and  $v+dv$  in the element of volume  $d\vec{r}$  at  $\vec{r}$ , and  $\Sigma_i(v)$  is the macroscopic neutron absorption cross section for neutrons of speed  $v$ . The absorption cross section is assumed to have no spatial dependence within the material. The thermal neutron energy range is taken to include neutrons with speeds up to  $v_c$ , the speed corresponding to the cadmium cutoff energy.

Equation (2.12) may be replaced by the expression:

$$a_i = \bar{n}_i \bar{v}_i \bar{\Sigma}_i V_i, \quad (2.13)$$

where the bars denote averages in space and velocity, defined as follows:

$$\bar{\Sigma}_i = \frac{\int_i \int_0^{v_c} v n(\vec{r}, v) \Sigma_i(v) dv d\vec{r}}{\int_i \int_0^{v_c} v n(\vec{r}, v) dv d\vec{r}}, \quad (2.14)$$

$$\bar{n}_i = \frac{\int_i \int_0^{v_c} n(\vec{r}, v) dv d\vec{r}}{\int_i d\vec{r}} \quad (2.15)$$

and

$$\bar{v}_i = \frac{\int_i \int_0^{v_c} v n(\vec{r}, v) dv d\vec{r}}{\int_i \int_0^{v_c} n(\vec{r}, v) dv d\vec{r}}. \quad (2.16)$$



The parameter  $V_i$  is the volume of the material  $i$  in a unit cell of the infinite reactor under consideration. More will be said about the cell concept in Sec. 4.3.1; for the present, a unit cell may be regarded as being composed of a single fuel rod and the moderator and added absorber associated with it. Table 2.2 indicates the index  $i$  for each

TABLE 2.2  
Index  $i$  Assigned to Materials in Cell

$i$	Material
0	Fuel
1	Moderator
2	Cladding
3	Added absorber

material used in the experiments to be discussed. The thermal neutron absorption in material  $i$  relative to the thermal neutron absorption in the fuel is denoted by  $A_i$ :

$$A_i = \frac{a_i}{a_0} = \frac{\bar{n}_i \bar{v}_i \bar{\Sigma}_i V_i}{\bar{n}_0 \bar{v}_0 \bar{\Sigma}_0 V_0} \quad (2.17)$$

The thermal utilization in the definition of Sec. 2.2 may then be expressed in terms of the  $a_i$  or  $A_i$  as follows:

$$f = \frac{a_0}{a_0 + a_1 + a_2 + a_3} = \frac{1}{1 + A_1 + A_2 + A_3} \quad (2.18)$$

The various factors appearing in the above equation may be evaluated by a combination of calculations and experiments. In the present work, the ratios of cross section in the  $A_i$  terms are calculated with the aid of a multigroup transport theory computer code (see Sec. 4.3.1), and the flux disadvantage factors are measured in activation experiments at the center of the subcritical assembly. Correction for the spatial variation of the neutron flux due to leakage from the assembly is readily made, in a manner described in detail in Sec. 4.3.2.

### 2.3.4 The Resonance Escape Probability (p)

The derivation of the expression for  $p$  in terms of experimentally measurable ratios is based on the corresponding derivation in Ref. KO 1. That treatment is modified in the present work to take into account epithermal absorption in copper,  $U^{235}$ , cladding, and moderator, and includes all absorptions, rather than just those occurring in resonances.

The epithermal neutron absorption rate in material  $i$ , relative to the thermal neutron absorption, is denoted by  $\rho_i$ . The same ratio for  $U^{238}$  is denoted by  $\rho_{28}$ . The epithermal neutron fission rate in  $U^{235}$ , relative to the thermal neutron fission rate, is defined as  $\delta_{25}$ .

These will now be related to the resonance escape probability through consideration of the relevant portion of the neutron life cycle in a finite reactor.

It is shown in Ref. KO 1 that if  $\epsilon$  is defined as in Sec. 2.3.1, then the number of fast captures in  $U^{238}$  per virgin  $U^{235}$  fission neutron is  $N_f$ :

$$N_f = \frac{(\epsilon-1)a_{28}}{\nu_{28} - 1 - a_{28}} \quad (2.19)$$

If  $\ell_f$  is the nonleakage probability in the high energy region,  $\epsilon\ell_f$  neutrons reach the resonance energy region. Of these,  $\epsilon\ell_f p$  avoid resonance capture, and  $\epsilon\ell_f(1-p)$  are captured. The nonleakage probabilities in the resonance and thermal energy regions are  $\ell_r$  and  $\ell_s$ , respectively; they are defined by equations analogous to Eq. (2.9). Then,  $\epsilon\ell_f\ell_r\ell_s p^2$  neutrons are absorbed in uranium at thermal energies.

If  $G$  is defined as the ratio of absorptions in  $U^{238}$  to total absorptions in fuel, at thermal energies, and  $a_{25}$  is the capture-to-fission ratio for  $U^{235}$  in the epithermal energy region, then the absorptions in the resonance region may be related to the thermal absorptions. We note that:

$$\rho_{28}G = \text{ratio of epithermal } U^{238} \text{ absorptions to thermal absorption in fuel,} \quad (2.20)$$

$$\rho_i A_i = \text{ratio of epithermal absorption in material } i \text{ to thermal absorption in fuel,} \quad (2.21)$$

$$\frac{\delta_{25}(1+a_{25})\eta(1-G)}{\nu_{25}} = \text{ratio of epithermal } U^{235} \text{ absorption to thermal absorption in fuel.} \quad (2.22)$$



Then, equating the total number of epithermal absorptions (relative to the thermal absorption in the fuel) to the expression for this quantity based on the neutron life cycle considerations above yields the following equation:

$$\rho_{28}G + \sum_{i=1}^3 \rho_i A_i + \frac{\delta_{25}(1+a_{25}) \eta(1-G)}{\nu_{25}} = \frac{\epsilon \ell_f^{(1-p)} + \frac{(\epsilon-1)a_{28}}{\nu_{28}-1-a_{28}}}{\epsilon \ell_f \ell_r \ell_s p f} \quad (2.23)$$

When this equation is solved for  $p$ , the result is:

$$p = \frac{1 + \frac{\epsilon-1}{\epsilon} \frac{a_{28}}{\nu_{28}-1-a_{28}} \frac{1}{\ell_f}}{1 + \ell_r \ell_s f \left[ \rho_{28}G + \sum_{i=1}^3 \rho_i A_i + \frac{\delta_{25}(1+a_{25}) \eta(1-G)}{\nu_{25}} \right]} \quad (2.24)$$

This is the desired expression for the resonance escape probability in an infinite assembly, based on parameters measured in a finite assembly. The measured quantities are  $R_{28}$ ,  $R_3$ ,  $\delta_{25}$ , and  $\delta_{28}$ , and the disadvantage factor implicit in the  $A_i$  terms. Where measured values of the first three quantities were unavailable, they have been calculated from measurements in similar assemblies, in a manner explained in Sec. 4.4. The constants used in the evaluation of Eq. (2.24) are presented in Table 2.1. The calculation of  $\eta$ ,  $G$ , and  $L_s^2$  is discussed in Sec. 4.3.

### 2.3.5 The Ratio of Epithermal to Thermal Fissions of $U^{235}$ ( $\delta_{25}$ )

Values of  $\delta_{25}$  measured in finite assemblies will be higher than those that would be observed in equivalent infinite assemblies, owing to neutron leakage in the resonance and thermal energy regions. The following derivation of the appropriate correction factor is based on a similar derivation in Ref. EN 1.

The treatment is similar to that of the preceding section. For the purposes of this discussion only, the resonance escape probability  $p$  will be replaced by two factors,  $p_{25}$  and  $p_{28}$ , defined as the probability of escaping  $U^{235}$  and  $U^{238}$  resonance absorption, respectively. For one virgin  $U^{235}$  fission neutron,  $\epsilon \ell_f$  neutrons slow down into the resonance region. The number captured in  $U^{235}$  resonances is  $\frac{\epsilon \ell_f (1-p_{25})}{2}$ , while  $\epsilon \ell_f \ell_r \ell_s f \left( \frac{p_{25}+p_{28}}{2} \right)$  slow down to thermal energies

and are absorbed in the fuel. Let  $\eta_r/v_{25}$  be the number of resonance fissions per resonance absorption in  $U^{235}$ , and  $\eta/v_{25}$  the corresponding quantity for thermal fission. Then the finite medium value of  $\delta_{25}$  is:

$$\delta_{25}(\text{finite}) = \frac{\eta_r}{\eta} \frac{1 - p_{25}}{p_{25} + p_{28}} \frac{1}{f} \frac{1}{\ell_r \ell_s} . \quad (2.25)$$

The infinite medium value of  $\delta_{25}$  is given by the same expression with the nonleakage probabilities set equal to unity; accordingly, it may be derived from the measured value as

$$\delta_{25} = \ell_r \ell_s \delta_{25}(\text{finite}) . \quad (2.26)$$

#### 2.4 EXPERIMENTAL DETERMINATION OF $k_\infty$ : ONE-REGION ASSEMBLY

The broad outline of the method devised for the measurement of  $k_\infty$  has been given in Secs. 1.2 and 1.3, under a set of restrictive assumptions. These restrictions will now be removed, and the corresponding expression for  $k_\infty$  will be derived for cases of practical interest.

Consider a subcritical, heterogeneous assembly of fuel and moderator, of sufficient size that an equilibrium spectrum exists everywhere except in regions near sources and boundaries, and let  $k_\infty$  be greater than unity. Consider also the introduction into the moderator of a uniformly distributed neutron absorber. Such an absorber will absorb thermal and epithermal neutrons. If the assembly is heterogeneous and the absorber is solid, some of the moderator will be expelled from the assembly. The neutron-multiplying characteristics of the medium, as summarized by Eq. (2.7), will be altered, to an extent depending on the amount and type of absorber added. If the absorber is selected properly, the value of  $k_\infty$  may be reduced to unity. As noted previously, this implies a null material buckling. For an assembly with null material buckling, Eq. (2.7) may be replaced by the equation,

$$1 = \epsilon^0 p^0 \eta^0 f^0 (1 + \delta_{25}^0) . \quad (2.27)$$

Superscript zeroes ( $^0$ ) refer to parameters characterizing such an



assembly. Division of Eq. (2.7) by Eq. (2.27) and use of Eq. (2.18) gives the result:

$$k_{\infty} = \left(\frac{\epsilon}{\epsilon^0}\right) \left(\frac{p}{p^0}\right) \left(\frac{\eta}{\eta^0}\right) \left(\frac{1 + \delta_{25}}{1 + \delta_{25}^0}\right) \left[1 + fA_3^0 + f \sum_{i=1}^2 (A_i^0 - A_i)\right]. \quad (2.28)$$

This equation is analogous to Eq. (1.5) but contains the necessary correction factors.

If the added absorber displaces little or no moderator, if it is predominantly a thermal neutron absorber, and if it is carefully placed within the assembly, the first four factors in parentheses on the right-hand side of Eq. (2.28) will all be near unity. Furthermore, the difference between  $A_i^0$  and  $A_i$  for the cladding and moderator can be made small. In the approximation that the former correction terms are indeed equal to unity, and the latter may be neglected, the similarity to Eq. (1.6) is more apparent:

$$k_{\infty} - 1 = fA_3^0 = \frac{a_3^0}{a_0 + a_1 + a_2}. \quad (2.29)$$

The factors entering the exact formulation of Eq. (2.28) account for spectral perturbations, epithermal absorptions in the added absorber, and effects of the heterogeneity of the lattice. In the present work, the values of the individual correction factors for spectral perturbations and epithermal absorptions differed from unity by no more than 3%; their product deviated from unity by less than 1.5%. The value of the correction factor  $f \sum_{i=1}^2 (A_i^0 - A_i)$  was from 0.15% to 0.4% of the bracketed term in which it appears in Eq. (2.28).

Although the correction factors are small, their nature is such that they are dependent on the moderator-to-fuel ratio of the lattice. To test the efficacy of the method, lattices spanning a wide range of moderator-to-fuel ratios of practical interest have been investigated.

Furthermore, it is to be noted that it is ratios of factors, not the factors themselves, which appear in Eq. (2.28). Thus, any systematic errors will tend to cancel; one obvious example of this is afforded by the factor  $(\eta/\eta^0)$ . The final value of  $k_{\infty}$  is independent of the value used for  $\nu_{25}$ , as well as that used for the macroscopic cross sections of the fuel.



Zero material buckling values are not attained experimentally. Varying amounts of absorber are added to the lattices, resulting in both positive and negative bucklings. In each assembly, the buckling, the fine structure of the thermal neutron distribution,  $R_{28}$ , and  $\delta_{28}$  are measured. The ratio  $\delta_{25}$  is measured in the unmodified lattice, and  $R_3$  in one or more of the assemblies. The correction factors of Eq. (2.28) and the ratio  $A_3$  are derived from these measurements, in a manner to be described in Sec. 4.3 and 4.4. These correction factors are plotted individually, with the measured material buckling as abscissa, and least squares fits employing low-order polynomials are made. (See Sec. 4.5.) The best estimate of the value of each parameter for an assembly with null material buckling is taken to be the y-intercept of the least squares line at zero buckling. These values are used in Eq. (2.28) to obtain an experimental value of  $k_\infty$ . The results are given in Sec. 5.4.

The values of  $k_\infty$  for each assembly may be derived from a formula analogous to Eq. (2.28). Quantities with superscript (') relate to an assembly containing added absorbers; those with superscript (°) relate to an assembly with null material buckling. The equation for  $k_\infty$  is:

$$k'_\infty = \left( \frac{\epsilon'}{\epsilon^\circ} \right) \left( \frac{p'}{p^\circ} \right) \left( \frac{\eta'}{\eta^\circ} \right) \left( \frac{1+\delta'_{25}}{1+\delta^\circ_{25}} \right) \left[ 1 + f' (A_3^\circ - A'_3) + f' \sum_1^2 (A_i^\circ - A'_i) \right]. \quad (2.30)$$

## 2.5 POSSIBLE APPLICATION OF THE METHOD TO A TWO-REGION ASSEMBLY

Many reactor physics parameters, including the material buckling, can be measured under appropriate experimental conditions in two-region subcritical assemblies (PE 2, RO 2, GO 1). Such assemblies consist of a central (or test) region, containing the mixture of fuel and moderator to be investigated, and an outer (or reference) region, containing a mixture of fuel and moderator whose properties are known. The measurements have the greatest chance of success when the differences between the test and reference regions are small.

It is of interest to consider the possibility of determining  $k_\infty$  in a two-region experiment. Combination of the high precision inherent in the Hanford technique (and attributed to the one-region subcritical



experiment described in the preceding section) with the minimal fuel requirements characterizing subcritical substitution measurements would be useful in experimental reactor physics.

The present study is aimed primarily at establishing the validity of the one-region subcritical technique for the measurement of  $k_{\infty}$ ; a simultaneous effort is under way to explore the limitations of subcritical substitution measurements of the buckling and other parameters in  $D_2O$  lattices (GO 1). The test of the possibility of combining the two methods must await completion of both projects, but one two-region assembly has been investigated as part of the present work. No attempt is made to determine a value of  $k_{\infty}$  on the basis of the measurements on this assembly, but exploratory measurements have been undertaken, in an attempt to investigate the feasibility of combining the two methods.

As indicated above, the two-region measurements are best-suited to situations where test and reference regions are not markedly different. Although other configurations are possible in two-region measurements of  $k_{\infty}$  (see Chap. VI), imbedding a test lattice modified by the addition of absorbers in a non-modified reference lattice presents the maximum possible economy in test fuel and absorber material. But the differences between the test and reference regions (in terms of material buckling, diffusion length, etc.) would, in this case, be very large, since the success of the determination of  $k_{\infty}$  depends on obtaining at least one modified lattice with a value of the material buckling at or near zero.

It was therefore deemed of interest to investigate a two-region assembly with a large difference between the test and reference regions. The flux distribution in the radial direction, and in the axial direction at three different radii, were investigated with bare and cadmium-covered foils. These measurements yield information about the regions of the assembly where an equilibrium spectrum may be expected and allow a comparison with the cadmium ratio values determined in the single-region measurements on the test and reference lattices. The assumption that the axial buckling  $\gamma^2$  is independent of radial position in a two-region assembly is important in most two-region determinations of test lattice bucklings. The above-mentioned measurements allow a test of the validity of this assumption in an



assembly where test and reference regions differ widely. The results of the measurements are discussed in Sec. 5.7.

## 2.6 DETERMINATION OF LATTICE PARAMETERS OTHER THAN $k_\infty$

### 2.6.1 Parameters Appearing in the Four-Factor Formula

While the method to be developed has been presented as a measurement of  $k_\infty$ , it may, with equal validity, be treated as a measurement of  $\eta$ ,  $p$ ,  $f$ , or  $(1+\delta_{25})$ . Since these parameters appear in Eq. (2.28) in ratios, the experimental value of  $k_\infty$  derived is independent of their absolute value, as discussed in Sec. 2.4. By solving Eq. (2.7) for the desired factor in terms of  $k_\infty$  and the other factors, and using the experimental values for them, an experimental value of the desired factor may be obtained. Such a procedure will be useful in cases where the percentage uncertainty in one of the factors is markedly greater than that in any of the others. The matter is further discussed in Sec. 5.5.

### 2.6.2 Parameters Relating to Neutron Leakage ( $L^2$ , $\tau$ )

The discussion to this point has centered on the neutron economy in an assembly so large that neutron leakage may be ignored. The parameter characterizing such an assembly is, of course, the neutron multiplication factor for an infinite medium,  $k_\infty$ . As indicated in Sec. 2.1.2, it may be related in a variety of ways to the material buckling. The equation stating this relationship is the so-called "criticality equation," the complexity of which is governed by the nature of the assumptions made concerning the slowing-down process. Detailed models have been evolved, but comparatively simple criticality equations, derived from elementary reactor theory, have been found adequate for correlating the available experimental data. References CR 3 and HE 7, which are critical evaluations of investigations of the physics of  $D_2O$ -moderated assemblies, have demonstrated the efficacy of such equations for parametric studies and correlation and intercomparison of data. Thus, the following equations have been used widely:

$$k_\infty = \left(1 + L^2 B_m^2\right) \left(1 + \tau B_m^2\right), \quad (2.30)$$

$$k_\infty = \left(1 + L^2 B_m^2\right) \left(e^{\tau B_m^2}\right). \quad (2.31)$$



In these equations,  $L^2$  is the thermal neutron diffusion area, and  $\tau$  is the Fermi age of neutrons. Equation (2.30) is derived from two-group theory; Eq. (2.31) is derived from age-diffusion theory.

The expression for the fast nonleakage probability derived from age theory,  $e^{-\tau B^2}$ , has been compared with a more precise expression calculated with the Greuling-Goertzel approximation, which does not involve the assumption of continuous slowing down basic to age theory (LE 1). The comparison was made for reactors moderated with deuterium. Although no single value of  $\tau$  was found for which the age theory expression gave results in agreement with those of the Greuling-Goertzel treatment for all values of  $B^2$ , for practical reactors ( $B^2 \leq 0.01 \text{ cm}^{-2}$ ) the range of values was found to be small (101.6  $\text{cm}^2$  to 107.2  $\text{cm}^2$  for the age from 2 Mev to 1.4 ev). The largest buckling encountered in this work is 0.0014  $\text{cm}^{-2}$ ; for bucklings of this magnitude or less, the age theory value of the nonleakage probability should not differ greatly from the value derived under the Greuling-Goertzel approximation.

Other workers have made experimental measurements of  $L^2$  and  $\tau$  by adding neutron absorbers to lattices, observing the change in the buckling and relating this to changes in  $k_\infty$  (see Appendix A). Under certain conditions, it is possible that both  $L^2$  and  $\tau$  can be simultaneously measured in experiments similar to those done here. The method proposed involves calculating the change in both  $L^2$  and  $\tau$  caused by the addition of the absorber, and leaving as unknowns the values of these two parameters for the unmodified lattice. The method is discussed in Appendix G. It is pointed out there that an assembly with zero material buckling contributes no information about  $L^2$  and  $\tau$ ; assemblies with low material buckling contribute very little information.

The main purpose of this study is the determination of  $k_\infty$ , in the manner described in Secs. 2.1 to 2.4. For this work, assemblies with zero material buckling are ideal; an effort was made to obtain buckling values near zero wherever possible. Thus, the available experimental data is not well-suited for the determination of  $L^2$  and  $\tau$ .

"Experimental" values of  $L^2$  may, however, be obtained from Eqs. (2.30) or (2.31), if calculated values of the Fermi age are used in conjunction with the measured values of  $k_\infty$  and the material buckling.

H. E. Bliss has calculated values of the age for the lattices studied (BL 2), using formulas given by A. D. Galanin (GA 1). Values of  $L^2$  calculated for the unmodified lattices in this way are given in Sec. 5.6.



## CHAPTER III

### EXPERIMENTAL APPARATUS

In this chapter, the apparatus used in these experiments is described. Where detailed descriptions of equipment used are readily available (e. g., the lattice facility), only a brief description will be given, together with the pertinent references. In addition, some details have been relegated to the appendices. The chapter closes with a listing of the experiments.

#### 3.1 SUBCRITICAL FACILITY AND M. I. T. REACTOR

The experiments took the form of foil irradiations in the M. I. T. Heavy Water Lattice Facility (HE 1). Its neutron source is the M. I. T. Research Reactor, a heavy water cooled and moderated, enriched uranium fueled, tank-type reactor, which was operated at a power level of 2 MW throughout the course of the experiments. Neutrons passing out of the reactor through the graphite thermal column enter the lattice tank from the bottom after making a 90° turn in the cavity which is situated as shown in Figs. 3.1 and 3.2. The neutron source is highly thermalized, having a gold-cadmium ratio of 3000-4000; the source strength is approximately  $10^{10}$  n/cm<sup>2</sup> sec at the bottom of the tank, when the reactor is operating at 2 MW. Because the subcritical facility is not on a direct "line-of-sight" with the reactor core, gamma rays from the core do not produce sufficient numbers of photoneutrons in the heavy water in the lattice to affect the measurements appreciably (PA 1).

The lattice facility consists of a cylindrical aluminum tank, three feet in diameter, covered on its sides with cadmium 0.020 inch thick. The subcritical lattices are made up by hanging the fuel rods on sets of parallel girders, which are notched to accept the rod top adapters. The rod bottom adapters notch into a grid plate, thus insuring accurate rod spacing. Lattices are assembled on the floor of the reactor building, then lifted into place with the overhead crane. The system is sealed and dried before heavy water is admitted. A cover gas of dry

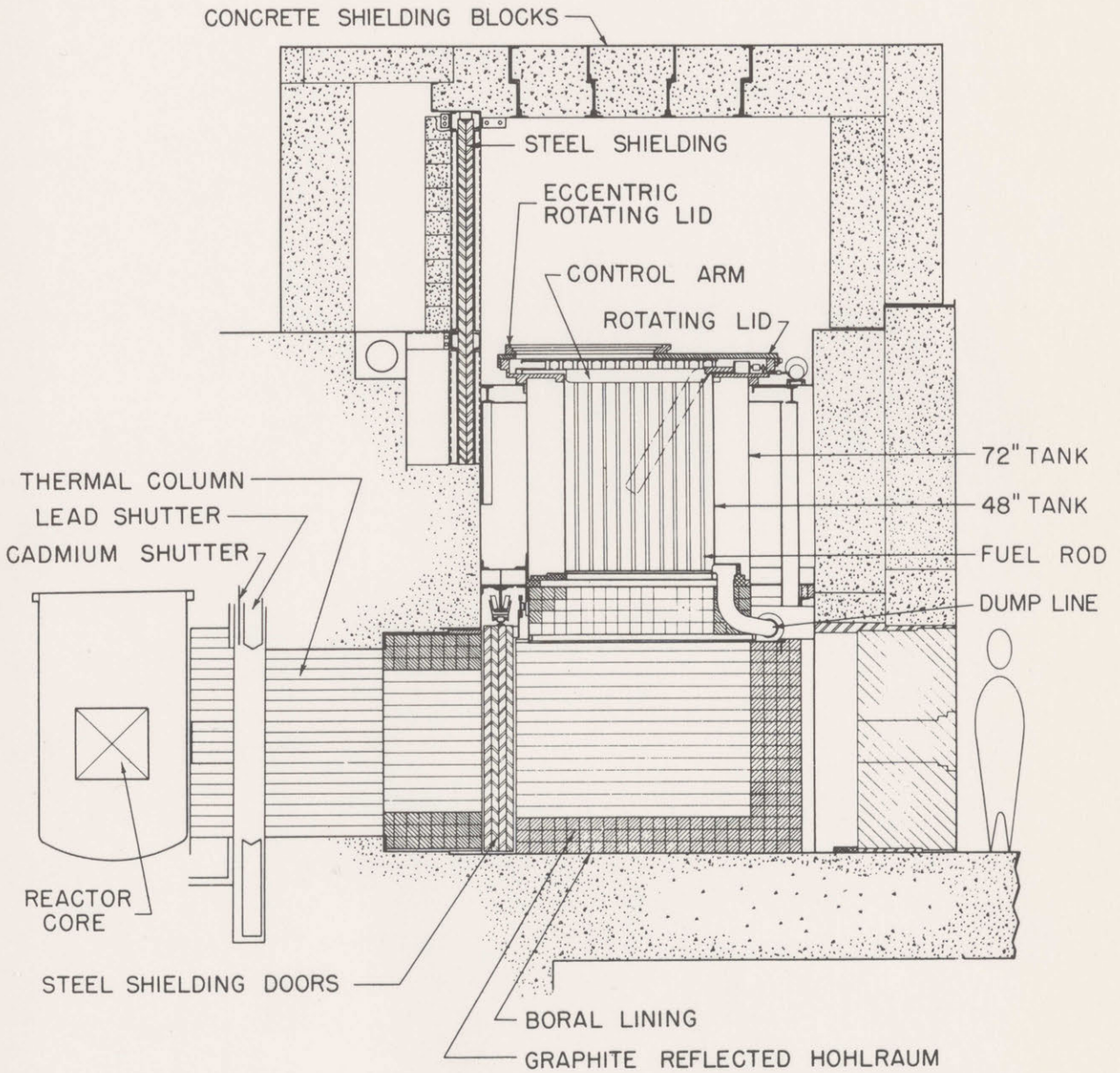


FIG. 3.1. VERTICAL SECTION OF THE SUBCRITICAL ASSEMBLY



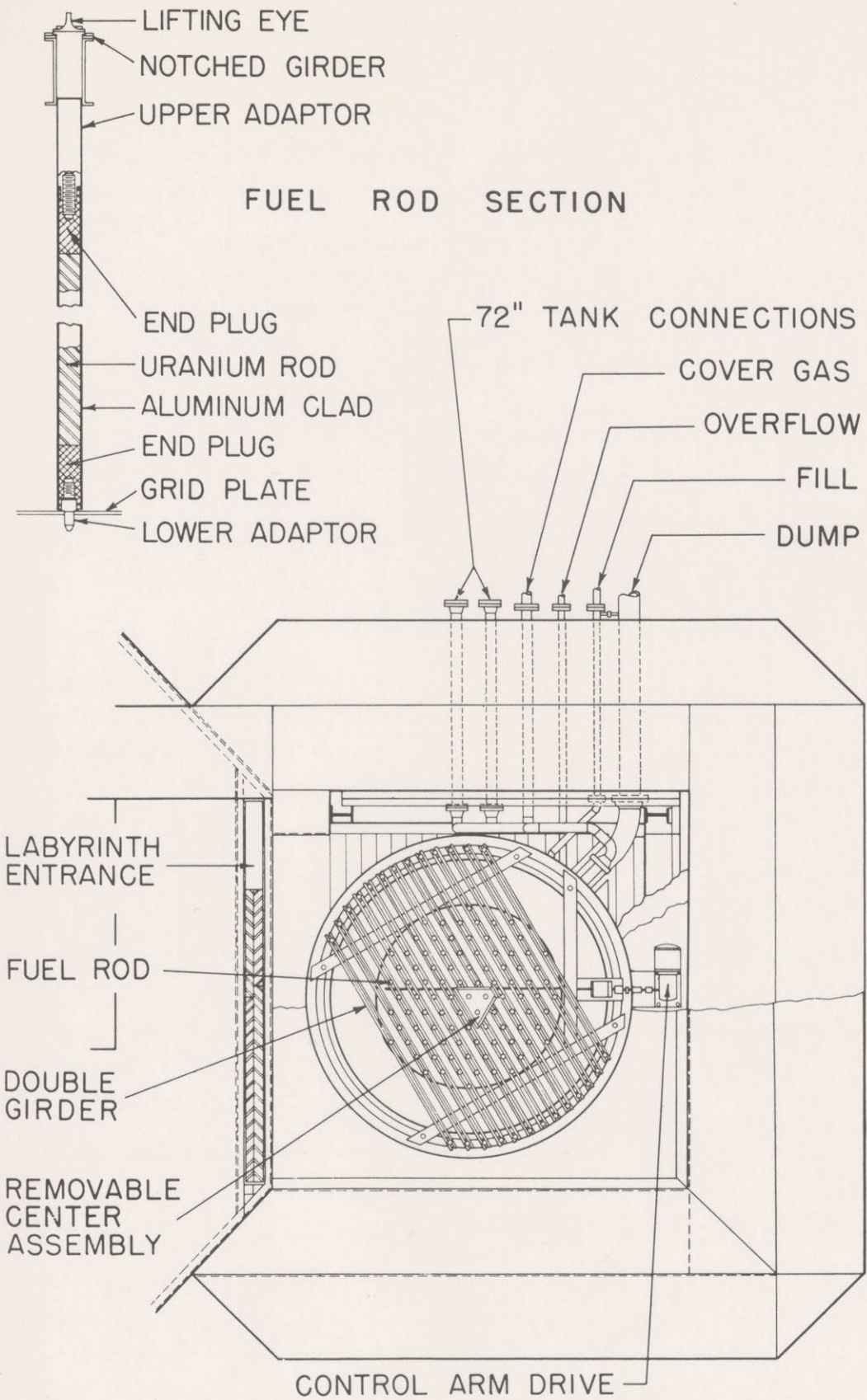


FIG. 3.2. PLAN VIEW OF THE SUBCRITICAL ASSEMBLY

nitrogen blankets all exposed  $D_2O$  surfaces, to prevent contamination from atmospheric moisture. The lattice can be reached, after sealing, only through the glove box mounted on the upper lid of the tank. By means of a set of eccentrically-mounted circular lids, this glove box may (with some effort) be positioned over any point in the lattice.

### 3.2 LATTICES STUDIED

All the lattices studied were made up of slightly enriched uranium metal rods, clad in aluminum, and arranged on a triangular spacing in heavy water moderator. The lattices were approximately 35 inches in diameter; the active fuel zone was 48 inches high. An arbitrary designator (based on the spacing) has been assigned to each lattice, for convenience of reference. The designators, and pertinent details, are listed in Table 3.1.

The lattices studied are the 250, 175, and 253 lattices. The 125 lattice is included in Table 3.1, even though it was not investigated by means of added absorbers. The results of independent investigations (HE 4, HE 5) on this lattice will be presented in Chap. V, for comparison with the results from the 250 and 175 lattices.

### 3.3 THERMAL NEUTRON ABSORBERS

Varying amounts of thermal neutron absorber had to be added to each of the lattices studied. The neutron absorber could have taken a number of different forms. The reasons for choosing the absorber used are given here.

The basic choice is between a homogeneous absorber dispersed uniformly in the moderator, and lumped absorbers placed at regular intervals through the assembly. The advantages and disadvantages of each are considered at greater length in Appendix B. The decision was in favor of lumped absorbers, for the reasons discussed there.

It was clear from the outset that the absorbers placed in the lattices ought to be continuous axially, to simplify interpretation of the results of the axial buckling measurements. Consideration was given to sheets, strips, rods, tubes, and bundles of rods or tubes. The following conclusions were reached: sheets would be very difficult to insert and remove from the lattices; they might buckle or ripple, and thus introduce positioning uncertainties; and they would severely limit



TABLE 3.1  
Description of Lattices Studied

Lattice Designator	Lattice Spacing (inches)	Fuel Slug Diameter (inches)	Air Gap (inches)	Clad Thickness (inches)	Fuel Rod Outer Diameter (inches)	Uranium Enrichment (weight %)	D <sub>2</sub> O Purity (mole %)	Moderator to Fuel Volume Ratio	Number of Rods
250	2.50	0.250	0.006	0.028	0.318	1.143	99.56	108.60	169
175	1.75	0.250	0.006	0.028	0.318	1.143	99.53	52.40	361
125	1.25	0.250	0.006	0.028	0.318	1.143	99.60	25.93	691
253	2.50	0.750	0.004	0.028	0.814	0.947	99.51	11.07	169

the already poor visibility in the lattice assembly. Strips would be easier to insert and remove, but retain the other disadvantages of sheets. Tubes offer considerably more rigidity than rods of the same cross-sectional area, but would be larger and more difficult to remove and insert. Bundles of rods or tubes had the disadvantage that the calculation of the disadvantage factors becomes unduly complicated. Finally, solid cylindrical rods were chosen for the lumped absorbers because of their simple shape, satisfactory rigidity, and because they do not substantially interfere with visibility in the assembly.

Desirable attributes for the absorber material include:

a well-known thermal neutron cross section, of such a magnitude that the lumped absorbers used have convenient sizes;

a thermal neutron cross section which varies with incident neutron velocity ( $v$ ) as  $1/v$ ;

availability at moderate or low cost in the form and purity desired;

moderate or low specific activation in neutron fluxes; short half life if possible;

small resonance neutron absorption integral; and

inertness to corrosion in the moderator.

Aluminum would be ideal except for its thermal neutron cross section, which is too small. Stainless steel and copper would both be acceptable. Copper was chosen because its macroscopic thermal neutron cross section is 50% larger than that of steel.

Copper, as it occurs naturally, has a thermal neutron cross section which varies as  $1/v$ ; its value for 2200 m/sec neutrons is  $3.79 \pm 0.04$  barns (DO 1); this cross section permits convenient rod sizes in the lattices studied. The rods used were thick enough to be readily manipulable, but, as will be seen, did not expel more than 1.71% of the moderator from any of the lattices studied.

The longest half life involved, when copper undergoes neutron irradiation, is 12.5 hours; the radioactive decay is mostly by electron or positron emission, with relatively little (3.5%) accompanying gamma emission, except for the annihilation gammas produced as a consequence



of the positron decay. An indication of the modest radiation levels involved is obtained from Table 3.2. The radiation level above background was measured with a portable radiation survey meter (Geiger tube) as a function of the distance of the tube face from the center of

TABLE 3.2

Radiation Level as a Function of Distance from Irradiated Rod

Distance (inches)	Radiation Level (mr/hr)
18.0	1.0
9.0	3.0
4.5	9.0
2.5	16.5

a single, 0.188-inch-diameter, copper rod, 1.3 hours after the shut-down of the last run of a three-week series of experiments. Three irradiations totaling 31.5 hours were made in the 44 hours prior to the radiation level measurement; the last run lasted 5.7 hours. The rod came from the center of the assembly.

The resonance absorption integral at infinite dilution, defined as,

$$\int_{0.415 \text{ eV}}^{\infty} \sigma_a(E) \frac{dE}{E}, \quad (3.1)$$

is 3.12 barns for copper (BE 1); over half of this may be assigned to the  $1/v$  component of the cross section.

#### 3.4 ABSORBER RODS USED

Two sets of rods were purchased, with nominal diameters of 0.188 inch and 0.144 inch, at a price of \$1.50 to \$2.00 per pound. These two types of rods are here designated "A" and "B," respectively. While cladding is apparently not strictly necessary when dealing with copper and  $D_2O$  of the purities involved (CR 2), all exposed surfaces were coated with 0.0005 inch of KANIGEN to remove any slight possibility of the copper causing corrosion of the aluminum tank and fuel cladding. KANIGEN, or "electroless nickel," consists of

nickel containing 1% to 15% phosphorus and is deposited chemically, without the use of externally applied voltages. The resulting coating is more nearly uniform in thickness than, for example, electroplated nickel or chromium. It is non-crystalline, non-porous, hard, and has corrosion properties equal or superior to those of pure electroplated nickel, as shown in a variety of cases tested by the Armour Research Foundation of the Illinois Institute of Technology (AR 1). The cost is comparable to that of equivalent thicknesses of less satisfactory electroplated coatings.

The 0.0005-inch cladding thickness of the KANIGEN was chosen with reference to experience with the control rod magnets in the MITR. The cladding, while it discolored during the course of the experiments, appeared to function satisfactorily, in that the conductivity of the lattice  $D_2O$  did not deviate appreciably from its normal value of 0.4 mhos/cm. Chemical analyses of the coating on the rods placed the weight percentage of phosphorous at 11.5% for the A rods and 9.2% for the B rods.

Qualitative spectrographic analysis of two samples of the copper used indicated that the only impurity present in an amount sufficient to alter the macroscopic thermal neutron absorption cross section by more than 0.002% was silver; the 0.01% (by weight) of this element increases the cross section by only 0.04%. Table 3.3 shows the major impurities present. The resonance absorption integral for the rod material should be very slightly (~0.5%) larger than that for pure copper, owing to the silver impurity. The resonance escape probability would be decreased by 0.2% at most.

### 3.5 POSITIONING AND SUPPORT OF ABSORBER RODS

The pattern in which the absorbing rods were placed in the lattice was chosen for two reasons. First, it was thought that the rods should be placed at regular intervals throughout the lattice, the interval being equal to, or an integral fraction of, the lattice spacing. If this is done, the "unit cell" associated with each fuel rod is identical throughout the lattice (see Sec. 4.3.2). This simplifies the interpretation of the radial buckling measurement; the material buckling of the lattices with added absorbers is then measured in the same way as the buckling of the normal lattices. Second, it was considered desirable to place each



TABLE 3.3

Impurities Present in Copper Used in Experiments<sup>\*</sup>  
 (Based on qualitative spectrographic analysis of two samples)

<u>Impurity</u>	<u>Weight Percentage (Max.)</u>
Pb	0.01
Ag <sup>**</sup>	0.01
Ni	0.01-0.001
Na	0.001
Si	0.001
Mg	0.001-0.0001
Ca	0.0001
Fe	0.0001

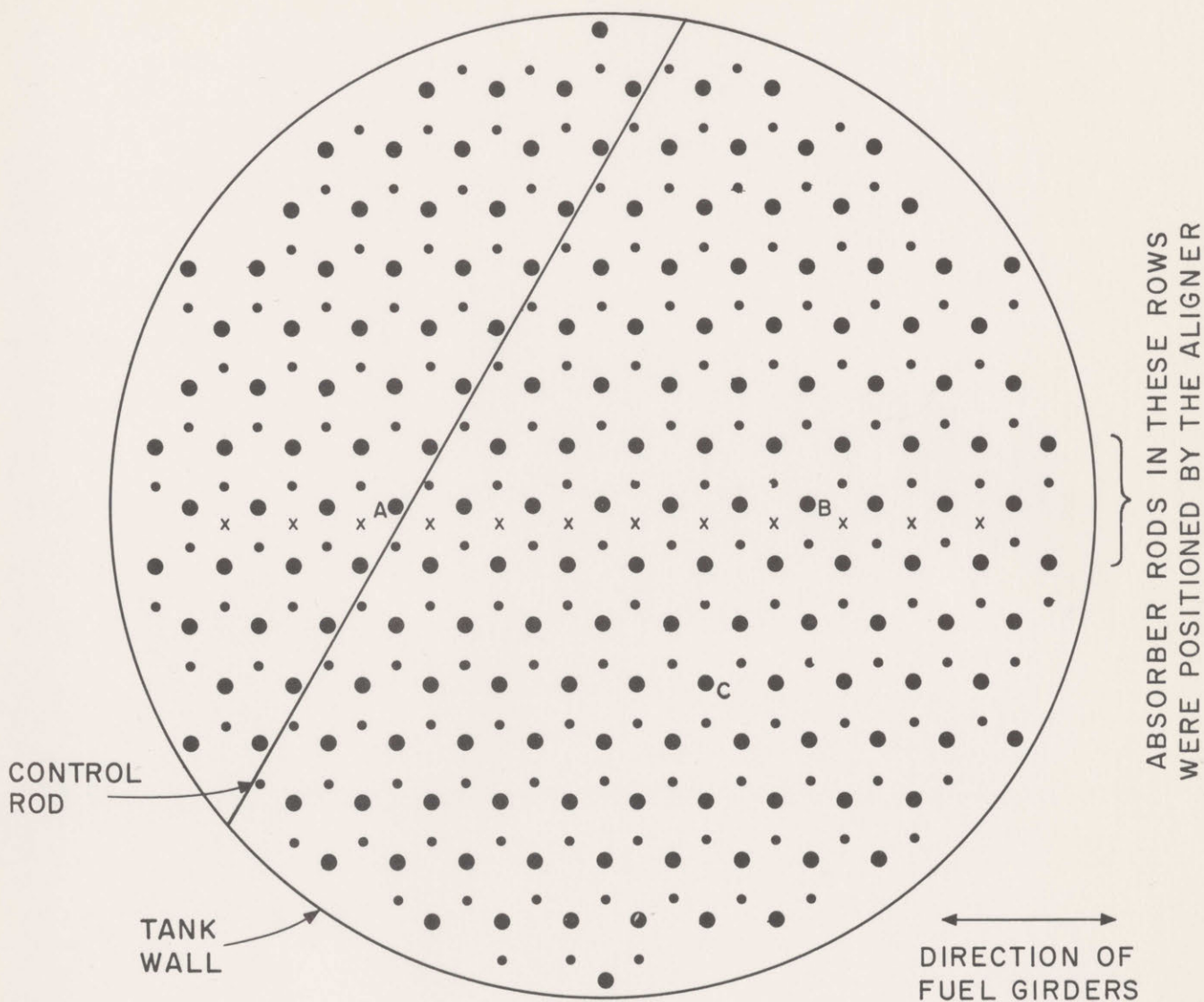
<sup>\*</sup> So-called OFHC (oxygen-free, high conductivity) copper.

<sup>\*\*</sup> Subsequent quantitative analysis placed the actual amount of silver present at  $0.0020\% \pm 0.0003\%$ .

absorber rod in a region of the cell where the neutron flux gradient is small. In this way, slight errors in absorber rod positioning should introduce only small perturbations in the results. The errors introduced in this fashion are thought to be negligible; they will be discussed further below.

These two requirements, together with mechanical limitations, served largely to define the positions of the absorbing rods in the lattices studied. In addition, the measurement of the thermal utilization is somewhat simplified if each absorber rod of a given size is located at the same position in the unit cell; this was found to be possible. The arrangement of the fuel rods and absorbing rods in the lattices studied is shown in Figs. 3.3 to 3.11. (See also Sec. 3.10.)

The leading requirement to be met by the mechanism for the support of the absorber rods was, of course, that of adequate mechanical strength. Furthermore, the supports had to be compatible with the equipment already in use in the subcritical assembly; no modifications were made to accommodate the new lattice elements. Simplicity in design was also held to be desirable. Finally, the mechanism had to



LEGEND

- |                                    |   |
|------------------------------------|---|
| ● FUEL ROD                         | A AXIAL TRAVERSE POSITION (CADMIUM COVERED FOILS)                               |
| • "B" COPPER ROD                   | B AXIAL TRAVERSE POSITION (BARE FOILS)  |
| x FOIL POSITION IN RADIAL TRAVERSE | C POSITION OF AXIAL TRAVERSE MADE TO DETERMINE EFFECT OF ALIGNER (SEE SEC. 3.5) |

FIG. 3.3. PLAN VIEW OF 250BI ASSEMBLY



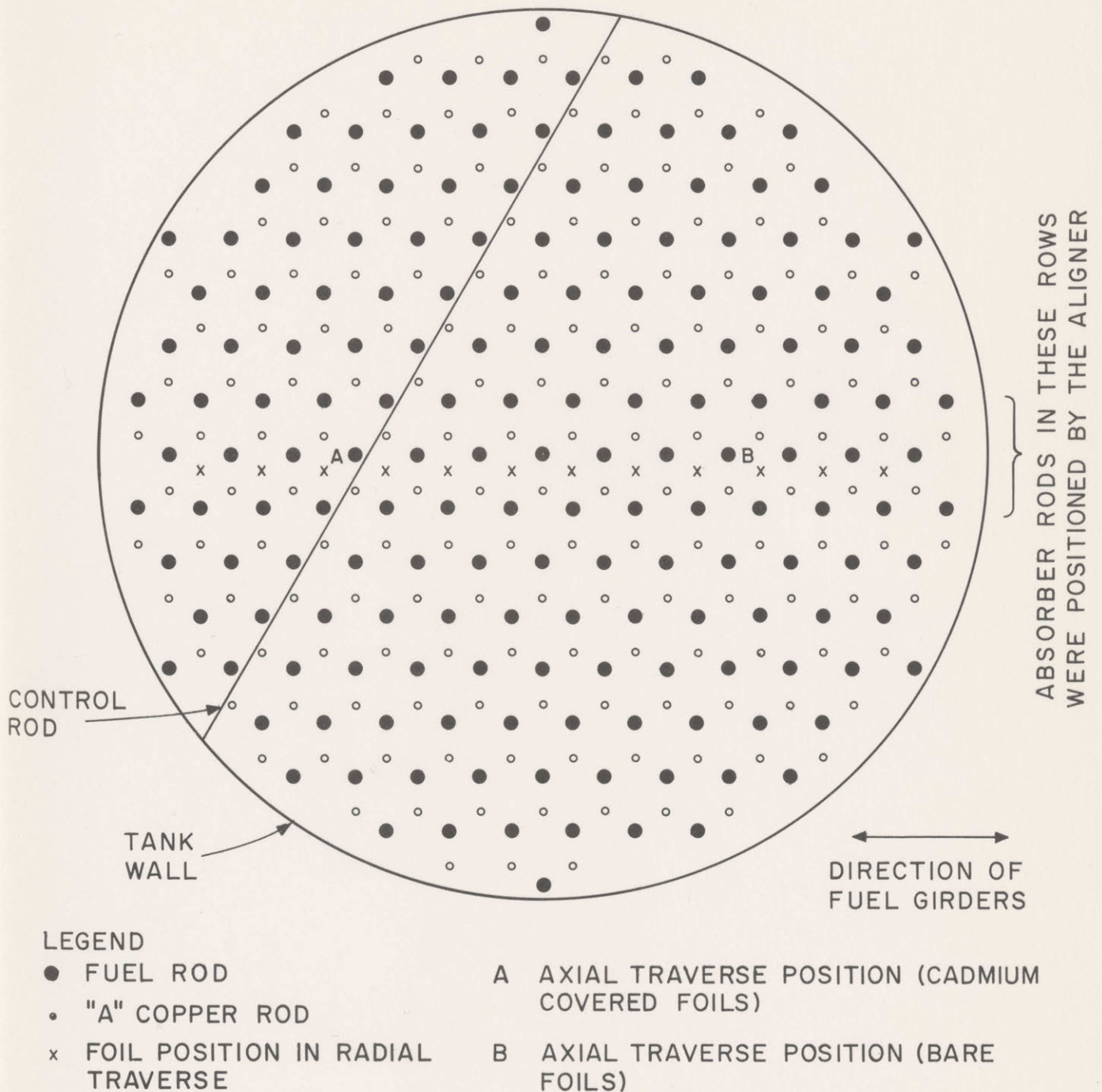


FIG. 3.4. PLAN VIEW OF 250AI ASSEMBLY

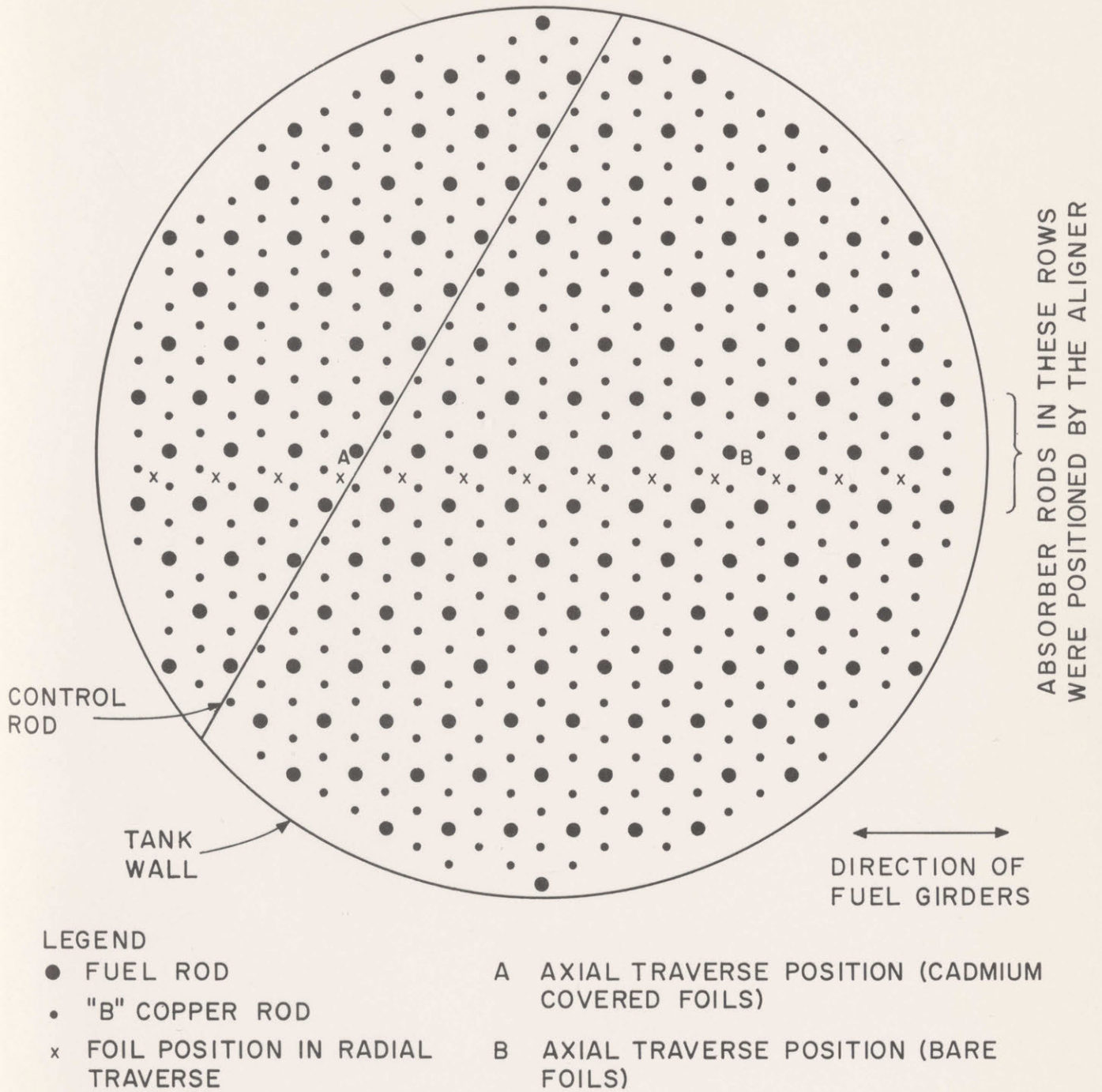


FIG. 3.5. PLAN VIEW OF 250B2 ASSEMBLY



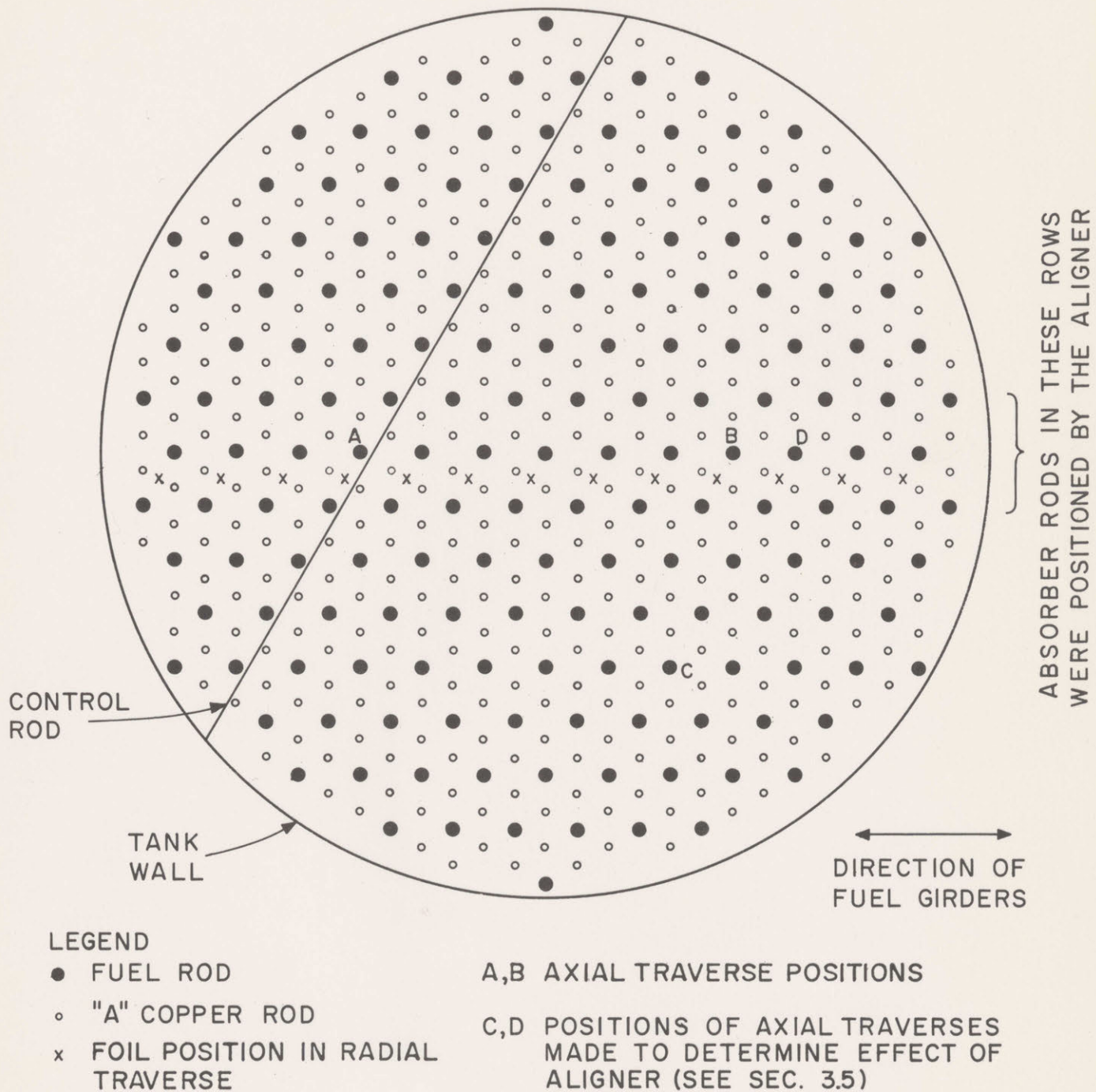


FIG. 3.6. PLAN VIEW OF 250A2 ASSEMBLY

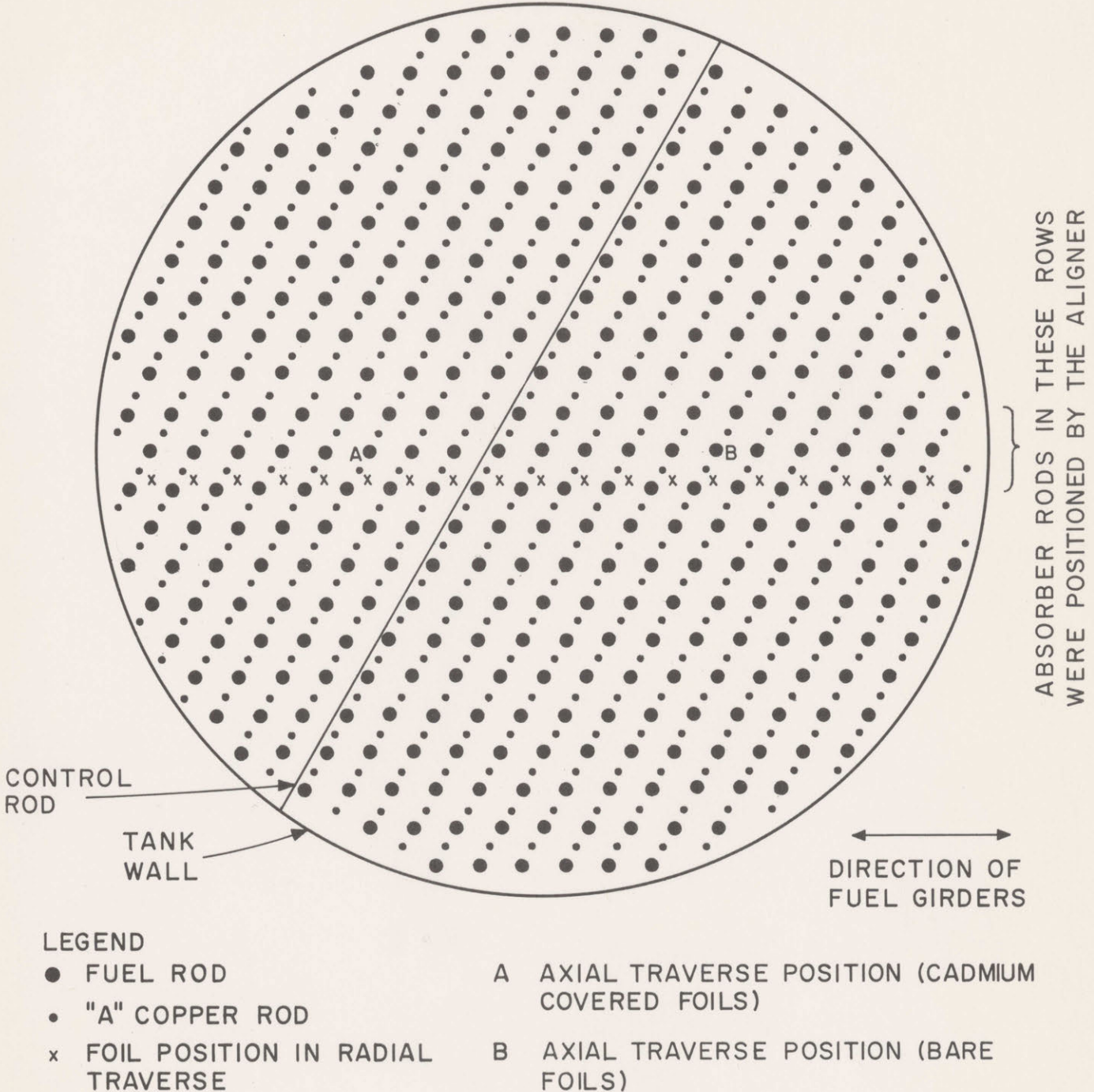


FIG. 3.7. PLAN VIEW OF 175Al ASSEMBLY





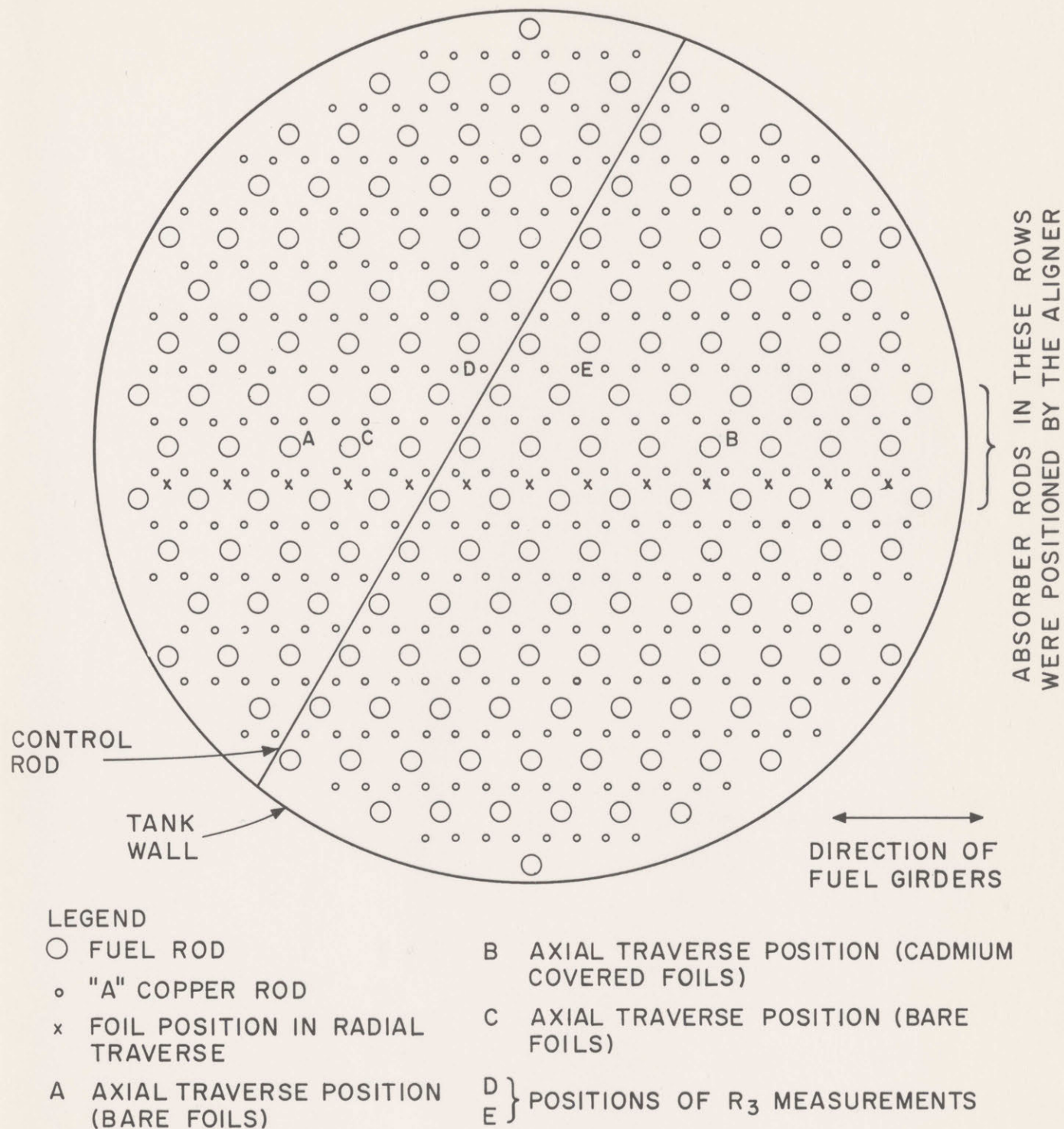


FIG. 3.9. PLAN VIEW OF 253A2 ASSEMBLY



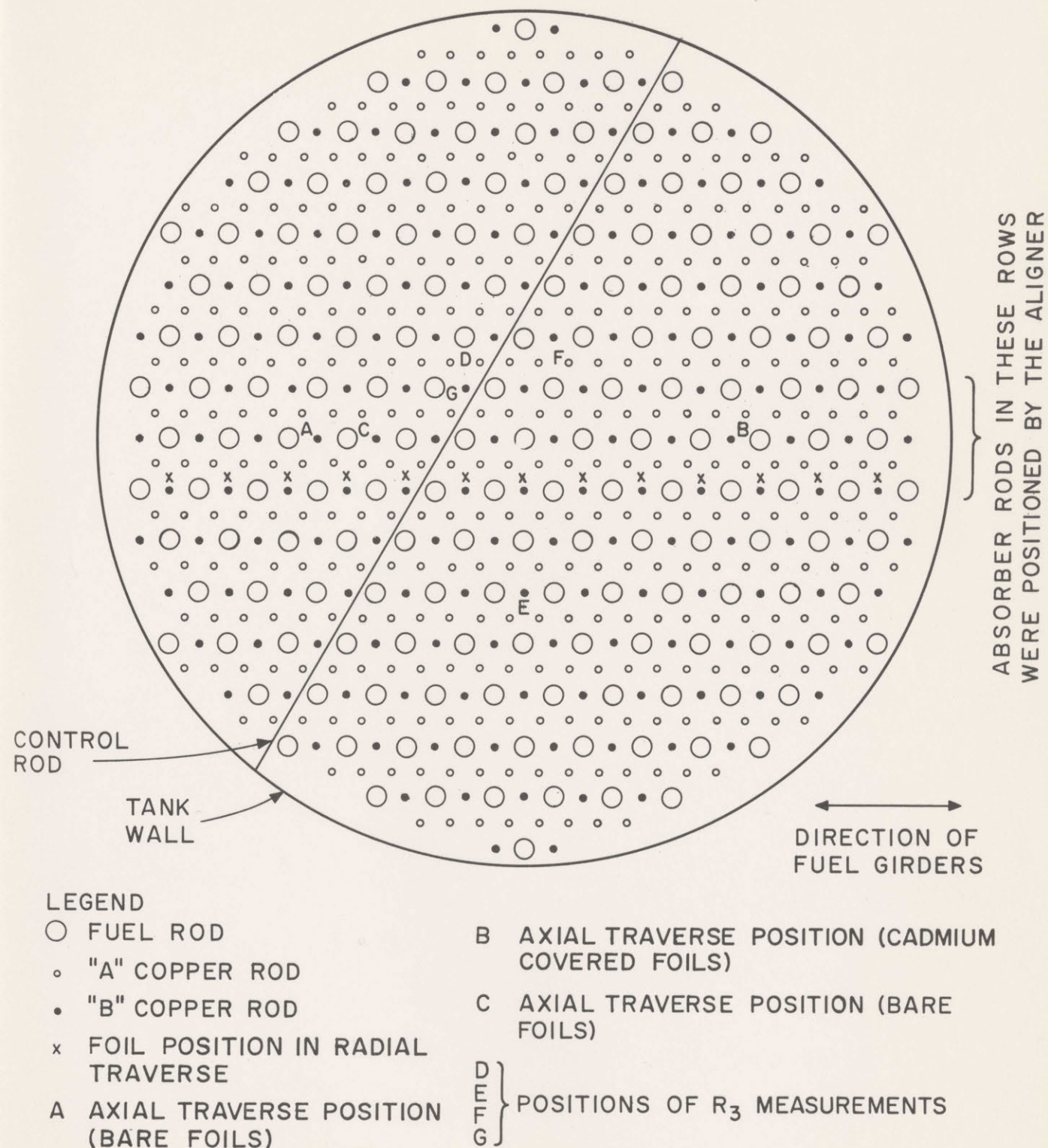


FIG. 3.10. PLAN VIEW OF 253A2BI(1R) ASSEMBLY

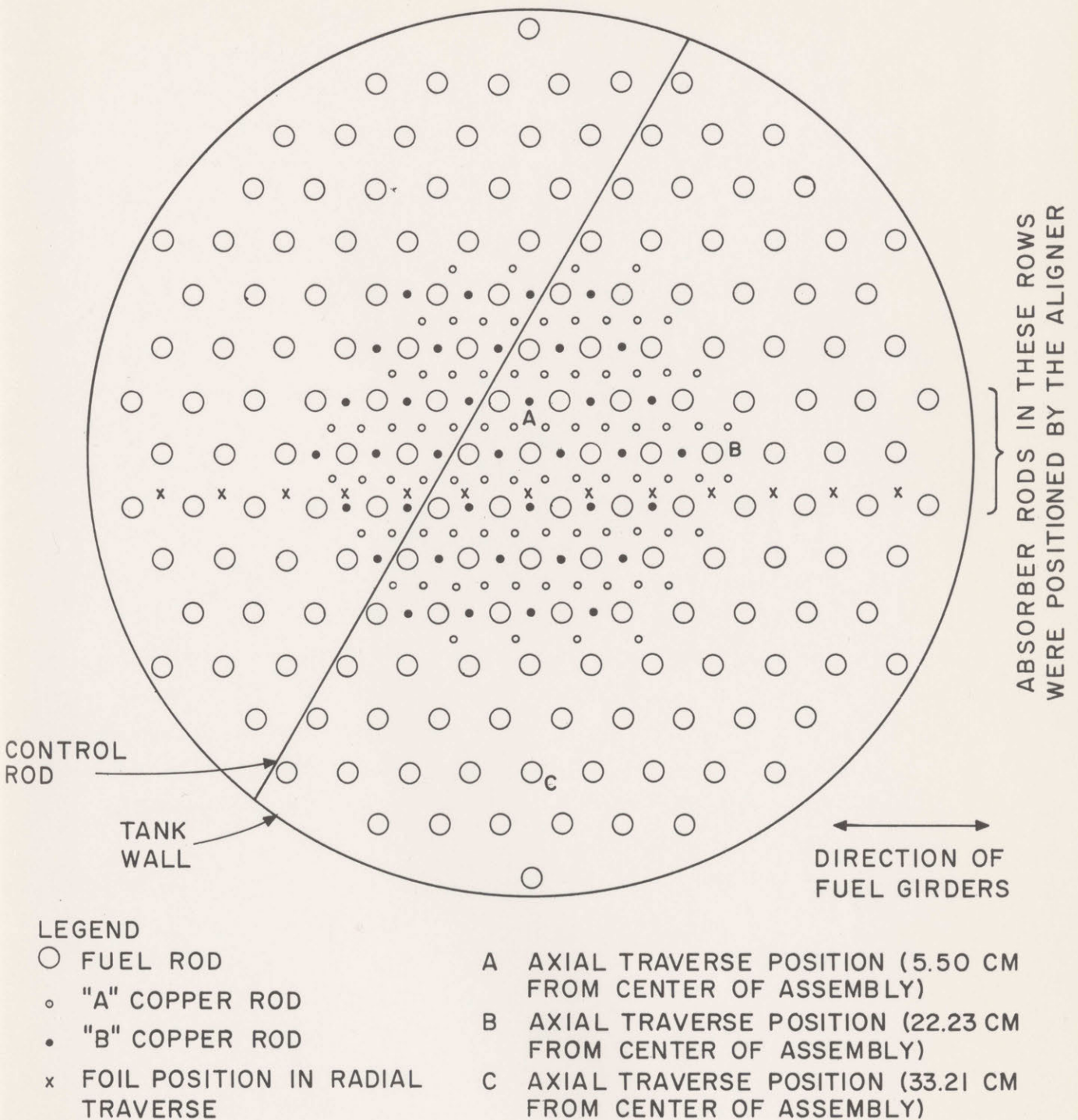


FIG. 3.II. PLAN VIEW OF 253A2BI(2R) ASSEMBLY



guarantee, insofar as possible, that the absorber rods were parallel to the fuel rods in the vertical direction.

In the 250 and 175 assemblies, the fuel support girders were spaced widely enough so that there was room between them for the absorber supports. The latter took the form of 1.25-inch by 1.25-inch aluminum channel with a wall thickness of 0.125 inch in the 250 assemblies, and of 1.25-inch by 0.625-inch aluminum bar stock in the 175 assemblies. The dimensions of the fuel support girders are such that, in each case, the absorber rod support elements described above fit tightly (press fit) between them. The support elements were wedged into place, carefully positioned, and checked at intervals during the work on each lattice, as well as after all work was complete. In no case was any lateral shift in the direction of motion parallel to the fuel girders detected.

In the 253 assemblies, space limitations precluded placing absorber rod supports between the rows of fuel. Instead, strips of 0.75-inch by 0.125-inch aluminum bar stock were laid on the top of the fuel support girders, parallel to the rows of fuel; they were held in place, in the direction transverse to the girders, by the fuel top adapters, against which they fit snugly. Absorber rods were also positioned within the rows of fuel rods in two of the assemblies studied in this lattice. A set of 1.25-inch by 1.375-inch by 0.125-inch rectangular aluminum coupons was fabricated; these fit snugly between the fuel top adapters within the rows. They were fabricated with special tabs, which fit into notches cut in the aluminum strips described above. This arrangement prevented the strips from sliding out of position along the direction of motion parallel to the fuel girders (see Fig. 3.12).

Each copper rod was fitted out with a top adapter (Fig. 3.13). The lower end of the adapter is spherical, as shown. The supports for the copper rods were made by machining 0.125-inch-deep depressions with a 0.5-inch ball end mill at the appropriate points on the channels, bars, strips, or coupons, and then boring through the support member with a 0.25-inch drill. The copper rods, when fitted with the top adapters, hung through the support members and were positioned at the center of the oversize hole by the spherical end of the adapter,



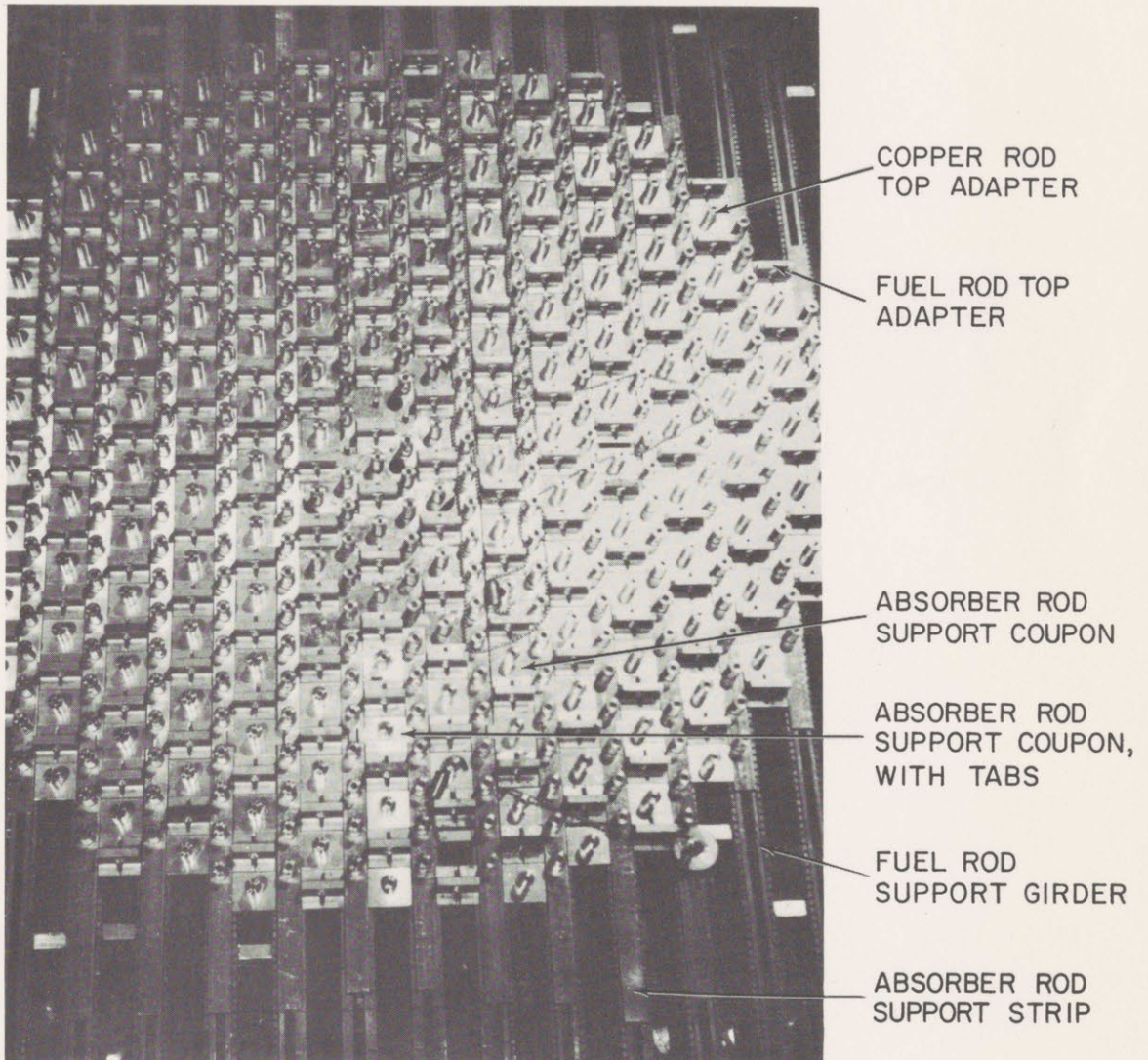


FIG. 3.12. ABSORBER ROD SUPPORTS IN 253 ASSEMBLIES



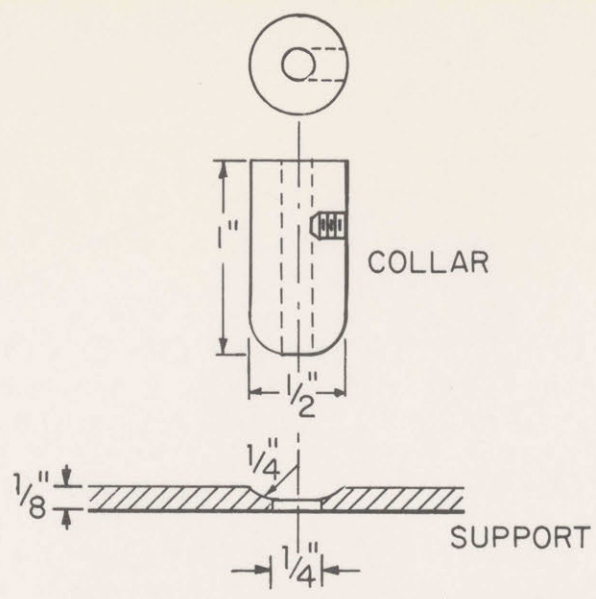


FIG. 3. 13a. COLLAR AND SUPPORT-DIMENSIONS

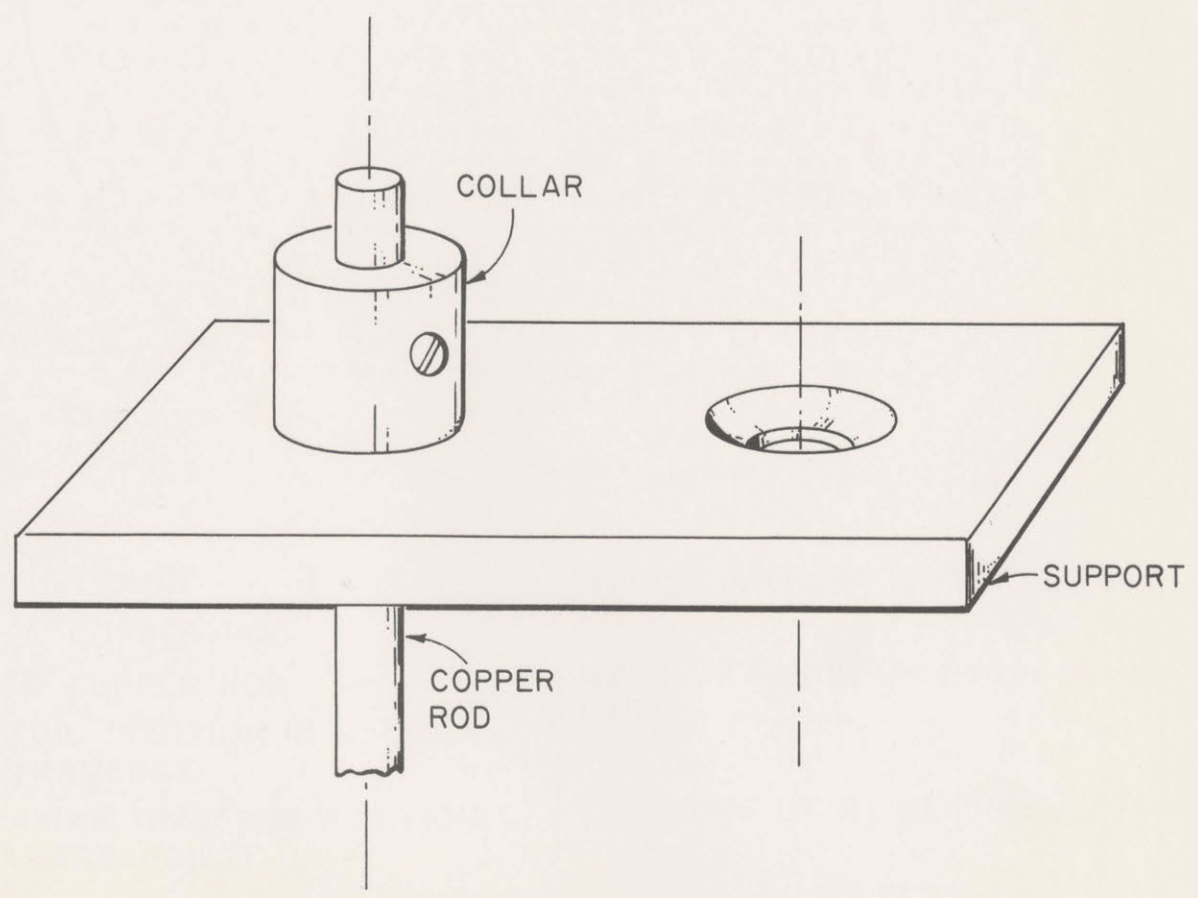


FIG. 3. 13b. PERSPECTIVE VIEW OF COPPER ROD FITTED WITH COLLAR AND IN PLACE, AND AN EMPTY ROD POSITION.

FIG. 3. 13. TOP ADAPTER FOR COPPER RODS

resting in the spherical depression. As described above, this proved to be a satisfactory means of supporting and positioning the absorber rods and guaranteeing their proper alignment. Rods were readily removable from, or replaceable in, the lattice throughout the series of experiments on any given assembly.

It was decided at the outset that a new grid plate would not be fabricated, and that the one normally in use would not be drilled to accept the copper rods. The rods hung free, from the top supports, with only those rods in the area where measurements were made (the central rows) held in place by a bottom aligner affixed to the grid plate. The rods used were carefully inspected for straightness before insertion in the lattice. After all rods had been inserted, and before the lattice was placed in the tank, careful inspections were made from all angles, by sighting down the rows of rods. Bent rods, or those which were out of line for any reason, were readily identifiable; they were replaced with straight rods.

Figure 3.14 shows the device used in the 250 assemblies to align the absorber rods in the central rows; it was constructed of 1.25-inch O.D., square aluminum tubing with a wall thickness of 0.125 inch, and securely affixed to the grid plate as shown. The location of the aligners is shown in Figs. 3.3 to 3.6. Because of the size of the device, experiments were made to determine its effect on the neutron flux distribution in the lattice. In the first and last of the assemblies investigated, axial distribution measurements with bare gold foils were made at points equidistant from the center of the lattice, one far from the aligner and one in the central row of fuel rods, as shown in Figs. 3.3 and 3.6. The results are given in Fig. 3.15. The ratio of foil activities in each of the two traverses does not differ from unity by a statistically significant amount (twice the S.D. of a single observation) for points above 35 cm. The axial buckling determinations are not based on any points below 35 cm (see Sec. 4.2), so the absorber rod aligner should have no effect on these results.

All radial and axial buckling measurements done with gold foils, with the exception of the axial measurements mentioned immediately above, and all microscopic traverses, were made in the region where the rods were positioned at the bottom by the aligners.



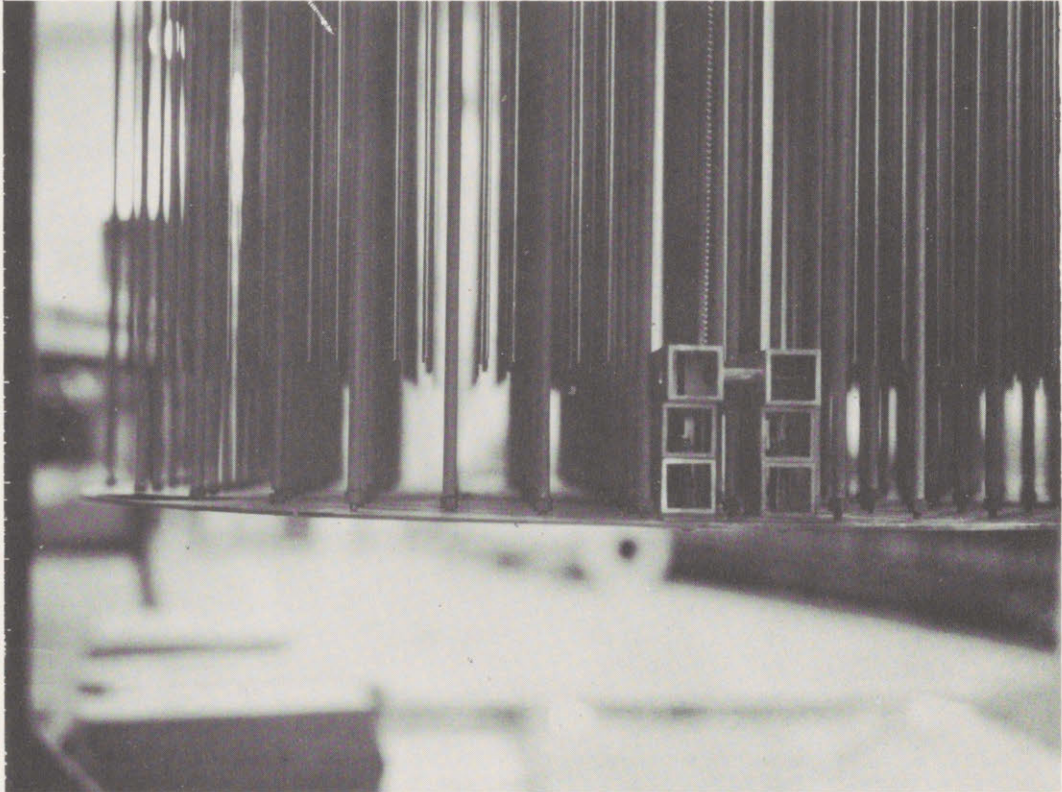


FIG. 3.14 ABSORBER ROD ALIGNER IN 250B2 ASSEMBLY

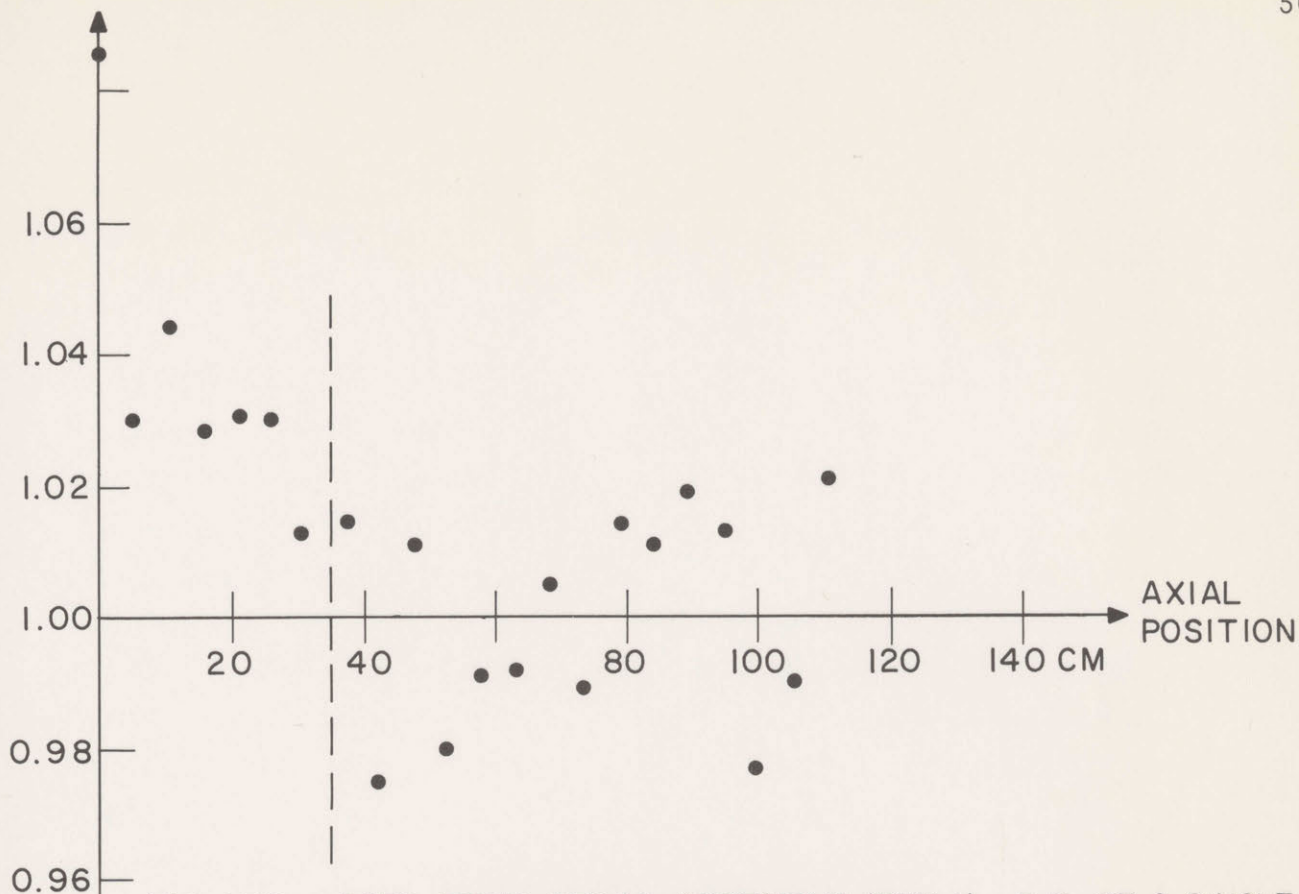


FIG. 3.15 a. DATA FROM 250A2 ASSEMBLY (RUN 1). S. D. OF A SINGLE OBSERVATION 1.6 %, S. D. OF THE MEAN 0.4 %. COUNTING STATISTICS CONTRIBUTE 0.4 % UNCERTAINTY TO EACH POINT.

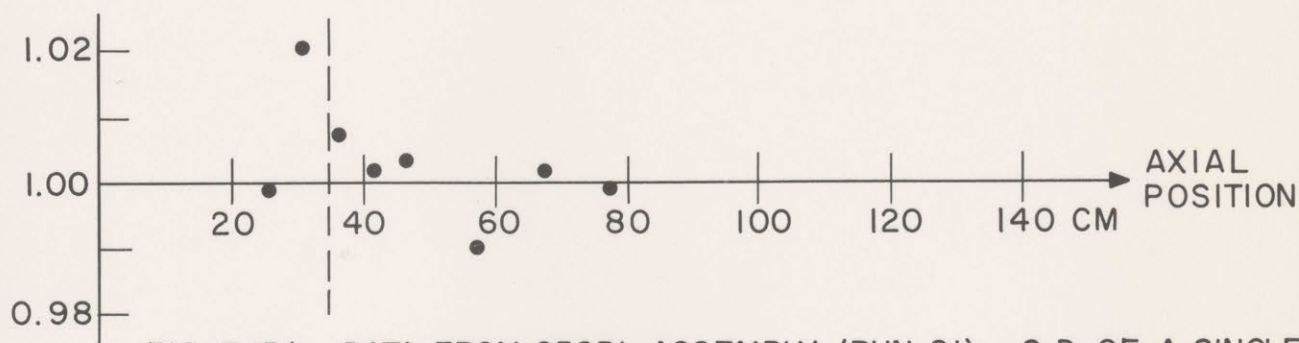


FIG. 3.15 b. DATA FROM 250B1 ASSEMBLY (RUN 21). S. D. OF A SINGLE OBSERVATION 0.7 %, S. D. OF THE MEAN 0.3 %. COUNTING STATISTICS CONTRIBUTE 0.2 % UNCERTAINTY TO EACH POINT.

FIG. 3.15. RATIO OF FOIL ACTIVITY IN OFF-CENTER AXIAL TRAVERSE TO FOIL ACTIVITY IN ON-CENTER TRAVERSE, AS A FUNCTION OF AXIAL POSITION. (BARE GOLD FOILS USED; RATIO OF ACTIVITIES NORMALIZED TO UNITY FOR ALL POINTS ABOVE 35 CM)



Aligners with a similar function were also used in the 175 and 253 assemblies (see Figs. 3.7 to 3.11), but were much smaller, consisting of 0.5-inch by 0.5-inch aluminum channel with a wall thickness of 0.0938 inch. No experiments to check for their effects were considered necessary in view of the foregoing results.

### 3.6 PURPOSE AND METHOD OF THE EXPERIMENTS

As stated at the beginning of this chapter, the experiments under discussion consisted of foil irradiations, chiefly of two kinds, called "macroscopic traverses" and "microscopic traverses," respectively. The purpose of the former is to establish the relative neutron flux distribution throughout the assembly, away from sources and boundaries; in practice, this involved mapping the activation distribution in the direction parallel to the axis of the cylindrical assembly, as well as perpendicular to it, with both bare and cadmium-covered gold foils. From such measurements, the material buckling may be derived, in the manner explained in Secs. 2.1 and 4.2. The second type of foil irradiation, the microscopic traverse, had as its purpose the determination of the relative thermal neutron activation distribution in the fuel, cladding, moderator, and copper absorber rods. Again, bare and cadmium-covered gold foils were irradiated; the way in which the thermal utilization may be derived from such experiments will be discussed in Sec. 4.3. The remainder of this section will be devoted to describing the foils, foil holders, and cadmium covers used in the experiments. Details concerning the irradiation and counting of the foils will be found in Appendix C.

A considerable effort has been in progress at the M. I. T. Heavy Water Lattice Project on the techniques for determining the material buckling and thermal utilization of subcritical lattices of uranium metal rods in heavy water. Reports on the material buckling have been presented by P. F. Palmedo (PA 1) and J. Harrington (HA 1); the thermal utilization experiments have been investigated by P. S. Brown (BR 1) and R. Simms (SI 1). While certain modifications of those techniques were made in the present work, particularly in the microscopic experiments, the experimental work described here is based, to a large extent, on the results of the preceding studies. Thus, the reader



is referred to the above-mentioned reports, or the Annual Reports of the project, for more detailed discussions. The foil irradiation experiments in the lattices with added absorbers were made, insofar as was possible, exactly as in lattices without added absorbers. The results in the two types of lattices should therefore be directly comparable.

### 3.7 NEUTRON-DETECTING FOILS

The foil material used was almost exclusively metallic gold. Gold has a large thermal neutron cross section which has been measured accurately (96 b. activation cross section for 2200 m/sec neutrons), and is very nearly a "1/v absorber" in the thermal neutron energy range (HU 1, WE 3). It is also readily activated by resonance energy neutrons; thus, activation of gold foils with and without cadmium covers makes it possible to determine the subcadmium and epicadmium activation distributions in a clear and relatively simple way. The significance of this is discussed in Sec. 2.1.3. Gold of the requisite purity is readily obtainable in sheets, is comparatively easy to form into satisfactory foils, and does not react to any appreciable extent with the heavy water moderator. Its 2.7-day half life and single isotope make it a convenient detector in practice; in the present work, for instance, many sets of foils could be counted twice because of the long half life.

Another possible foil material, the use of which would have facilitated some aspects of the analysis, is copper. A number of the properties of copper which make it an ideal added absorber turn out, however, to constitute disadvantages for a foil material. Its macroscopic activation cross section for thermal neutrons is only 4% that of gold, so that larger foils and longer irradiations are needed to obtain the statistical accuracy possible with gold foils. Furthermore, the small resonance absorption integral of copper means that it is a less efficient epithermal neutron detector than gold. Finally, the 12-hour half life of copper, while it does not preclude its use as a detector, would certainly reduce greatly the flexibility in the scheduling of experiments possible with gold. (In view of the fact that the addition of absorbers rendered the main exponential facility useless to most of the other members of the Project, the experiments had to be completed as quickly as possible.)



The foils used were, for the most part, made up from fresh (previously unirradiated) sheets of gold, although some foils were reused after a minimum of two months' cooling time. A punch and die press in standard use on the Project was used in manufacturing the foils; care was taken to see that all foils used in a given traverse were

- 1) made with the same punch and die,
- 2) punched from the same sheet of gold, and
- 3) as nearly matched in weight as possible.

The foils punched from a given sheet of gold, with a given punch and die, were made up into "libraries" of 200 to 400 foils, arranged in order of weight. The foils were weighed on a microgram balance; the standard deviation for a single measurement with this device has been determined to be 6 micrograms for an 0.038-gram foil. This constitutes an uncertainty of 0.015% and is negligible in comparison with the uncertainties due to counting statistics, which were never less than 0.11%. The lightest and heaviest foils in each experiment did not differ in weight by more than 2% of the mean.

The foils used in the macroscopic traverses were circular, 0.125 inch in diameter and 0.010 inch thick. Those used in the microscopic traverses in the 250 and 175 assemblies were circular, 0.0625 inch in diameter and 0.010 inch thick; 0.0625-inch-diameter, 0.005-inch-thick foils were used for the microscopic measurements in the 253 assembly. The purity of the gold was in all cases 99.95% or better.

### 3.8 FOIL HOLDERS - MACROSCOPIC DISTRIBUTION MEASUREMENT

All foil holders used were constructed of aluminum, the minimum amount consistent with the objectives of the experiment being used. The purer alloys of aluminum (1100, 6063, and 6061) were used throughout. Following general practice on the Project, "bare" foils were placed in aluminum pillboxes with an O.D. of 0.25 inch and a height of 0.060 inch; "cadmium-covered" foils were placed in similar pillboxes of cadmium. The thickness of the top, bottom, and wall of one of these pillboxes was 0.020 inch.



### 3.8.1 Radial Foil Holders

The radial foil holders were constructed of extruded, rectangular bar stock, 0.25 inch by 0.375 inch or 0.25 inch by 0.5 inch, and were positioned in the moderator by suspending them at the ends with aluminum bead chain, from carefully positioned support points. Circular depressions, 0.010 inch deep and capable of accommodating a gold foil in an aluminum or cadmium pillbox, were milled at intervals corresponding to the spacing of the lattice in which the holder was to be used; the accuracy of the location of these positioning depressions is about 0.0005 inch. Foils were secured to the holders with mylar tape; previous work indicates that the perturbation caused by the tape is negligible (SI 1). The foil holders were positioned in the lattices at heights from 70.6 cm to 71.4 cm above the bottom of the core. Positioning of the radial foil holders is further discussed in Sec. 4.2.1. As indicated in Figs. 3.3 to 3.11, they were parallel to the fuel support girders, in the first or second channel away from the lattice center.

### 3.8.2 Axial Foil Holders

Axial traverses were made in three different ways. In all assemblies studied (except the two-region assembly), at least one set of foils was imbedded in a fuel rod and irradiated. (In the 250 and 175 assemblies, all axial traverses were made in this way.) In the 253 assemblies, axial traverses were made by positioning foils in the moderator between fuel rods on aluminum foil holders. Finally, to explore a third alternative for the axial buckling measurement, in the last two assemblies to be investigated, fresh copper rods were irradiated at positions close to the center of the lattice, removed shortly after shutdown and sawed into pieces from which foils were cut; the positions from which foils were to be taken were accurately measured and marked before the irradiation. The positions of the various axial traverses are given in Figs. 3.3 to 3.11. Foils were generally placed at 2-inch intervals, from 12 inches to 40 inches above the bottom of the core.

As noted above, most of the axial distribution measurements were made with foils imbedded in the fuel. Several "experimental rods," consisting of hollow aluminum tubes with positioning tabs corresponding



to the top adapter of a normal fuel rod, were available for use with each lattice. Two-inch-long uranium slugs were also available; a total of 24 of these slugs, 15 or more with aluminum- or cadmium-boxed foils imbedded in one end, were placed in an experimental rod in a typical experiment of this kind. A fuel rod near the center of the lattice was withdrawn to make room for the experimental rod. After irradiation, the experimental rod was removed and disassembled, and the foils recovered for counting. The principal drawback in the use of this method is the high radiation level encountered by personnel while loading and unloading the experimental rods. Fuel slugs 0.75 inch in diameter, irradiated near the bottom of the lattice, had contact radiation levels in excess of 1 R (beta plus gamma). Extreme care was taken during experimental preparation and breakdown to minimize radiation exposure to all individuals concerned. There is also another drawback to the method: the experimental rods occasionally leak. Of the 32 axial traverses made in the manner described, three were rendered questionable by waterlogging — leaky gaskets allowed heavy water to seep into the rod during the course of the experiment. In all cases where experimental rods were waterlogged, the foils were cleaned with extra care before counting. More will be said about the results of these experiments in Sec. 4.2.2.

The aluminum foil holders used in the 253 lattice were fabricated in much the same manner as the radial foil holders previously described. The cross section of the extruded aluminum was, however, T-shaped and not rectangular (see Fig. 3.16). The back of the T measured 0.4375 inch, the leg 0.75 inch, and the wall thickness was 0.125 inch. Foils were secured in place with mylar tape. The holders were positioned at the top by means of a fuel rod top adapter which was fastened to the body of the holder. The pointed tip of the holder fitted into a hole in the fuel rod grid plate, which positioned the bottom of the holder.

Two traverses were made with the third technique, which involved the cutting of cross-sectional foils from an irradiated copper rod. The results are further discussed in Sec. 4.2.2. Considerably more effort was necessary to do the experiment with copper foils than it was to do the gold foil experiment. The drawbacks previously associated with

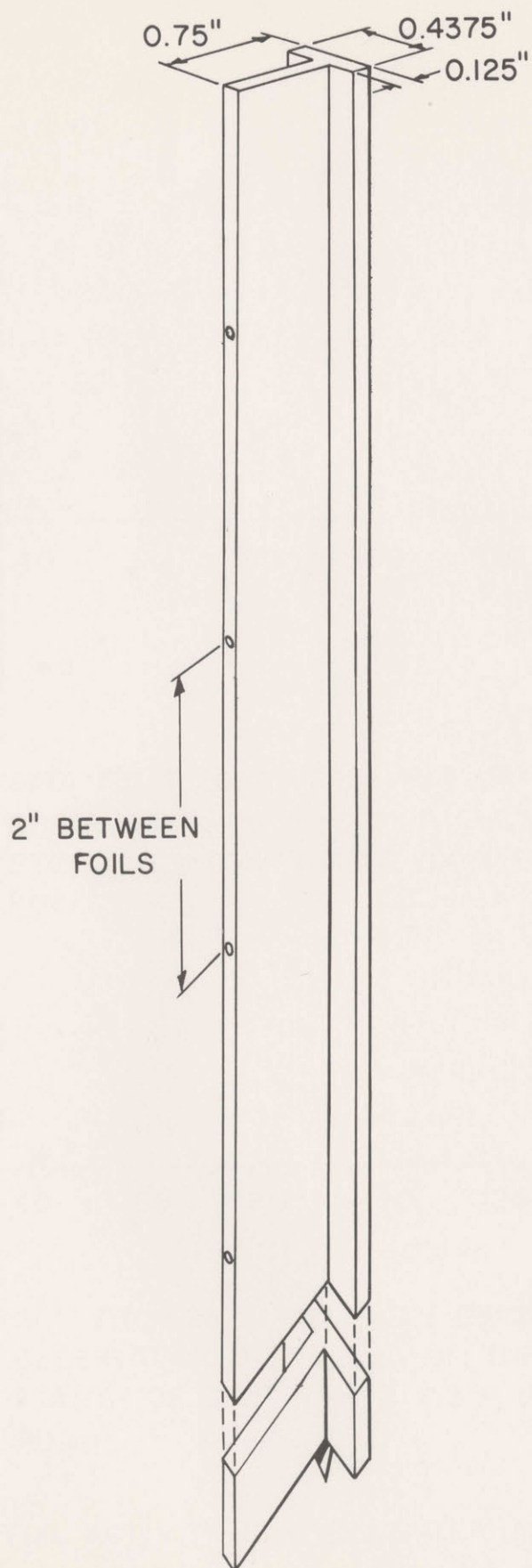


FIG. 3.16. AXIAL FOIL HOLDER USED IN 253 ASSEMBLIES.



copper as foil material (comparatively small cross section and half life), together with the difficulties involved in machining radioactive materials in short times, account for most of the additional effort needed.

A fourth method of measuring the axial buckling, involving the construction of a wire or rod scanner, was considered but not employed. It was felt that the measurement could be made more readily with foils, as described above, and that it would be very difficult to obtain both satisfactory collimation and a count rate high enough to allow good statistics.

The locations of the various axial traverses are shown in Figs. 3.3 to 3.11.

### 3.9 FOIL HOLDERS – MICROSCOPIC DISTRIBUTION MEASUREMENT

The purpose of the microscopic or intracellular traverses was, as previously noted, to determine the thermal neutron activation distribution in the fuel, moderator, and added absorber. In all the assemblies investigated, the central rod or rods were removable, together with the immediately adjacent copper rods. The "central cluster" could then be fitted out with the necessary foil holders, lowered into the lattice through the glove box by a winch, and replaced in position for the irradiation. The bottom adapter on the central fuel rod notched into the grid plate: a lower plate securely fixed to the central rod, below the bottom of the active fuel zone, prevented the other rods in the assembly from rotating or getting out of position. The upper plate of the central cluster was fabricated from plexiglass, so that the foil holders were visible when in position in the lattice. This upper plate positioned all the rods properly with respect to each other and fit snugly between the fuel support girders in such a way as to ensure proper positioning of the entire central cluster. Similar devices have been in use on the Project since its inception (BR 1, SI 1).

#### 3.9.1 Activation Distribution in Moderator

To map the activation distribution in the moderator, foils were placed on flat aluminum holders. In the 250 and 175 assemblies, these holders were 0.012 inch thick, in keeping with previous practice on the Project. To accommodate the bare foils, holes 0.065 inch in diameter



were drilled in the holder at the positions desired. The foils fit easily into these holes and were held in place with one or two layers of mylar tape on the top and the bottom. The body of the foil holder for the cadmium-covered foils was constructed similarly, but the holes were drilled out to 0.125 inch in diameter; cadmium pillboxes of the type shown in Fig. 3.17 were then inserted into the holes and cemented into place with epoxy resin. The foil holders were secured to the central fuel and absorber rods with mylar tape, at positions from 20 inches to 26 inches above the bottom of the core.

Although the results obtained with the foil holders described are considered reliable, in practice, an inordinate amount of effort was necessary to carry through a successful experiment with this equipment. Difficulty was experienced in positioning the holders and in securing them in position; mylar tape can be most inconvenient to work with, in this connection. Previous experiments have shown that as many as eight layers of mylar tape, in the immediate vicinity of the foils, do not perturb the measurement (SI 1). Anchoring the foil holder in place with a minimum amount of tape is, however, difficult at best. Finally, the epoxy resin cement proved not to be wholly reliable. Accordingly, in cooperation with Project personnel, a new kind of foil holder substantially different from those previously used was designed and built for use in the 253 assemblies.

The new holders consisted of flat aluminum plates, 0.060 inch thick. They were roughly triangular in shape and, as shown in Fig. 3.18, could be positioned by the three central fuel rods. Three fuel rods were equipped with circular rings which fit around the rods snugly and provided positive positioning for the foil holders. Bare foils lay in shallow (0.006-inch-deep) circular depressions 0.065 inch in diameter and were secured to the holder by a layer or two of mylar tape. The foil holder for the cadmium-covered foils was again constructed by drilling out holes 0.125 inch in diameter at each of the foil positions, but a modified cadmium box having no lower flanges was used. These boxes fit tightly (press fit) into the 0.125-inch holes. The foil holders, as constructed, were used successfully in three microscopic traverses and were an improvement over their predecessors.

To determine whether the foil holder caused a local depression in



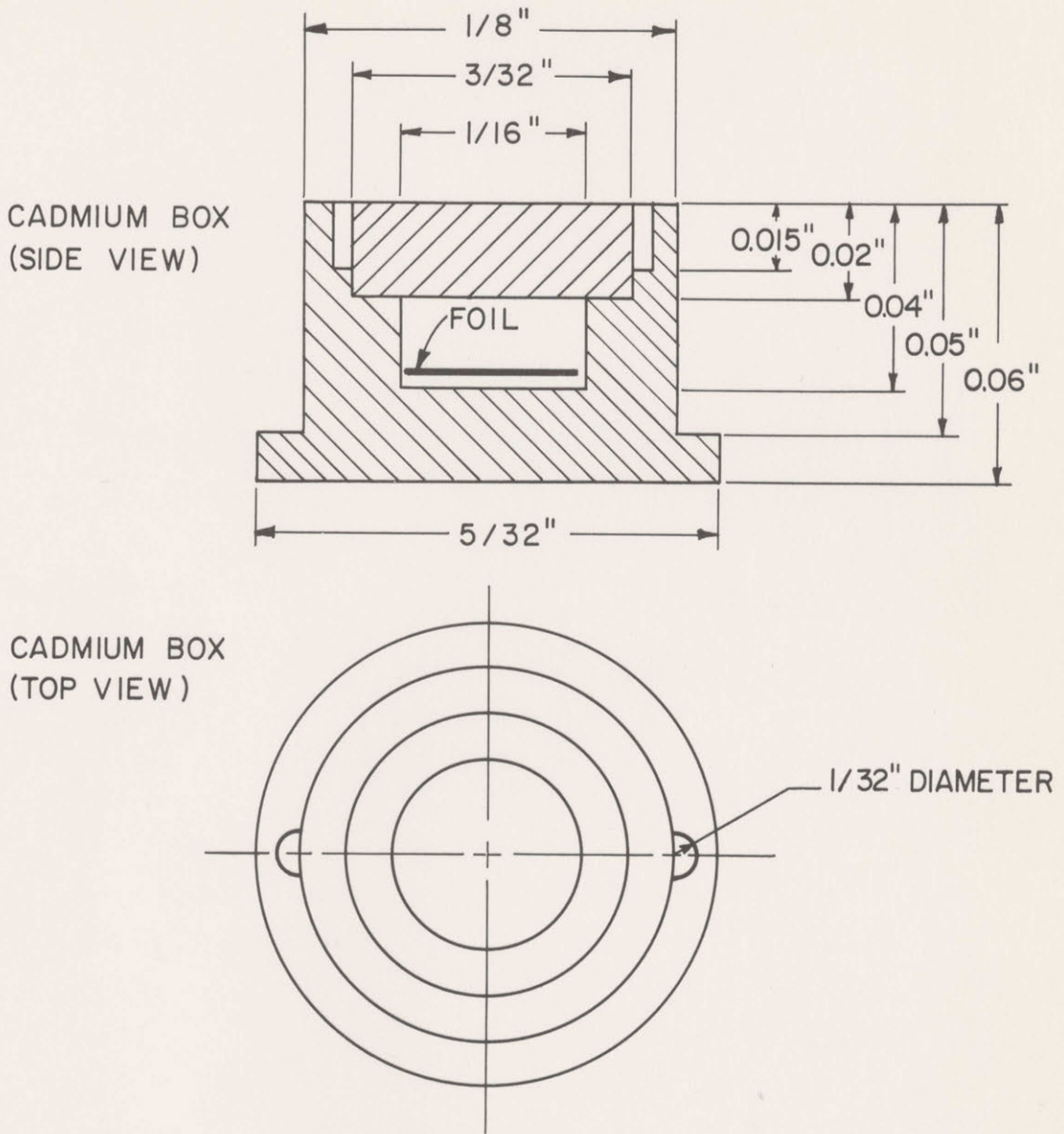


FIG. 3.17. THE CADMIUM BOX USED IN THE MICROSCOPIC DISTRIBUTION MEASUREMENT (FROM REF. SI 1)

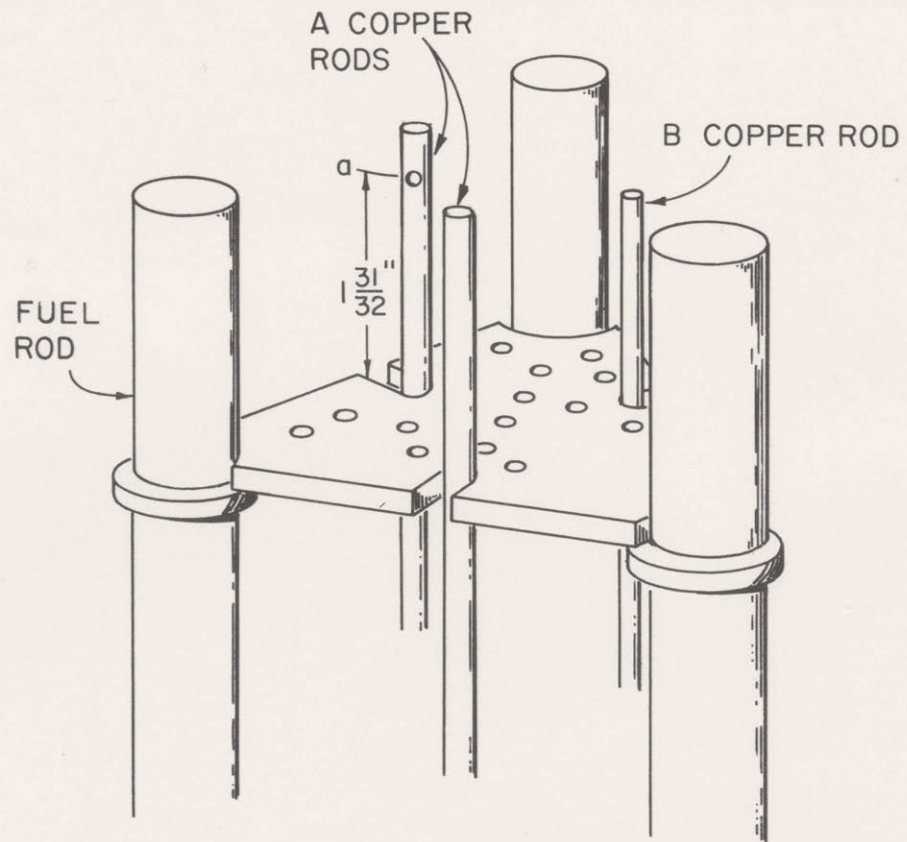


FIG. 3.18. FOIL HOLDER USED IN MICROSCOPIC DISTRIBUTION MEASUREMENT IN 253 ASSEMBLIES



the neutron flux for which a correction would have to be made, foils were irradiated on the surface of a copper rod at two positions. The first foil was taped into position at the point marked "a" in Fig. 3.18; the second was two inches directly below it, taped to the absorber rod at the height of the foil holder, so that it was between the foil holder edge and the rod surface. The experiment was done twice; the activity of the "a" foil was found to be  $1.0\% \pm 0.5\%$  higher than that of the lower foil, when both activities were corrected to the same reference height. No correction factor was applied to the activities of the foils on the holder; the effect of a 1% increase in their activity would be to decrease the thermal utilization by 0.005%, which is negligible in comparison to other uncertainties in this parameter.

### 3.9.2 Activation Distribution in Rods

In addition to the foils irradiated in the moderator, foils were also placed within the central fuel rod, within the copper rods, and on the surface of the fuel rods and copper rods. The surface foils were simply fixed in position with mylar tape. The foils in the fuel rod were positioned on a 0.125-inch-thick "button" of fuel material whose diameter was the same as that of a normal fuel slug. Such buttons are available for routine use on the Project; the foils could be positioned satisfactorily in milled depressions, and a single piece of mylar tape held them in place (see Fig. 3.19). An experimental rod, identical to that described in connection with the axial traverses, was used as a central fuel rod when microscopic traverses were made. This rod was loaded with slugs of fuel totaling 48 inches in length; two buttons were loaded with foils and placed between the slugs so that their positions in the experimental rod were approximately 20 inches and 24 inches, respectively, from the bottom of the core. The lower button was sandwiched between unmilled, 0.125-inch-thick buttons; 0.020-inch-thick cadmium foils were placed above and below the three buttons. A one-inch-long, 0.020-inch-thick, cadmium sleeve was placed on the rod so that its center was at the same height as the lower set of foils. Thus, the lower set of foils was surrounded by cadmium, and the upper set was bare.

The problem of determining the relative activation within the copper rods was solved by fabricating a special set of rods (see Fig. 3.20). They were constructed by cutting a copper rod into two

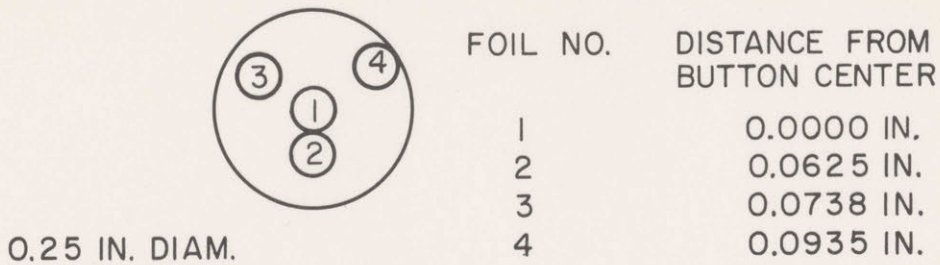


FIG. 3.19 a. TOP VIEW OF FUEL BUTTON USED IN 250 AND 175 LATTICES, SHOWING LOCATION OF FOILS.

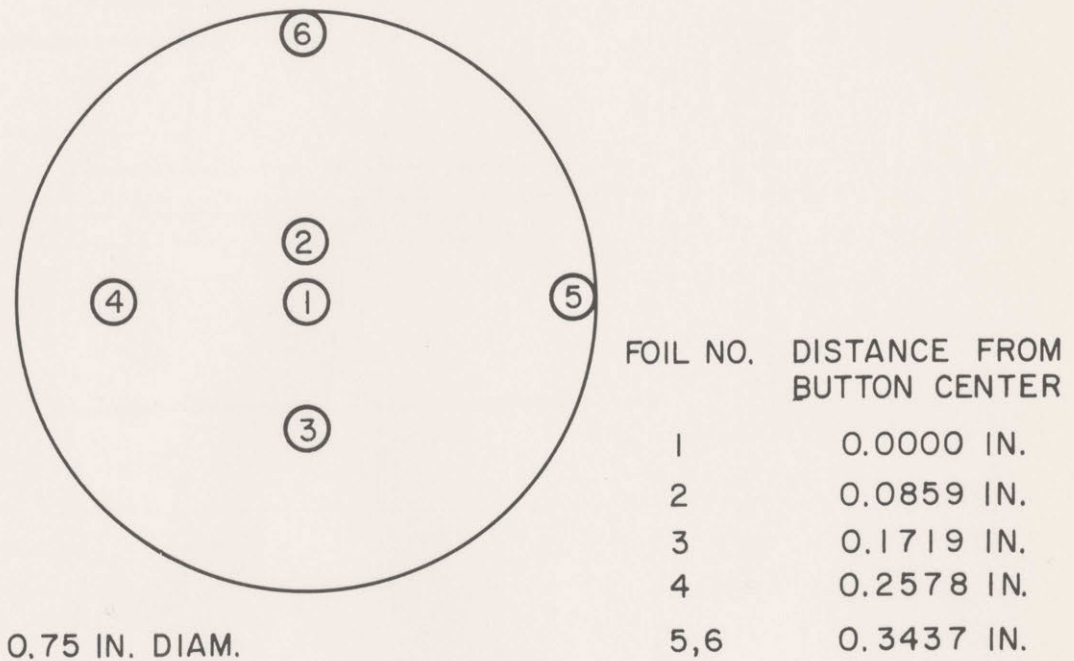
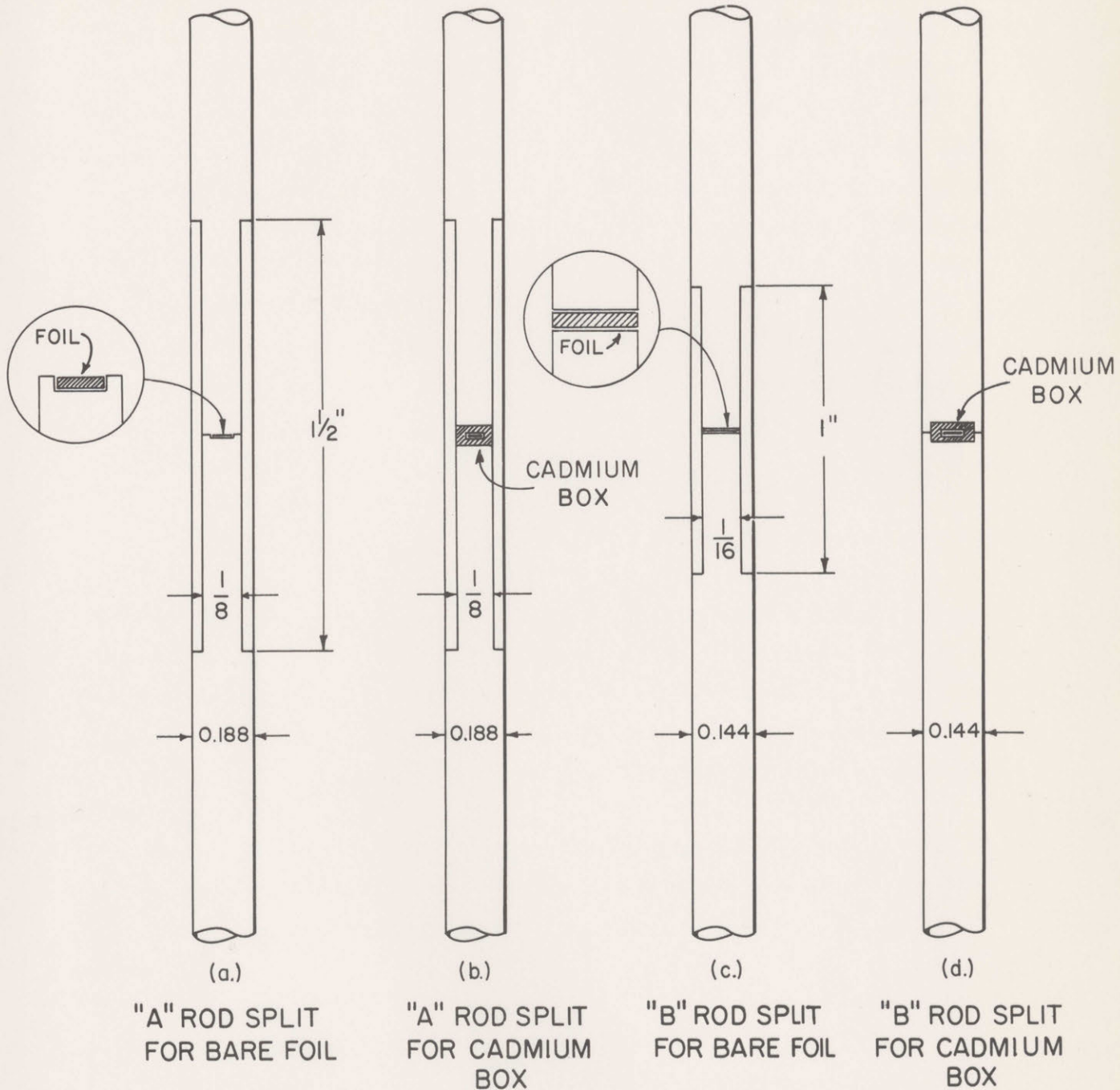


FIG. 3.19 b. TOP VIEW OF FUEL BUTTON USED IN 253 LATTICE, SHOWING LOCATION OF FOILS.

FIG. 3.19. FOIL HOLDERS FOR THE MEASUREMENT OF THE MICROSCOPIC DISTRIBUTION IN FUEL





(THE RODS ACCOMMODATE  $\frac{1}{16}$ " DIAMETER FOILS, OR  $\frac{1}{8}$ " DIAMETER CADMIUM BOXES WHICH ARE 0.060" THICK.)

FIG. 3.20 COPPER RODS USED IN MICROSCOPIC DISTRIBUTION MEASUREMENTS (VERTICAL SECTION).

pieces and turning a shoulder on the two pieces, at their meeting point. A sleeve having the same outer diameter as the rod, and with a thickness fixed by the diameter of the shoulder and the requirement of an easy fit ("slip" fit), completed the device. This sleeve was clad with KANIGEN just as was the body of the rod. Both the special "A" rod, and the "B" rod designed to accept a bare foil, were constructed in this manner. In use, the three parts of each rod were joined with mylar tape; the smallest amount of tape commensurate with the requisite mechanical strength was used. The tape also served to keep  $D_2O$  out of the rods; foils were dry when removed from the rods. The rods were fixed to the bottom plate of the central cluster in such a manner as to support them from the bottom.

Owing to the very thin wall (less than 0.010 inch) that would have been necessary for a similar rod capable of accepting a cadmium-covered foil in a "B" rod, the simpler design of Fig. 3.20d was used. The drawbacks to this arrangement were:

- 1) low mechanical strength,
- 2) the possibility of neutron streaming at the point where the two parts of the rods join.

In practice, the two parts of the rod fit tightly over the cadmium box, a press fit being necessary to join them. This, together with several wraps of mylar tape and support by the bottom plate of the central cluster, generally kept the two parts of the rod together snugly. This rod required more careful handling than the others, but in general performed satisfactorily.

The cadmium boxes used for the foils imbedded in copper rods, and for those on the rod surfaces, were like those shown in Fig. 3.17, without the flange; 0.020 inch of cadmium surrounded the foil on all sides.

### 3.10 SUMMARY OF THE EXPERIMENTS

Nine assemblies have been studied in the present series of experiments: four based on the 250 lattice, two based on the 175 lattice, and three based on the 253 lattice. One of the latter was a two-region assembly. The assembly configurations, together with the location of the experimental apparatus in the various experiments, have already



been presented (Figs. 3.3 to 3.11). Tables 3.4 and 3.5 give pertinent data about the nature of each of these assemblies, the time spent in studying them, and the experiments made in each. The designator for each assembly is somewhat arbitrarily made up of the three digits which form the designator of the host lattice, together with letters indicating the number of each kind of copper rod in a unit cell. Rods of 0.188-inch diameter are designated "A"; those of 0.144-inch diameter are designated "B." These designators are purely for convenience of reference to the various assemblies.

In addition to the types of experiment already described, three additional measurements were made in several of the assemblies, as indicated in Table 3.5. The first two of these involved irradiation of natural and depleted uranium foils in the central rod of the assembly, and had as their purpose the determination of the ratios  $R_{28}$  and  $\delta_{28}$  (see Sec. 2.3). The work was done by C. Robertson, H. Guéron, and S. Hellman; the details are available in theses by Robertson and Hellman (RO 1, HE 8) and in the Lattice Project Annual Report for 1965 (HE 5).

Some of the measurements usually done were not made in the 175A1 and 253A2 assemblies, for lack of time. The variation of  $\delta_{28}$  with material buckling is so slight that it was unnecessary to measure it in every assembly (see Sec. 5.3). The variation of  $R_{28}$  is not small, but it may be calculated in a manner described in Sec. 4.4. No radial distribution measurement with cadmium-covered foils was made in the 253A2 assembly; the region of spectral equilibrium was taken to be the same as that in the 253A2B1 assembly, which is very similar to the 253A2.

Finally, measurements were made of the cadmium ratio for a copper rod in the lattice ( $R_3$ ). The experiment was done in conjunction with the previously described measurement of the axial distribution with foils sawn from an irradiated copper rod. The rods were located at positions shown in Figs. 3.9 and 3.10. One end of a rectangular strip of cadmium, 1 inch wide and 0.002 inch thick, was secured to the copper rod and then wrapped around the rod 10 times, resulting in a sleeve thickness of 0.020 inch. The sleeve was generally placed at a point on the rod 18 inches above the bottom of the assembly. After irradiation,

TABLE 3.4

## Description of Assemblies Studied

Designator	Number of A Rods Per Fuel Rod	Number of B Rods Per Fuel Rod	Percentage of Moderator Expelled by Added Absorbers	Number of Weeks Spent in Study	Run Numbers
250A2	2	0	1.04	2	1-8
250A1	1	0	0.52	1	9-13
250B2	0	2	0.62	1	14-18
250B1	0	1	0.31	1	19-23
175A1B1	1	1	1.71	1.5	24-29
175A1	1	0	1.08	1	30-34
253A2B1(2R)*	(2)	(1)	(1.47)	1	35-40
253A2B1	2	1	1.47	1.5	41-46
253A2	2	0	1.14	0.5	47-49

\* (2R) signifies two-region assembly.



TABLE 3.5

Number and Type of Experiments Done in Each Assembly

Designator	Radial Distribution Measurement		Axial Distribution Measurement		Microscopic Distribution Measurement	$R_{28}$ Measure- ment	$\delta_{28}$ Measure- ment	$R_3$ Measure- ment
	Bare Foil	Cd-covered Foil	Bare Foil	Cd-covered Foil				
250A2	3	1	4	2	2	4	3	0
250A1	2	1	2	2	2	2	3	0
250B2	2	1	2	2	2	4	3	0
250B1	2	1	4	2	2	4	3	0
175A1B1	2	1	3	3	2	4	3	0
175A1	2	1	2	2	2	8	0	0
253A2B1(2R)	1	1	3	3	0	0	0	0
253A2B1	1	2	3	2	2	2	2	8
253A2	1	0	2	1	2	0	0	3

\* (2R) signifies two-region assembly.

the sleeve was removed, and 0.015-inch- and 0.030-inch-thick foils were cut from the rod at 18 inches and at several other points higher up on the rod. The bare foil activities were used to determine the axial flux distribution as previously noted; the activity of the foils cut at 18 inches, together with the average activity of the bare foils corrected to 18 inches, were used to determine the desired cadmium ratio.

During all but two of the 49 runs, a gold foil, 0.0625 inch in diameter and 0.0025 inch thick, was exposed in the cavity beneath the lattice assembly as a monitor. After all runs in a given assembly had been completed, the monitor foils for these runs were counted. In this way, the relative flux time for each irradiation was determined. Knowledge of the relative flux time is needed for the determination of cadmium ratios, when the bare and cadmium-covered foils are irradiated in separate runs, as was done with the radial traverses (see Sec. 4.1).



## CHAPTER IV

### ANALYSIS OF DATA

The theoretical basis of the experimental work and the experiments made have been discussed in the previous chapters. In this chapter, the analytical methods developed and used to derive the values of parameters from the experimental data are treated.

#### 4.1 RELATIVE ACTIVATION DISTRIBUTION AND CADMIUM RATIOS

As noted in Chap. III, the purpose of many of the experiments was the determination of the relative activation distribution for bare and cadmium-covered gold foils, in the immediate neighborhood of the central fuel rod, or along one of the two major coordinate axes. The techniques used to count the foils and correct the observed activity of each foil to the appropriate relative activity are not new and will only be summarized here; the reader is referred to Appendix C for the details.

Foils were counted with NaI crystal scintillation counters equipped with single-channel analyzers adjusted for integral counting above a particular energy. Automatic sample changers facilitated the taking of data. Observed activities were corrected for radioactive decay during the time from the end of the irradiation to the beginning of each count, and for decay during counting. Each foil activity was also divided by the weight of the foil, so that minor variations in foil size were accounted for. Counter dead times were carefully measured by the two-source method (PR 1). Background counts were taken before and after each set of foils was counted. The background count rate used in the analysis of the data was taken as the average of the two count rates, except when copper foils were being counted. In this case, the background, over the period when foils were being counted, varied by nearly a factor of two, owing to decay of the foil activities. The variation in the background count rate between the counts made before and after was assumed to be linear.



In almost every case, each set of foils was counted three or more times and the results for each foil averaged to give the final activity; each activity was weighted with the inverse square of its standard deviation in forming this average. The standard deviation assigned each activity was derived as indicated in Appendix C.

The measurement of the cadmium ratio as a function of axial position was generally made by irradiating simultaneously a set of bare foils and a set of cadmium-covered foils at equivalent positions. Thus, it was presumed that azimuthal variations in the neutron flux density at points well within the assembly were negligible; experiments in previous lattices have shown the validity of this assumption (PA 1 and HA 1). Foil holders were placed at positions 13.3 cm to 22.3 cm from the center rod of the assembly, in the center girder (see Figs. 3.3 to 3.11). After irradiation, the cadmium-covered foils were counted first because of their lower activity. Following this, the bare foils were counted; one or two of the cadmium-covered foils were counted with the bare foils, to detect any changes in the counter sensitivity. All activities were corrected back to the time the irradiation ended; if the activities of the foils counted both times differed by an amount greater than that accounted for by statistical fluctuations, a correction for the drift in counter sensitivity was made. After the other corrections mentioned earlier in this section were made, the cadmium ratio was obtained simply as the ratio of the corrected activities of the bare and cadmium-covered foils.

The measurement of the cadmium ratio as a function of position within the central cell of the assembly was made in a similar manner. But, rather than exposing the foil holders at two equivalent radial positions, the holders were loaded into the same cell, axially separated by a distance of 4 to 6 inches. Since both holders were always within a region (17 to 26 inches above the bottom of the assembly) where the axial flux variation is well described by a single exponential function, correction of the observed relative activations to an intermediate reference height (20 inches) was straightforward. Values of the cadmium ratio or, what is of greater interest, the relative thermal activation, as a function of position, were then readily derived as before.

Measurement of the cadmium ratio as a function of radial position



involved an additional complication because the bare and cadmium-covered foils were not irradiated simultaneously but in consecutive experiments. Since the source strength as well as the irradiation time generally differed for the two experiments, the relative activation of the "monitor foils" described at the close of the preceding chapter was used to correct the observed relative activities. All corrected foil activities were divided by the monitor foil activation before cadmium ratios were computed.

## 4.2 DETERMINATION OF THE MATERIAL BUCKLING

As indicated in Sec. 2.1.3, the material buckling is obtained by fitting functions of the form  $J_0(aR)$  and  $\sinh \gamma(H_0 - z)$  to radial and axial activation distributions, respectively, measured within the region of spectral equilibrium;  $a$  and  $\gamma$  are determined by an iterative least-squares fitting process, and the material buckling obtained from Eq. (2.5),

$$B_m^2 = a^2 - \gamma^2 . \quad (4.1)$$

The unit used here for buckling is the "microbuck" ( $\mu B$ ):

$$0.01 \text{ m}^{-2} = 0.000001 \text{ cm}^{-2} = 1 \mu B . \quad (4.2)$$

The analysis of the large amount of data was facilitated by the use of two digital computer codes written by P. F. Palmedo (PA 1) and modified by J. Harrington (HA 1, HA 2).

### 4.2.1 The RADFIT Code

The input to the radial buckling code (RADFIT) consists of the positions of the foils on the holder, the distance of the foil holder from the center of the assembly, the foil activities (and standard deviations, if desired), an initial estimate of the buckling to start the iterative process, and a few iteration parameters. An iterative least-squares fit is made to the parameters  $A$  and  $a$  in the expression  $AJ_0(aR)$ . The quantity minimized is

$$\sum_{i=1}^m W_i d_i^2 , \quad (4.3)$$



where  $d_i$  is the residual for foil  $i$  (the difference between the foil activity and the value of the fitted function at  $R_i$ ),  $W_i$  is the weight associated with point  $i$ , and  $m$  is the number of foils. The appropriate value for  $W_i$  is the inverse square of the standard deviation of the activity of foil  $i$ ; if the standard deviation is not supplied,  $W_i$  is taken to be equal to the inverse square of the activity. The latter option is appropriate when all foils have been counted for the same number of counts. The iterative process ceases when the change in both  $A$  and  $a$  is less than a preset amount, here taken as  $10^{-5}$ .

In thirteen of the twenty-five radial distributions, foils at equal distances from the center of the assembly, but on opposite sides of the assembly, showed unequal activities; the differences were greater than those to be expected from counting statistics. An example is given in Fig. 4.1. This result is indicative of one of two deviations from ideal experimental conditions. Either the foil holder as a whole has shifted to one side or the other (parallel to itself), or the holder was tilted (one end lower than the other). Because of the design of the foil holder, the former possibility is highly unlikely. The holders hung free, from carefully located support points, and were observed in position before and after most runs. The second possibility almost certainly accounts for the observed behavior of the radial distributions. An effort was made to insure that foil holders were level; in fact, the holders were never more than 0.25 inch out of level. The aluminum bead chain used to support the holders has advantages over other means, many of which have been investigated earlier (PA 1, HA 1). Its major advantage is that exact positioning of a collar with set screw on the chain is difficult because of the knobbiness of the chain; it can, with some effort, be done to within approximately 0.04 inch. The disadvantage is smaller in clean lattices than in the modified lattices because the axial relaxation length in the clean lattices is larger, making the effect of foil holder tilt less serious.

A small amount of foil holder tilt does not invalidate the distribution for use in obtaining the radial buckling. The axial activation distribution is exponential in character at the point in question (71 cm). Over the very small distances involved (less than 1 cm), the difference in foil activities ( $\phi_1 - \phi_2$ ) is (to an excellent approximation) proportional



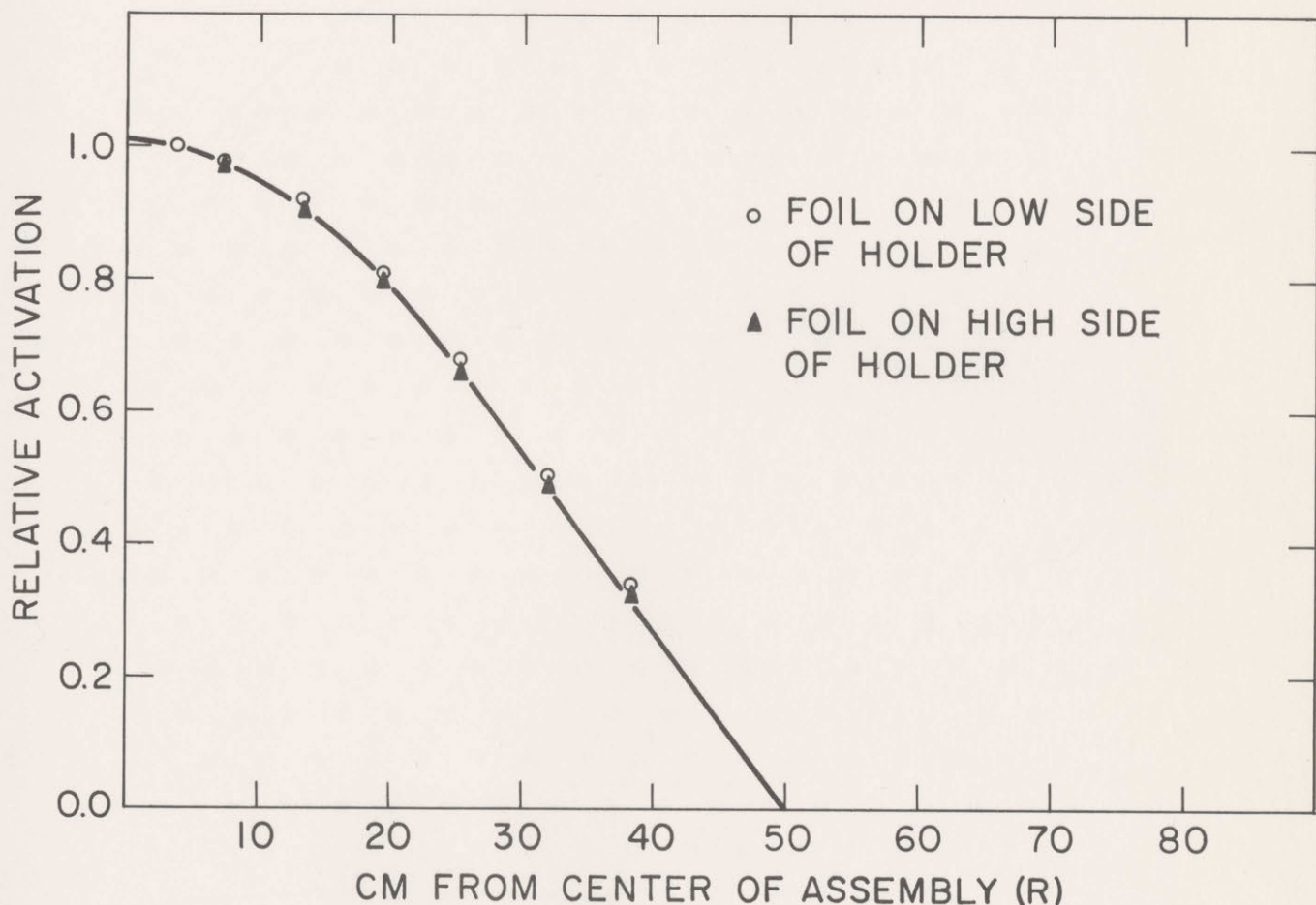


FIG. 4.1. RELATIVE ACTIVATION DISTRIBUTION AS A FUNCTION OF RADIAL POSITION (R), MEASURED IN ASSEMBLY 253A2 WITH BARE 0.010 INCH GOLD FOILS. FUNCTION  $AJ_0(\alpha R)$  FITTED TO POINTS LESS THAN 22.5 CM FROM CENTER; VALUE OF A IS 1.0065, VALUE OF  $\alpha^2$  IS 2313  $\mu\text{B}$ . STANDARD DEVIATION IN FOIL ACTIVITIES DUE TO COUNTING STATISTICS 0.15%.

to the separation between the foils ( $z_1 - z_2$ ):

$$(\phi_1 - \phi_2) \sim \left[ \sinh \gamma(H_0 - z_1) - \sinh \gamma(H_0 - z_2) \right] \sim \left[ 1 - e^{-\gamma(z_2 - z_1)} \right] \sim \gamma(z_2 - z_1). \quad (4.4)$$

Consider a foil holder at a small angle  $\beta$  to the horizontal. A foil on the low end of the holder, at a distance  $x$  from the center, will be a distance  $\beta x$  below the height of a foil at the exact center of the foil holder. A foil equidistant from the center on the high end of the holder will be a distance  $\beta x$  above the center foil. The activity of the foil on the high end of the holder is decreased from the activity that would be observed if the angle  $\beta$  were zero; the activity of the foil on the low end is increased above this activity by the same fraction, to a high degree of approximation. The desired activity is thus the average of the two observed activities.

In practice, it is not necessary to average observed activities at points equidistant from the center and on either side of the center before making least-squares fits to the distributions. Test runs indicated that the same value of  $\alpha^2$  was obtained (to within one microbuck), whether the observed distribution (such as that of Fig. 4.1) or the distribution with averaged activities was used. This result can be traced to the fact that it is the sum of the squares of the fractional (not absolute) residuals that is minimized in the least-squares fitting process. (This is rigorously true only where foils were counted for a preset number of counts, but it holds approximately in all instances under consideration here.) Thus, the fitting process does not distinguish between two points at  $(\phi, R)$  and two points, one at  $(\phi + \delta, R)$  and the other at  $(\phi - \delta, R)$ .

In all but one of the assemblies, radial traverses were made with bare and cadmium-covered foils (see Table 3.5). The positions of the foil holders are shown in Figs. 3.3 to 3.11; the height of the center of the holder varied from 70.6 cm to 71.4 cm. The height of the holder is known to within about 0.0625 inch, or 0.16 cm. Cadmium ratios were derived as described in Sec. 4.1 and plotted against radial position; Fig. 4.2 shows the results for the 175A1B1 assembly. The values of the cadmium ratio for points less than about 28 cm from the center of



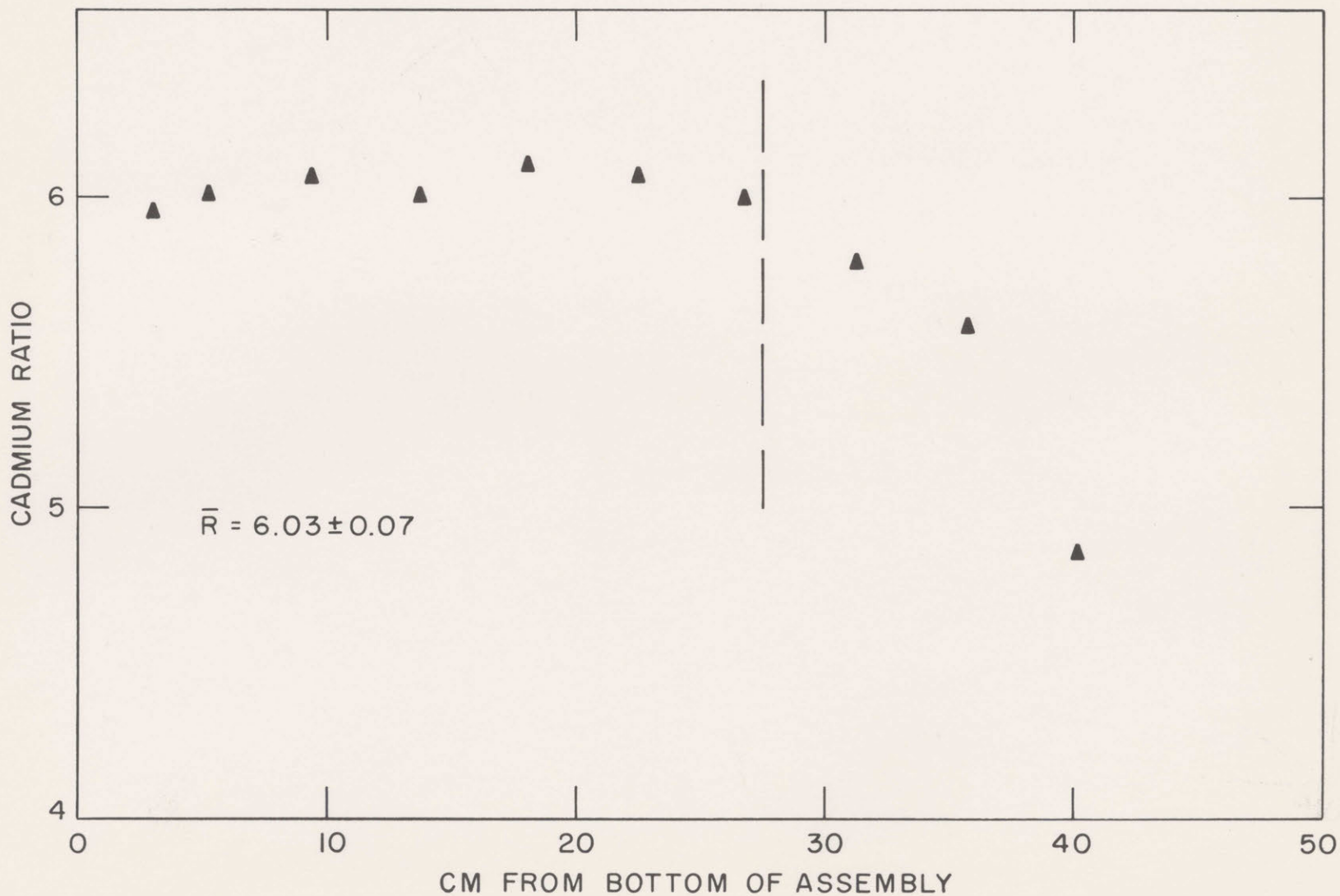


FIG. 4.2. CADMIUM RATIO IN I75AIBI ASSEMBLY AS A FUNCTION OF RADIAL POSITION (RUNS 25, 27)

the assembly show a random behavior about the mean values. Accordingly, an equilibrium spectrum was assumed present in this region. Table 4.1 summarizes the results for the assemblies studied. The number of foils within the equilibrium region varied from 7 to 13.

TABLE 4.1  
Region of Equilibrium Cadmium Ratio (Radial)

Assembly	Radial Region of Equilibrium Cadmium Ratio (cm)	Value of Cadmium Ratio ** IN MODERATOR
250B1	0 - 30.0	12.41 ± 0.13
250A1	0 - 25.0	12.57 ± 0.12
250B2	0 - 28.0	11.39 ± 0.14
250A2	0 - 27.5	11.06 ± 0.15
175A1	0 - 27.5	6.37 ± 0.05
175A1B1	0 - 27.5	6.03 ± 0.07
253A2	(0 - 22.5)*	
253A2B1	0 - 22.5	2.99 ± 0.03

\* Assumed on basis of measurements in 253A2B1 assembly.  
\*\* Gold foils were 0.125 inch in diameter and 0.010 inch thick.

The mean value of the cadmium ratio within the equilibrium region, based on all the available data, and the standard deviation of the mean are given also. Where only one traverse with either bare or cadmium-covered foils is available, the standard deviation includes the effect of the 0.16-cm uncertainty in foil holder position. Further comments on the cadmium ratios will be made in Sec. 4.2.2.

Figures 4.3 to 4.5 are samples of the results of the radial traverses. They consist of the experimental activities, normalized to unity at the innermost point and plotted as a function of radial position. Activities of foils equidistant from the center have been averaged. The  $J_0$  Bessel function fitted to the points within the equilibrium region is given for comparison. The residuals are also plotted as a function of radial position. In all but four of the twenty-three radial traverses done in one-region assemblies, the residuals outside the region of



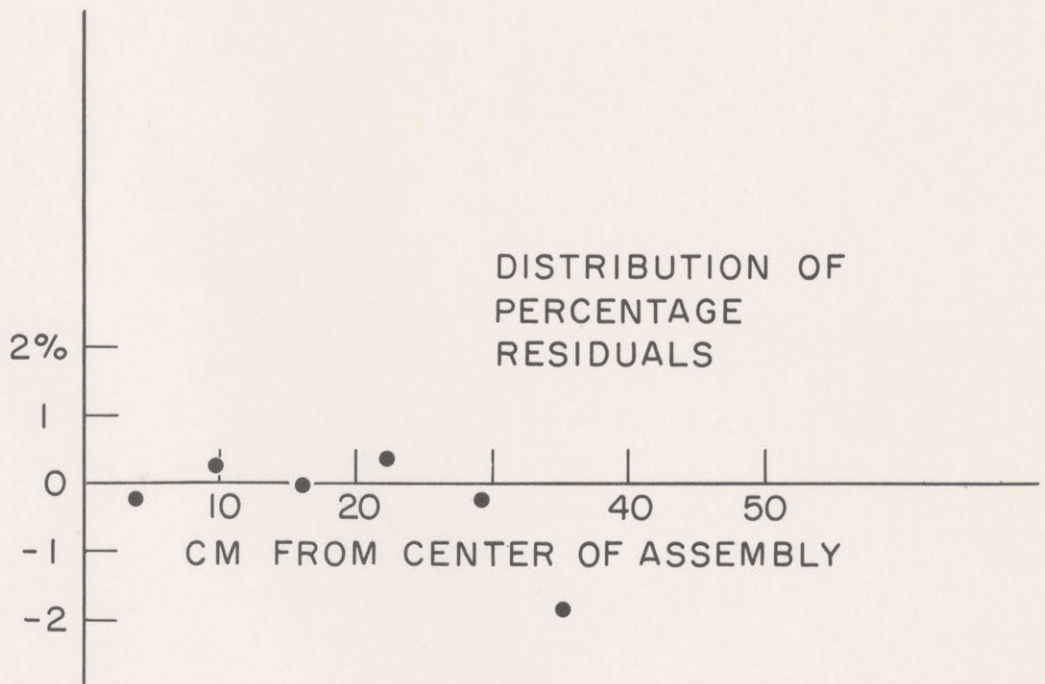
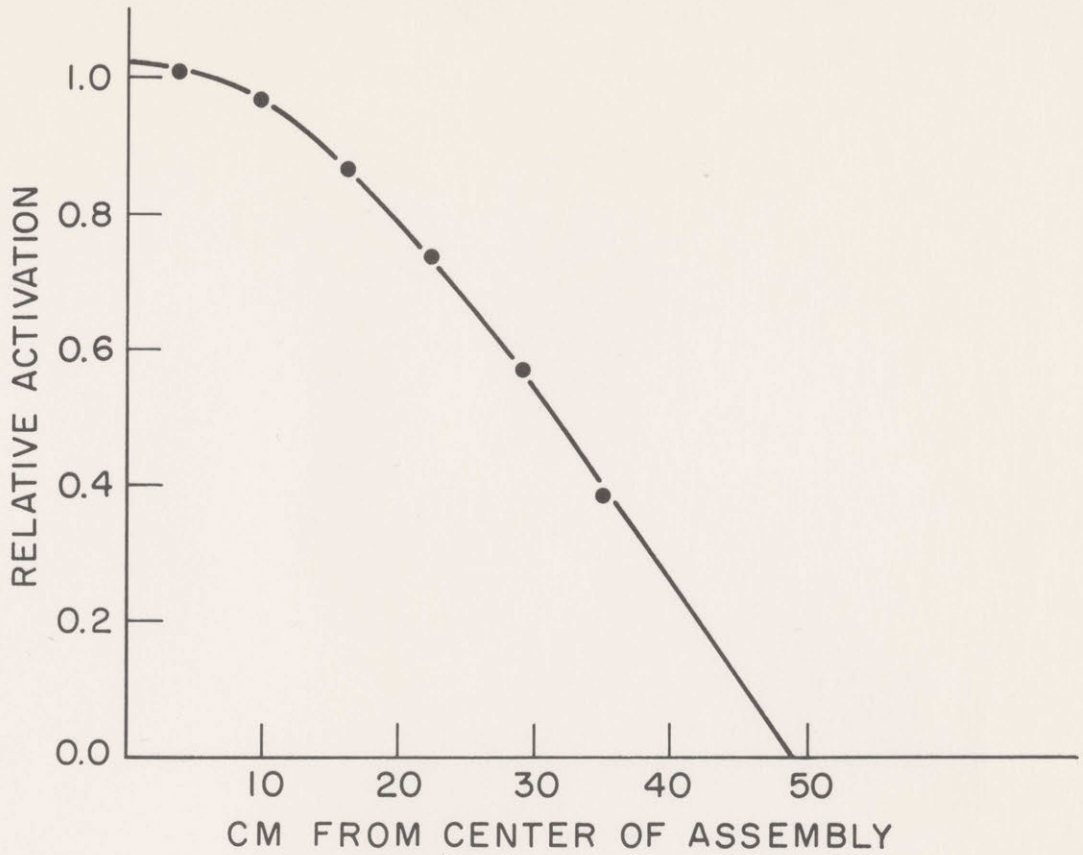


FIG. 4.3. RELATIVE ACTIVATION DISTRIBUTION IN 250BI ASSEMBLY AS A FUNCTION OF RADIAL POSITION (RUN 19, BARE FOILS; RADIAL BUCKLING IS  $2418 \mu\text{B.}$ )

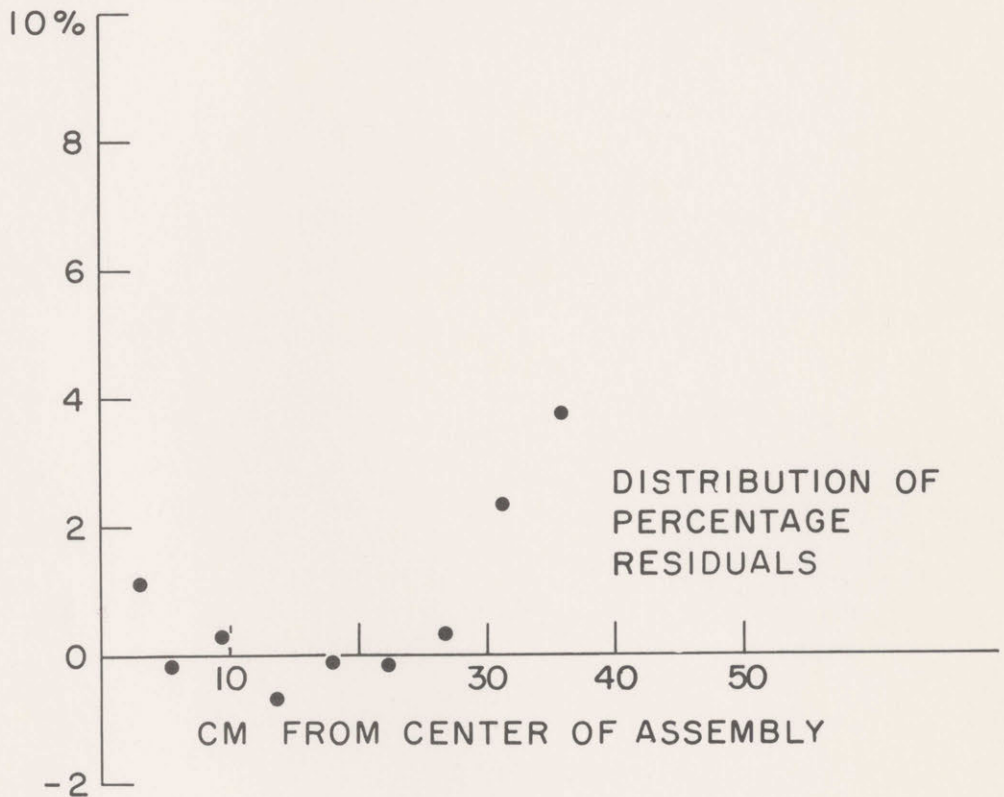
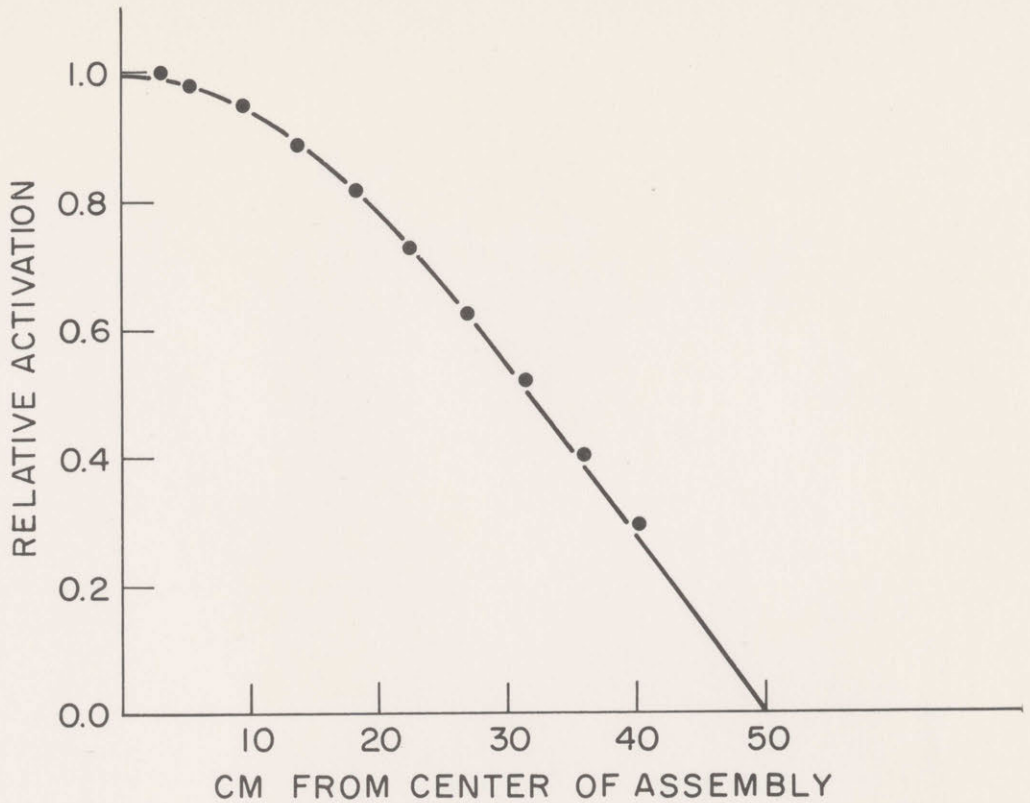


FIG.4.4. RELATIVE ACTIVATION DISTRIBUTION IN 175Al ASSEMBLY AS A FUNCTION OF RADIAL POSITION (RUN 33, CADMIUM COVERED FOILS; RADIAL BUCKLING IS  $2311 \mu\text{B.}$ )



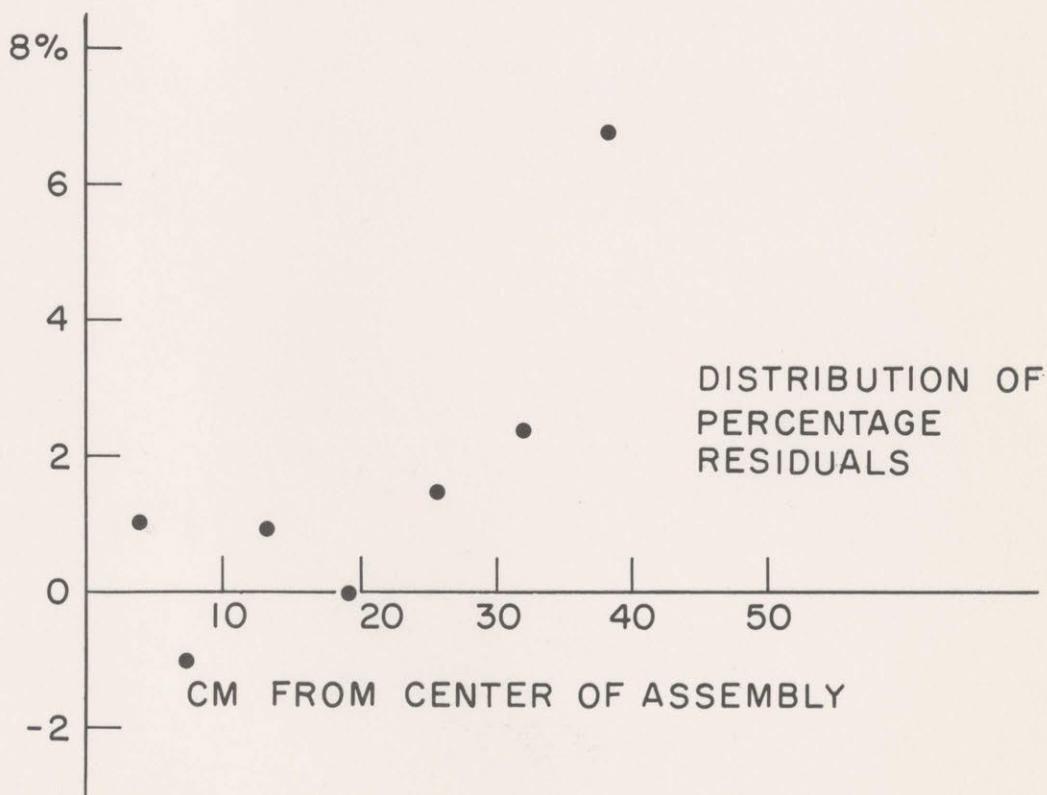
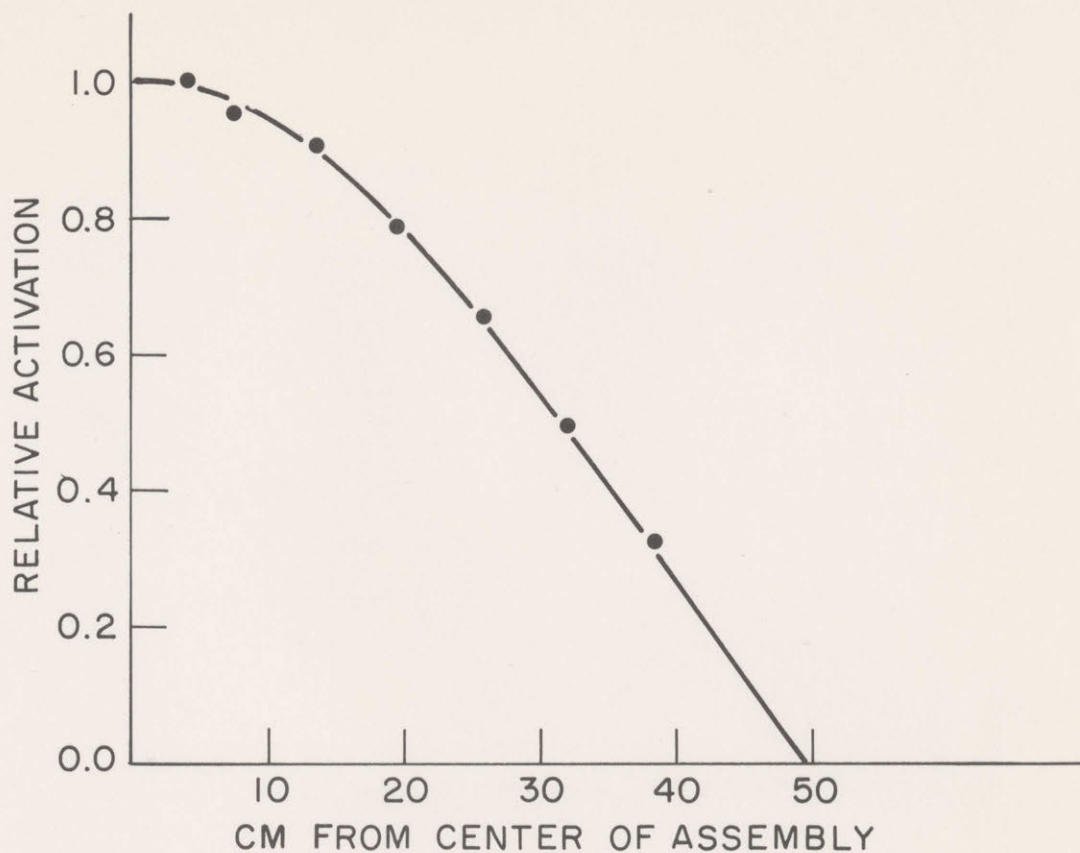


FIG. 4.5. RELATIVE ACTIVATION DISTRIBUTION IN 253A2BI ASSEMBLY AS A FUNCTION OF RADIAL POSITION (RUN 43, BARE FOILS; RADIAL BUCKLING IS  $2361 \mu\text{B.}$ )

equilibrium cadmium ratio were positive when cadmium-covered foils were used and negative when bare foils were used (see Figs. 4.3 and 4.4). Four traverses made with bare foils did display positive residuals outside the equilibrium region; Fig. 4.5 gives an example.

Of the 25 radial traverses made, one had to be discarded because of malfunctions of the counting equipment; in addition, one point had to be dropped from each of three runs because of difficulties with experimental apparatus.

The radial buckling for each run was obtained from a least-squares fit to all points within the equilibrium region; the residuals appeared in each case to be randomly distributed about the value of zero within this region. The radial buckling for each assembly was taken as the mean of the values for all runs made in that assembly. The uncertainty is the standard deviation of the mean; the Student correction for small sample size was applied. The results are reported in Sec. 5.1.

The extrapolated radius,  $R_o$ , has been defined in Sec. 2.1.3 by the equation,

$$R_o = \frac{2.4048}{\alpha}. \quad (4.5)$$

The extrapolation distance (the difference between the value of  $R_o$  and the physical radius of the lattice) is needed for the axial buckling analysis described in the next section. If the cross-sectional area of a lattice of  $N$  fuel rods is taken to be  $N$  times the area,  $A_{\text{cell}}$ , assigned to each rod in an infinite lattice, then the physical radius of the lattice,  $R_{\text{lat}}$ , is  $(NA_{\text{cell}}/\pi)^{1/2}$ . For a lattice on a triangular spacing  $S$ , the value of  $A_{\text{cell}}$  is  $(0.75)^{1/2}S^2$  (see Sec. 4.3.1). Thus, the physical radius of the lattice is given by the equation,

$$R_{\text{lat}} = \left[ \frac{3^{1/2}}{2\pi} \right]^{1/2} N^{1/2}S = 0.52504 N^{1/2}S. \quad (4.6)$$

The values of the extrapolation distance are given in Table 4.2, in centimeters and in units of the transport mean free path,  $\lambda_{\text{tr}}$ . The value of  $\lambda_{\text{tr}}$  for each assembly was taken as  $3\bar{D}$ , where  $\bar{D}$  is the diffusion coefficient calculated with Eq. 4.12; the values of  $\bar{D}$  are listed in Table 5.2. The extrapolation distance varies from 2.1 to 2.6, in units of  $\lambda_{\text{tr}}$ ; for the 250, 175, and 253 lattices (unmodified by the addition of absorbers), the extrapolation distance varies from 1.7 to 2.2, in units of  $\lambda_{\text{tr}}$ .



TABLE 4.2  
Radial Extrapolation Distance,  $R_o - R_{lat}$

Assembly	Extrapolation Distance	
	(cm)	(units of $\lambda_{tr}$ )
250B1	5.65	2.2
250A1	6.73	2.6
250B2	5.87	2.2
250A2	6.23	2.4
175A1	5.51	2.1
175A1B1	6.60	2.5
253A2	6.67	2.4
253A2B1	6.23	2.2

#### 4.2.2 The AXFIT Code

The technique for calculating the axial buckling is similar to that just described for the radial buckling. The axial buckling code (AXFIT) functions much as does the RADFIT code; the parameters varied in the fitting process are  $A$  and  $\gamma$ , in the expression  $A \sinh \gamma(H_o - z)$ . The height,  $H_o$ , at which the extrapolated flux goes to zero, is an input parameter, and provision is made in the code for trying several values.

Axial traverses were made with bare and cadmium-covered foils in all assemblies. The foil holders were placed at radial positions from 13.3 to 22.3 cm from the center of the assembly in all cases except those used in the experiments on the effect of the absorber rod aligner, described in Sec. 3.5. The positions of all the axial traverses are shown in Figs. 3.3 to 3.11. Cadmium ratios were obtained as described in Sec. 4.1 and plotted against axial position; Fig. 4.6 shows the results for the 250B2 assembly. The region from 35 cm to 95 cm is taken as the equilibrium region. Table 4.3 gives the results for all the assemblies studied. The equilibrium value of the cadmium ratio is also given. Where two independent sets of measurements of the cadmium ratio as a function of axial position are available, the value reported is the mean of all values in the equilibrium region. The

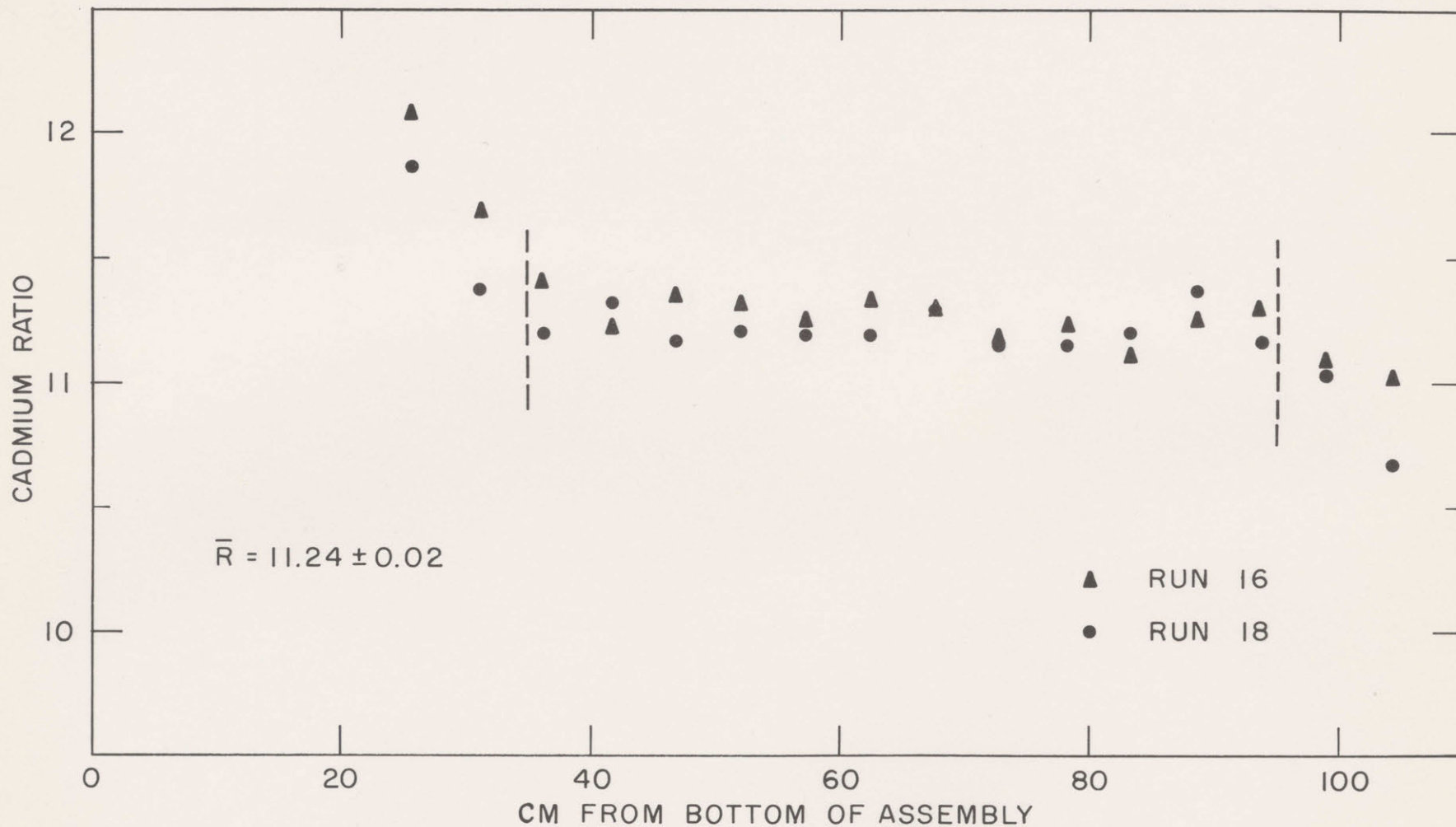


FIG. 4.6. CADMIUM RATIO IN 250B2 ASSEMBLY AS A FUNCTION OF AXIAL POSITION (RUNS 16, 18)



TABLE 4.3  
Region of Equilibrium Cadmium Ratio (Axial)

Assembly	Axial Region of Equilibrium Cadmium Ratio (cm)	Value of Cadmium Ratio*	
		IN MODERATOR	IN FUEL
250B1	35 - 100	—	11.77 ± 0.06
250A1	45 - 100	—	11.76 ± 0.06
250B2	35 - 95	—	11.24 ± 0.02
250A2	35 - >100	—	11.15 ± 0.04
175A1	<30 - >100	—	6.16 ± 0.02
175A1B1	<30 - >100	—	5.78 ± 0.03
253A2	32.5 - 100	3.10 ± 0.02	—
253A2B1**	32.5 - 100	3.21 ± 0.02	—

\* Gold foils were 0.125 inch in diameter and 0.010 inch thick.

\*\* See text.

standard deviation is the standard deviation of the mean. Where only one set of measurements of the cadmium ratio was available, the standard deviation reported is based on the two independent sources of error, foil positioning and the scatter about the mean value. The uncertainty in foil positioning is about 0.0313 inch, or 0.079 cm.

The value of the cadmium ratio in the 253A2B1 assembly is suspected to be in error; it is higher than the value reported for the 253A2 assembly and higher than the value reported in Table 4.1, with which it should be in agreement. Although the result is believed to be in error, a careful check of all the available data fails to reveal a reason for discarding it, and it is therefore included here. However, the value of the cadmium ratio measured in the three radial traverses in the 253A2B1 assembly (see Tables 3.5 and 4.1), not the value reported in Table 4.3, is taken as the appropriate one for comparison with the cadmium ratios measured in radial traverses in the two-region assembly (see Sec. 5.7). There are two other minor anomalies in Tables 4.1 and 4.3, but the calculated uncertainties more than account for them. The absolute value of the cadmium ratio is important only in the analysis of the two-region experiment; thus, no further discussion is necessary.

As with the radial buckling measurement, all points from regions where the cadmium ratio was not stable, or the asymptotic distribution was not observed, were rejected. The method used to determine the region where the asymptotic distribution existed will be considered next.

Initially, only those points more than 50 cm from the bottom of the assembly were used. Least-squares fits were made, first to all points in the resulting distribution, then to successively fewer, dropping the point nearest the top of the assembly after each fit and repeating the analysis. The process was continued until the axial distribution of the residuals was random.

To the resulting distribution were then added the points within 50 cm of the bottom of the assembly. Least-squares fits to the data were again made with successively fewer points; after each fit, the point nearest the bottom of the assembly was dropped. The process was continued until the axial distribution of the residuals was random.

The "asymptotic region" was defined as the largest portion of the assembly over which the axial distribution of the residuals was random for all traverses (see Table 4.4). Since the asymptotic region fell within the region of equilibrium cadmium ratio for all the assemblies, Table 4.4 defines the region for each assembly from which points were taken in the axial buckling analysis. The least-squares fits from which the buckling values were derived included from 6 to 9 points.

TABLE 4.4  
Axial Region Where Asymptotic Distribution Prevails  
in Each Assembly

Assembly	Asymptotic Region (cm)
250B1	35.0 - 73.0
250A1	45.0 - 73.0
250B2	36.0 - 78.0
250A2	50.0 - 78.0
175A1	41.0 - 77.7
175A1B1	30.6 - 73.0
253A2	40.6 - 71.0
253A2B1	35.5 - 71.0



Because all points in the distributions were two or more relaxation lengths from the extrapolated end point  $H_0$ , it was not possible to determine the best value of  $H_0$  from the fitting process alone. However, the dependence of the buckling  $\gamma^2$  on the value chosen for  $H_0$  is very weak; a 1-cm change in the value of  $H_0$  results in a 1-3  $\mu\text{B}$  change in the value of  $\gamma^2$ . The axial extrapolation distance was assumed to be the same as the radial, and the value of  $H_0$  was obtained by adding the radial extrapolation distance (from Table 4.2) to the physical length of the fuel rods (121.92 cm). The resulting values of  $H_0$  are given in Table 4.5. The values determined by least-squares fits to data from the clean lattices range from 127 cm to 131 cm, in good agreement with the values reported here.

TABLE 4.5  
Value of Extrapolated Height,  $H_0$ , for Each Assembly

Assembly	Extrapolated Height (cm)
250B1	127.57
250A1	128.65
250B2	127.79
250A2	128.15
175A1	127.43
175A1B1	128.52
253A2	128.59
253A2B1	128.15

Figures 4.7 and 4.8 are samples of the results of the axial traverses. They consist of the experimentally observed foil activities plotted with semilogarithmic coordinates as a function of axial position. Fitted values of the function  $A \sinh \gamma(H_0 - z)$  are plotted in the asymptotic region, for comparison. All theoretical and experimental points have been normalized by dividing by  $A \sinh \gamma H_0$ .

The results of the two axial traverses made in the 253 assemblies with foils sawn from a copper rod (see Sec. 3.8) were consistent with the results of the axial traverses made with gold foils. Because of

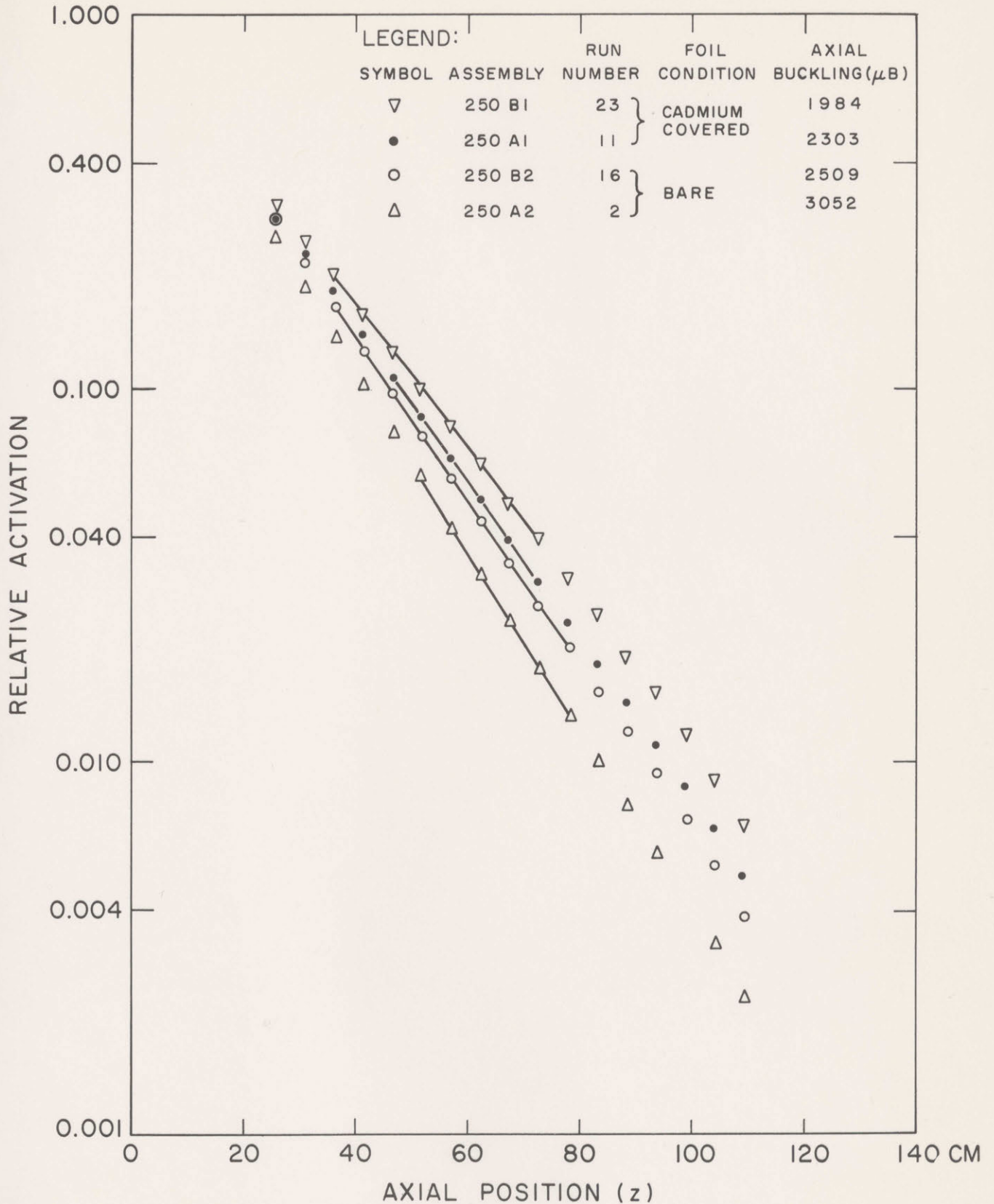


FIG. 4.7 RELATIVE ACTIVATION DISTRIBUTION IN FOUR 250 ASSEMBLIES AS A FUNCTION OF AXIAL POSITION. (GOLD FOILS USED WERE 0.010 INCHES THICK, 0.125 INCHES IN DIAMETER. UNCERTAINTY DUE TO COUNTING STATISTICS 0.2% TO 0.4%)



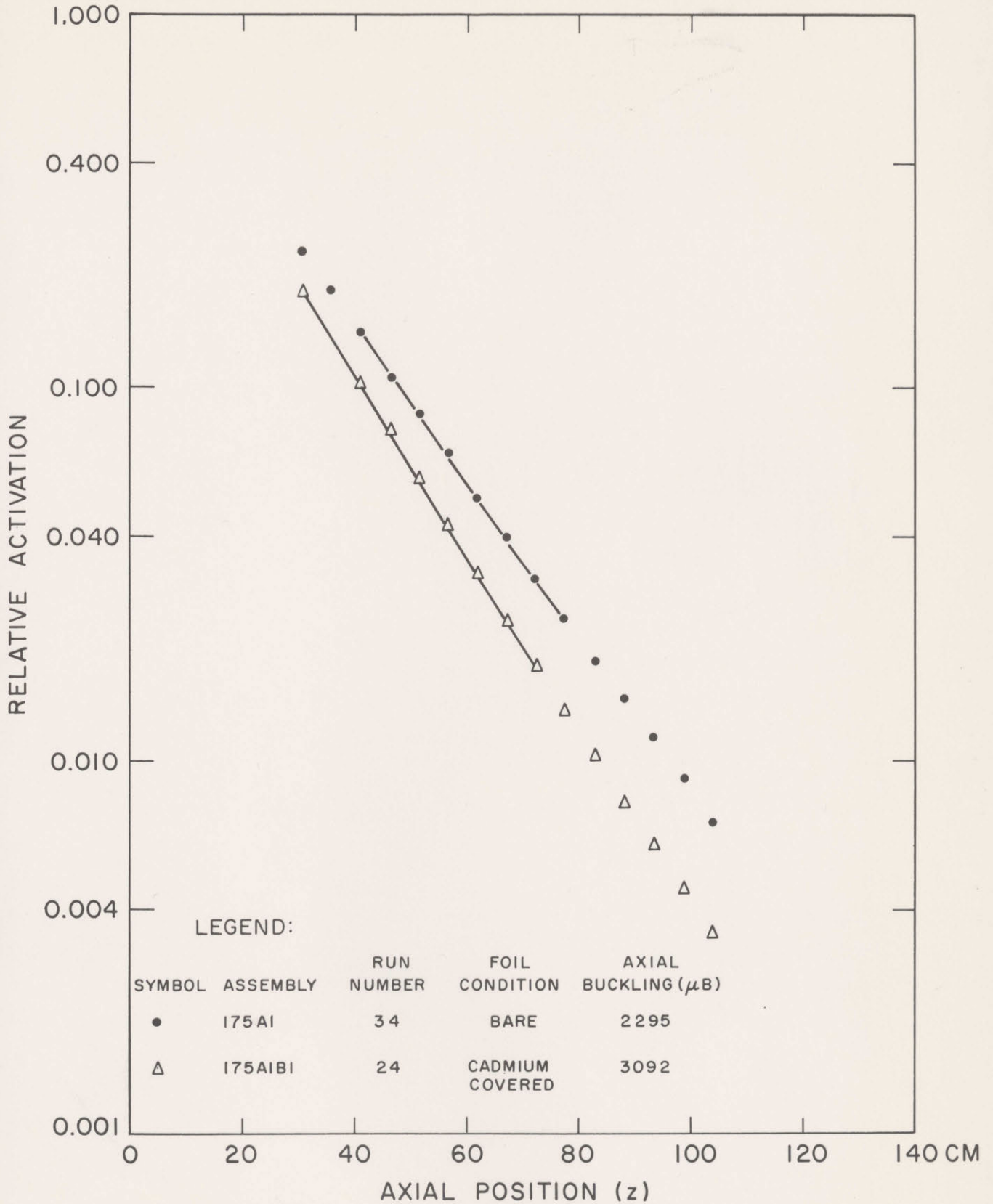


FIG.4.8 RELATIVE ACTIVATION DISTRIBUTION IN TWO 175 ASSEMBLIES AS A FUNCTION OF AXIAL POSITION. (GOLD FOILS USED WERE 0.010 INCHES THICK, 0.125 INCHES IN DIAMETER. UNCERTAINTY DUE TO COUNTING STATISTICS 0.2% TO 0.4%)

unfavorable experimental conditions only, the results of these exploratory measurements are not believed to be as reliable as those obtained with gold foils. Only four points remained in each distribution after the activities of foils above 71 cm in height, or within 10 cm of the cadmium sleeve used in the  $R_3$  measurement (see Sec. 3.10), had been dropped. The four points in each case spanned an axial distance of only 15.24 cm, and the uncertainties due to counting statistics are significantly greater than those in the traverses made with gold foils (0.33% as opposed to 0.20% or less). Although the data do not show statistically significant differences, for the sake of consistency with data from other assemblies, the value of the axial buckling for each assembly was derived solely from measurements with gold foils. Of the 44 axial traverses made with gold foils, five had to be discarded because of mechanical difficulties. A bent experimental fuel tube was used twice, and foil holders were improperly positioned twice. In one of the three experiments in which fuel rods were waterlogged (see Sec. 3.8.2), it was impossible to clean the foils satisfactorily; this run was discarded.

Of the approximately 700 experimentally observed foil activities, four were dropped because of difficulties with experimental equipment; five foils were accidentally lost in the course of the experiments.

The value of the axial buckling for each assembly was calculated by averaging the values for all traverses free of mechanical difficulties in that assembly; results are given in Sec. 5.1.

If a computed standard deviation for each fitted value of the buckling were available, the final value taken for the assembly could be the weighted average of the individual values, to which a standard deviation based on the computed uncertainties could be assigned. No such computed standard deviation is presently available, but an approximate upper limit can be calculated in the case of the axial fitting process. The technique used involves the calculation of the change in the buckling ( $\Delta\gamma_i^2$ ) necessary to reduce the residual at point  $i$  to zero, for all points of the distribution. The value of the coefficient  $A$  in the expression  $A \sinh \gamma(H_0 - z_i)$  is assumed to be constant. The r m s value of the buckling increments gives an indication of the standard deviation that should be assigned to the fitted value of  $\gamma^2$ , due to statistical scatter in the data points about the asymptotic distribution, provided



TABLE 4.6  
Comparison of RMS Value of Buckling Increment  
with S. D. of the Mean

Assemblies	Range of the S.D. of the mean of the axial buckling, from Table 5.1 ( $\mu$ B)	Range of the rms value of the buckling increment, calculated as described in text ( $\mu$ B)
250	4 - 22	3 - 15
175	15 - 35	5 - 39
253	12 - 14	7 - 16

the points in the distribution are far from the extrapolated end point of the assembly, as is the case here. In Table 4.6, the standard deviation of the mean for the axial buckling measurements in each of the three sets of assemblies is compared to the rms value of the buckling increments. The fact that the two are comparable in magnitude is taken as an indication that the scatter in the axial buckling data about the mean is not caused by a series of experimental errors but is caused by counting statistics. It does not, however, exclude the possibility of a systematic error.

The values of the buckling for the clean lattices were obtained by other workers on the Heavy Water Lattice Project (HE 4, HE 5). Close coordination and cooperation ensured that the same equipment and techniques were used in taking and analyzing the data in the unmodified lattices and in the assemblies with added absorbers. There should, therefore, be no systematic discrepancy between the two sets of buckling values. The generally smaller standard deviations assigned to the results for the unmodified lattices reflect the increased precision that could be obtained from the larger number of traverses made in these lattices. Furthermore, the assemblies containing added absorber rods showed a more complicated fine structure, with a greatly reduced area between rods where the flux was relatively flat. Hence, slight foil positioning errors tended to produce larger deviations from ideal behavior in the assemblies with added absorbers than in the unmodified lattices. This factor is particularly important in considering the results of the radial buckling determinations.



### 4.3 THE CALCULATION OF THE SPATIALLY-DEPENDENT THERMAL NEUTRON SPECTRUM AND THE THERMAL UTILIZATION

Although the present work is mainly experimental in nature, there are some parameters which are more readily calculated than measured or which can be measured only with great difficulty. In this connection, it is useful to be able to calculate the neutron energy spectrum as a function of position within the assembly, to provide a means of computing spectrum-dependent parameters, such as hardened cross sections for use in the calculation of the thermal utilization.

#### 4.3.1 Thermal Energy Range – Unmodified Lattices

The various alternatives for calculating the thermal neutron spectrum as a function of position, in lattices similar to those studied here, have been considered in detail by P. Brown (BR 1) and R. Simms (SI 1). Excellent agreement with experiment has been observed when the thermalization transport theory code THERMOS (HO 1, HO 2) was used in its modified one-dimensional form (HO 3). An independent investigation of the usefulness of THERMOS is offered by the work of Salah and Parkinson (SA 2). A thermal neutron beam extracted from various points in a subcritical, natural uranium fueled, heavy water moderated lattice was analyzed with a crystal spectrometer; excellent agreement with the results of THERMOS was reported. In view of these findings, this code was used extensively in the present work.

The calculation relates to a "unit cell" of a heterogeneous medium, infinite in extent. The unit cell is composed of a single fuel rod and the moderator associated with it. All unit cells are identical; thus, the neutron distribution throughout an infinite medium is known if the distribution in the unit cell is known. From considerations of symmetry, it is possible to specify the neutron distribution throughout the unit cell (and hence throughout the infinite medium) if the distribution is known over an appropriately chosen segment of the unit cell. The smallest such segment is here referred to as the "smallest repeating cell segment."

For a lattice of fuel rods on a triangular spacing  $S$ , the unit cell is a hexagon; the length of the sides is  $3^{-1/2} S$  and the area is  $(0.75)^{1/2} S^2$ . The smallest repeating cell segment is a right triangle, the area of which is  $1/12$  that of the unit cell (see Fig. 4.9). The



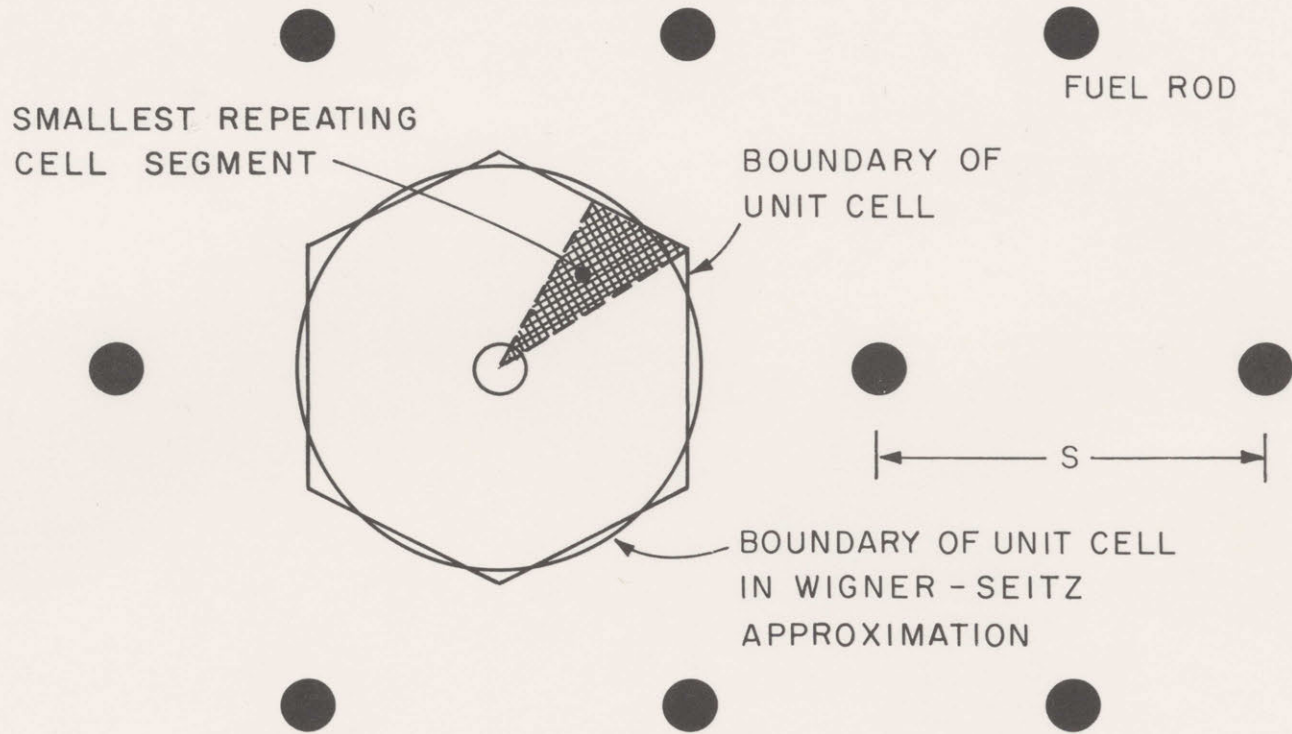


FIG.4.9 UNIT CELL AND SMALLEST REPEATING CELL SEGMENT IN A LATTICE ON A TRIANGULAR SPACING, S

Wigner-Seitz approximation consists of replacing the hexagonal boundary of the unit cell by a circle enclosing the same area; the problem of calculating the neutron distribution becomes a one-dimensional one. This approximation reduces greatly the effort necessary to calculate the neutron distribution and has been found to be appropriate in lattices of the type studied here (BR 1, SI1). For lattices on a triangular spacing  $S$ , the radius of the Wigner-Seitz cell is  $(3)^{1/4}(2\pi)^{-1/2} S$ , or  $0.52504 S$ .

The THERMOS code, as used here, obtains the space-dependent thermal neutron spectrum in one-dimensional cylinders by solving the integral transport equation numerically. Thirty energy groups (up to 0.78 eV) and twenty space points are used. The scattering kernel used for the moderator is the Nelkin kernel, adapted for heavy water by Honeck (HO 4). Diagonal elements have been corrected for anisotropic scattering, in keeping with Simms' conclusions on this point (SI 1). Free gas kernels are used for the other nuclides present. A spatially uniform  $1/E$  slowing-down source above 0.78 eV is assumed.

The cell boundary is assumed perfectly reflecting. It has been found necessary to include an extra cylindrical region outside the cell proper, composed of a very thin, very dense, fictitious medium of high scattering cross section (BR 1, SI 1, HO 3). The presence of this region has the effect of making the spatial distribution of neutrons reflected back into the cell from the boundaries less dependent on the neutrons' angle of incidence and greatly improves the agreement with experiment for tightly-packed lattices. This outer scattering region was used in all calculations.

The input data to the code consist of the dimensions of the regions in the cylindrical cell, the concentrations of the several isotopes in each region, and their cross sections. The input data used are tabulated in Appendix D.

The calculation of spectrally averaged quantities is made by the edit portion of the code after the spectrum at each space point has been calculated. The following definitions are used:



$$\bar{\Sigma}_i = \frac{\int_i \int_0^{v^*} v \Sigma(v) N(r, v) dv (2\pi r dr)}{\int_i \int_0^{v^*} v N(r, v) dv (2\pi r dr)}, \quad (4.7)$$

$$\bar{\phi}_i = \frac{\int_i \int_0^{v^*} v N(r, v) dv (2\pi r dr)}{V_i}, \quad (4.8)$$

$$\bar{N}_i = \frac{\int_i \int_0^{v^*} N(r, v) dv (2\pi r dr)}{V_i}, \quad (4.9)$$

$$V_i = \int_i (2\pi r dr), \quad (4.10)$$

$$\bar{v}_i = \frac{\int_i \int_0^{v^*} v N(r, v) dv (2\pi r dr)}{\int_i \int_0^{v^*} N(r, v) dv (2\pi r dr)}, \quad (4.11)$$

$$\bar{D}_{\text{mod}} = \frac{\int_{\text{mod}} \int_0^{v^*} \frac{\lambda_{\text{tr}}(v)}{3} v N(r, v) dv (2\pi r dr)}{\int_{\text{mod}} \int_0^{v^*} v N(r, v) dv (2\pi r dr)}. \quad (4.12)$$

In the equations,  $r$  is the position coordinate in the cylindrical cell,  $v$  is the neutron velocity,  $N(r, v)$  is the space-dependent neutron spectrum,  $\Sigma(v)$  is the energy-dependent reaction cross section,  $\lambda_{\text{tr}}(v)$  is the energy-dependent transport mean-free path, and  $v^*$  is the upper velocity limit on the integrations. The cross sections used are tabulated in Refs. HO 2 and HU 1. The values of  $\lambda_{\text{tr}}(v)$  in each of the thirty energy groups are derived and listed in Ref. PE 1. The integrations are, of course, replaced by appropriate summations in the numerical calculations.

The relative reaction rate in region  $i$  is  $\bar{\Sigma}_i \bar{N}_i \bar{v}_i V_i$ . If the averages are understood to be over the fuel rod volume, and the energy region below the cadmium cutoff, the calculated values of  $\eta$  and  $G$ , two parameters defined in Sec. 2.3, are:

$$\eta = v_{25} \frac{\bar{\Sigma}_{\text{fission}}(\text{U}^{25})}{\bar{\Sigma}_{\text{abs}}(\text{U}^{25}) + \bar{\Sigma}_{\text{abs}}(\text{U}^{28})}, \quad (4.13)$$

and

$$G = \frac{\bar{\Sigma}^{\text{abs}}(U^{28})}{\bar{\Sigma}^{\text{abs}}(U^{25}) + \bar{\Sigma}^{\text{abs}}(U^{28})} \quad (4.14)$$

The thermal utilization  $f$  may be calculated as:

$$f = \frac{\bar{\Sigma}_o^{\text{abs}} \bar{N}_o \bar{v}_o V_o}{\sum_{i=0}^2 \bar{\Sigma}_i^{\text{abs}} \bar{N}_i \bar{v}_i V_i} \quad (4.15)$$

with the subscript notation of Table 2.2. As discussed in Ref. PE 1, a good estimate of the diffusion coefficient  $\bar{D}$  averaged over the entire cell is afforded by Eq. (4.12) because of the similarity of  $\lambda_{\text{tr}}$  for the fuel and the moderator. Since the diffusion coefficient enters the calculation of  $k_\infty$  only through the correction factor  $\ell_s$ , and because the results are not strongly dependent on the value of the diffusion coefficient, the estimate afforded by Eq. (4.12) will here be used. If the lattice average absorption cross section  $\bar{\Sigma}^{\text{abs}}(\text{cell})$  is defined by Eq. (4.7) with the spatial integration done over the entire cell, a value of the diffusion area  $L^2$  is obtained from the relationship:

$$L^2 = \bar{D}_{\text{mod}} / \bar{\Sigma}^{\text{abs}}(\text{cell}) \quad (4.16)$$

#### 4.3.2 Thermal Energy Range – Modified Lattices

In lattices modified by the addition of an absorber distributed homogeneously throughout the moderator, the method of the foregoing section could be applied for the calculation of the neutron energy spectrum as a function of position. However, if the lattice is modified by the addition of lumped absorbers, the treatment must be extended. Provided that the lumped absorbers are distributed uniformly and their spacing is equal to the lattice spacing  $S$  or an integral fraction thereof, the hexagonal unit cell remains as described above. Each such cell is identical and is composed of the central fuel rod, the surrounding moderator, and one or more lumped absorbers. The size of the smallest repeating cell segment is generally larger in a modified lattice, although this need not be true.



As in the preceding discussion, knowledge of the neutron distribution over the smallest repeating cell segment is sufficient to specify the distribution throughout an infinite medium. However, neither the smallest repeating cell segment nor the unit cell is convenient for the calculation of the thermal neutron distribution in space and energy. It is more convenient to regard each element as being centered in a cylindrical cell and carry out independent THERMOS calculations for each cell.

Determination of Cell Sizes. The sizes of the various cells are no longer known a priori, as Suich has pointed out (SU 1). They can, however, be determined a posteriori: on the basis of calculations, as in the case of Suich's work; or on the basis of measurements, as is done here. Using heterogeneous source-sink theory, Suich shows that the cross-sectional area to be assigned to the cell about each lattice element is directly proportional to the number of absorptions in the element. In his work, a weakly-absorbing moderator, a uniform slowing-down source across the cell, and invariance of the cell boundaries with neutron energy are assumed; all these assumptions may be made for the lattices considered here.

These considerations seem to indicate an iterative approach. Consider an assembly composed of an equal number of fuel rods and copper rods, uniformly distributed. (Examples of such assemblies in this work are the 250B1, 250A1, and 175A1 assemblies, shown in Figs. 3.3, 3.4, and 3.7.) Cell sizes for cylindrical "fuel" and "copper" cells may be chosen on the basis of Suich's algorithm and reasonable guesses of the relative absorption in each (see Appendix F), subject to the requirement that the sum of the fuel cell area and the copper cell area is equal to the area of a unit cell. Separate THERMOS calculations may then be made for each of the two cells. From these calculations, a good approximation to the spectrally-averaged absorption cross sections of the fuel and copper rods is obtained.

In order to scale the relative neutron densities in the decoupled cells, the results of the microscopic traverses described in Sec. 3.9 are used. The experimental results, and the corrections applied to account for the effect of neutron leakage, are discussed later in this section. The corrected distribution is normalized to the distributions



calculated with the THERMOS code, at the center of each cell, as described in Appendix E.

New estimates of the relative absorption in the fuel and the copper, and the thermal utilization, are made next; THERMOS-calculated cross sections and relative neutron densities based on experiment are used wherever possible. (In the fuel rod cladding, and the annular region which surrounds the foils imbedded in the copper rods, the THERMOS-calculated neutron density distribution is used.) New cell sizes are calculated, and the THERMOS calculations repeated. Only two iterations were necessary; convergence was achieved rapidly. For instance, the value of the thermal utilization taken as an initial guess for the 250A2 assembly was 0.570; the value obtained from the first set of calculations was 0.534, and the value obtained from the second set was 0.533. Since the change in the value of the thermal utilization resulting from the second set of calculations was less than the uncertainty associated with it in every case, a third set of calculations was unnecessary.

Confidence in the iterative method just described is increased by the fact that values of  $\bar{v}$  at the outer edges of the two cells in the final calculation always agreed within 0.8% or less; the same is true for  $\bar{\Sigma}$ .

The values of  $\bar{\Sigma}_i$ ,  $\bar{\phi}_i$ ,  $\bar{N}_i$ ,  $V_i$ ,  $\bar{v}_i$ ,  $\bar{D}_{\text{mod}}$ ,  $\eta$ ,  $G$ ,  $f$ , and  $L^2$  for the modified lattices were obtained from Eqs. (4.7) to (4.16). The results of the second set of THERMOS calculations provided the values of  $\bar{\Sigma}_i$  and  $\bar{v}_i$ ; values of  $\bar{N}_i$  were derived from observed foil activities wherever possible. The analysis was made with the aid of a digital computer; the method is discussed in greater detail in Appendix E.

The generalization to two or more copper rods per unit cell is straightforward; the rods need not be of the same size.

The Microscopic Traverses. Since the THERMOS calculation to which the results of the microscopic traverses are compared is made for a cylindrical cell in an infinite assembly, the observed foil activities had to be corrected for the effect of neutron leakage from the finite assembly. The correction was made by dividing all activities by the function  $J_0(aR)$ , where  $R$  is the radial position of the foil and  $a$  is the square root of the radial buckling (SI 1). Because all foils were near the center of the assembly, the correction factor deviated from unity by at most 3%.

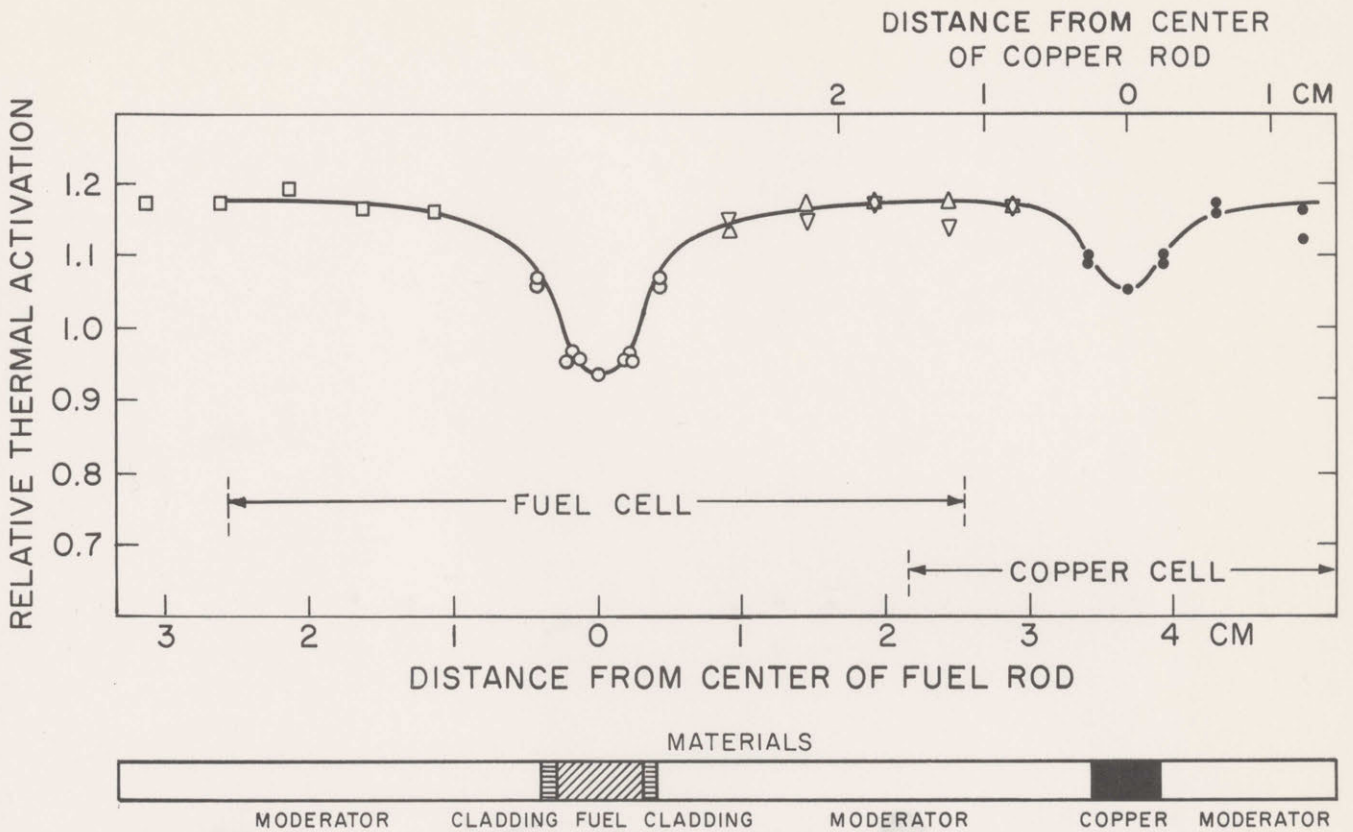


Foil activities also had to be corrected for differences in axial position. All activities were multiplied by the function  $e^{\gamma(z-z_0)}$ , where  $\gamma$  is the square root of the axial buckling,  $z$  the distance of the foil from the bottom of the assembly, and  $z_0$  a reference height taken, for convenience, as 20 inches.

The assumption is made here that the microscopic and macroscopic distributions are completely separable in the region where the microscopic traverses were done, and that the corrections just described are sufficient to account for the effects of neutron leakage. In Ref. CR 1, an inseparability effect peculiar to assemblies with separated fuel and absorbers is mentioned; it causes the ratio of the neutron flux in the fuel to that in the absorbers to vary as the macroscopic distribution  $J_0(aR)$ . The source of the effect is not described, but a formula correcting the value of the thermal utilization to the infinite medium value is given. The ratio of the value of  $f$  for an infinite medium to the value measured in an experiment in the neighborhood of a fuel rod at a distance  $R_u$  from the center of the assembly is given as  $[1 - A_3 f(1 - J_0^{-1}(aR_u))]^{-1}$ , where  $A_3$  is the ratio of thermal absorptions in the absorber rods to thermal absorptions in the fuel. Since all microscopic traverses were done in the neighborhood of the central fuel rod of the assembly, the value of  $R_u$  is zero, and no correction factor is necessary.

Two microscopic traverses were made in each assembly, resulting in two independent measurements of the relative absorption in all the materials present. The two values of the thermal utilization agree, on the average, within 0.45%. The maximum discrepancy is 1.13%. Difficulties caused by counter malfunctions, and errors in assembling the central cluster, place the results of both runs in the 175A1B1 assembly in question; the values of the thermal utilization agree within 0.90%. The effect on the value of  $k_\infty$  derived for the 175 lattice is slight and is discussed further in Sec. 5.4.

Two examples of microscopic distributions, corrected for neutron leakage, are given in Figs. 4.10 and 4.11. The activation distribution calculated by THERMOS is given for comparison.



LEGEND:

- ◻ ◻  
 ▽ ▽
 
{
 EXPERIMENTAL ACTIVITIES  
 PLOTTED AS A FUNCTION OF  
 DISTANCE FROM CENTER OF  
 FUEL ROD
  
- {
 EXPERIMENTAL ACTIVITIES  
 PLOTTED AS A FUNCTION OF  
 DISTANCE FROM CENTER OF  
 COPPER ROD

PLAN VIEW OF MICROSCOPIC TRAVERSE  
SHOWING POSITIONS OF RODS AND FOILS

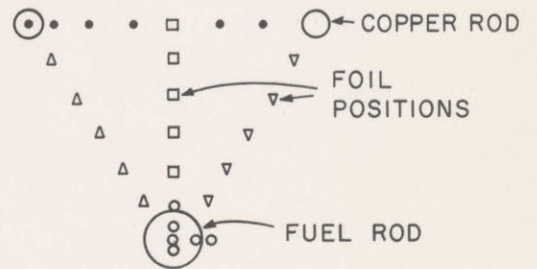
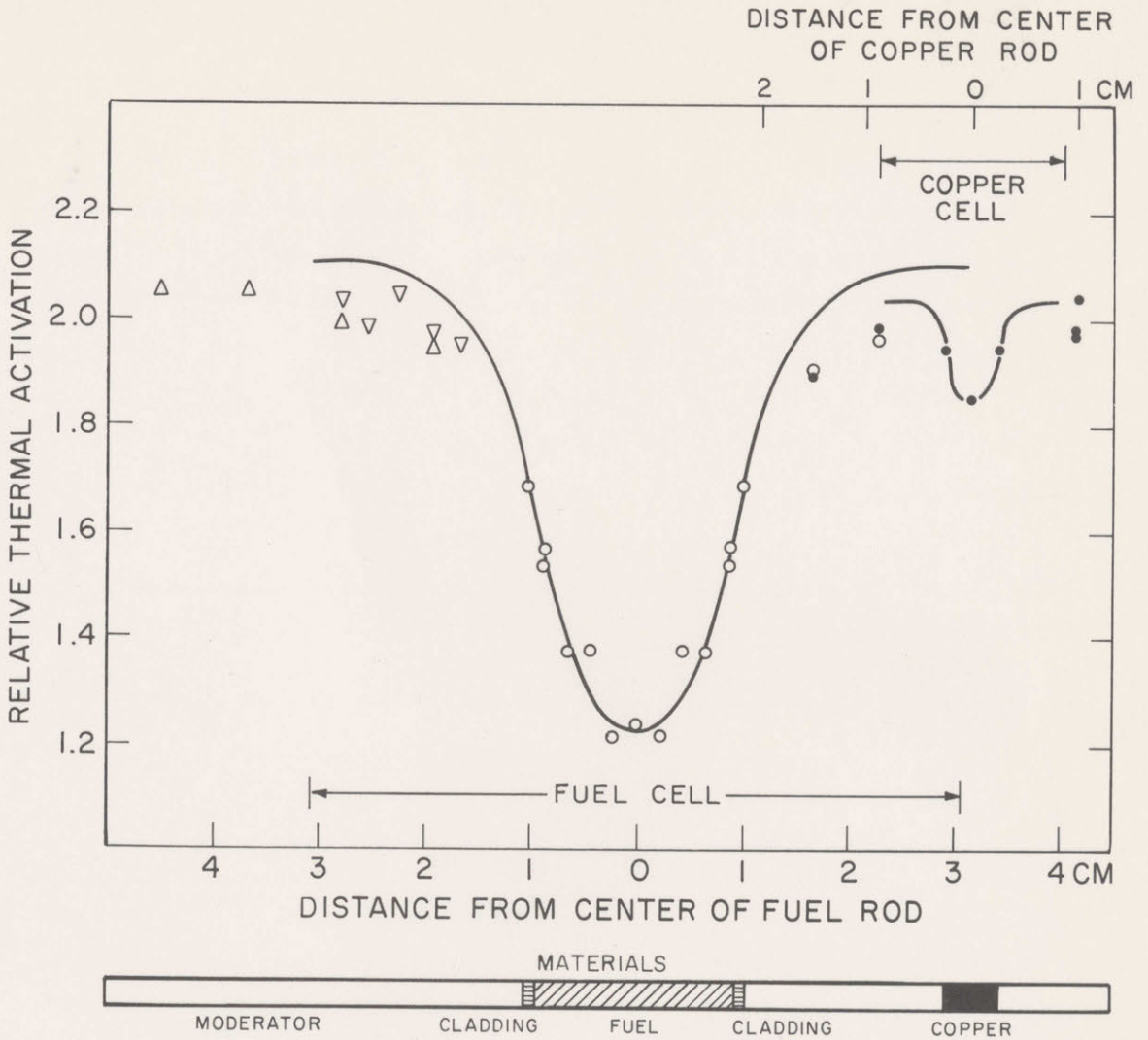


FIG. 4.10 RELATIVE THERMAL ACTIVATION DISTRIBUTION NEAR CENTER FUEL ROD IN 250A2 ASSEMBLY (RUN 7). (GOLD FOILS USED WERE 0.010 INCHES THICK, 0.0625 INCHES IN DIAMETER. UNCERTAINTY DUE TO COUNTING STATISTICS 0.28%. SOLID LINES SHOW THERMOS-CALCULATED RELATIVE THERMAL ACTIVATION DISTRIBUTION.)





PLAN VIEW OF MICROSCOPIC TRAVERSE, SHOWING POSITIONS OF RODS AND FOILS

LEGEND:

$\Delta$   $\nabla$  { EXPERIMENTAL ACTIVITIES PLOTTED AS A FUNCTION OF DISTANCE FROM CENTER OF FUEL ROD

$\circ$  { EXPERIMENTAL ACTIVITIES PLOTTED AS A FUNCTION OF DISTANCE FROM CENTER OF COPPER ROD

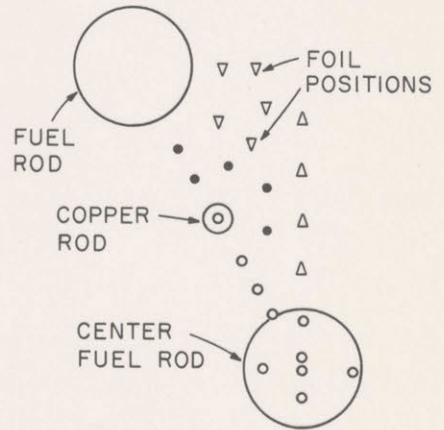


FIG. 4.11 RELATIVE THERMAL ACTIVATION DISTRIBUTION NEAR CENTER FUEL ROD IN 253A2 ASSEMBLY (RUN 48). (GOLD FOILS USED WERE 0.005 INCHES THICK, 0.0625 INCHES IN DIAMETER. UNCERTAINTY DUE TO COUNTING STATISTICS 0.65%. SOLID LINES SHOW THERMOS-CALCULATED RELATIVE THERMAL ACTIVATION DISTRIBUTION.)

#### 4.4 CALCULATION OF RATIO OF EPITHERMAL AND THERMAL REACTION RATES ( $\rho_i, \delta_{25}$ )

Although the neutron energy spectrum in the epithermal energy range does not need to be treated in great detail, it is necessary to make some assumptions concerning it because some of the ratios of epithermal to thermal reaction rates ( $\rho_i, \delta_{25}$ ) appearing in the formula for the resonance escape probability (Eq. 2.24) have been calculated rather than measured. Measurements of  $\delta_{25}$  were made in unmodified lattices only;  $\rho_3$  for the copper rods was measured only in the 253A2B1 and 253A2 assemblies; and the values of  $\rho_1$  and  $\rho_2$ , which relate to the moderator and cladding, were calculated.

The method makes extensive use of the results of the THERMOS calculations for the fuel and copper cells described in the preceding subsection, but it is not a part of the THERMOS code and should not be confused with it.

It is assumed that the epithermal neutron flux varies as  $1/E$ . This energy dependence is derived in the theoretical treatments of media with low absorption cross sections, but experiments show that it is also valid in many practical cases (AN 2), and it is commonly used. Cross sections are assumed to vary with neutron velocity as  $1/v$  in the thermal energy region. The cladding and moderator are also treated as  $1/v$  absorbers in the epithermal region, while  $U^{235}$  and copper are treated as resonance absorbers. Resonance integrals are derived from measurements in closely related assemblies.

Consider first the calculation of  $\rho_1$  and  $\rho_2$ . We have:

$$\rho_i = \frac{\int_i \int_{v_c}^{v_T} \phi(\vec{r}, v) \Sigma_i(v) dv d\vec{r} + \int_i \int_{v_T}^{\infty} \phi(\vec{r}, v) \Sigma_i(v) dv d\vec{r}}{\int_i \int_0^{v_c} \phi(\vec{r}, v) \Sigma_i(v) dv d\vec{r}}. \quad (4.17)$$

The spatial constancy of the absorption cross section  $\Sigma_i(v)$  within the region  $i$  is assumed. The upper limit of the neutron speed in the thermal region is  $v_c$ , and that of the highest-energy group in the THERMOS calculation is  $v_T$ . From the definition of the neutron flux, we have:

$$\phi(\vec{r}, v) = vn(\vec{r}, v). \quad (4.18)$$



The continuous function  $n(\vec{r}, v)$  is approximated in practice (over the range  $0 \leq v \leq v_T$ ) by the matrix  $N(K, I)$  calculated by the THERMOS code;  $K$  is a spatial index relating to the several subregions in region  $i$ , and  $I$  is the energy group index ( $1 \leq I \leq 30$ );  $N$  is a density in both space and velocity. If it is assumed that the epithermal neutron flux varies as  $1/E$ , then the epithermal neutron density varies as  $1/v^2$ . The requirement that the neutron density be continuous at  $v_T$  specifies the constant of proportionality:

$$n(\vec{r}, v) = \frac{[N(K, 30)][v_{30}][v_{31}]}{v^2}, \quad v_c \leq v. \quad (4.19)$$

Here,  $v_{30}$  and  $v_{31}$  are the lower and upper velocity limits of the 30<sup>th</sup> group of the THERMOS calculation. On the assumption that the velocity dependence of the absorption cross sections for the cladding and moderator are adequately represented by a  $1/v$  variation, we may write:

$$\Sigma_i(v) = \frac{\Sigma_i v_0}{v}, \quad 0 \leq v \leq \infty. \quad (4.20)$$

Here,  $\Sigma_i$  is the absorption cross section of the  $i^{\text{th}}$  material for neutrons of energy  $v_0$ . Under these assumptions, Eq. (4.17) may be written in the form:

$$\rho_i = \frac{[\bar{N}_i \bar{v}_i \bar{\Sigma}_i V_i]_{28}^{30} + \Sigma_i v_0 v_{30} \bar{N}(i, 30) V_i}{[\bar{N}_i \bar{v}_i \bar{\Sigma}_i V_i]_1^{27}}. \quad (4.21)$$

Here, Eqs. (4.7), (4.9), (4.10), and (4.11) have been applied; the sub- and superscripts on the bracketed expressions refer to the lower and upper limits of the summation over the discrete spectrum produced by THERMOS;  $\bar{N}(i, 30)$  is the volume-averaged value of  $N(K, 30)$ , over material  $i$ . For the 0.020-inch-thick cadmium covers used in the experiments, summation over the first 27 THERMOS groups is appropriate. The upper limit of the thermal energy range is then 0.415 ev.

For a  $1/v$  absorber,  $\bar{v}_i \bar{\Sigma}_i$  is equal to  $v_0 \Sigma_i$ , as reference to Eqs. (4.7), (4.11), and (4.20) will show. This permits the following simple expression for  $\rho_i$ :

$$\rho_i = \frac{[\bar{N}_i]_{28}^{30} + v_{30} \bar{N}(i, 30)}{[\bar{N}_i]_1^{27}}. \quad (4.22)$$

Values of all parameters appearing in Eq. (4.22) may be obtained from the output of the THERMOS code, either directly from the printed output or from the matrix  $N(K, I)$  which is printed and punched on data cards. The velocity is a dimensionless variable based on 2200 m/sec; for the usual THERMOS velocity mesh,

$$\begin{aligned} v_0 &= 1, \\ v_{30} &= 5.285, \\ v_{31} &= 5.855. \end{aligned} \quad (4.23)$$

The derivation of the expression for  $\delta_{25}$  and  $\rho_3$  is similar to that just used: Eq. (4.17) is again the defining expression, with the integrations over the volume of the rod in question. Equations (4.18) and (4.19) also apply. But it is necessary to assume that  $N(K, 30)$  is constant in all parts of the rod; this requirement is met in the cases of interest here, to within 1.1%. If an effective resonance integral is defined as:

$$\text{ERI}(i) = \frac{\int_i d\vec{r} \int_{v_c}^{\infty} \Sigma_i(v) \frac{dv}{v}}{V_i}, \quad (4.24)$$

for the rod, then Eq. (4.17) may be rewritten in the manner of Eq. (4.21) as follows:

$$\rho_i = \frac{[\bar{N}_i \bar{v}_i \bar{\Sigma}_i V_i]_{28}^{30} + \bar{N}(i, 30) v_{30} v_{31} V_i \text{ERI}(i)}{[\bar{N}_i \bar{v}_i \bar{\Sigma}_i V_i]_1^{27}}. \quad (4.25)$$

This expression may be further simplified, in the same manner as Eq. (4.22):

$$\rho_i = \frac{[\bar{N}_i]_{28}^{30} + v_{30} v_{31} \bar{N}(i, 30) \left[ \frac{\text{ERI}(i)}{\Sigma_i} \right]}{[\bar{N}_i]_1^{27}}. \quad (4.26)$$

Equation (4.26) relates  $\rho_i$ , the ratio of epithermal to thermal events, to an appropriate resonance integral, in terms of parameters obtainable as before from the THERMOS output.

It has been assumed throughout that only small perturbations in



the neutron distribution in the epithermal energy range are caused by the addition of copper rods to the lattices. In particular, the value of the effective resonance integral is taken as constant. At least one measurement of  $\rho_i$ , e. g. from measured cadmium ratios, is necessary to establish the value of  $ERI(i)$  in an assembly for which a THERMOS calculation is available. Once this is done, values of  $\rho_i$  may be calculated in any similar assemblies for which THERMOS calculations have been performed.

It is important that parameters measured in finite assemblies be corrected by means of an equation analogous to Eq. (2.26) to their infinite medium values, since the foregoing treatment does not otherwise account for the effect of leakage.

The assumptions made in the course of these two derivations would appear to limit their usefulness severely. To test the method, values of  $(ERI/\Sigma)$  were calculated from the measured values of  $\rho_{28}$ ; results are given in Table 4.7. Although, in this case, the assumptions appear least applicable, no value deviated more than 8.2% from the mean. When the mean value of  $ERI/\Sigma$  for each rod type was used to calculate values of  $\rho_{28}$  for each assembly, no value deviated more than 8.7% from the measured value; the r m s value of the deviations was 3.9% (see Table 4.7). The method was, therefore, considered to be sufficiently accurate for use in the present application, as the following considerations show.

The resonance escape probability is calculated from Eq. (2.24):

$$p = \frac{1 + \frac{\epsilon - 1}{\epsilon} \frac{a_{28}}{v_{28} - 1 - a_{28}} \frac{1}{\ell_f}}{1 + \ell_r \ell_s f \left[ \rho_{28} G + \sum_{i=1}^3 \rho_i A_i + \frac{\delta_{25} (1 + a_{25}) n (1 - G)}{v_{25}} \right]} \quad (4.27)$$

The value of the second term in the numerator is always less than 0.0027 here, so that the value of  $p$  is almost completely determined by the second term in the denominator. In the 250 and 175 assemblies, the term  $\rho_{28} G$  accounts for 62% to 83% of the value of the second term in the denominator; measured values of  $\rho_{28}$  with uncertainties less than 2% are available for all the assemblies, and the values of the  $\rho_i$  and  $\delta_{25}$  terms are calculated. If an upper limit on the uncertainty in

TABLE 4.7  
Measured and Calculated Value of  $\rho_{28}$

Assembly	Measured Value of $\rho_{28}$	$\left[ \frac{\text{ERI}}{\Sigma} \right]$ (See Note 1)	Calculated Value of $\rho_{28}$ (See Note 2)	Deviation of Calculated Value from Measured Value (%)
250	0.234	2.473	0.239	+ 1.9
250B1	0.247	2.495	0.249	+ 1.0
250A1	0.262	2.687	0.246	- 6.0
250B2	0.272	2.637	0.260	- 4.3
250A2	0.291	2.314	0.317	+ 8.7
175	0.475	2.518	0.489	+ 2.9
175A1	0.527	2.653	0.515	- 2.2
175A1B1	0.592	2.604	0.589	- 0.4
253	1.358	2.181	1.374	+ 1.2
253A2			1.407	
253A2B1	1.442	2.235	1.425	- 1.2

Note 1: Value of  $\left[ \frac{\text{ERI}}{\Sigma} \right]$  based on measured value of  $\rho_{28}$ .

Note 2: Average value of  $\left[ \frac{\text{ERI}}{\Sigma} \right]$  used for each lattice:

<u>Lattice</u>	
250	2.521
175	2.592
253	2.208



these terms, due to the method of calculation, is taken as 5%, the uncertainty in the expression in brackets in the second term in the denominator is 2.2% at most; the resulting uncertainty in the value of  $p$  is limited to less than 0.22%. In the 253 lattice and the two 253 assemblies, the term  $\rho_{28}G$  accounts for 81% to 85% of the resonance absorptions. The two measured values of  $\rho_{28}$  have uncertainties of 1.9% and 2.1%. Assuming the  $\rho_{28}G$  term to be known, in all three cases, within 4.0%, the measured values of the  $\rho_3A_3$  term to within 2.0%, and the calculated values of the  $\rho_i$  and  $\delta_{25}$  terms within 5%, the uncertainty in the expression in brackets in the second term in the denominator is 3.5% at most. The resulting uncertainty in the value of  $p$  is 1.0% or less.

The value of the expression  $(1+\delta_{25})$  is also obtained from the values of  $\delta_{25}$  calculated for each of the assemblies. An uncertainty of 5% in the calculated values results in an uncertainty in the value of  $(1+\delta_{25})$  which varies from 0.11% to 0.44%.

The method just described has advantages over other methods in which a maxwellian spectrum is joined to a "1/E tail." First, the assumption of a maxwellian is unnecessary, since the THERMOS-calculated spectrum is used. Second, there is no problem of deciding how and where to join the two spectra; the THERMOS calculation carries the spectrum into the 1/E region.

#### 4.5 LEAST SQUARES FITTING

As stated in Chap. II, the values of the parameters appearing in Eq. (2.28) are obtained by a least squares fitting process. Each parameter is plotted against the material buckling, and a first or second degree polynomial is fitted to the data. The leading (constant) term of the polynomial is taken as the best estimate of the value of the parameter for an assembly with zero material buckling. Points were not weighted in the fitting process.

The variations in the correction terms  $\left(\frac{\epsilon}{\epsilon'}\right)$ ,  $\left(\frac{\eta}{\eta'}\right)$ ,  $\left(\frac{p}{p'}\right)$ ,  $\left(\frac{1+\delta_{25}}{1+\delta'_{25}}\right)$ ,  $(A'_1-A_1)$ , and  $(A'_2-A_2)$  over the entire range of bucklings are so small (see Tables 5.3 and 5.8) that the polynomial order is not of great consequence in determining the value of these quantities at zero buckling. The degree of fit was calculated each time a least squares fit was made, and the fit corresponding to a minimum value of this quantity was used. The degree of fit is defined as:



$$\frac{\sum_{i=1}^M (x_i - P_i)^2}{M - N - 1}, \quad (4.28)$$

where  $x_i$  is a data point,  $M$  is the number of such data points,  $N$  the order of the polynomial approximation to the data, and  $P_i$  the value of the polynomial at point  $i$  (WO 2).

The quantity  $A_3^0$  determines the value of  $k_\infty$  almost completely, and thus it is important that an appropriate function be fitted to the measured and calculated values of  $A_3$  in the several assemblies. Assume that the material buckling  $B_m^2$  is related to  $k_\infty$  by Eq. (2.31) and that thermal neutron absorptions in cladding and moderator may be neglected, so that the expression for the thermal utilization,  $f$ , (Eq. (2.18)) becomes  $(1+A_3)^{-1}$ . If the spectral perturbation is small, the diffusion area of the modified lattices is approximated by the quantity  $fL^2$ , where  $L^2$  is the diffusion area of the unmodified lattice. The Fermi age,  $\tau$ , may be presumed constant (see Appendix G). Substitution of these expressions for the thermal utilization and the diffusion area into Eq. (2.31), and use of Eq. (2.7) for  $k_\infty$ , leads to the result,

$$A_3 = \eta\epsilon\rho(1+\delta_{25}) \left[ 1 - \tau B^2 + \frac{1}{2}(\tau B^2)^2 - \dots \right] - (1+L^2 B^2), \quad (4.29)$$

$$A_3 = [\eta\epsilon\rho(1+\delta_{25}) - 1] - [L^2 + \tau\eta\epsilon\rho(1+\delta_{25})] B^2 + \\ + \left[ \frac{1}{2}\eta\epsilon\rho(1+\delta_{25})\tau^2 \right] B^4 - \dots \quad (4.30)$$

Because the magnitude of the quantity  $\tau B^2$  is always less than 0.2 here, the series in brackets in Eq. (4.29) converges quickly. It is evident from this equation that, in this approximation at least, a polynomial of low degree in  $B^2$  should correlate the data well. Polynomials of degree one, two, and three were tried in the fitting process on the data from the 250 assemblies; the degree of fit was minimal for a second degree polynomial. Accordingly, second degree polynomials were used to obtain the value of  $A_3^0$ .

It may therefore be reasonably assumed that the fitting process itself does not introduce significant errors into the fitted value of  $A_3^0$ .



To ascertain the effect on the value of  $A_3^0$  of the uncertainty in the buckling value of a particular assembly, the least squares analysis by which  $A_3^0$  was determined was repeated twice, once with the buckling for the assembly in question equal to the observed value plus one standard deviation, and once with the buckling equal to the observed value minus one standard deviation. The average change in the value of  $A_3^0$  is the uncertainty in the fitted value caused by the uncertainty in the buckling value of the assembly in question. To obtain the standard deviation of the value of  $A_3^0$ , the uncertainty caused by the uncertainties in the buckling values and  $A_3$  values for each of the assemblies was evaluated; since these are independent, the total uncertainty was calculated as the square root of the sum of their squares.

## CHAPTER V

### RESULTS AND CONCLUSIONS

The results of the investigation are given in this chapter. Sections 5.1 to 5.5 concern the determination of  $k_{\infty}$  for the three lattices studied (250, 175, 253). For the sake of comparison, values of measured and calculated parameters (HE 4, HE 5) for the 125 lattice are also given, although this lattice was not studied as part of the present work. Section 5.6 concerns the measurement of the age and the diffusion area; the results of the exploratory experiments on the two-region assembly are given in Sec. 5.7. The conclusions drawn from the work are given in Sec. 5.8.

#### 5.1 BUCKLING

The determination of the material buckling is discussed in Secs. 2.1.3 and 4.2. The results are listed in Table 5.1. The extrapolated radius  $R_0$  corresponding to the measured value of the radial buckling is also given in Table 5.1. The  $D_2O$  temperature during the measurements varied from a reference value of 25°C by no more than 5°C. In independent work on the Heavy Water Lattice Project, the dependence of the material buckling on temperature has been studied. The material buckling of a lattice identical to the 250 lattice (except for its enrichment, which was 1.027%) was measured at 18°C, 27°C, and 60°C (HE 4). The temperature coefficient of the buckling ( $\partial B_m^2 / \partial T$ ) was less than 1.8  $\mu B / ^\circ C$ . Thus, any corrections to the measured bucklings would be less than 9  $\mu B$ , which is insignificant in comparison to the uncertainty already assigned to most of them.

The moderator purity for each lattice is listed in Table 3.1. Measurements of the variation of material buckling with moderator purity have not been undertaken. The variation of the moderator purity over the course of the work on any one lattice is smaller (0.01%) than the uncertainty (0.03%) in the measured values of the purity, rendering such corrections insignificant in the present study.

The values of the radial buckling for the modified assemblies are



TABLE 5.1  
Measured Bucklings

Designator	Radial Buckling ( $\mu\text{B}$ )	Extrapolated Radius (cm)	Axial Buckling ( $\mu\text{B}$ )	Material Buckling ( $\mu\text{B}$ )
250	2403 $\pm$ 16 (10)	49.00	1396 $\pm$ 7 (8)	1007 $\pm$ 17
250B1	2410 $\pm$ 19 (3)	48.99	1997 $\pm$ 9 (6)	413 $\pm$ 21
250A1	2307 $\pm$ 89 (3)	50.07	2313 $\pm$ 16 (4)	-6 $\pm$ 90
250B2	2388 $\pm$ 11 (3)	49.21	2512 $\pm$ 4 (4)	-124 $\pm$ 12
250A2	2353 $\pm$ 43 (4)	49.57	3073 $\pm$ 22 (4)	-720 $\pm$ 48
175	2418 $\pm$ 4 (10)	48.90	1013 $\pm$ 12 (10)	1405 $\pm$ 13
175A1	2327 $\pm$ 19 (3)	49.85	2309 $\pm$ 35 (4)	18 $\pm$ 40
175A1B1	2229 $\pm$ 30 (2)	50.94	3083 $\pm$ 15 (5)	-854 $\pm$ 34
125*	2392 $\pm$ 6 (14)	49.17	948 $\pm$ 8 (7)	1444 $\pm$ 10
253	2364 $\pm$ 8 (5)	49.40	1395 $\pm$ 7 (9)	969 $\pm$ 11
253A2	2313 $\pm$ 74 (1)	50.01	2125 $\pm$ 12 (3)	188 $\pm$ 75
253A2B1	2353 $\pm$ 76 (3)	49.57	2339 $\pm$ 14 (3)	14 $\pm$ 77

Note: The number in parentheses following the radial and axial buckling values is the number of independent measurements of the value that were made.

\* See Ref. HE 4.

lower than the values for the unmodified lattice in all cases but one, although the difference is generally less than two standard deviations. This is in keeping with the observation that values of the radial buckling measured in lattices are lower than those measured in pure moderator. The value of the radial buckling measured in pure moderator in the tank used for these measurements has been measured and found to be  $2539 \pm 2 \mu\text{B}$  (HA 1, HE 3).

The uncertainties assigned to the values of the material buckling of the lattices without added absorber are smaller than those assigned to the values for the modified lattices, chiefly because of the larger number of experiments done in the former, as discussed at the end of Sec. 4.2.2. The three measured values of the radial buckling in the 250A1 assembly did not agree well, and the large uncertainty calculated reflects this fact. The same is true of the radial buckling value of the 253A2B1 assembly. The radial buckling value of the 175A1B1 assembly appears suspiciously low; only two measurements are available ( $2214 \mu\text{B}$  and  $2241 \mu\text{B}$ ). As noted previously (see Table 3.5), only one measurement of the radial buckling was made in the 253A2 assembly. The uncertainty assigned is the average value of the standard deviation for a single observation of the radial buckling in the other assemblies, for which three or more measurements are available.

The effect of these uncertainties on the measured values of  $k_\infty$  is discussed in Sec. 5.4.

## 5.2 PARAMETERS CHARACTERIZING THE THERMAL ENERGY REGION

The values of  $\eta$ ,  $\bar{D}$ ,  $\bar{\Sigma}_a(\text{cell})$ , and  $L_s^2$ , calculated for each of the lattices and assemblies by means of Eqs. (4.15), (4.14), (4.9), and (4.18), respectively, are listed in Table 5.2. No value of  $\bar{D}$  for the 125 lattice was available; the value of  $L_s^2$  for a similar lattice with slightly lower enrichment (1.027%) was used (DA 1). Values of  $G$  calculated by means of Eq. (4.16) are in Table 5.3, as are values of the  $A_1$  and  $f$  determined by the combination of measurement and calculation described in Sec. 2.3.3. The subscript 4 refers to the cladding on the copper rods. Absorption in the  $\text{H}_2\text{O}$  present in the heavy water is included in the  $A_1$  term (and, incidentally, accounts for



TABLE 5.2

Parameters Characterizing the Thermal Energy Region (I)

Designator	Neutron Regeneration Factor ( $\eta$ )	Diffusion Coefficient ( $\bar{D}$ ) (cm)	Average Macroscopic Absorption Cross Section ( $(\bar{\Sigma}_a(\text{cell}))$ ) ( $\text{cm}^{-1}$ )	Diffusion Area ( $L_s^2$ ) ( $\text{cm}^2$ )
250	1.5319	0.8623	0.003270	264
250B1	1.5314	0.8659	0.004148	209
250A1	1.5311	0.8678	0.004504	192
250B2	1.5309	0.8688	0.004835	180
250A2	1.5303	0.8726	0.005768	151
175	1.5300	0.8745	0.006446	136
175A1	1.5284	0.8844	0.008925	99
175A1B1	1.5276	0.8895	0.010195	87
125	1.5265		0.011915	74
253	1.4408	0.9128	0.01775	51
253A2	1.4392	0.9204	0.02046	46
253A2B1	1.4388	0.9226	0.02142	44

TABLE 5.3

## Parameters Characterizing the Thermal Energy Region (II)

Designator	Ratio of Absorptions in Various Materials to Absorptions in Fuel					
	Moderator (A <sub>1</sub> )	Fuel Rod Cladding (A <sub>2</sub> )	Copper (A <sub>3</sub> )	Copper Rod Cladding (A <sub>4</sub> )	U <sup>238</sup> (G)	Thermal Utilization (f)
250	0.03433	0.01609	0.	0.	0.2606	0.9520
250B1	0.03314	0.01609	0.2490	0.00377	0.2607	0.7681
250A1	0.03401	0.01609	0.4057	0.00473	0.2608	0.6847
250B2	0.03341	0.01609	0.4905	0.00742	0.2608	0.6463
250A2	0.03350	0.01609	0.8178	0.00954	0.2609	0.5328
175	0.01716	0.01609	0.	0.	0.2610	0.9678
175A1	0.01666	0.01608	0.4043	0.00471	0.2614	0.6936
175A1B1	0.01643	0.01608	0.6198	0.00826	0.2616	0.6022
125	0.00743	0.01624	0.	0.	0.2619	0.9769
253	0.00536	0.00624	0.	0.	0.3022	0.9885
253A2	0.00504	0.00623	0.1271	0.00147	0.3025	0.8773
253A2B1	0.00494	0.00622	0.1673	0.00208	0.3026	0.8470



approximately 77% of that term). Thermal neutron absorption in the air in the gap between the fuel and the cladding was calculated to be 0.00172% of the absorption in the fuel in the 250 and 175 assemblies, and 0.00048% of the absorption in the fuel in the 253 assemblies. These absorptions were neglected in the calculation of the thermal utilization.

### 5.3 PARAMETERS CHARACTERIZING THE EPITHERMAL ENERGY REGION

The values of  $R_3$ ,  $\rho_3$ ,  $R_{28}$ ,  $\rho_{28}$ ,  $\rho_1$ ,  $\rho_2$ ,  $\rho_4$ ,  $\delta_{25}$ , and  $\delta_{28}$  are listed in Tables 5.4 to 5.6. Measured parameters are listed in Tables 5.4 and 5.5; calculated parameters are given in Table 5.6. The values of the parameters listed are those associated with the finite assembly.

Measured values of  $R_3$ , the cadmium ratio for a copper rod, are given in Table 5.5, together with the corresponding values of  $\rho_3$ . The value of  $\left(\frac{\text{ERI}}{\Sigma}\right)_{\infty}$  appropriate for use in Eq. (4.28) was found to be 0.2673 for the A copper rods, and 0.2517 for the B copper rods. The subscript ( $\infty$ ) indicates that the value of  $\rho_3$  obtained with this value of  $\left(\frac{\text{ERI}}{\Sigma}\right)_{\infty}$  is that for an infinite lattice; it must be corrected, as indicated in Sec. 4.4, to obtain the value for a finite assembly.

The calculated value of  $\rho_{28}$  for the 253A2 assembly is given in Table 5.6; the resonance integral used is given in Table 4.7. Values of  $\rho_i$  (for  $i=1, 2$ , and  $4$ ) obtained from Eq. (4.24) are listed in Table 5.6.

Values of  $\delta_{25}$  are also given in Table 5.6. Equation (4.28) was used, with a value of  $\left(\frac{\text{ERI}}{\Sigma}\right)_{\infty}$  of 0.1146 for the 250 assemblies, a value of 0.1194 for the 175 assemblies, and a value of 0.1178 for the 253 assemblies. The first two values were derived from the measurements in the 250 and 175 lattices, the latter from measurements in a lattice identical to the 253 lattice in every respect except for the spacing. The spacing was 5 inches, and the measured value of  $\delta_{25}$  was  $0.0299 \pm 0.0004$  (HE 6).

### 5.4 CALCULATION OF $k_{\infty}$

In Secs. 2.1 to 2.4, the neutron multiplication factor for an infinite medium,  $k_{\infty}$ , was discussed, and two independent methods for measuring it were described. For convenience of reference, values of  $k_{\infty}$  determined with Eqs. (2.28) or (2.30) are here denoted  $k_{\infty 1}$ ; values

TABLE 5.4

Measured Parameters Characterizing the Epithermal Energy Region (I)

Designator	Ratio of Epithermal Fissions of U-235 to Thermal Fissions of U-235 ( $\delta_{25}$ )	Ratio of Fissions of U-238 to Fissions of U-235 ( $\delta_{28}$ )	Cadmium Ratio for U-238 ( $R_{28}$ )	Ratio of Epithermal Absorptions in U-238 to Thermal Absorptions in U-238 ( $\rho_{28}$ )
250	0.0163 ± 73	0.0164 ± 1	5.268 ± 94	0.2343 ± 51
250B1		0.0156 ± 5	5.048 ± 13	0.2470 ± 8
250A1		0.0169 ± 10	4.821 ± 24	0.2617 ± 16
250B2		0.0171 ± 3	4.676 ± 42	0.2720 ± 31
250A2		0.0173 ± 3	4.434 ± 29	0.2912 ± 24
175	0.0334 ± 16	0.0205 ± 3	3.105 ± 23	0.4750 ± 52
175A1			2.897 ± 24	0.5271 ± 67
175A1B1		0.0237 ± 39	2.690 ± 25	0.5917 ± 87
125	0.0579 ± 11	0.0265 ± 7	2.230 ± 18	0.8130 ± 119
253		0.0615 ± 21	1.736 ± 14	1.358 ± 26
253A2				
253A2B1		0.0630 ± 31	1.693 ± 15	1.442 ± 31



TABLE 5.5

Measured Parameters Characterizing the Epithermal Energy Region (II)

Designator	Copper Rod Type	Cadmium Ratio for Rod ( $R_3$ )	Ratio of Epithermal Absorptions to Thermal Absorptions ( $\rho_3$ )
253A2	A	$8.19 \pm 0.09$	$0.1392 \pm 0.0017$
253A2B1	A	$7.81 \pm 0.09$	$0.1468 \pm 0.0019$
253A2B1	B	$8.53 \pm 0.27$	$0.1328 \pm 0.0048$

of  $k_\infty$  determined with the four-factor formula, Eq. (2.7), are denoted  $k_{\infty 2}$ .

The values of  $\eta$  and  $f$  from Tables 5.2 and 5.3, and the values of  $\epsilon$ ,  $p$ , and  $(1+\delta_{25})$  obtained by means of Eqs. (2.8), (2.24), and (2.26), by using data in Tables 5.1 to 5.6, are given in Table 5.7. All parameters are those associated with an infinite medium. The value of the fast fission factor,  $\epsilon$ , for the 175A1 and 253A2 assemblies was calculated by assuming a linear variation of  $\epsilon$  with material buckling. The factors  $(\eta/\eta')$ ,  $(p/p')$ ,  $(\epsilon/\epsilon')$ , and  $\left(\frac{1+\delta_{25}}{1+\delta'_{25}}\right)$  are obtained directly from them, and are listed in Table 5.8. These factors were fit to first or second degree polynomials as explained in Sec. 4.5, in order to obtain the value of each factor at zero buckling. These values  $((\eta/\eta')^0)$ ,  $(\epsilon/\epsilon')^0$ , etc.) have also been included in Table 5.8; they are the correction factors which appear in Eq. (2.28). The correction factors appearing in Eq. 2.30 are given in Table 5.9.

As stated in Sec. 4.5, the value of  $k_\infty$  is determined almost completely by the value of  $A_3^0$ , which is the ratio of thermal neutron absorptions in copper to thermal neutron absorptions in fuel, for an assembly with zero material buckling. Figures 5.1 to 5.3 show the variation in  $A_3$  with material buckling,  $B_m^2$ , for the three lattices studied. The standard deviations of the values of  $A_3$  were calculated from the uncertainties in the cross sections of copper and uranium,

TABLE 5.6

Calculated Parameters Characterizing the Epithermal Energy Region

Designator	Ratio of Epithermal Fissions of U-235 to Thermal Fissions of U-235 ( $\delta_{25}$ )	Ratio of Epithermal Absorptions in U-238 to Thermal Absorptions in U-238 ( $\rho_{28}$ )	Ratio of Epithermal Absorptions to Thermal Absorptions, in Various Materials			
			Moderator ( $\rho_1$ )	Fuel Rod Cladding ( $\rho_2$ )	Copper ( $\rho_3$ )	Copper Rod Cladding ( $\rho_4$ )
250			0.01268	0.01402		
250B1	0.0170		0.01566	0.01817	0.02134	0.01356
250A1	0.0168		0.01782	0.02037	0.02540	0.01735
250B2	0.0177		0.01891	0.02156	0.02546	0.01847
250A2	0.0216		0.02303	0.02624	0.03416	0.02333
175			0.02619	0.02857		
175A1	0.0351		0.03719	0.04147	0.05384	0.03677
175A1B1	0.0405		0.04400	0.04872	0.06490 (A rod) 0.06179 (B rod)	0.04455
125			0.04529	0.04860		
253	0.1079		0.08479	0.10102		
253A2	0.1105	1.407	0.09823	0.11724		0.09394
253A2B1	0.1119		0.10235	0.12211		0.09801



TABLE 5.7

Values of  $\eta$ ,  $\epsilon$ ,  $p$ ,  $f$ , and  $1+\delta_{25}$  Based on Measured and Calculated Parameters

Designator	Neutron Regeneration Factor ( $\eta$ )	Fast Fission Factor ( $\epsilon$ )	Resonance Escape Probability ( $p$ )	Thermal Utilization ( $f$ )	Resonance Fission Factor ( $1+\delta_{25}$ )
250	$1.532 \pm 28$	$1.0117 \pm 4$	$0.9530 \pm 41$	$0.9520 \pm 15$	$1.0116 \pm 52$
250B1	$1.531 \pm 28$	$1.0110 \pm 5$	$0.9473 \pm 36$	$0.7681 \pm 19$	$1.0149 \pm 67$
250A1	$1.531 \pm 28$	$1.0119 \pm 8$	$0.9412 \pm 37$	$0.6847 \pm 23$	$1.0168 \pm 75$
250B2	$1.531 \pm 28$	$1.0120 \pm 4$	$0.9411 \pm 37$	$0.6463 \pm 24$	$1.0177 \pm 79$
250A2	$1.530 \pm 28$	$1.0122 \pm 4$	$0.9398 \pm 36$	$0.5328 \pm 28$	$1.0216 \pm 97$
175	$1.530 \pm 28$	$1.0147 \pm 5$	$0.9055 \pm 47$	$0.9678 \pm 8$	$1.0242 \pm 17$
175A1	$1.528 \pm 28$	$1.0159 \pm 18$	$0.8861 \pm 20$	$0.6936 \pm 25$	$1.0350 \pm 17$
175A1B1	$1.528 \pm 28$	$1.0167 \pm 27$	$0.8807 \pm 23$	$0.6022 \pm 35$	$1.0405 \pm 19$
125	$1.527 \pm 28$	$1.0190 \pm 7$	$0.8374 \pm 75$	$0.9769 \pm 13$	$1.0450 \pm 24$
253	$1.441 \pm 26$	$1.0439 \pm 20$	$0.7105 \pm 54$	$0.9885 \pm 3$	$1.0927 \pm 49$
253A2	$1.439 \pm 26$	$1.0444 \pm 25$	$0.6953 \pm 81$	$0.8773 \pm 13$	$1.1073 \pm 56$
253A2B1	$1.439 \pm 26$	$1.0445 \pm 25$	$0.6896 \pm 52$	$0.8470 \pm 17$	$1.1117 \pm 58$

TABLE 5.8

Ratios Used in the Determination of Correction Factors

Designator	Ratio of Neutron Regeneration Factors $(\eta/\eta')$	Ratio of Resonance Escape Probabilities $(p/p')$	Ratio of Fast Fission Factors $(\epsilon/\epsilon')$	Ratio of Resonance Fission Factors $\left(\frac{1+\delta_{25}}{1+\delta'_{25}}\right)$
250	1.	1.	1.	1.
250B1	1.00031	1.0061	0.0006	0.9967
Value for a hypothetical zero buckling assembly	1.00054	1.0114	0.9999	0.9947
250A1	1.00051	1.0125	0.9998	0.9949
250B2	1.00065	1.0126	0.9997	0.9940
250A2	1.00101	1.0141	0.9995	0.9902
175	1.	1.	1.	1.
175A1	1.00105	1.0219	0.9988	0.9896
Value for a hypothetical zero buckling assembly	1.00106	1.0221	0.9988	0.9895
175A1B1	1.00160	1.0282	0.9980	0.9843
253	1.	1.	1.	1.
253A2	1.00106	1.0219	0.9995	0.9868
253A2B1	1.00140	1.0304	0.9994	0.9829
Value for a hypothetical zero buckling assembly	1.00143	1.0311	0.9994	0.9826



TABLE 5.9  
Correction Factors for Use in Equation (2.30)

Designator	Ratio of Neutron Regeneration Factors $(\eta'/\eta^0)$	Ratio of Resonance Escape Probabilities $(p'/p^0)$	Ratio of Fast Fission Factors $(\epsilon'/\epsilon^0)$	Ratio of Resonance Fission Factors $\left(\frac{1+\delta'_{25}}{1+\delta^0_{25}}\right)$
250B1	1.0002	1.0053	0.9992	0.9979
250A1	1.0000	0.9988	1.0001	0.9998
250B2	0.9999	0.9987	1.0002	1.0007
250A2	0.9995	0.9973	1.0004	1.0045
175A1	1.0000	1.0002	1.0000	0.9999
175A1B1	0.9995	0.9941	1.0008	1.0052
253A2	1.0003	1.0090	0.9999	0.9958
253A2B1	1.0001	1.0007	1.0000	0.9997

and the uncertainty (based on counting statistics) in the relative thermal neutron density in copper and uranium. The 1.1% uncertainty in the thermal neutron cross section of copper dominates; the maximum uncertainty in  $A_3$  is 1.4%. The second degree polynomial fitted to the data is shown in Figs. 5.1 to 5.3.

The determination of the value of  $A_3^0$  and its standard deviation is discussed in Sec. 4.5. The value calculated for the 250 lattice was  $0.423 \pm 0.017$ , the value for the 175 lattice  $0.409 \pm 0.011$ , and the value for the 253 lattice  $0.171 \pm 0.027$ . The large uncertainty in the material buckling of the 250A1 assembly, discussed in Sec. 5.1, accounts for most of the uncertainty in the value of  $A_3^0$  for the 250 lattice. The least-squares analysis of the  $A_3$  data for these assemblies was repeated, with the 250A1 data point omitted (see Fig. 5.4). The degree of fit associated with the second degree polynomial fitted to the data was smaller by a factor of five than that associated with the polynomial fitted to all five data points (Fig. 5.1), suggesting that a more reliable estimate of  $A_3^0$

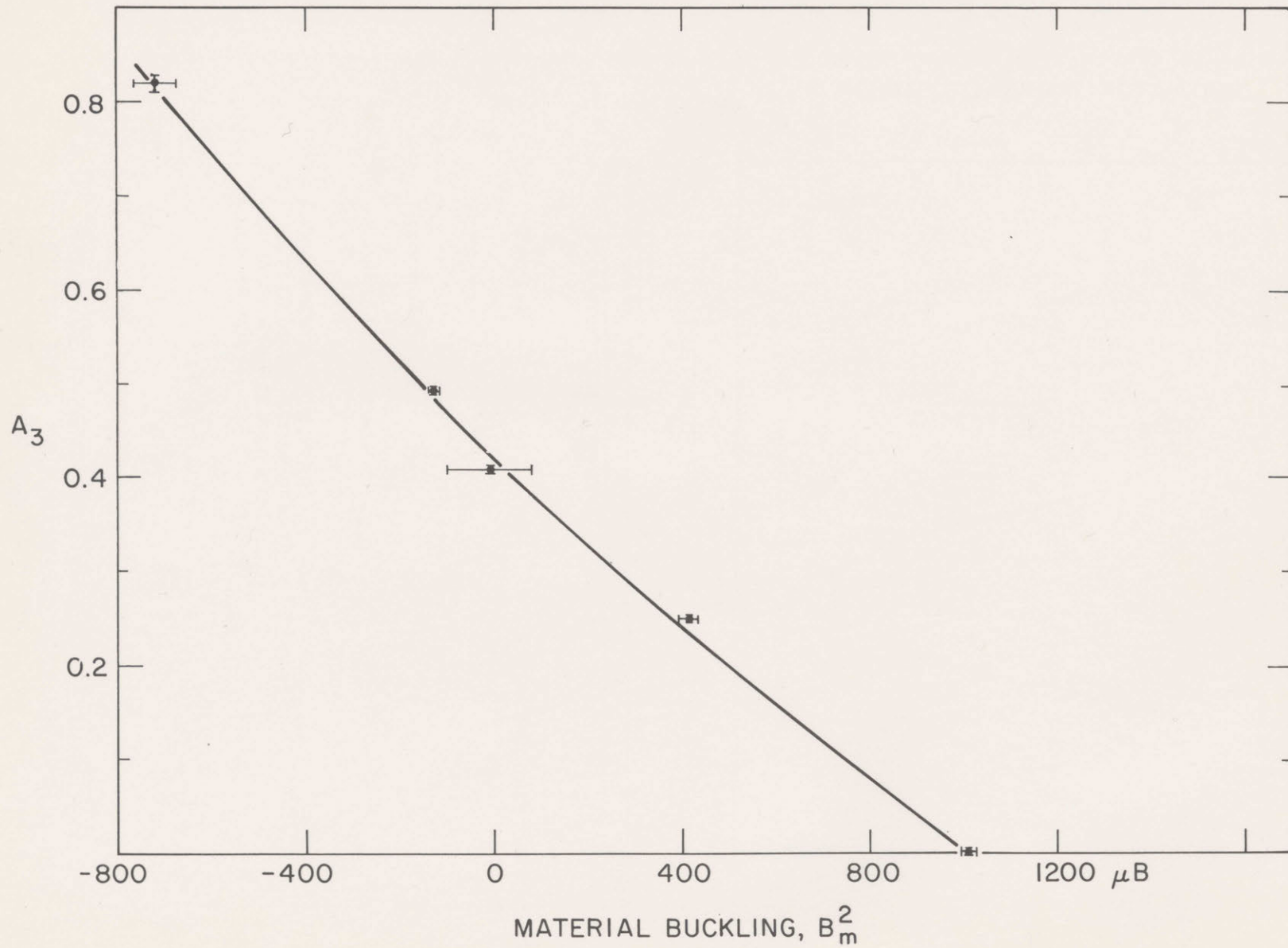


FIG.5.1 RELATIVE ABSORPTION OF THERMAL NEUTRONS IN COPPER,  $A_3$ , AS A FUNCTION OF MATERIAL BUCKLING,  $B_m^2$ , FOR 250 ASSEMBLIES



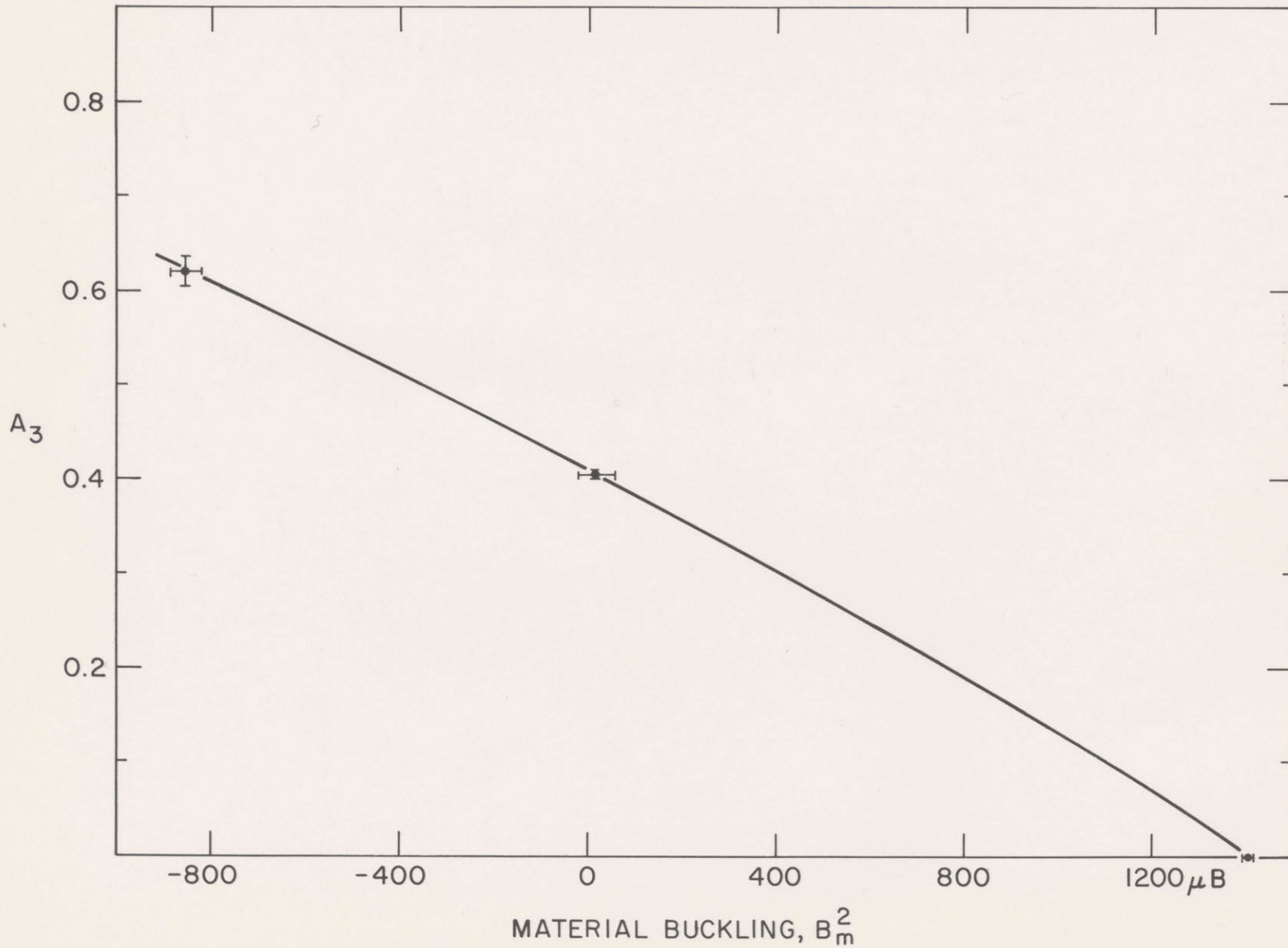


FIG. 5.2 RELATIVE ABSORPTION OF THERMAL NEUTRONS IN COPPER,  $A_3$ , AS A FUNCTION OF MATERIAL BUCKLING,  $B_m^2$ , FOR 175 ASSEMBLIES

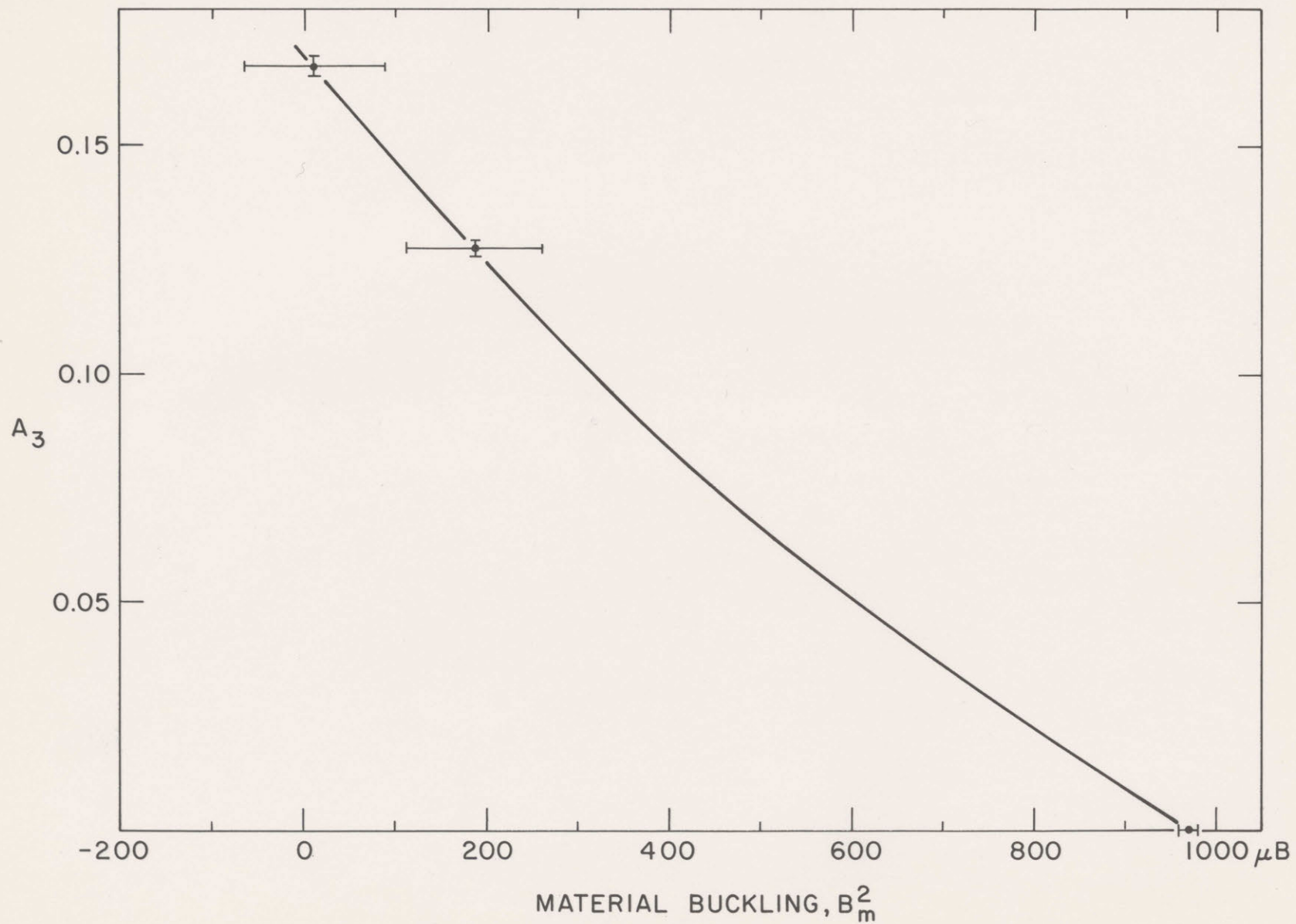


FIG.5.3 RELATIVE ABSORPTION OF THERMAL NEUTRONS IN COPPER,  $A_3$ , AS A FUNCTION OF MATERIAL BUCKLING,  $B_m^2$ , FOR 253 ASSEMBLIES



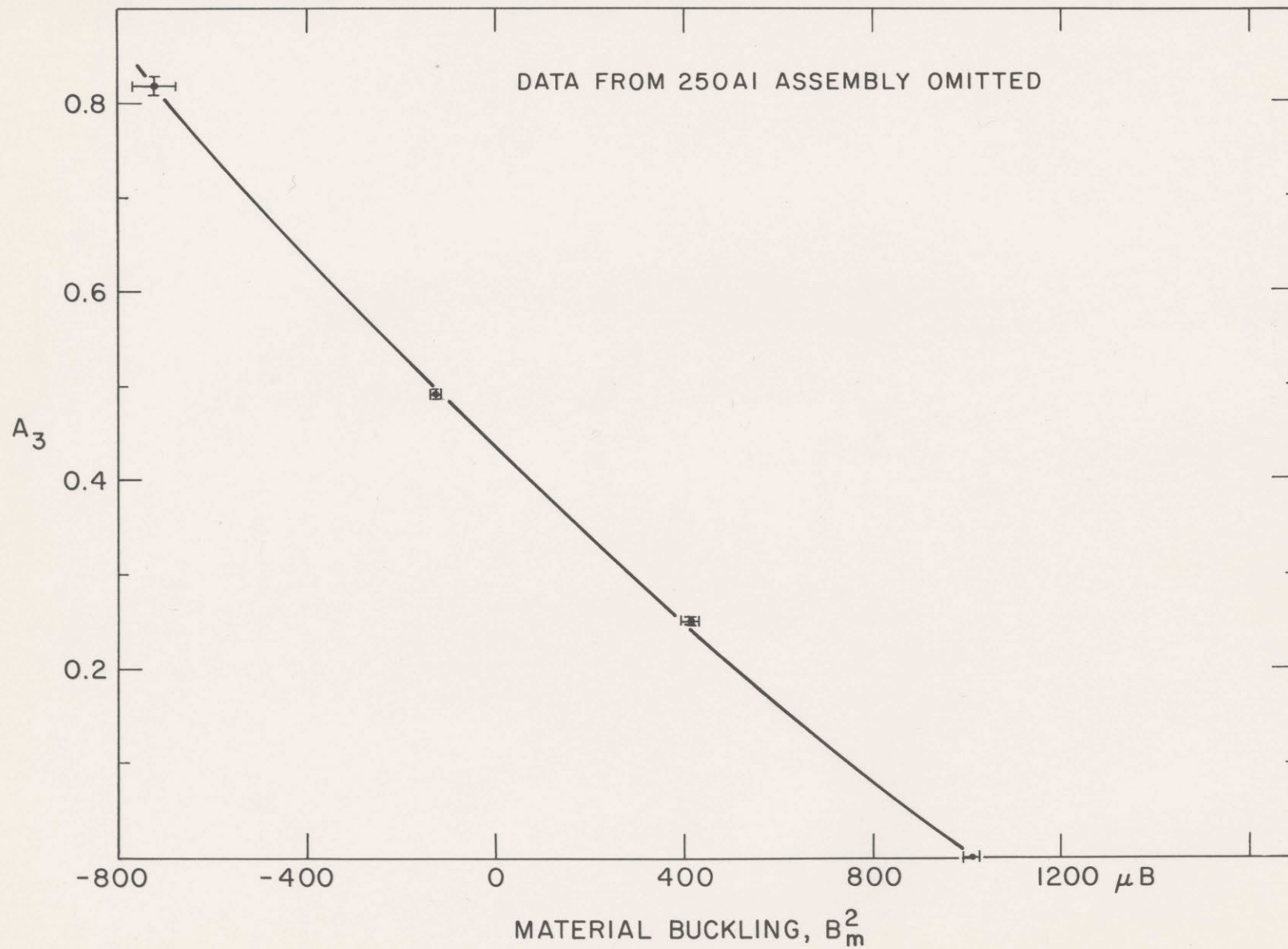


FIG.5.4 RELATIVE ABSORPTION OF THERMAL NEUTRONS IN COPPER,  $A_3$ , AS A FUNCTION OF MATERIAL BUCKLING,  $B_m^2$ , FOR 250 ASSEMBLIES

may be derived by omission of the 250A1 data. The value of  $A_3^0$  calculated is  $0.435 \pm 0.007$ ; this value of  $A_3^0$  was used for the calculation of  $k_{\infty 1}$  for the 250 lattice.

As stated in Sec. 4.3.2, the value of  $A_3$  for the 175A1B1 assembly is open to question because of difficulties with experimental equipment. The calculated uncertainty takes account of the discrepancy between the two independent measurements of  $A_3$  made in this assembly.

The value of the radial buckling for this assembly is discussed in Sec. 5.1; the fact that the curve of Fig. 5.2 is concave downward, rather than concave upward as the curves of Figs. 5.1, 5.3, and 5.4 are, is another reason for thinking that the radial buckling value of this assembly is indeed too low. (The predicted shape of the curves is discussed in Sec. 4.5.)

The analysis of the data from the 175 assemblies was repeated with the 175A1B1 data omitted; a linear extrapolation was used to obtain the value of  $A_3^0$ . The change in the calculated value of  $A_3^0$  was 0.12%, indicating that the calculated value of  $k_{\infty 1}$  is insensitive to inclusion or omission of the 175A1B1 data. The value of  $A_3^0$  calculated from all three data points has been used.

Table 5.10 contains the values of  $k_{\infty 1}$  and  $k_{\infty 2}$ . The uncertainty in the values of  $k_{\infty 1}$  is determined by the uncertainty in  $A_3^0$ , which varies from 1.6% to 15.8%. The term  $\sum_{i=1,2,4} (A_i^0 - A_i)$  is at most 0.4% of the term in which it appears; hence, uncertainties introduced by this term may be neglected. The multiplicative correction factors which account for the change in the values of  $\epsilon$ ,  $p$ , and  $(1 + \delta_{25})$  also contribute uncertainties small in comparison with that contributed by the  $A_3^0$  term because they consist of ratios of the form,  $\frac{1+x}{1+y}$ , where  $y$  and  $x$  are nearly equal. Because the values of these ratios are near unity, they are insensitive to systematic errors which affect both  $x$  and  $y$  equally or nearly equally, such as changes in the values of  $\nu_{25}$ ,  $\nu_{28}$ ,  $a_{28}$ , and the various cross sections used in the calculation of the correction factors. The multiplicative correction factor which accounts for the change in the value of  $\eta$  is independent of the value of  $\nu_{25}$  and the fission cross section of  $U^{235}$ . Because this correction factor deviates from unity by at most 0.16%, uncertainties in the absorption cross sections of  $U^{238}$  and  $U^{235}$  introduce no significant uncertainties into this factor.



TABLE 5.10

Values of the Multiplication Factor  $k_{\infty}$ 

Designator	Source of Value of $k_{\infty}$		
	Equation (2.28)	Equation (2.30)	Equation (2.7)
250	$1.429 \pm 0.007$		$1.422 \pm 0.028$
250B1		$1.148 \pm 0.007$	$1.143 \pm 0.023$
250A1		$1.020 \pm 0.010$	$1.015 \pm 0.021$
250B2		$0.963 \pm 0.005$	$0.959 \pm 0.020$
250A2		$0.796 \pm 0.006$	$0.792 \pm 0.017$
175	$1.416 \pm 0.011$		$1.393 \pm 0.026$
175A1		$1.004 \pm 0.009$	$0.988 \pm 0.018$
175A1B1		$0.871 \pm 0.012$	$0.857 \pm 0.017$
125			$1.330 \pm 0.027$
253	$1.187 \pm 0.027$		$1.154 \pm 0.023$
253A2		$1.044 \pm 0.027$	$1.015 \pm 0.024$
253A2B1		$1.003 \pm 0.026$	$0.976 \pm 0.020$

The uncertainties in the values of  $k_{\infty 2}$  are calculated from the uncertainties in  $\nu_{25}$ ,  $\nu_{28}$ ,  $a_{28}$ , cross sections, in the measured parameters  $\delta_{28}$ ,  $\rho_{28}$ ,  $\delta_{25}$ ,  $\rho_3$ , and in the measured relative thermal neutron density in the copper rods.

The values of  $k_{\infty}$  reported in Table 5.10 are in good agreement, within the quoted uncertainties, although the values of  $k_{\infty 1}$  are consistently higher than those of  $k_{\infty 2}$ .

## 5.5 DISCUSSION OF RESULTS

As discussed in Sec. 5.4, the values of  $k_{\infty 1}$  depend chiefly on the measured values of the material buckling, on the measured thermal neutron disadvantage factor of the fuel (relative to the added absorber), and on the values of the thermal neutron absorption cross sections for the fuel and absorber. The values of  $k_{\infty 2}$  depend chiefly on the measured ratios  $\rho_{28}$ ,  $\delta_{25}$ , and  $\delta_{28}$ ; on the values of the absorption cross sections for the fuel, moderator, and cladding, and the fission

cross section of the fuel; and on the values of  $\nu_{25}$  and  $\nu_{28}$ . Strong efforts have been made by different workers to eliminate sources of systematic error from both methods for determining  $k_{\infty}$ ; the two values of  $k_{\infty}$  given for each assembly in Table 5.10 are in agreement within statistical uncertainties in every case. This lends confidence in both methods for measuring  $k_{\infty}$ , at least for lattices composed of slightly enriched uranium metal fuel and heavy water moderator, with moderator-to-fuel ratios between 10 and 100. However, because there are fewer sources of error in the measurement of  $k_{\infty 1}$ , these results are likely to be more trustworthy.

The results for the 250 and 175 lattices show that values of  $k_{\infty 1}$  with uncertainties between 0.5% and 1.0% can be measured by making use of thermal neutron absorbers in the manner described. These uncertainties are smaller than those associated with values of  $k_{\infty 2}$ , which range from 1.9% to 2.0%; this is another reason for preferring the values of  $k_{\infty 1}$ . The uncertainty in the value for the 253 lattice (2.3%) shows, however, that such precision is achieved only when accurate values of the material buckling are obtained.

The uncertainty in  $(k_{\infty 1} - 1)$  is 1.6% for the 250 lattice, 2.6% for the 175 lattice, and 14.4% for the 253 lattice. The "null reactivity" method of measuring  $k_{\infty}$ , developed at the Physical Constants Testing Reactor (PCTR), was discussed in Sec. 1.2; R. E. Heineman (HE 9) has noted that such measurements yield an accuracy of about 3% in  $(k_{\infty} - 1)$ . The null reactivity technique was also used by T. C. Engelder et al. (EN 1), to measure the multiplication factors of lattices fueled with  $\text{UO}_2$  and  $\text{UO}_2\text{-ThO}_2$  and moderated with mixtures of  $\text{D}_2\text{O}$  and  $\text{H}_2\text{O}$ ; the quoted uncertainties in Ref. EN 1 range from 3.3% to 8.3% in  $(k_{\infty} - 1)$ . It may be concluded that the use of added absorbers in subcritical assemblies, as described here, can result in measurements of  $(k_{\infty} - 1)$  as accurate as those obtained with the null reactivity technique, if the buckling measurements are sufficiently precise.

It was pointed out in Sec. 2.6.1 that the measurements made here may be treated as measurements of any one of the factors appearing in Eq. (2.7). It is of interest, for reasons discussed below, to use the results to calculate a value of the neutron regeneration factor,  $\eta$ . If the right-hand sides of Eqs. (2.7) and (2.28) are equated, and the resulting equation is solved for  $\eta$ , we obtain:



$$\eta = \left( \frac{\eta}{\eta^0} \right) \left[ \frac{1 + \sum_i^4 A_i^0}{\epsilon^0 p^0 (1 + \delta_{25}^0)} \right]. \quad (5.1)$$

This equation is simply a statement of the fact that the value of the multiplication factor  $k_\infty$  is unity for an assembly with zero material buckling.

Equation (5.1) is of interest because direct measurements of  $\eta$  in a lattice spectrum are not easily made (CR 1); values calculated with an equation like Eq. (2.11) are usually used. The uncertainties assigned to such values generally range from 1% to 2%, owing to uncertainties in the values of  $\nu_{25}$  and in the fission and absorption cross sections of the fuel (DA 1). Values of  $\eta$  calculated with Eq. (5.1) are independent of these sources of error, however; if the buckling measurements are sufficiently precise, as is the case here with the 250 and 175 lattices, the uncertainty in the value of  $\eta$  is smaller than the uncertainty in values calculated with Eq. (2.11).

The values of  $\eta$  calculated for the 250 and 175 lattices with Eq. (2.11) are  $1.532 \pm 0.028$  and  $1.530 \pm 0.028$ , respectively. The values computed for the same lattices with Eq. (5.1) are  $1.525 \pm 0.014$  and  $1.555 \pm 0.008$ , respectively. The results are in agreement within the calculated uncertainties. Because of this, and because of the small number of experiments, no special significance can be attached to the disagreement between the values for the 175 lattice, which is somewhat greater than that between the values for the 250 lattice. The values of  $\eta$  calculated with Eq. (5.1) are chiefly of interest because of the smaller uncertainties associated with them.

## 5.6 CALCULATION OF DIFFUSION AREA ( $L^2$ )

The use of the available experimental data for the measurement of the diffusion area and the Fermi age is discussed in Sec. 2.6.2. In this section, "experimental" values of  $L^2$  obtained from the two-group and age-diffusion criticality equations, with calculated values of the Fermi age supplied by H. E. Bliss (BL 2), are given; measured values of  $k_{\infty 1}$  and the material buckling were used with Eqs. (2.30) and (2.31); the results are given in Table 5.11. These may be compared with the value of  $L^2$  calculated with Eq. (4.16); the



TABLE 5.11

Measured and Calculated Values of the Diffusion Area ( $L^2$ )  
for the Unmodified Lattices

Lattice Designator	Fermi Age ( $\tau$ ) $\text{cm}^2$	Source of Value of $L^2$		
		Eq. (2.30) $\text{cm}^2$	Eq. (2.31) $\text{cm}^2$	Eq. (4.16) $\text{cm}^2$
250	$123 \pm 3$	$269 \pm 8$	$261 \pm 9$	264
175	$125 \pm 3$	$145 \pm 7$	$134 \pm 7$	136
125	$129 \pm 3$	$84 \pm 16$	$72 \pm 15$	74
253	$128 \pm 3$	$58 \pm 25$	$51 \pm 25$	51

values of  $\bar{\Sigma}_a$  and  $\bar{D}$  were obtained by averaging cross-section values taken from the literature over the spatial and energy distribution calculated by the THERMOS code, as discussed in Sec. 4.3 (see Table 5.2). The values calculated with Eq. (2.31), which is based on age-diffusion theory, are in better agreement with the calculated values than are the values calculated with Eq. (2.30), which is based on two-group theory. The large uncertainties calculated for the values of  $L^2$  for the 125 and 253 lattices are in part a result of the fact that the uncertainties in the values of  $k_\infty$  for these lattices are larger than those for the 250 and 175 lattices. The values of  $L^2$  calculated with Eqs. (2.30) and (2.31) are roughly proportional to  $(k_\infty - 1)$ ; thus they are very sensitive to the uncertainty in  $k_\infty$ . For instance, in the case of the 250 lattice, if the value of  $k_{\infty 2}$  is used instead of the value of  $k_{\infty 1}$ , the uncertainty in the values of  $L^2$  increases from 8 or 9  $\text{cm}^2$  to 25 or 26  $\text{cm}^2$ .

## 5.7 EXPLORATORY EXPERIMENTS ON TWO-REGION ASSEMBLY

Figure 3.11 is a diagram of the two-region assembly, designated the 253A2B1(2R) assembly. The outer region was identical to the unmodified 253 lattice; the pattern of fuel and absorber rods in the central region was identical to the pattern of the 253A2B1 assembly. The material buckling values for the outer and inner regions, measured in independent one-region experiments, are  $969 \pm 11 \mu\text{B}$  and  $14 \pm 77 \mu\text{B}$ ,



respectively. The radius of the inner region, determined with Eq. (4.6), was 20.28 cm.

### 5.7.1 Cadmium Ratio

Figures 5.5 and 5.6 show the radial activation distributions measured with bare and cadmium-covered gold foils. Each point represents the average of two foil activities. The foil holders were located 71.12 cm above the bottom of the assembly. The traverse with bare foils shows significant deviations from the asymptotic distribution for a one-region assembly ( $J_0$  Bessel function); the traverse with cadmium-covered foils does not. Figure 5.7 shows the variation in the cadmium ratio as a function of radial position within the two-region assembly. Values obtained from the radial traverses show somewhat larger uncertainties than those obtained from the axial traverses because of the uncertainty in the foil holder position discussed in Sec. 4.2.1. The equilibrium cadmium ratios characteristic of the unmodified 253 lattice and the 253A2B1 assembly are also shown in Fig. 5.7 for comparison.

Figure 5.8 shows the variation in the cadmium ratio as a function of axial position, at three different radial positions. At each position, equilibrium appears to exist between 45 cm and 100 cm from the bottom of the assembly, although there is a slight upward trend in the values measured at a radial position of 22.23 cm. The mean values of the cadmium ratio, and standard deviation of the mean, are given in Table 5.12.

TABLE 5.12

Equilibrium Cadmium Ratio  
in Two-Region Assembly (253A2B1(2R))

Radial Position (cm)	Mean Value
5.50	3.10 ± 0.02
22.23	3.21 ± 0.02
33.21	3.26 ± 0.02

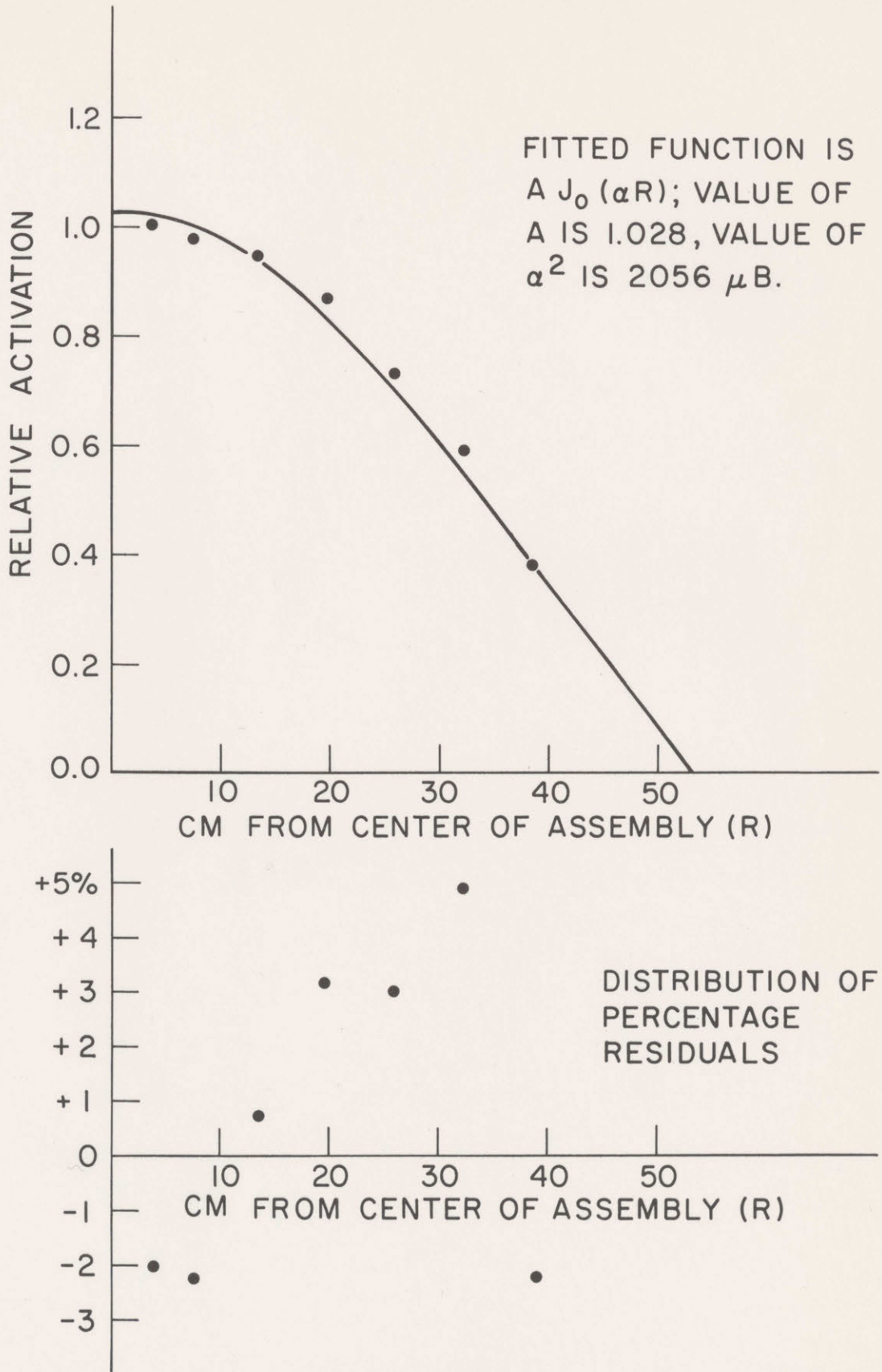


FIG. 5.5 RELATIVE ACTIVATION DISTRIBUTION IN 253A2BI (2R) ASSEMBLY AS A FUNCTION OF RADIAL POSITION (RUN 35, BARE FOILS)



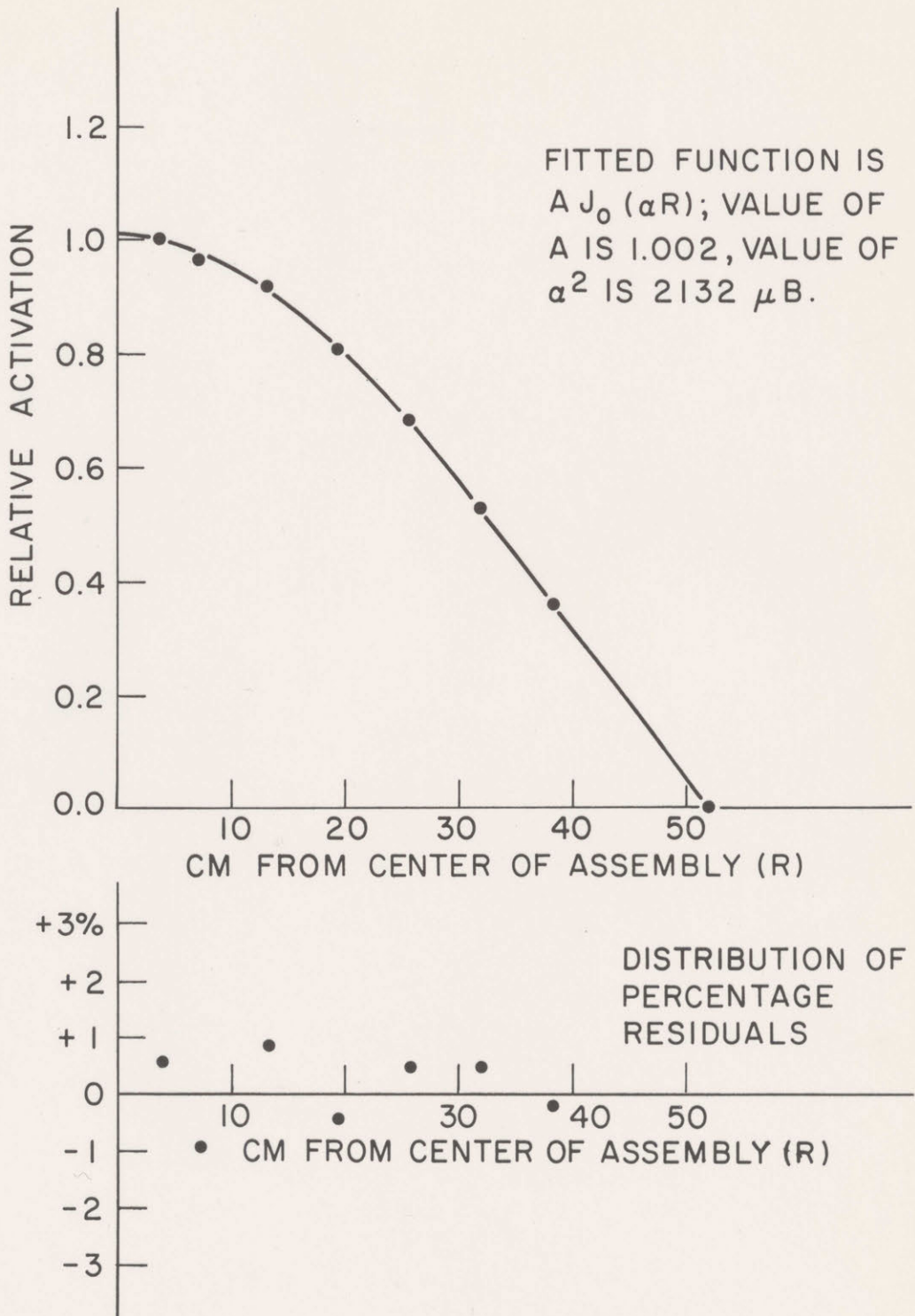


FIG. 5.6 RELATIVE ACTIVATION DISTRIBUTION IN 253A2BI (2R) ASSEMBLY AS A FUNCTION OF RADIAL POSITION (RUN 37, CADMIUM COVERED FOILS)

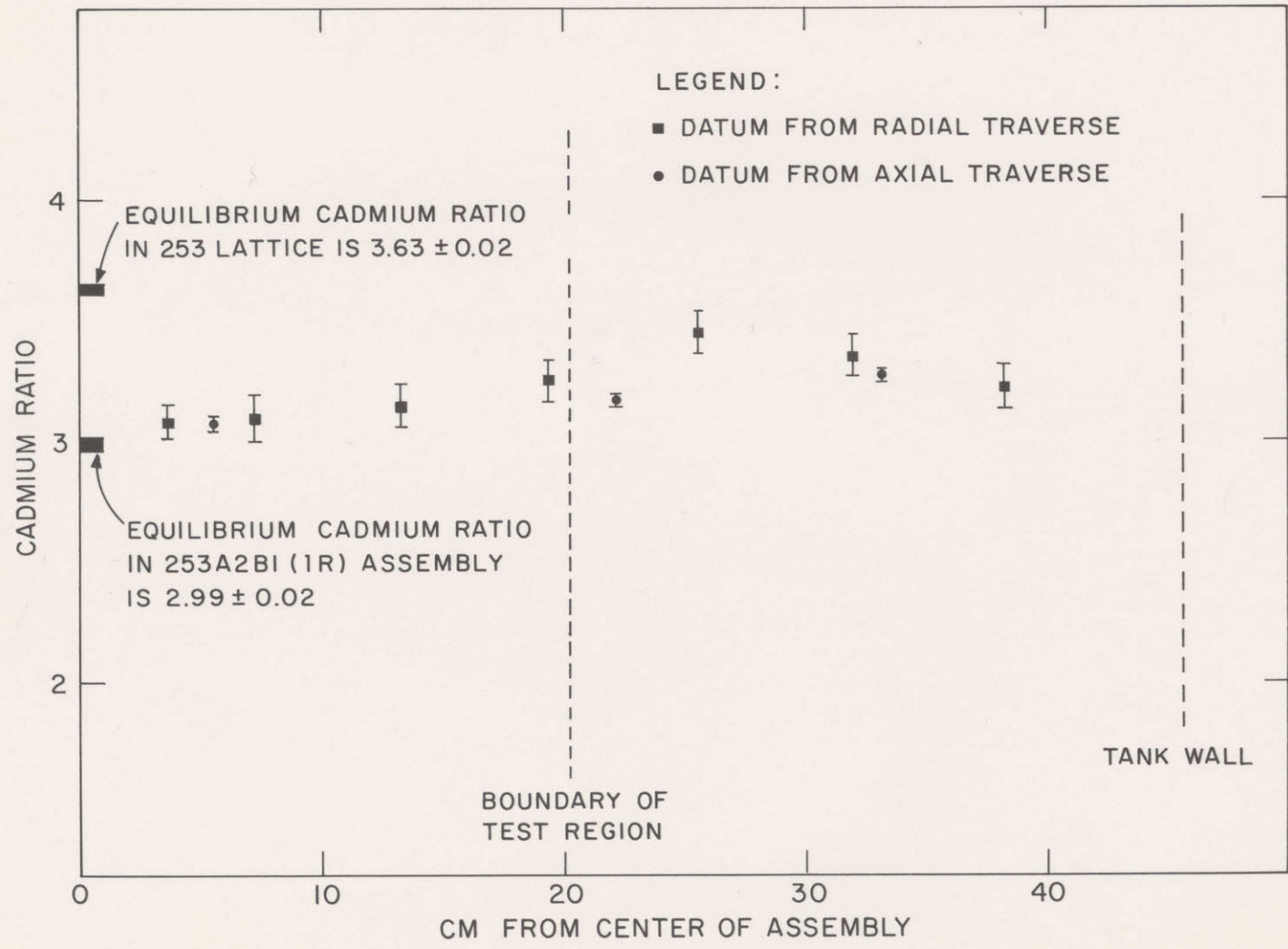


FIG. 5.7 CADMIUM RATIO IN 253A2BI (2R) ASSEMBLY AS A FUNCTION OF RADIAL POSITION



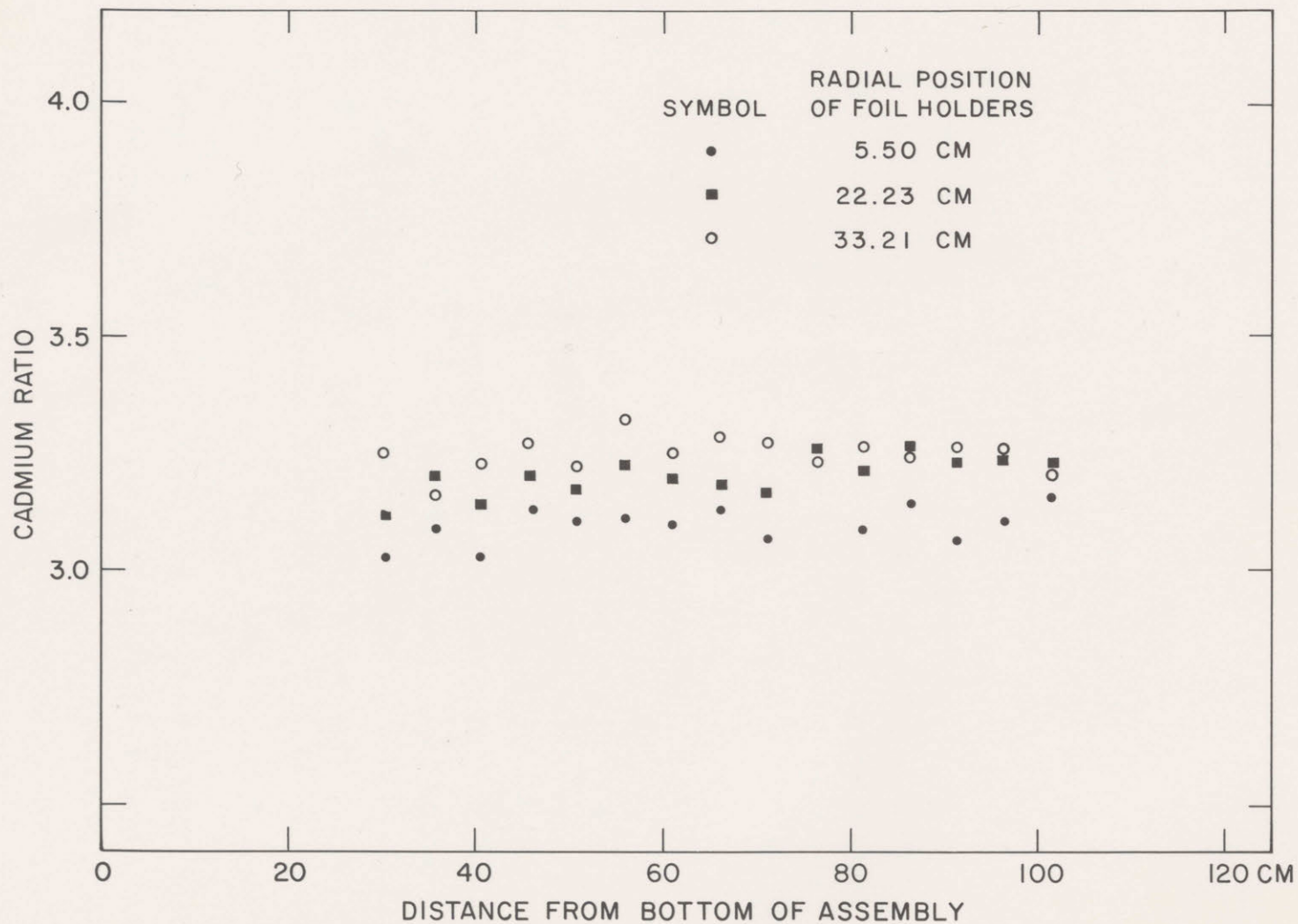


FIG.5.8    CADMIUM RATIO IN 253A2BI (2R) ASSEMBLY AS A FUNCTION OF RADIAL AND AXIAL POSITION

The cadmium ratio appears to reach an equilibrium value within a region approximately 16 cm in diameter, at the center of the assembly. The three values of the cadmium ratio measured in this region are  $3.08 \pm 0.08$ ,  $3.07 \pm 0.03$ , and  $3.10 \pm 0.09$ ; the average value, weighted with the inverse square of the standard deviation, is  $3.07 \pm 0.03$ . This value is 2.7 standard deviations higher than the equilibrium value for the 253A2B1 one-region assembly.

The question whether or not an equilibrium cadmium ratio is attained must thus be left open; the most that can be said on the basis of the experiments done so far is that the value of the cadmium ratio approaches the value measured in the experiments in the 253A2B1 one-region assembly, as shown in Fig. 5.7. Further study under a variety of experimental conditions will be necessary to determine whether an equilibrium cadmium ratio is achieved over a large enough region so that measurements of  $\delta_{28}$ ,  $\delta_{25}$ ,  $\rho_{28}$ , and  $f$  can be made in the central cell of two-region assemblies similar to the one studied here. The experimental results reported here give some grounds for thinking that this can be done.

### 5.7.2 Buckling

Least squares fits to the data from the macroscopic traverses made in the 253A2B1(2R) assembly were analyzed in the manner described in Sec. 4.2. Values of the radial buckling,  $\alpha^2$ , obtained by least squares fits to various sets of points from the traverse made with cadmium-covered foils (see Fig. 5.6) are given in Table 5.13; the sets of points selected are indicated in the table. The results of the traverse with bare foils do not approach the asymptotic  $J_0$  distribution (see Fig. 5.5); hence, fitted values of  $\alpha^2$  are not meaningful and will not be presented.

The values of the axial buckling,  $\gamma^2$ , obtained from least squares fits to the measured axial distributions, are given in Table 5.14. Points less than 45 cm or more than 76 cm from the bottom of the assembly were not used in the fitting process. The points in this region were randomly distributed about the fitted distribution ( $A \sinh \gamma(H_0 - z)$ ) in all experiments but one, the traverse with cadmium-covered foils at 33.21 cm. It is possible that the foil holder was not properly engaged in position at the bottom during this experiment, but



TABLE 5.13  
 Values of Radial Buckling  
 for Two-Region Assembly (253A2B1(2R))

Points Used	Radial Buckling (Cadmium-Covered Foils) ( $\mu\text{B}$ )
All seven	2132
Inner six	2115
Inner five	2107
Outer three	2148

TABLE 5.14  
 Values of Axial Buckling  
 for Two-Region Assembly (253A2B1(2R))

Radial Position of Foil Holder (cm)	Foil Condition	Axial Buckling ( $\mu\text{B}$ )	RMS Value of Buckling Increment ( $\mu\text{B}$ )
5.50	Bare	1863	7
5.50	Cadmium covered	1795	5
22.23	Bare	1803	10
22.23	Cadmium covered	1813	9
33.21	Bare	1706	8
33.21	Cadmium covered	1727	20

this is not thought to be the cause of the deviation from the asymptotic shape. The position at which the traverses were made was 12.6 cm from the wall of the tank; it is possible that edge effects, such as fast neutron reflection from the concrete shielding, are responsible for the effect observed. Such effects have been investigated at M. I. T. by D. Goebel (HE 5), and observed at distances up to 12.2 cm from the tank wall.

As stated in Sec. 2.5, the axial buckling in a two-region assembly is usually assumed to be constant as a function of radial position, in calculating the value of the material buckling for the assembly. The low values given in Table 5.14 for the outermost traverses may be caused by the edge effects mentioned above. The results of D. Goebel's work show that the axial buckling would indeed be expected to decrease, for positions near the edge of the assembly. Of the remaining four measurements, done at interior points, three are in good agreement. The value of 1863  $\mu\text{B}$  measured with bare foils near the center of the assembly indicates that more experiments are necessary before it can be concluded that the axial buckling of assemblies like the one studied can be presumed constant as a function of radial position.

## 5.8 CONCLUSIONS

The most important conclusion to be drawn from the results presented in this chapter is that values of  $k_{\infty}$  and  $\eta$  can be measured, with uncertainties between 0.5% and 1.0%, by making use of thermal neutron absorbers in subcritical assemblies in the manner described in Secs. 2.4 and 2.6.1. The measured values of the multiplication factor ( $k_{\infty 1}$ ) are independent or nearly independent of many parameters associated with values of the multiplication factor calculated with the four-factor formula ( $k_{\infty 2}$ ); among these are  $\nu_{25}$ ,  $\nu_{28}$ ,  $\delta_{25}$ ,  $\delta_{28}$ ,  $\rho_{28}$ , the macroscopic fission cross section of the fuel, and all absorption cross sections except that of the fuel. The values of  $k_{\infty 1}$  for the three lattices studied are in good agreement within experimental uncertainties with the values of  $k_{\infty 2}$ , if account is taken of fission of  $\text{U}^{235}$  in the epithermal energy range. Because the sources of error in the values of  $k_{\infty 1}$  are fewer in number than the sources of error in  $k_{\infty 2}$ , and because the uncertainties calculated for the values of  $k_{\infty 1}$  are smaller than those calculated for the values of  $k_{\infty 2}$ , the values of  $k_{\infty 1}$  are believed to be more trustworthy.



The measured values of the neutron regeneration factor,  $\eta$ , are independent of the value of  $\nu_{25}$  and the fission cross section of the fuel; they are in agreement, within experimental uncertainties, with values of  $\eta$  calculated from values of  $\nu_{25}$  and the ratio of the fission and absorption cross sections of the fuel (Eq. (2.11) or Eq. (4.13)), averaged over the spectrum calculated with a multigroup transport theory code (THERMOS).

The foregoing conclusions are based on the results of single-region experiments in a subcritical assembly. Exploratory experiments, discussed in Sec. 2.5, were made to see if the measurements could be done in two-region subcritical assemblies. No grounds for belief that the experiment could not be done in this way were discovered; there is considerable reason to believe, on the basis of the experiments done, that this can, in fact, be done if the material buckling can be measured in a two-region subcritical experiment. More measurements will be necessary, however, before a conclusion can be definitely established.

The values of  $k_{\infty 1}$  were used, in conjunction with a calculated value of the Fermi age and the measured value of the material buckling, to obtain values of the diffusion area with the two-group and age-diffusion criticality equations. The values were compared with values of the diffusion area calculated with Eq. 4.16, using values of the absorption cross section and diffusion coefficient averaged over the spatial and energy distribution calculated with the THERMOS code. The values obtained with the age-diffusion equation were in slightly better agreement with the calculated values than were those obtained with the two-group equation. It was found that the uncertainties in the experimental values of the diffusion area were greater by a factor of three if the values of  $k_{\infty 2}$  were used.

## CHAPTER VI

## SUMMARY AND SUGGESTIONS FOR THE FUTURE

The conclusions given in Sec. 5.8 show that the objectives set forth in Sec. 1.3 have been realized. The work is summarized in this chapter, and suggestions for future work are given.

## 6.1 SUMMARY

The first objective of the work was to develop a method for the measurement of  $k_{\infty}$ , to be based on the Hanford technique described in Sec. 1.2, but to utilize a subcritical, not a critical, facility. The method is described in Secs. 2.1 to 2.4, and consists basically of a determination of the amount of thermal neutron absorber necessary to reduce the value of the material buckling to zero, or equivalently, to reduce the value of  $k_{\infty}$  to unity. The value of  $k_{\infty}$  for the lattice without added absorbers may be computed from the amount of absorber necessary, with Eq. (2.28); correction factors are included for spectral perturbations, epithermal absorption in the added absorber, and effects of the heterogeneity of the lattice.

There are two important advantages to this method of measuring  $k_{\infty}$ , as compared with the usual method involving direct use of the four-factor formula (Eq. (2.7)). The first advantage is that the measured value is independent of the values of  $\nu_{25}$  and the macroscopic fission cross section of the fuel, and nearly independent of the values of  $\nu_{28}$ ,  $\delta_{25}$ ,  $\delta_{28}$ ,  $\rho_{28}$ , and all absorption cross sections except those of the fuel and the added absorber. A second advantage is that higher precision is possible than with the four-factor formula, since the method is really a measurement of  $(k_{\infty}-1)$ . The measurements can, with equal validity, be treated as an experimental measurement of  $\eta$  (see Sec. 2.6.2); this fact is significant because experimental measurements of this factor are otherwise difficult to make.

The second objective of the work was to apply the method. Three lattices were investigated; each consisted of slightly enriched uranium metal fuel rods immersed in heavy water moderator; the volume ratio



of moderator to fuel varied from 11.07 to 108.60 (see Sec. 3.2). Solid copper rods clad in nickel were chosen for use as added absorbers, for reasons discussed in Secs. 3.3 and 3.4. Diagrams of the nine assemblies investigated are given in Chap. III. The following quantities were measured: the macroscopic activation distribution with gold foils; the fine structure of the thermal neutron activation distribution with gold foils; the ratios  $\delta_{25}$  and  $\delta_{28}$ ; and the cadmium ratios for gold,  $U^{238}$ , and copper, for the assemblies with added absorbers. The techniques used in these measurements were not new, for the most part. They are described in Secs. 3.6 to 3.10.

The analysis of the macroscopic activation distributions to obtain the values of the material buckling of the assemblies with added absorbers proceeded much as in the now standard way used for unmodified lattices, with two exceptions (see Sec. 4.2). The first is that the radial extrapolation distance in units of the mean free path  $\lambda_{tr}$  is slightly larger for the modified assemblies ( $2.4 \pm 0.3$ ) than it is for the unmodified lattices ( $2.0 \pm 0.3$ ). The second is that the region of equilibrium cadmium ratio in the modified lattices is smaller than that in the unmodified lattices. Because data taken near the top of the assembly were unusable for this reason, the extrapolated height of the lattice was taken as the physical height plus the radial extrapolation distance. The values of the axial buckling are not sensitive to the value chosen for the extrapolated height.

The multigroup transport theory code THERMOS was used to obtain calculated, space-dependent spectra in decoupled cylindrical cells centered on fuel rods and copper rods (see Sec. 4.3.1). Use was made of a result of heterogeneous source-sink theory given by J. E. Suich (see Sec. 4.3.2) to determine the cell sizes and normalize the THERMOS-calculated activation distributions to the experimentally observed distributions. The calculated spectra were used to obtain hardened cross sections for use in calculating values of  $\eta$ ,  $f$ , and various thermal reaction rate ratios. A method was developed which makes use of the THERMOS-calculated spectra, and experimentally observed ratios of epithermal events to thermal events, to predict values of the same ratio in assemblies similar to the one in which the measurement was made (see Sec. 4.4). If the reaction rate cross



section is assumed to vary with neutron velocity ( $v$ ) as  $1/v$  throughout the epithermal energy range, no measurements are necessary. Fair agreement with experiment was observed when the method was used to predict values of  $\rho_{28}$ , the ratio of epithermal absorptions in  $U^{238}$  to thermal absorptions in  $U^{238}$ ; the method was sufficiently accurate to be useful for calculating values of  $\delta_{25}$ , and values of the ratio of epithermal absorptions to thermal absorptions in cladding, moderator, and added absorber.

The results of the investigation show that values of  $k_{\infty}$  and  $\eta$  can be measured in the manner proposed, with uncertainties between 0.5% and 1.0%, if the buckling measurements are sufficiently precise (see Secs. 5.1 to 5.5). Agreement with values of  $k_{\infty}$  calculated from the four-factor formula is good if the latter is modified to take into account epithermal fissions in  $U^{235}$ . The values of  $\eta$  obtained from the measurements were in good agreement with values calculated with THERMOS-hardened cross sections. The measurement of  $(k_{\infty}-1)$  is comparable in precision to that of the PCTR technique; this is significant because it shows that it is possible to obtain precise measurements of  $k_{\infty}$  without a critical facility.

A major advantage which the PCTR technique offers is economy of test lattice fuel; as little as one cell of the test lattice may be used. In order to investigate the possibility of similar economies in the sub-critical measurement of  $k_{\infty}$  with added absorbers, exploratory experiments in a two-region assembly were done (see Sec. 2.5). No final conclusion can be reached on the basis of these experiments, but it seems likely that the fine structure measurement and the measurements of  $\rho_{28}$ ,  $\delta_{28}$ , and  $\delta_{25}$  can be done in suitable two-region assemblies (see Sec. 5.7). The measurement of the material buckling in a two-region assembly is the subject of a separate study by another worker; final conclusions must await completion of this work.

It was found that the uncertainty in "experimental" values of the diffusion area,  $L^2$ , were smaller by a factor of three if the measured values of  $k_{\infty}$  were used instead of the values obtained with the four-factor formula (see Sec. 5.6). Criticality equations derived from two-group theory and age-diffusion theory were used, with calculated values of the Fermi age, and measured buckling values. The values of  $L^2$  derived from the age-diffusion equation were in slightly better



agreement with calculated values than were those derived from the two-group equation.

Simultaneous measurement of both parameters related to neutron leakage from finite assemblies during slowing down and diffusion ( $L^2, \tau$ ) was hampered by the low buckling values of the modified lattices, which render them unsuitable for determinations of these quantities (see Secs. 2.6.2 and 5.6).

## 6.2 SUGGESTIONS FOR THE FUTURE

### 6.2.1 One-Region Measurements

On the basis of the work done to date, it appears that thermal neutron absorbers can be used in one-region loadings in subcritical assemblies similar to those investigated here, to obtain measured values of  $k_\infty$  with an accuracy in  $(k_\infty - 1)$  of 3% or better, and an accuracy of 0.5% to 1.0% in  $\eta$ . At M. I. T., one to two weeks of experimentation per lattice, in addition to the normal experiments in the unmodified lattices, should provide sufficient data, if the added absorber concentrations are carefully chosen (see Appendix F). On the basis of these results, and the development of Sec. 4.4, it would appear that the parameters  $R_{28}$ ,  $\delta_{25}$ , and  $\delta_{28}$  need only be measured in the unmodified lattice and, at most, one modified lattice, preferably the one with the lowest buckling value. Measurements of  $R_3$  in one assembly in each series should suffice; if a body of effective resonance integral data for each copper rod size is built up, it may be possible to dispense with this measurement altogether and rely entirely on the method of Sec. 4.4 for values of  $\rho_3$ .

The microscopic distribution experiments could be improved by reducing the number of foils in the moderator, particularly in tightly-spaced lattices, and increasing the number of foils irradiated on the rod surfaces. The evidence gathered to date indicates that the THERMOS-calculated activation distribution in and on the surface of the copper rods and the fuel rods is in good agreement with the measured distribution. It may, therefore, be possible to dispense with irradiation of the foils within the rods, irradiate a number of foils on the rod surfaces instead, and use the THERMOS results to calculate the distribution within the rod. One of the most time-consuming aspects of the microscopic experiments is the loading of foils into the fuel and copper rods; certainly some of



the microscopic traverses could be done in this way in each assembly.

It was noted in Sec. 5.4 that the uncertainty in  $k_{\infty}$  depends strongly on the uncertainty in  $A_3^0$ , the ratio of thermal neutron absorptions in added absorber to thermal neutron absorptions in fuel, for an assembly with a material buckling value of zero. The measurement of  $k_{\infty}$  can be improved by reducing the uncertainties in  $A_3^0$ . Figures 5.1 to 5.4 show that the value of  $A_3^0$  is usually more strongly influenced by uncertainties in the values of the material buckling than by uncertainties in the values of  $A_3$ . Table 5.1 shows that increasing the number of buckling measurements would result in considerable improvements in the uncertainties; the desirability of this has to be weighed against the increased time necessary for the measurements. If the uncertainties in the values of the buckling are markedly reduced, then the uncertainties in the values of  $A_3$  for each assembly will make a more important contribution to the uncertainty in  $A_3^0$ . The uncertainty in  $A_3$  is dominated by the 1.1% uncertainty in the microscopic absorption cross section of copper for thermal neutrons (see Sec. 5.4). Remeasurement of this parameter with greater precision, or use of a different absorber with a better-known absorption cross section, would reduce the uncertainties in the values of  $A_3$ . If substantial reductions in the uncertainty in the absorption cross section can be made, counting statistics on the foils in the microscopic traverses will make a more important contribution and should be improved correspondingly.

The measurements could be improved in some respects by the use of a homogeneous added absorber, such as boric acid dissolved in the moderator. The advantages and disadvantages of this, and the reasons for the use of lumped absorbers here, are discussed in Appendix B.

Improvements in the precision with which  $k_{\infty}$  is measured will result in corresponding improvements in the uncertainties in the "experimental" values of the diffusion area,  $L^2$ . As noted in Secs. 2.6.2 and 5.6, and in Appendix G, the requirements for the measurement of  $k_{\infty}$  and the requirements for the simultaneous measurement of  $L^2$  and  $\tau$  conflict with each other, so that separate sets of experiments will probably be necessary if both measurements are to be made.



### 6.2.2 Two-Region Measurements

It has been shown that approximately equal precision in the measurement of  $(k_{\infty}-1)$  may be expected from the Hanford technique (see Sec. 1.2) and the subcritical measurement described here. The Hanford technique requires much less fuel, but a critical facility is necessary, and the so-called "spectral mismatch" problem is important in the interpretation of the results. Care must be taken to measure the extent to which the neutron spectrum incident on the central cell of the reactor differs from the equilibrium spectrum, and correct the measured values of  $k_{\infty}$  accordingly. The subcritical technique circumvents the spectral mismatch problem; thus, if enough test fuel is available for the construction of an exponential assembly, it should give results as good as those given by the Hanford technique, possibly at less cost.

In the Introduction, the need for accurate results from assemblies utilizing minimum amounts of fuel was noted. Accordingly, the next step in the development of the subcritical measurement of  $k_{\infty}$  should be a detailed investigation of the two-region experiment. Such measurements involve a spectral mismatch problem just as does the PCTR measurement, but if theoretical correction factors can be derived, the method holds promise of combining high precision and economy in test fuel, as well as the safety and low operating costs associated with an exponential facility. Some of the alternatives for future experimentation are given in Table 6.1. One "Type 1" experiment has been done already; the results are given in Sec. 5.7. Type 1 and Type 2 experiments represent no improvement over the one-region measurement, since a full subcritical loading of fuel is required; such experiments will be chiefly of interest in the development of the method. A successful Type 3 experiment is the ultimate objective; problems of theoretical interpretation will be greatest in this case, but the required amount of test fuel and added absorber are at a minimum. If Type 3 experiments cannot be done, a Type 4 experiment would be nearly as useful; by adding absorbers to the reference region, the differences between the test and reference region may be made small, and problems of theoretical interpretation eased.

The problem deserves further study.

TABLE 6.1

Possible Configurations for Subcritical Two-Region Measurements of  $k_{\infty}$ 

Experiment Type	Reference Region	Test Region	Full Subcritical Loading of Test Fuel Required?	Comment
1	Lattice I without added absorbers.	Lattice I with added absorbers in several different amounts, varied to obtain several values of $B_m^2$ near zero.	Yes	Large difference between test and reference regions.
2	Lattice I with added absorbers sufficient to make value of $B^2$ near zero.		Yes	Minimal difference between test and reference regions.
3	Lattice II without added absorbers.		No	Large difference between test and reference regions.
4	Lattice II with added absorbers sufficient to make value of $B^2$ near zero.		No	Difference between test and reference regions depends on choice of test and reference fuel; may be made small.

Note: Lattice I is the lattice to be investigated; lattice II is a reference lattice presumably available in large enough amounts so that its characteristics may be established in one-region measurements.



## APPENDIX A

### LITERATURE RESEARCH

The purpose of this appendix is to note briefly some references to work that has been done in areas of interest closely allied to this study.

#### A.1 MEASUREMENT OF $k_{\infty}$ AND $\eta$

Experimental determinations of  $k_{\infty}$  are usually made by measuring quantities such as  $\delta_{28}$ ,  $\delta_{25}$ ,  $\rho_{28}$ , and the fine structure of the thermal neutron distribution, using the measurements to calculate values of  $\epsilon$ ,  $p$ ,  $f$ , and  $(1+\delta_{25})$  in a manner similar to that described in Sec. 2.3, calculating  $\eta$ , and then computing  $k_{\infty}$  from an equation like Eq. (2.7). The measurements can be done in critical or subcritical lattices. Other ways of measuring  $k_{\infty}$  include the Hanford technique, described in Sec. 1.2, and pulsed neutron experiments (MA 1). A review of measurements of  $k_{\infty}$  and intracell lattice parameters (including  $\eta$ ) in lattices fueled with uranium and moderated with light water, heavy water, or graphite is given in Ref. KA 1; the Hanford technique is also discussed. Another more detailed survey, confined to assemblies moderated with heavy water, is found in Ref. CR 3; measurements of both  $k_{\infty}$  and  $\eta$  are discussed.

Measurements of  $k_{\infty}$  are being made in Europe with the Hanford technique; one example is the work done at the Institute of Technology in Munich by G. Riesch (RI 1).

Results of measurements of  $\eta$  as a function of energy for  $U^{235}$  and other nuclides are given in Refs. AN 1 and SA 3. Values of  $\eta$  in a lattice spectrum have been obtained from analyses of the variation of other measured lattice parameters as a function of  $U^{235}$  concentration (KO 1) and lattice spacing (MU 1). Values of  $\eta$  have also been measured at the Savannah River Laboratory by a cadmium ratio technique (CR 3, HU 2).

The subcritical technique for the measurement of  $k_{\infty}$  described in Sec. 2.4 is applicable only for lattices with values of  $k_{\infty}$  greater than unity. A complementary technique restricted to lattices for which the value of  $k_{\infty}$  is less than unity has been evolved at the University of

Virginia. The method involves the use of added absorbers, but does not appear to be closely related to the Hanford technique. The method is described in Ref. BU 1; experimental results for a lattice of natural uranium rods in light water moderator are given. The value of  $k_{\infty}$  obtained was  $0.929 \pm 0.002$ ; the calculated value obtained with the four-factor formula for the same lattice was  $0.944 \pm 0.011$ . The value of  $k_{\infty}$  measured in pulsed neutron experiments was  $0.939 \pm 0.012$ .

## A.2 USE OF ADDED ABSORBERS IN SUBCRITICAL LATTICES

Added absorbers are often used in critical experiments, but their use in subcritical lattices is much less common. An early example of such work is reported by E. R. Cohen et al. in Ref. CO 1. Lattices of natural uranium rods in heavy water moderator were studied; in one of these, measurements of the Fermi age were made by borating the moderator. Changes in the radial buckling,  $\eta$ ,  $\rho$ , and  $\epsilon$  were assumed negligible,  $f$  and  $L^2$  were calculated, and the age evaluated by measuring the change in the axial buckling; Eq. (2.31) was used. Heterogeneous absorbers have been added to subcritical lattices moderated with heavy water at the Savannah River Laboratory (CR 2); in one such experiment, unclad copper tubes were used (DU 1). The work was part of an effort to measure migration areas and anisotropy for a particular lattice; the results were used in conjunction with critical experiments.

Boric acid was added to the light water moderator of a number of lattices of slightly enriched uranium metal rods studied at Brookhaven National Laboratory (KO 1) in experiments to determine the migration area,  $M^2$ . Equations derived from simple reactor models were used to relate  $k_{\infty}$  and the buckling; one of these is:

$$k_{\infty} = 1 + M^2 B_m^2 . \quad (\text{A.1})$$

The buckling was measured for the modified lattices, and the thermal utilization was calculated. From Eqs. (A.1) and (1.1), a formula for the thermal utilization as a function of the material buckling can be written:

$$f = \frac{1}{\eta\epsilon\rho} + \frac{M^2}{\eta\epsilon\rho} B_m^2 . \quad (\text{A.2})$$

Values of the migration area, which was assumed to be unaffected by



the added absorber, were calculated from the slope of the curve of  $f$  against  $B^2$ . The measured values of  $\eta$ ,  $\epsilon$ , and  $p$  for the unmodified lattice were used. Similar analyses were done with equations like Eqs. (2.30) and (2.31) in place of Eq. (A.1); the migration area was determined from the relationship:

$$M^2 = L^2 + \tau . \quad (\text{A.3})$$

The value of  $k_\infty$  obtained from Eq. (A.1), with the experimental values of  $M^2$  and  $B_m^2$ , can be shown to be the same as that which would be obtained if the experiments were analyzed with the technique described in Sec. 2.4, under the assumption that the correction terms in Eq. (2.28) are all unity.

English workers have done experiments similar to those done at Brookhaven in lattices of natural uranium rods in light water moderator at Queen Mary College in London (MA 2). The work on natural uranium-water lattices at the University of Virginia has been mentioned in Sec. A.1.

As far as is presently known, the present study represents the first published account of experiments made in an attempt to adapt the Hanford technique to subcritical measurements, although the possibility is mentioned in one of the earliest articles on the technique (HE 10).

APPENDIX B  
USE OF ADDED ABSORBERS  
HOMOGENEOUSLY DISPERSED IN LIQUID MODERATOR

Although lumped absorbers were chosen for use here (see Sec. 3.3), the absorber could equally well have been dissolved in the liquid moderator. This method has advantages, to be discussed below. It will be noted that the description of the theory, the equipment, and the analysis of data in Chaps. I to IV applies equally well to either case, except in some respects in which the use of homogeneously dispersed absorber results in a simplification of the treatment. The purpose of this appendix is to discuss the advantages and disadvantages of each method of adding absorber, and give the reasons for using lumped absorbers here.

The first and most important difference between the two methods concerns the measurement of the thermal utilization, or equivalently, the relative absorption in the added absorber. As noted at the beginning of Sec. 4.3.2, if the absorber is uniformly dispersed in the moderator, a THERMOS calculation may be made for the modified lattice exactly in the manner described in Sec. 4.3.1 for the unmodified lattices. The treatment of Sec. 4.3.2 may thus be dispensed with entirely. It is possible that no microscopic traverses would be necessary at all, if it were proven that the THERMOS results were as reliable as an experiment, as is the case with an unmodified lattice of the type considered here. In either event, an important decrease in the time needed for experiments would result. The preliminary calculations described in Appendix F would also be made simpler and more precise.

A second difference between the heterogeneous and homogeneous methods concerns the determination of the ratio of epithermal absorptions to thermal absorptions in the absorber,  $\rho_3$ . If, for example, an absorber such as boric acid were to be dissolved in the moderator, and the assumption could be made that the absorber cross section varies as  $1/v$  throughout the epithermal energy range, the value of  $\rho_3$  could simply be obtained with Eq. (4.22). A further decrease in the amount of



time needed for the experiments would be effected.

Another (minor) advantage of a homogeneous absorber is that it displaces virtually no moderator. This is inconsequential in assemblies moderated with heavy water, as has been shown here, but it is possible that in the more tightly packed assemblies moderated with light water, solid absorbers would displace enough moderator to cause an undesirably large change in the resonance escape probability.

A fourth difference between the two methods under discussion concerns the ease with which buckling values near zero may be attained practically. If a homogeneous absorber is used, the absorber concentration may more readily be varied in small amounts. If this were done after preliminary analysis of buckling measurements, it would be possible to attain buckling values very near zero, or bunched about that point. This procedure should result in increased accuracy, or equivalently, should require fewer experiments than the heterogeneous method, to obtain equal accuracy in  $k_{\infty}$ .

Against the foregoing advantages of homogeneously dispersed absorber, some disadvantages must be considered. Determination of the amount of absorber added, which can be done without significant uncertainties for heterogeneous absorbers, is not always simple, and may become an added source of error in the most important parameter in the measurements,  $A_3^0$  (see Sec. 4.5). For boric acid, titration techniques have been used (KO 1, CR 2). A sigma-pile measurement (WE 1) might also be done in the exponential tank with the fuel rods removed. Care must also be taken to ensure that no absorber is plated out or deposited in the piping of the system. Also, if a relatively expensive moderator such as heavy water is used, it is important to be sure that all of the absorber can be removed when the experiments are over. Finally, if two-region measurements such as those discussed in Secs. 2.5, 5.7, and 6.2.2 are to be done, heterogeneous absorbers are required unless the test region is to be isolated from the reference region. Such measurements involve varying the absorber concentration in the test region, without varying it in the reference region. Obviously, unless the test region is separated from the reference region, heterogeneous absorbers are required.

Heterogeneous absorbers were used in this work principally to avoid contamination of the heavy water moderator and the plumbing of

the subcritical facility; the work described here is only a small part of the Lattice Project research, and it was thought that it should on no account endanger the success of other experiments in progress. Furthermore, experiments with two-region assemblies may be done in the future; as noted above, this all but requires heterogeneous absorbers. Finally, as discussed earlier, the heterogeneous method is more complicated than the homogeneous method; since it has been used successfully, it would appear clear that the homogeneous method should work as well or better, resulting in even more accurate measurements of  $k_{\infty}$ . Had homogeneous absorber been used, little could have been said about heterogeneous absorbers.



## APPENDIX C

## FOIL COUNTING: PROCEDURES AND ANALYSIS OF DATA

The foils used, the procedures for counting them, and the methods of data analysis have been discussed in Secs. 3.7 and 4.1. The purpose of this appendix is to give further details on these aspects of the work.

The counting equipment used is described in detail in Ref. SI 1. The practices followed here in counting the foils are much the same as those described there. Dead times for the two NaI scintillation counters were remeasured by the two-source method (PR 1); the values obtained, and used in this analysis, were between  $10^{-7}$  minute and  $3 \times 10^{-7}$  minute. The counting equipment was calibrated regularly; integral counting was used throughout, with the cutoff energy set at the low point in the gamma spectrum between the 411-keV photopeak and the Compton edge.

Foils were washed in acetone before they were weighed, before they were mounted on foil holders for irradiation, and before they were counted. Foils that were scratched in the process of removal from the holders were reweighed; usually, the weight did not differ by a statistically meaningful amount, but in the few cases where it did, the new weight was used in the analysis. Scratched foils were not reused.

In general, each set of foils was counted at least three times, for a preset number of counts. The total number of counts on foils from the macroscopic traverses was always between 60,000 and 600,000, and usually was between 100,000 and 300,000. The total number of counts on the foils from the microscopic traverses varied from 30,000 to 300,000, and usually was between 40,000 and 200,000. Because the thermal activation was sought, the bare foils were counted for two to four times as many counts as the cadmium-covered foils. Because the printer-timer accuracy is  $\pm 0.01$  minute, no counting intervals were less than 2.50 minutes; most were longer than 5.00 minutes. No count rates were higher than 50,000 counts per minute, to ensure that the dead time correction did not introduce appreciable error.

The measurement of the background count rate is discussed in Sec. 4.1. The measurements made before and after the counting runs



did not differ by a statistically meaningful amount, except in one instance, to be discussed below. The variation in background count rate due to the movement of foils by the automatic sample changers is greater; variations by nearly a factor of two are possible. Accordingly, background count rates were always measured with all foils in the sample changer, at several points in the counting cycle, and the average value used. Because the counters were well shielded, the background count rate was usually 5% of the lowest count rate, or less. A sufficient number of background counts was taken so that the uncertainty in the foil count rate due to the uncertainty in the background was less than the uncertainty due to counting statistics on the foil itself.

The foil data analysis was done with a computer code described in Refs. SI 1 and SI 3. The fractional standard deviation based on counting statistics (PR 1) and the fractional standard deviation based on scatter about the mean, for all foils, are calculated and printed out for comparison. The two were in good agreement, within 10% of each other, except as noted below. The fractional deviation from the mean is also printed out, for each count on each foil.

In Sec. 4.3.2, malfunctions of counting apparatus were mentioned which affect the results of experiments in the 175A1B1 assembly. It was observed repeatedly that one of the counting setups had two distinct background levels, 30 counts per minute and 120 counts per minute. The background count rate was constant at one of these two levels, for periods long compared to the duration of a single foil count, but it did alternate between the two. No other counting equipment was available, and no remedy could be found for the difficulty on short notice. Accordingly, the foils were counted with the faulty apparatus. The data were analyzed twice, with the background count rate taken first as 30 counts per minute and then as 120 counts per minute. Foils were counted three to six times; inspection of the table of deviations from the mean count rate allowed an estimate to be made of which of the two backgrounds was appropriate for each foil count. The data were then reanalyzed with the variable background count rate determined in this way. The fractional standard deviation based on scatter about the mean for all foils was always reduced by this reanalysis. No counting runs were used for which this quantity was more than twice the value calculated from the total number of counts.



The foregoing procedure was an emergency measure, and it is realized that it is not wholly satisfactory. The counter difficulty was subsequently remedied and did not reoccur. The effect of the 175A1B1 measurements on the results is discussed in Sec. 5.4 and shown to be negligible.

Usually, all foils from a given macroscopic traverse were counted in the same counting run. This was not possible, however, in the case of the axial distribution measurements in the 250 assemblies. Because the activities of the foils at opposite ends of the foil holder differed by as much as a factor of 100 (see Fig. 4.7), counting all foils for a preset number of counts in one counting run was impractical. Accordingly, the 17 foils in each traverse were split into two batches. The eleven least active foils were counted first, followed by the nine most active foils. Three intermediate foils were counted in both batches and provided a means of correcting for counter drift; these corrections were made as explained in Sec. 4.1. During the experiments on the 175 and 253 lattices, counting equipment was available which allowed all foils from a given axial traverse to be counted in one run. Instead of simply presetting the number of counts, both a preset time and a preset number of counts could be used; counts were terminated when either limit was reached. This equipment was used for analysis of all axial traverses in the 175 and 253 assemblies.

It should be noted that in the experimental measurement of  $R_3$  described in Sec. 3.10, it is actually the cadmium ratio of  $\text{Cu}^{63}$ , here defined as  $R_{\text{Cd}}^{63}$ , which is determined. The other isotope of natural copper,  $\text{Cu}^{65}$ , activates to form  $\text{Cu}^{66}$ , which has a 5.2-minute half life. Since more than two hours always elapsed between the end of the irradiations and the beginning of the foil counting, no account was taken of  $\text{Cu}^{65}$  in the measured cadmium ratio. The average value of the ratio  $\frac{R_{\text{Cd}}^{63} - 1}{R_{\text{Cd}}^{65} - 1}$  was experimentally measured by workers at Hanford, with foils varying from 0.0013 inch to 0.020 inch in thickness, and found to be  $1.00 \pm 0.07$  (BE 1). It is shown in the reference cited that the resonance integrals of natural copper,  $\text{Cu}^{63}$ , and  $\text{Cu}^{65}$  may be inferred from their thermal cross sections and measurements of  $R_{\text{Cd}}^{63}$  only. Accordingly, no measurement of  $R_{\text{Cd}}^{65}$  was made, and the measured value of  $R_{\text{Cd}}^{63}$  was used in the calculation of  $\rho_3$ , the ratio of epithermal absorptions to thermal absorptions in natural copper.

APPENDIX D  
 DIMENSIONS, DENSITIES, AND NUCLEAR CROSS SECTIONS  
 OF MATERIALS USED

In this appendix, the physical dimensions and properties of the various materials used in the assemblies are given.

D.1 DIMENSIONS AND DENSITIES

The dimensions of the fuel rods are given in Table 3.1. The diameter of the "A" copper rods is  $0.1872 \pm 0.0001$  inch; the diameter of the "B" copper rods is  $0.1438 \pm 0.0001$  inch. The cladding thickness is  $0.0005 \pm 0.0002$  inch. The uncertainties are standard deviations of the mean of eight to twelve measurements. The rods are very uniform in diameter, as indicated by the small uncertainties.

The density taken for the uranium metal fuel in the 250 and 175 assemblies was  $18.92 \text{ gm/cm}^3$ . The density taken for the fuel in the 253 assemblies was  $18.90 \text{ gm/cm}^3$ . For the determination of the density of the copper, three cylindrical samples were prepared by circular grinding. Their dimensions were carefully measured with a micrometer, and they were weighed with a microgram balance. Table D.1 gives the results. The uncertainty calculated on the basis of the uncertainty in the measurements is given; the standard deviation of the mean of the three measurements is  $0.012 \text{ gm/cm}^3$ .

TABLE D.1  
 Density of Copper Samples

Sample	Weight (gm)	Volume ( $\text{cm}^3$ )	Density ( $\text{gm/cm}^3$ )
1	5.351138	0.600908	8.905
2	5.302960	0.596276	8.894
3	5.828190	0.656631	8.876
Average			$8.892 \pm 0.015$



The density of KANIGEN is listed in Ref. AR 1 as  $7.85 \pm 0.03 \text{ gm/cm}^3$ . The purity of the  $\text{D}_2\text{O}$  is given in Table 3.1; it is based on the assumption of a linear variation in the purity between two measurements made at the beginning and at the end of the experiments on the lattices for which results are reported. The uncertainty in a single measurement is about 0.03 mol %.

## D.2 NUCLEAR CROSS SECTIONS USED IN THERMOS CALCULATIONS

The THERMOS code was used as described in Sec. 4.3.1. The moderator temperature was taken as  $20^\circ\text{C}$ ; the mass used in calculating the high energy source term was the mass number. The standard cross section data described and tabulated in Refs. DA 1, HO 2, SI 1, and SI 2 were used for the cross sections of  $\text{U}^{235}$ ,  $\text{U}^{238}$ ,  $\text{N}^{14}$ ,  $\text{O}^{16}$ ,  $\text{Al}^{27}$ ,  $\text{D}_2\text{O}$ , and  $\text{H}_2\text{O}$ ; the original data sources are Refs. HU 1, NE 1, and SA 1. Cross-section data for the copper rods and their KANIGEN cladding are given in Table D.2. The source of the data is Ref. HU 1, except that the thermal neutron absorption cross section of copper is taken from Ref. DO 1.

TABLE D.2  
Nuclear Cross Sections of Added Absorbers

Material	Microscopic Absorption Cross Section for 2200 m/sec Neutrons (barns)	Microscopic Scattering Cross Section for Slow Neutrons (barns)
Cu	3.79	7.2
Ni	4.6	17.5
P	0.19	5.0

For the convenience of future workers, the concentrations calculated from the foregoing data for use with the THERMOS code are given in Table D.3. The absorption cross sections of the nitrogen in the air gap and the copper, nickel, and phosphorus in the added absorbers were assumed to vary as  $1/v$  with incident neutron velocity  $v$ ; the scattering cross sections were treated as constant. The scattering cross sections used in the high energy source calculation are given in Table D.3 also.

TABLE D.3 THERMOS Input Data: Concentrations and High Energy Cross Sections

Region	Lattice	Material	Isotope Identification Numbers	Concentration for Calculation Proper (at./barn cm)	Isotope	High Energy Scattering Cross Section (barns)	Concentration* for High Energy Source Calculation (at./barn cm)			
Fuel	250-175	Uranium	23592-1	0.00055444	U <sup>235</sup>	10.0				
			23592-2							
	253	Uranium	23892-1	0.047349	U <sup>238</sup>	8.5				
			23592-1							
		23592-2	0.00045888	U <sup>235</sup>	10.0					
		23892-1				0.047393	U <sup>238</sup>	8.5		
Air gap	All	Air	3000-20	0.00008	N <sup>14</sup>				9.9	0.0001
			2000-20	0.00024						
Fuel rod cladding	All	Aluminum	168-1	0.0000538	O <sup>16</sup>	3.75				
			2713-1	0.060275	Al <sup>27</sup>	1.40				
Moderator	250	Light and heavy water	20-51	0.066229	D	3.4				
			18-51	0.0002927	H	20.4				
			168-1	0.033261	O	3.75				
	175	Light and heavy water	20-51	0.066209	D	3.4				
			18-51	0.0003127	H	20.4				
			168-1	0.033261	O	3.75				
	253	Light and heavy water	20-51	0.066196	D	3.4				
			18-51	0.0003260	H	20.4				
			168-1	0.033261	O	3.75				
Added absorber	All	Copper	3000-20	0.31954	Cu(nat)	7.2	0.08431			
			2000-20	0.60704						
		KANIGEN	3000-20	0.33127				Ni(nat)	17.5	0.07129
			2000-20	1.33543				P(nat)	3.4	0.01757
Fictitious scattering region	All	-	2000-20	200.	-	-	0.			

\* Concentration is the same as for calculation proper, unless otherwise given.



## APPENDIX E

CALCULATION OF SPECTRALLY AVERAGED PARAMETERS  
IN A MODIFIED LATTICE WITH THE TULIP CODE

The method in which THERMOS calculations and the results of the microscopic traverses have been used to calculate spectrally averaged parameters for the modified lattices is described in Sec. 4.3.2. The purpose of this appendix is to give some details concerning the method, and describe a computer code written to do the calculations.

## E.1 CALCULATION OF FOIL ACTIVITIES

The experimentally observable quantity in studying the fine structure of the thermal neutron distribution in an assembly is the activity of foils positioned in and around the fuel and absorber rods (BR 1, SI 1). For a precise comparison with theory, foil activities must be calculated from the theoretical distribution in space and energy. The calculated thermal activity of foil  $j$  is  $\underline{A}_j$ , where

$$\underline{A}_j = \int_j \int_0^{v_c} v N(\vec{r}, v) \Sigma^*(v) dv d\vec{r}, \quad (\text{E.1})$$

and the notation of Sec. 4.3 is used;  $\Sigma^*(v)$ , the activation cross section as a function of velocity, is also a function of foil thickness, owing to self-absorption effects (SI 1). The spatial integration is over the surface of the foil  $j$ . In the formulation for a cylinder, with  $r$  the radial position coordinate, the expression for  $\underline{A}_j$  may be written:

$$\underline{A}_j = \int_j A^*(r) (2\pi r dr), \quad (\text{E.2})$$

with

$$A^*(r) = \int_0^{v_c} v N(r, v) \Sigma^*(v) dv. \quad (\text{E.3})$$

The quantity  $A^*(r)$  is the specific activation at  $r$ ; it must be integrated over the foil surface to obtain  $\underline{A}_j$ .

The THERMOS code can be used to calculate values of  $A^*(r)$ ; since all quantities are taken to be constant within each of the twenty space

regions, the graph of  $A^*(r)$  against  $r$  is really a histogram (see Fig. E.1), although it is generally shown in graphs like Figs. 4.10 and 4.11 as a continuous curve. This histogram may be integrated over the surfaces of the foils, or it may be converted to an appropriate smoothed function before the integration is done.

Normalization of the experimental results to the THERMOS-calculated distribution for unmodified lattices is discussed by P. Brown in Ref. BR 1; Brown concluded that the normalization should be done at the cell edge, where the neutron distribution is fairly constant over a large area. Here, on the other hand, the inclusion of absorber rods in the lattices reduces the area over which the distribution is constant; furthermore, good agreement with the THERMOS-calculated distribution everywhere in the moderator is not expected or required. Accordingly, experiment has been normalized to theory at the center of the fuel rod, where good agreement is to be expected.

The gradient of the neutron density distribution is relatively large in the fuel rod, and it was not clear at the beginning of the work that the foils used were small enough, compared to the fuel rod size, to be treated as point detectors. It was thought worthwhile to treat the problem of calculating the foil activities in more detail than is customary in analyzing the results of the experiments in the unmodified lattices.

Accordingly, four methods for calculating the foil activities have been tried. The first, and simplest, involves treating  $A^*(r)$  as a histogram, and using the values of  $A^*(r)$  at the foil center ( $r_j$ ) to compute  $\underline{A}_j$ :

$$\underline{A}_j = FA^*(r_j) , \quad (\text{E.4})$$

where  $F$  is the area of the foil. The second involves integration of  $A^*(r)$  in its histogram form over the foil surface to obtain  $\underline{A}_j$  (Eq. (E.2)). The third and fourth methods were identical to the first and second, respectively, except that the histogram  $A^*(r)$  was converted to a continuous, piecewise linear distribution before the  $\underline{A}_j$  were calculated. The linearization was made by requiring continuity at the interfaces between regions, as well as constancy of the integral

$$\int A^*(r)(2\pi r dr) \quad (\text{E.5})$$

over each region, in both approximations to the true  $A^*(r)$ . The



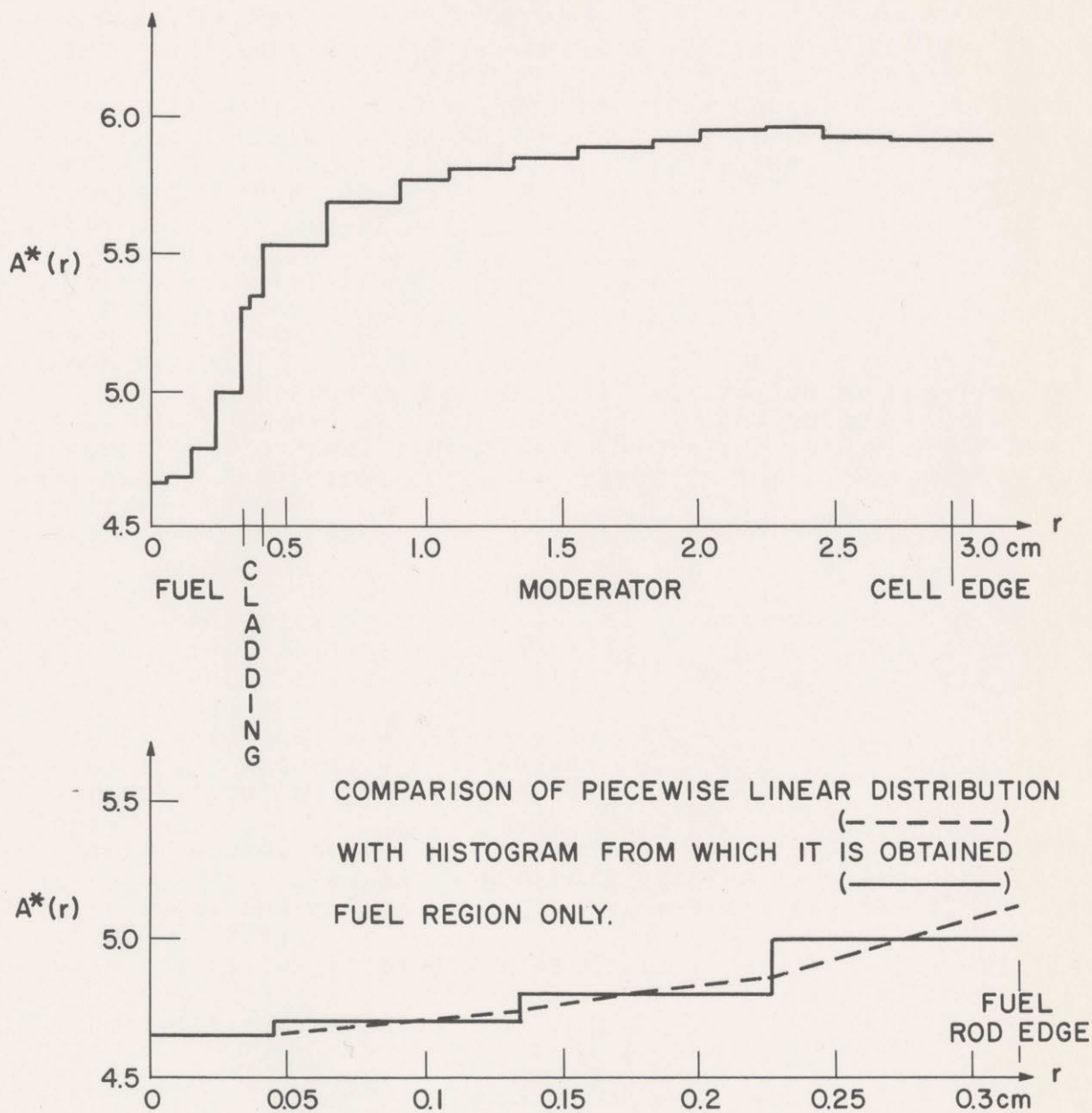


FIG. E. I. SPECIFIC ACTIVATION  $A^*(r)$  AS A FUNCTION OF RADIAL POSITION IN CELL ( $r$ ). HISTOGRAM CALCULATED BY THERMOS FOR 0.010-INCH GOLD FOILS IN 250BI ASSEMBLY.

calculation was begun by assuming that  $A^*(r)$  was flat throughout the center region. An example of the results obtained is shown in Fig. E.1.

Activities for the foils in the fuel rod in each of the sixteen independent microscopic traverses were calculated by the four methods described, and compared with experiment by calculating the r m s value of the percentage differences. The results are given in Table E.1. (The slightly larger r m s values in the 253 assemblies are caused by counting statistics, which were not as good as those in the 250 and 175 experiments, where thicker foils were used.) It does not appear that any one of the methods can definitely be excluded on the basis of these results. The linearization of the THERMOS-calculated distribution (methods 3 and 4) seems to improve agreement with experiment slightly, particularly in the 250 and 175 assemblies, probably because the histogram for  $A^*(r)$  gives over- or underestimates for the specific activity near the interfaces between regions (see Fig. E.1). Although method 4 would be expected to be more precise than method 3 for the experiments done here, both appear to yield equally good agreement with experiment. The difference between the two values of the thermal utilization derived with methods three and four is very small, and is less than the uncertainty in this quantity. Method 4 has been used consistently throughout the work.

## E.2 NORMALIZATION OF CALCULATED NEUTRON DENSITIES

Let the experimental activity of foil  $j$  be  $E_j$ . Then the proportionality factor  $a_j$  between experimental and calculated activities for foil  $j$  may be written:

$$a_j = \frac{A_j}{E_j} . \quad (\text{E.6})$$

The average proportionality factor  $\bar{a}$  is defined for the fuel cell as:

$$\bar{a} = \frac{1}{M} \sum_1^M a_j , \quad (\text{E.7})$$

where  $M$  is the number of foils in the fuel. If average quantities, defined as in Sec. 4.3 are used, Eq. (E.1) may be written:

$$\bar{A}_j = \bar{v}_j \bar{N}_j \bar{\Sigma}_j^* F . \quad (\text{E.8})$$



TABLE E.1

Comparison of Four Methods for Normalizing Theory and Experiment:  
RMS Value of Percentage Residuals

Assembly	Run No.	$\bar{A}^*(r)$ Taken as Histogram		$\bar{A}^*(r)$ Linearized	
		Eq. (E.4)	Eq. (E.2)	Eq. (E.4)	Eq. (E.2)
		Method 1	Method 2	Method 3	Method 4
250A2	7	1.96	1.23	1.17	1.29
250A2	8	1.10	0.85	0.80	0.80
250A1	11	1.41	1.43	1.50	1.41
250A1	13	1.77	1.40	1.30	1.39
250B2	16	1.11	0.72	0.68	0.69
250B2	18	1.19	0.96	0.86	0.91
250B1	21	1.11	0.82	0.73	0.77
250B1	23	1.60	0.74	0.75	0.85
175A1B1	26	0.62	1.33	1.30	1.21
175A1B1	29	0.79	0.51	0.42	0.43
175A1	32	0.77	0.84	0.78	0.76
175A1	34	1.09	1.05	1.12	1.03
253A2B1	44	2.10	1.54	1.55	1.62
253A2B1	46	2.98	2.59	2.29	2.39
253A2	48	2.04	2.52	2.64	2.59
253A2	49	2.07	2.24	2.38	2.22

Solving for the relative neutron density in terms of the experimentally observed activity yields the following equation:

$$\bar{N}_j = \frac{\bar{a}E_j}{\bar{v}_j \bar{\Sigma}_j^* F} \quad (\text{E.9})$$

It has been found convenient in practice to normalize all neutron densities to the calculated neutron density for the fuel cell. The values of  $\bar{N}_i$  for use in Eqs. (4.7), (4.8), (4.11), (4.12), and (4.15) are then obtained as follows:  $\bar{N}_i$  for the fuel and its cladding are obtained directly from the THERMOS calculation; the value of  $\bar{a}$  determined for the foils in the fuel allows determination of the  $\bar{N}_i$  throughout most of the rest of the cell from the experimental values of  $E_j$ . The copper cladding and the outer region of the copper rod have no foils imbedded in them, so that an appropriate value of  $\bar{N}_i$  for these regions must be taken from the copper cell calculation, with proper normalization.

### E.3 CALCULATION OF THERMAL UTILIZATION AND OTHER PARAMETERS

Insofar as is possible, the derived values of  $f$  and other parameters are experimental in nature. The disadvantage factors ( $\bar{N}_i/\bar{N}_0$ ) are obtained as outlined above;  $\bar{v}_i$  and  $\bar{\Sigma}_i$  are taken from the THERMOS calculation and are independent of the normalization just discussed. The  $V_i$  are fixed by the dimensions of the various lattice elements. The moderator region was split up into subregions, each roughly centered on a foil, and the neutron density taken to be constant over the subregion and given by Eq. (E.9) (see Fig. E.2). Although this is a somewhat drastic assumption, it is acceptable in practice because the neutron distribution is nearly "flat" in the moderator region and because very few neutrons are absorbed there. Several different moderator subregion sets were tried in each assembly; the values of the thermal utilization were not appreciably affected.

The calculation of the diffusion coefficient,  $\bar{D}$ , is described in Sec. 4.3.1; it is evaluated for the moderator with Eq. (4.12), and the assumption is made that this is a good approximation to the value for the lattice, since the volume of fuel is usually small compared to the volume of moderator, and the diffusion coefficients for the fuel and moderator are not markedly different (see Table E.2). The same



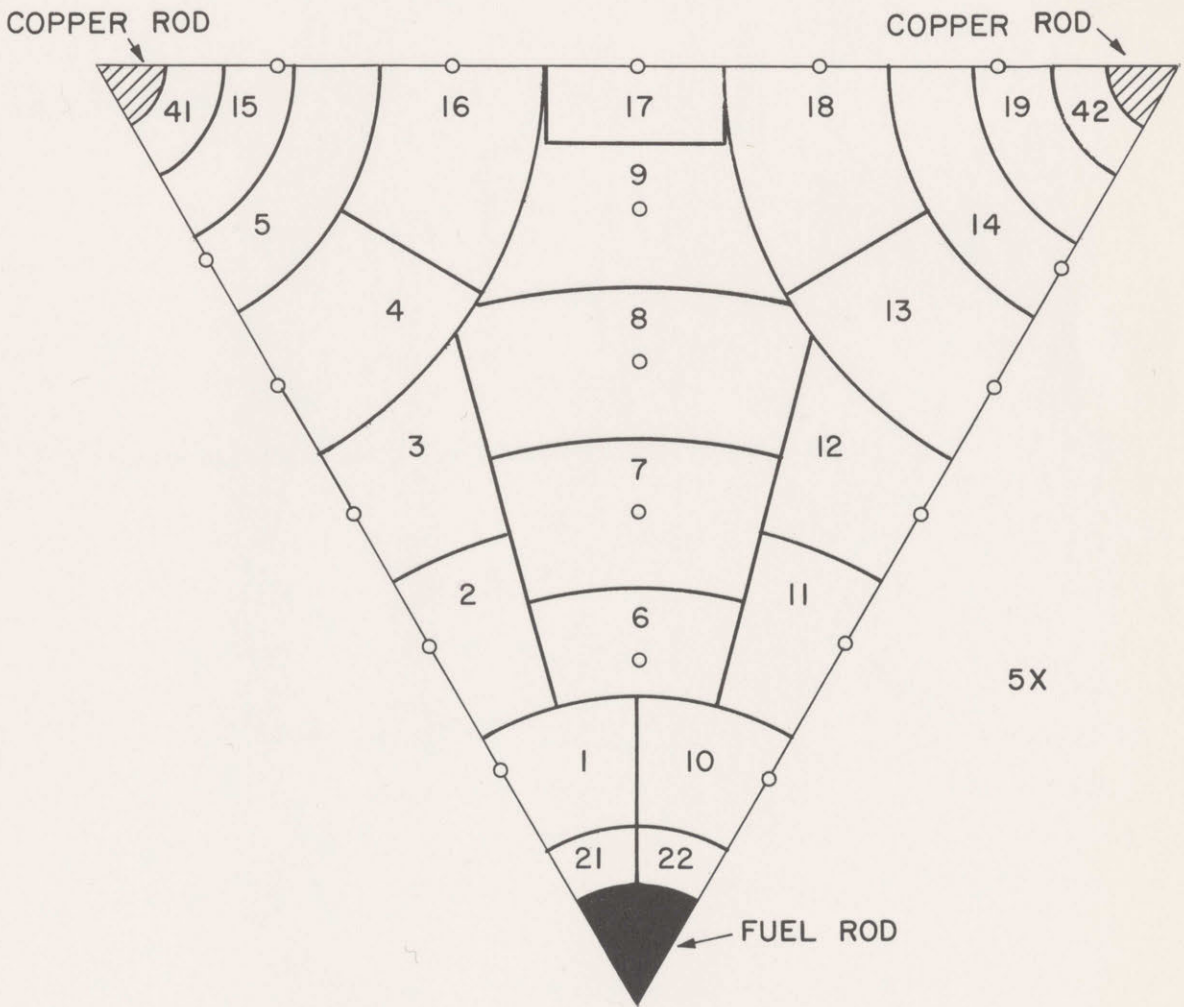


FIG. E.2. MODERATOR SUBREGIONS IN 250A2 ASSEMBLY. SUBREGION ARRANGEMENT BASED ON POSITIONS OF FOILS IN MICROSCOPIC TRAVERSES.

TABLE E.2

Transport Cross Section ( $\Sigma_{tr}$ ) and Mean Free Path ( $\lambda_{tr}$ ) of Lattice Materials Based on 2200 m/sec Microscopic Cross Sections

Material	$\Sigma_{tr}$ ( $\text{cm}^{-1}$ )	$\lambda_{tr}$ (cm)
D <sub>2</sub> O (99.5%)	0.449	2.23
U	0.770	1.30
Cu	0.923	1.08

$$\lambda_{tr} = \Sigma_{tr}^{-1} = [\Sigma_s(1-\mu_o) + \Sigma_a]^{-1}$$

approximation is used here for the modified lattices. The volume of copper is 1.71% of the moderator volume or less (see Table 3.4); the transport cross sections and mean free paths are given in Table E.2.

#### E.4 THE TULIP CODE

A computer code (TULIP, Thermal Utilization of Lattices Including Poison) has been written in the IBM FORTRAN language to do the numerical computations involved in the normalization of experiment and theory, and calculation of the thermal utilization ( $f$ ), relative thermal neutron absorption in various materials ( $A_i$ ), and the average macroscopic absorption cross section for the assembly ( $\Sigma_a(\text{cell})$ ). The purpose of this section is to describe and list the code, and indicate how it may be used.

The unit cell of the modified lattice is assumed to consist of ten regions: the fuel, the air gap, the fuel rod cladding, an arbitrary number of copper rods of no more than three different sizes, each with cladding, and the moderator. Each region consists of an arbitrary number of subregions, corresponding to the subregions in the THERMOS calculation in the rods, and to a pattern like that shown in Fig. E.2 in the moderator.

The input data required by the code include the experimental



activities of the foils in the microscopic traverse, the radial positions of the foils in the fuel, the diameter of the foils and of the fuel rod, THERMOS-calculated values of  $\bar{v}_i$ ,  $\bar{\Sigma}_i^{abs}$ , and  $\bar{\Sigma}_i^*$  for each subregion, values of  $\bar{N}_i$  for subregions where no foils were irradiated, and values of  $A^*(r_i)$  for the subregions in the fuel. Input data are read in by the main program. MAIN prints out titles and the values of all input quantities, and calls the subroutines in proper order, according to the method of analysis desired. Subroutine GEOM computes fuel rod subregion volumes. Subroutine LIN linearizes  $A^*(r)$  in the fuel if desired (see Fig. E.1); subroutine FLOP is called by LIN. Subroutine ACTY calculates the foil activities by whichever of the four methods of Sec. E.1 is desired, calling subroutines ISEEK and INTEGR in the process. Subroutine NORM does the normalization described in Sec. E.2, and calculates values of  $\bar{N}_j$  for the moderator subregions with Eq. (E.9). Subroutine UTIL calculates  $\Sigma_a(\text{cell})$ ,  $A_i$  and  $f$ . Communication between routines is via COMMON storage, except for subroutines FLOP, INTEGR, and ISEEK.

Multiple calculations may be made in one job. Several completely separate cases may be run, or the same case may be analyzed repeatedly under varying conditions. These conditions are prescribed by a card of "switch settings" which are read in before the computations are begun. The total number of printed lines for one case is approximately

$$100 + 3[\text{NUMBER OF FOILS}] + 2[\text{NUMBER OF SUBREGIONS}].$$

Analysis of one case takes from 10 to 25 seconds of IBM 7094 computer time.

Table E.3 describes the input formats for the TULIP code. Listings of the code and of a sample input deck follow. The upper limits on the size of the arrays may be deduced from the DIMENSION statements.

TABLE E.3

## Input Format for the TULIP Code

Card Type	Variables	Format	Description
1	None	(72H )	Comments or problem identification.
2	(NSW(I), I=1, 5)	(5I5)	Switches; see TULIP listing.
3	(NSR(I), I=1, 10)	(10I5)	Number of subregions in each of the ten regions.
4	(NFR(I), I=1, 10)	(10I5)	Number of foils in each of the ten regions.
5	(DFUEL, DFOIL)	(2E10.5)	Diameters of fuel rod and foils.
6	(ACT, RF)	(E12.5, F12.4)	Activities and positions of the foils in fuel.
7	(ENDEN*VOL, VBAR, SIGABS, VOL, SIGACT, RELACT, ACTFAC, MAL)	(7E10.5, I2)	Quantities calculated by user or by THERMOS for subregion k: $\bar{N}_k, V_k, \bar{v}_k, \bar{\Sigma}_k^a, V_k, \bar{\Sigma}_k^*, A^*(r_k)$ , and two multiplicative factors included for convenience (see listings). One card for each region.
8	(ACT)	(E12.5)	Activities of the foils not in the fuel. One activity per card.

More Type 7 cards may be included, for moderator, if desired (see NSW(4)).  
If reanalysis of data is desired, put in appropriate cards of Types 1 and 2 next. If analysis of separate case is to follow, put in cards of Types 1 to 8 next. This may be continued indefinitely. Two blank cards terminate the job.



```

C      TULIP -- A DATA REDUCTION CODE FOR EVALUATION OF THERMAL
C      UTILIZATION OF LATTICES INVOLVING POISON.  INPUTS -- CELL
C      DIMENSIONS, EXPERIMENTAL RELATIVE THERMAL NEUTRON ACTIVATION
C      DISTRIBUTIONS, CALCULATED MICROSCOPIC QUANTITIES, AND
C      NON-NORMALIZED RELATIVE THERMAL NEUTRON DENSITIES AND THERMAL
C      ACTIVATIONS CALCULATED BY THERMOS.  OUTPUT -- NORMALIZED RELATIVE
C      THERMAL NEUTRON ABSORPTION IN ALL REGIONS OF LATTICE.
C      MIT HEAVY WATER LATTICE PROJECT.  J. HARRINGTON, 4/65.
COMMON NSW, NREG, NSR, NFR, PI, NFF, DFUEL, DFOIL, ACT, RF, NFUEL,
1N1, ENDEN, VBAR, SIGAB5, VOL, SIGACT, RELACT, ACTFAC, MAL, CALACT,
2ALF, DIF, VOLMAL, RO, RC, RI, FEDGE1, FEDGE2, C0, C1, NFM, VFOIL,
3 ALFBAR, DDLSEZ
  DIMENSION NSW(8), NSR(10), NFR(10), ACT(10,50), RF(20), ENDEN(10,5
1 0), VBAR(10,50), SIGAB5(10,50), VOL(10,50), SIGACT(10,50),
2 RELACT(10,50), ACTFAC(10,50), MAL(10), CALACT(20), ALF(20),
3 DIF(20), VOLMAL(10,50),RO(20), RC(20), RI(20), FEDGE1(20),
4 FEDGE2(20), C0(20), C1(20), DDLSEZ(20), FRACT1(20), FRACT2(20)
  DIMENSION ACTIV(10,50)
101  READ 104
104  FORMAT(72H
1
  READ 3, (NSW(I), I=1,8)
C      NSW(1) MUST BE NONZERO TO OBTAIN FURTHER EXECUTION.
C      NSW(2) = 0 ... A(R) TAKEN AS CONTINUOUS, PIECEWISE LINEAR.
C      NSW(2) = 1 ... A(R) TAKEN AS HISTOGRAM.          SEE (LIN).
C      NSW(3) = NUMBER OF SUBDIVISIONS PER SUBREGION IN INTEGRATION OVER
C      FOIL.      TAKEN AS 20 IF NOT OTHERWISE SPECIFIED.  SEE (ACTY).
C      NSW(4) = NUMBER OF ADDITIONAL SETS OF MODERATOR SUBREGIONS TO BE
C      TRIED.          SEE (UTIL).
C      NSW(5) CONTROLS PRINTOUT OF ALTERNATIVE CALCULATION OF FOIL
C      ACTIVITIES.          SEE 51 BELOW.
  IF(NSW(3)) 17,18,17
18  NSW(3) = 20
17  PRINT 1
1  FORMAT(          76H1CODE TULIP -- EVALUATES THERMAL UTILIZATION OF LA
1TTICES INVOLVING POISON.  /37HOM.I.T. HEAVY WATER LATTICE PROJEC
2T.  //)
  PRINT 104
  PRINT 105
105  FORMAT(/////////38H RECORD OF TIME OF DATA PROCESSING... )
  CALL CLOCK(2)
  IF (NSW(1)) 103,6,102
103  IF (NSW(1) + 1) 41,42,42
102  NREG = 10
  READ 3, (NSR(I), I= 1,NREG)
  READ 3, (NFR(I), I= 1,NREG)
  PI = 3.1415927
3  FORMAT(14I5, 2X)
  NFF = NFR(1)
  READ 2, DFUEL, DFOIL
  VFOIL = (PI/4.) * DFOIL**2
  READ 91, (ACT(1,J), RF(J), J=1,NFF)
91  FORMAT(E12.5, F12.4 )
  NFUEL = NSR(1)
  DO 60 J=1,NFUEL

```

```

READ 2, ENDEN(1,J), VBAR(1,J), SIGABS(1,J), VOL(1,J), SIGACT(1,J),
1  RELACT(1,J), ACTFAC(1,J), MAL(1)
60 RELACT(1,J) = RELACT(1,J)*ACTFAC(1,J)
CALL GEOM
DO 61 J=1,NFUEL
61 ENDEN(1,J) = ENDEN(1,J) / VOL(1,J)
IF (N1) 7,6,7
6 CALL EXIT
7 DO 5 I=2,NREG
NSRI = NSR(I)
IF (NSRI) 15,15,9
15 ENDEN (I,1) = 0.
VBAR (I,1) = 0.
SIGABS (I,1) = 0.
VOL (I,1) = 0.
SIGACT (I,1) = 0.
RELACT (I,1) = 0.
VLMAL (I,1) = 0.
GO TO 5
9 DO 4 J=1,NSRI
READ 2, ENDEN(I,J), VBAR(I,J), SIGABS(I,J), VOL(I,J), SIGACT(I,J),
1 RELACT(I,J), ACTFAC(I,J), MAL(I)
2 FORMAT(7E10.5, I2)
VLMAL(I,J) = VOL(I,J) * FLOATF(MAL(I))
ENDEN(I,J) = ENDEN(I,J) / VOL(I,J)
4 CONTINUE
5 CONTINUE
PRINT 20
20 FORMAT (71H1NON-NORMALIZED INPUT QUANTITIES BROKEN DOWN BY REGION
1AND SUBREGION //13H REGION ,2X, 12H SUBREGION , 2X,
212H NDEN , 2X, 12H AVE VEL , 2X, 12H SIGMA A , 2X,
312H VOLUME , 2X, 12H VOLUME , 2X, 12H SIGMA ACT , 2X,
412H REL ACT / 70X, 14H(SINGLE CELL), 4X, 7H(TOTAL)/ )
DO 21 I=1,NREG
NSRI = NSR(I)
IF (NSRI) 23,23,21
23 NSRI = 1
21 PRINT 22, (I,J,ENDEN(I,J), VBAR(I,J), SIGABS(I,J),VOL(I,J),
1 VLMAL(I,J), SIGACT(I,J), RELACT(I,J), J=1,NSRI)
22 FORMAT(1H0, I7, 11X, I3, 5X, 1P7E14.5/(I8, 11X, I3, 5X,7E14.5))
DO 10 I=2,NREG
IF(NFR(I)) 8,10,8
8 NFRI = NFR(I)
DO 12 J=1,NFRI
READ 92, ACT(I,J)
92 FORMAT(E12.5 )
12 CONTINUE
10 CONTINUE
41 CALL LIN
42 PRINT 30
30 FORMAT(42H1MEASURED AND CALCULATED FOIL ACTIVITIES //13H )
CALL ACTY
PRINT 31
31 FORMAT(/////59H MEASURED AND CALCULATED FOIL ACTIVITIES FOR FOILS
1IN FUEL //13H REGION , 2X, 12H FOIL NO. , 2X,

```



```

2   12H MEAS ACT , 2X, 12H CALC ACT , 2X, 12HPROP FACTOR ,
3   15H PCT DEV FM AVE/)
RMSVAL = 0.
KKK = 1
DO 32 J=1,NFF
RMSVAL = RMSVAL + DIF(J)**2
32  PRINT 93, KKK, J, ACT(1,J), CALACT(J), ALF(J), DIF(J)
93  FORMAT(18, 11X, I3, 5X, 1P3E14.5, 2PF11.2)
RMSVAL = SQRTF(RMSVAL/FLOATF(NFF))
PRINT 33, ALFBAR
33  FORMAT( 1H0, 38X, 18HAVE PROP FACTOR = , 1PE12.5)
PRINT 16, RMSVAL
16  FORMAT(1H0, 38X, 33HRMS VALUE OF PCT DEV FROM AVE = , 2PF8.2)
PRINT 34, ALFBAR
34  FORMAT(/////26H MEASURED FOIL ACTIVITIES /////
1   13H REGION ,2X, 12H FOIL NO. , 2X, 12H MEAS ACT
2   2X, 12H MEAS ACT X /43X, 1PE12.5//)
DO 70 I=1,NREG
IF(NFR(I)) 68,70,68
68  NFRI = NFR(I)
DO 72 J=1,NFRI
ACTIV(I,J) = ACT(I,J)*ALFBAR
72  PRINT 93, I, J, ACT(I,J), ACTIV(I,J)
70  CONTINUE
CALL NORM
IF(NSW(5)) 51,52,51
51  PRINT 55
55  FORMAT(/////93H COMPARISON OF MEASURED ACTIVITY WITH ACTIVITY CA
1LCULATED ON BASIS OF A(R) AT FOIL CENTER )
PRINT 31
ALF2 = 0.
DO 54 J=1,NFF
CALL ISEEK(J,0,N3)
IF(NSW(2)) 62,63,62
62  DDLSEZ(J) = VFOIL*(REACT(1,N3))
GO TO 64
63  DDLSEZ(J) = VFOIL*(C0(N3) + C1(N3)*RF(J))
64  ALF(J) = DDLSEZ(J)/ACT(1,J)
54  ALF2 = ALF2+ALF(J)
ALF2 = ALF2/FLOATF(NFF)
RMSVAL = 0.
DO 56 J=1,NFF
FRACT1(J) = ALF(J)/ALF2 - 1.
PRINT 93, KKK,J,ACT(1,J), DDLSEZ(J),ALF(J), FRACT1(J)
56  RMSVAL = RMSVAL + FRACT1(J)**2
RMSVAL = SQRTF(RMSVAL/FLOATF(NFF))
PRINT 33, ALF2
PRINT 16, RMSVAL
52  PRINT 58
58  FORMAT(1H1)
PRINT 104
CALL UTIL
GO TO 101
END

```

```

SUBROUTINE GEOM
SUBROUTINE FOR CODE TULIP.      J. HARRINGTON, 4/65.
COMMON NSW, NREG, NSR, NFR, PI, NFF, DFUEL, DFOIL, ACT, RF, NFUEL,
1 IN1, ENDEN, VBAR, SIGABS, VOL, SIGACT, RELACT, ACTFAC, MAL, CALACT,
2 ALF, DIF, VOLMAL, RO, RC, RI, FEDGE1, FEDGE2, C0, C1, NFM, VFOIL,
3 ALFBAR, DDLSEZ
DIMENSION NSW(8), NSR(10), NFR(10), ACT(10,50), RF(20), ENDEN(10,5
1 0), VBAR(10,50), SIGABS(10,50), VOL(10,50), SIGACT(10,50),
2 RELACT(10,50), ACTFAC(10,50), MAL(10), CALACT(20), ALF(20),
3 DIF(20), VOLMAL(10,50), RO(20), RC(20), RI(20), FEDGE1(20),
4 FEDGE2(20), C0(20), C1(20), DDLSEZ(20), FRACT1(20), FRACT2(20)
T = DFUEL/2.
RO(1) = T/FLOATF(2*NFUEL - 1)
RC(1) = 0.5*RO(1)
RI(1) = 0.
VOL(1,1) = PI*RO(1)**2
VOLMAL(1,1) = VOL(1,1)
DO 1 I = 2, NFUEL
RI(I) = RO(I-1)
RC(I) = RO(I-1) + RO(1)
RO(I) = RO(I-1) + 2.*RO(1)
VOL(1,I) = PI*(RO(I)**2-RI(I)**2)
1 VOLMAL(1,I) = VOL(1,I)
PRINT 10
10 FORMAT(29H1FUEL REGION GEOMETRY DATA /5HOREG., 2X, 8HR(INN
IER), 4X, 9HR(CENTER), 3X, 8HR(OUTER), 5X, 7HVOLUME )
PRINT 11, (I, RI(I), RC(I), RO(I), VOL(1,I), I=1,NFUEL)
11 FORMAT(I3, 1X, 1P4E12.5)
IF(RF(1)) 2,2,3
2 FEDGE1(1) = 0.
FEDGE2(1) = DFOIL/2.
IF(NFF-1) 14,14,15
15 N1 = 2
GO TO 4
3 N1 = 1
4 DO 8 I = N1, NFF
FEDGE1(I) = RF(I) - (DFOIL/2.)
FEDGE2(I) = FEDGE1(I) + DFOIL
IF (FEDGE1(I)) 6,7,7
7 IF (FEDGE2(I)-T) 8,8,6
6 PRINT 9
9 FORMAT (78H1A FOIL IS PLACED IN SUCH A MANNER THAT THE INTEGRATION
IS CAN NOT BE PERFORMED. )
N1 = 0
8 CONTINUE
14 PRINT 12, DFOIL
12 FORMAT(/////10H FOIL DATA/11H0FOILS ARE ,F6.4, 17H CM. IN DIAMETER
1. / 11H0LOCATIONS- /6H0FOIL , 10HINNER EDGE, 4X, 6HCENTER, 4
2X, 10HOUTER EDGE /)
PRINT 13, (I, FEDGE1(I), RF(I), FEDGE2(I), I=1,NFF)
13 FORMAT(I4, 1X, 1P3E12.5)
RETURN
END

```



```

SUBROUTINE LIN
C  SUBROUTINE FOR CODE TULIP.      J. HARRINGTON, 4/65.
COMMON NSW, NREG, NSR, NFR, PI, NFF, DFUEL, DFOIL, ACT, RF, NFUEL,
1N1, ENDEN, VBAR, SIGABS, VOL, SIGACT, RELACT, ACTFAC, MAL, CALACT,
2ALF, DIF, VOLMAL, RO, RC, RI, FEDGE1, FEDGE2, C0, C1, NFM, VFOIL,
3 ALFBAR, DDLSEZ
DIMENSION NSW(8), NSR(10), NFR(10), ACT(10,50), RF(20), ENDEN(10,5
1 0), VBAR(10,50), SIGABS(10,50), VOL(10,50), SIGACT(10,50),
2 RELACT(10,50), ACTFAC(10,50), MAL(10), CALACT(20), ALF(20),
3 DIF(20), VOLMAL(10,50),RO(20), RC(20), RI(20), FEDGE1(20),
4 FEDGE2(20), C0(20), C1(20), DDLSEZ(20), FRACT1(20), FRACT2(20)
DIMENSION TABLE (20,3)
IF(NFUEL-1) 6,6,12
12 IF(NSW(2)) 6,7,6
7 C0(1) = RELACT(1,1)
C1(1) = 0.
PRINT 13
13 FORMAT(/////
1 131H1HISTOGRAM FOR SPECIFIC ACTIVATION AS FUNCTION OF RADIU
1S WITHIN FUEL HAS BEEN CONVERTED TO A CONTINUOUS, PIECEWISE LINEAR
2 FUNCTION /58X, 17HA(R) = C0 + C1*R./ 102H THE INTEGRAL OF A(
3R) OVER EACH REGION EQUALS THE VALUE OF THE STEP FUNCTION TIMES TH
4E REGION VOLUME. )
10 NN2 = 2*NFUEL - 2
DO 2 I=2,NN2,2
I2 = I/2
2 CALL FLOP (1., RI(I2+1), VOL(1,I2+1), (2.*PI/3.)*
1 (RO(I2+1)**3-RI(I2+1)**3), C0(I2) C1(I2)*RO(I2),
2 RELACT(1,I2+1)*VOL(1,I2+1), C0(I2+1), C1(I2+1))
DO 4 I = 1,NFUEL
TABLE(I,1) = C0(I) + C1(I)*RI(I)
TABLE(I,2) = C0(I) + C1(I)*RC(I)
4 TABLE(I,3) = C0(I) + C1(I)*RO(I)
11 PRINT 3
3 FORMAT(4HOREG, 5X, 13HHISTOGRAM FOR, 5X, 36H LINEARIZED FUNCTIO
1N VALUE AT ,5X, 6X, 12HCOEFFICIENTS/4H (I), 5X, 12H REL ACT
2 , 5X, 4X, 4HR(I), 8X, 4HR(C), 8X, 4HR(O), 4X, 5X, 12H C0(I)
3, 12H C1(I) )
PRINT 5, (I, RELACT(1,I), (TABLE(I,J), J=1,3), C0(I), C1(I), I=1,
1 NFUEL)
5 FORMAT (I3, 7X, 1P6E14.5)
6 RETURN
END

```

```

SUBROUTINE ACTY
SUBROUTINE FOR CODE TULIP.      J. HARRINGTON, 4/65.
COMMON NSW, NREG, NSR, NFR, PI, NFF, DFUEL, DFOIL, ACT, RF, NFUEL,
1N1, ENDEN, VBAR, SIGABS, VOL, SIGACT, RELACT, ACTFAC, MAL, CALACT,
2ALF, DIF, VOLMAL, RO, RC, RI, FEDGE1, FEDGE2, CO, C1, NFM, VFOIL,
3 ALFBAR, DDLSEZ
DIMENSION NSW(8), NSR(10), NFR(10), ACT(10,50), RF(20), ENDEN(10,5
1 0), VBAR(10,50), SIGABS(10,50), VOL(10,50), SIGACT(10,50),
2 RELACT(10,50), ACTFAC(10,50), MAL(10), CALACT(20), ALF(20),
3 DIF(20), VOLMAL(10,50), RO(20), RC(20), RI(20), FEDGE1(20),
4 FEDGE2(20), CO(20), C1(20), DDLSEZ(20), FRACT1(20), FRACT2(20)
IF (NSW(2)) 50,1,50
1 PRINT 16, NSW(3)
16 FORMAT(109H0CALCULATED FOIL ACTIVITY FOR EACH FOIL OBTAINED BY RE
1GION-BY-REGION INTEGRATION OF A(R) OVER FOIL SURFACE. /
2 1H0, 13, 33H SUBREGIONS TAKEN IN EACH REGION.)
IF (RF(1)) 2,2,23
2 N1 = 2
J=1
R1=0.
ISW=0
CALACT(1) = 0.
7 IF(RO(J) - FEDGE2(1)) 4,3,3
4 R2 = RO(J)
GO TO 5
3 R2 = FEDGE2(1)
ISW = 1
5 BITTY = CO(J)*PI*(R2**2-R1**2) + 2.*PI*C1(J)*(R2**3-R1**3)/3.
CALACT(1) = CALACT(1) + BITTY
IF (ISW) 6,6,24
6 R1=R2
J=J+1
GO TO 7
23 N1 = 1
24 DO 48 K=N1,NFF
CALACT(K) = 0.
R1 = FEDGE1(K)
ISW = 0
CALL ISEEK (K, -1, J)
37 IF(RO(J)-FEDGE2(K)) 34,33,33
34 R2 = RO(J)
GO TO 35
33 R2 = FEDGE2(K)
ISW = 1
35 NSW3 = NSW(3)
DEL = (R2-R1)/FLOATF(NSW3)
DO 40 I = 1,NSW3
FI = I
HT = CO(J) + C1(J)*(R1 + (FI-0.5)*DEL)
RINNER = R1 + (FI-1.)*DEL
ROUTER = RINNER + DEL
CALL INTEGR (RINNER, ROUTER, K, BITTY)
40 CALACT(K) = CALACT(K) + HT * BITTY
IF (ISW) 36,36,48
36 R1 = R2

```



```

J=J+1
GO TO 37
48 CONTINUE
49 GO TO 101
50 PRINT 15
15 FORMAT(          65HUSPECIFIC ACTIVATION AS FUNCTION OF RADIUS TREATED
1AS HISTOGRAM. /131HUCALCULATED FOIL ACTIVITY FOR FOIL J OBTAINED
2BY SUMMING PRODUCT OF SPECIFIC ACTIVATION IN REGION I AND AREA OF
3FOIL J IN REGION I, /42H FOR ALL REGIONS IN WHICH FOIL J APPEARS
4.          )
IF(RF(1)) 52,52,73
52 N1=2
J=1
R1=0.
ISW=0
CALACT(1) = 0.
57 IF(RO(J) - FEDGE2(1)) 54,53,53
54 R2 = RO(J)
GO TO 55
53 R2 = FEDGE2(1)
ISW = 1
55 BITTY = PI*(R2**2 - R1**2)*RELACT(1,J)
CALACT(1) = CALACT(1) + BITTY
IF (ISW) 56,56,74
56 R1 = R2
J=J+1
GO TO 57
73 N1 = 1
74 DO 100 I=N1,NFF
CALACT(I) = 0.
R1 = FEDGE1(I)
ISW=0
CALL ISEEK (I, -1, J)
87 IF(RO(J)-FEDGE2(I)) 84,83,83
84 R2 = RO(J)
GO TO 85
83 R2 = FEDGE2(I)
ISW = 1
85 CALL INTEGR(R1,R2,I, BITTY)
CALACT(I) = CALACT(I) + BITTY*RELACT(1,J)
IF(ISW) 86,86,100
86 R1 = R2
J= J+1
GO TO 87
100 CONTINUE
101 ALFBAR = 0.
DO 102 I=1,NFF
ALF(I) = CALACT(I)/ACT(1,I)
102 ALFBAR = ALFBAR + ALF(I)
ALFBAR = ALFBAR/FLOATF(NFF)
DO 103 I=1,NFF
103 DIF(I) = ALF(I)/ALFBAR-1.
RETURN
END

```

```

SUBROUTINE NORM
SUBROUTINE FOR CODE TULIP.      J. HARRINGTON, 4/65.
COMMON NSW, NREG, NSR, NFR, PI, NFF, DFUEL, DFOIL, ACT, RF, NFUEL,
1N1, ENDEN, VBAR, SIGABS, VOL, SIGACT, RELACT, ACTFAC, MAL, CALACT,
2ALF, DIF, VOLMAL, RO, RC, RI, FEDGE1, FEDGE2, C0, C1, NFM, VFOIL,
3 ALFBAR, DDLSEZ
  DIMENSION NSW(8), NSR(10), NFR(10), ACT(10,50), RF(20), ENDEN(10,5
1 0), VBAR(10,50), SIGABS(10,50), VOL(10,50), SIGACT(10,50),
2 RELACT(10,50), ACTFAC(10,50), MAL(10), CALACT(20), ALF(20),
3 DIF(20), VOLMAL(10,50),RO(20), RC(20), RI(20), FEDGE1(20),
4 FEDGE2(20), C0(20), C1(20), DDLSEZ(20), FRACT1(20), FRACT2(20)
  NFM = NFR(10)
  DO 1 J = 1,NFM
1  ENDEN (10,J)= (ALFBAR*ACT(10,J))/(VBAR(10,J)*VFOIL*SIGACT(10,J))
  DO 3 I = 4,8,2
  IF (ENDEN(I,1)) 2,3,2
2  DUMDEN = (ALFBAR*ACT(I,1)/(VBAR(I,1)*VFOIL*SIGACT(I,1)))
  BETA = DUMDEN/ENDEN(I,1)
  I1 = I+1
  DO 4 K=I,I1
  NSRK = NSR(K)
  DO 4 J=1,NSRK
4  ENDEN(K,J) = BETA*ENDEN(K,J)
  X = (VFOIL-VOL(I,1))/VFOIL
  IF(ABS(X)-0.0001) 3,3,5
5  PRINT 6, I, X
6  FORMAT(58H1FOIL AREA DIFFERS FROM AREA OF INNER SUBREGION OF REGIO
1N ,I1, 4H BY , 2PF5.2, 9H PERCENT., 27H STRICT EQUALITY ASSUMED.
2  )
3  CONTINUE
  RETURN
  END

```



```

SUBROUTINE UTIL
C SUBROUTINE FOR CODE TULIP.      J. HARRINGTON, 4/65.
COMMON NSW, NREG, NSR, NFR, PI, NFF, DFUEL, DFOIL, ACT, RF, NFUEL,
1 IN1, ENDEN, VBAR, SIGABS, VOL, SIGACT, RELACT, ACTFAC, MAL, CALACT,
2 ALF, DIF, VOLMAL, RO, RC, RI, FEDGE1, FEDGE2, C0, C1, NFM, VFOIL,
3 ALFBAR, DDLSEZ
DIMENSION NSW(8), NSR(10), NFR(10), ACT(10,50), RF(20), ENDEN(10,5
1 0), VBAR(10,50), SIGABS(10,50), VOL(10,50), SIGACT(10,50),
2 RELACT(10,50), ACTFAC(10,50), MAL(10), CALACT(20), ALF(20),
3 DIF(20), VOLMAL(10,50),RO(20), RC(20), RI(20), FEDGE1(20),
4 FEDGE2(20), C0(20), C1(20), DDLSEZ(20), FRACT1(20), FRACT2(20)
DIMENSION ABSO(10), ABS(10,50), RELABS(10)
DIMENSION FLUX(10), FLX(10,50)
FINV = 0.
TOTABS = 0.
TOTFLX = 0.
DO 2 I=1,NREG
ABSO(I) = 0.
FLUX(I) = 0.
NSRI = NSR(I)
DO 1 J= 1,NSRI
ABS(I,J) = VBAR(I,J)*ENDEN(I,J)*SIGABS(I,J)*VOLMAL(I,J)
FLX(I,J) = VBAR(I,J)*ENDEN(I,J)*VOLMAL(I,J)
FLUX(I) = FLUX(I) + FLX(I,J)
1 ABSO(I) = ABSO(I) + ABS(I,J)
RELABS(I) = ABSO(I)/ABSO(1)
TOTABS = TOTABS + ABSO(I)
TOTFLX = TOTFLX + FLUX(I)
2 FINV = FINV + RELABS(I)
F = 1./FINV
TOTSIG = TOTABS/TOTFLX
PRINT 3
3 FORMAT( 76HONORMALIZED RELATIVE ABSORPTION RATE BROKEN DOWN BY REG
1ION AND SUBREGION      )
PRINT 4
4 FORMAT(///13H      REGION      ,2X, 12H SUBREGION  , 2X,12H AVE VEL
1,2X, 12H NDEN      , 2X, 12H SIGMA A   , 2X, 12H TOT VOL  ,2X,
2 12H TOT FLUX   , 2X, 12H ABSORPTIONS ,2X, 12HABS REL FUEL/)
DO 9 I=1,NREG
NSRI=NSR(I)
DO 6 J=1,NSRI
PRINT 5, I,J,VBAR(I,J), ENDEN(I,J), SIGABS(I,J), VOLMAL(I,J),
1 FLX(I,J), ABS(I,J)
5 FORMAT(I8,11X, I3, 5X, 1P6E14.5)
6 CONTINUE
GO TO (11, 12, 13, 14, 15, 16, 15, 17, 15, 18), I
11 PRINT 110
110 FORMAT(1X, 12H      FUEL      )
GO TO 8
12 PRINT 120
120 FORMAT(1X, 12H AIR GAP      )
GO TO 8
13 PRINT 130
130 FORMAT(1X, 12H      CLAD      )
GO TO 8
UTIL

```

```

14 PRINT 140
140 FORMAT(1X, 12H A POISON )
GO TO 8
15 PRINT 150
150 FORMAT(1X, 12HPOISON CLAD,
GO TO 8
16 PRINT160
160 FORMAT(1X, 12H B POISON )
GO TO 8
17 PRINT 170
170 FORMAT(1X, 12H C POISON )
GO TO 8
18 PRINT 180
180 FORMAT(1X, 12H MODERATOR )
8 PRINT 7, FLUX(I), ABSO(I), RELABS(I)
7 FORMAT(1H+, 14X, 12H TOTAL ,56X, 1P3E14.5/)
9 CONTINUE
19 PRINT 20, FINV, F , TOTSIG , TOTABS, TOTFLX
20 FORMAT(113X, 12H-----//108X,5H1/F =,1PE12.5//110X,3HF =,
1 1PE12.5, // 96X, 17HLATTICE SIGMA A =,1PE12.5//
2 94X,19HTOTAL ABSORPTIONS =,1PE12.5//101X,12HTOTAL FLUX = ,
3 1PE12.5)
IF(NSW(4)) 100,100,21
21 READ 22,(ENDEN(10,J), VBAR(10,J),SIGABS(10,J), VOL(10,J),SIGACT(10
1,J), RELACT(10,J), ACTFAC(10,J), MAL(10) , J=1,NFM)
22 FORMAT (7E10.5,I2)
TOTABS = TOTABS - ABSO(10)
TOTFLX = TOTFLX - FLUX(10)
ABSO(10) = 0.
FLUX(10) = 0.
DO 23 J=1,NFM
VOLMAL(10,J) = VOL(10,J) * FLOATF(MAL(10))
ENDEN(10,J) = (ALFBAR*ACT(10,J))/(VBAR(10,J)*VFOIL*SIGACT(10,J))
ABS(10,J) = VBAR(10,J)*ENDEN(10,J)*SIGABS(10,J)*VOLMAL(10,J)
FLX(10,J) = VBAR(10,J)*ENDEN(10,J)*VOLMAL(10,J)
FLUX(10) = FLUX(10) + FLX(10,J)
23 ABSO(10)= ABSO(10) + ABS(10,J)
TOTABS = TOTABS + ABSO(10)
TOTFLX = TOTFLX + FLUX(10)
TOTSIG = TOTABS/TOTFLX
FINV = FINV-RELABS(10)
RELABS(10) = ABSO(10)/ABSO(1)
FINV = FINV + RELABS(10)
F = 1./FINV
I=10
PRINT 25
PRINT 4
DO 24 J=1,NFM
24 PRINT 5, I, J,VBAR(10,J) ,ENDEN(10,J), SIGABS(10,J), VOLMAL(10,J)
1 , ABS(10,J)
25 FORMAT(54H1RECALCULATION WITH NEW SET OF MODERATOR SUBREGIONS. )
PRINT 180
PRINT 7, ABSO(10), RELABS(10)

```



```
NSW(4) = NSW(4) - 1  
GO TO 19  
100 RETURN  
END
```

```

SUBROUTINE ISEEK (K1, K2, K3)
C   SUBROUTINE FOR CODE TULIP.      J. HARRINGTON, 4/65.
C   SUBROUTINE TO FIND FUEL SUBREGION IN WHICH INNER EDGE, CENTER,
C   OR OUTER EDGE OF FOIL K1 IS LOCATED.
COMMON NSW, NREG, NSR, NFR, PI, NFF, DFUEL, DFOIL, ACT, RF, NFUEL,
IN1, ENDEN, VBAR, SIGABS, VOL, SIGACT, RELACT, ACTFAC, MAL, CALACT,
2ALF, DIF, VOLMAL, RO, RC, RI, FEDGE1, FEDGE2, CO, C1, NFM, VFOIL,
3 ALFBAR, DDLSEZ
DIMENSION NSW(8), NSR(10), NFR(10), ACT(10,50), RF(20), ENDEN(10,5
1 0), VBAR(10,50), SIGABS(10,50), VOL(10,50), SIGACT(10,50),
2 RELACT(10,50), ACTFAC(10,50), MAL(10), CALACT(20), ALF(20),
3 DIF(20), VOLMAL(10,50),RO(20), RC(20), RI(20), FEDGE1(20),
4 FEDGE2(20), CO(20), C1(20), DDLSEZ(20), FRACT1(20), FRACT2(20)
IF (K2) 1,2,3
1  R = FEDGE1(K1)
GO TO 4
2  R = RF(K1)
GO TO 4
3  R = FEDGE2(K1)
4  DO 5 I=1,NFUEL
IF (R-RO(I)) 7,5,5
5  CONTINUE
PRINT 6, K2, K1
6  FORMAT(27H1SUBROUTINE (ISEEK) IN MODE, I3, 20H FAILED TO FIND FOIL
1, I3, 1H.)
CALL EXIT
7  K3 = I
RETURN
END

```

```

SUBROUTINE FLOP (A,B,C,D,E,F,G,H)
C   SUBROUTINE FOR CODE TULIP.      J. HARRINGTON, 4/65.
C   SUBROUTINE TO SOLVE SYSTEM ( AX+BY=E, CX+DY=F )
C   ANSWER ( X = G      Y = H )
COMMON NSW, NREG, NSR, NFR, PI, NFF, DFUEL, DFOIL, ACT, RF, NFUEL,
IN1, ENDEN, VBAR, SIGABS, VOL, SIGACT, RELACT, ACTFAC, MAL, CALACT,
2ALF, DIF, VOLMAL, RO, RC, RI, FEDGE1, FEDGE2, CO, C1, NFM, VFOIL,
3 ALFBAR, DDLSEZ
DIMENSION NSW(8), NSR(10), NFR(10), ACT(10,50), RF(20), ENDEN(10,5
1 0), VBAR(10,50), SIGABS(10,50), VOL(10,50), SIGACT(10,50),
2 RELACT(10,50), ACTFAC(10,50), MAL(10), CALACT(20), ALF(20),
3 DIF(20), VOLMAL(10,50),RO(20), RC(20), RI(20), FEDGE1(20),
4 FEDGE2(20), CO(20), C1(20), DDLSEZ(20), FRACT1(20), FRACT2(20)
DEN = A*D-B*C
IF (DEN) 1,2,1
1  G = (E*D-B*F)/DEN
H = -(A*F-E*C)/DEN
RETURN
2  PRINT 3,C
3  FORMAT (60H1DETERMINANT OF SYSTEM TO BE SOLVED IS ZERO. VALUE OF
1C IS ,1PE12.5)
PRINT 4
4  FORMAT(48H C = VOLUME OF REGION TO WHICH SYSTEM APPLIES.
CALL EXIT
END

```



```

SUBROUTINE INTEGR(R1, R2, J, VAL)
SUBROUTINE FOR CODE TULIP.      J. HARRINGTON, 4/65.
SUBROUTINE EVALUATES INTEGRAL OF
      (2*R*ARCCOS(BIGR) * DR)
OVER INTERVAL (R1,R2) FOR FOIL J.
THIS IS THE AREA OF THE FOIL BETWEEN THE TWO RADII.
COMMON NSW, NREG, NSR, NFR, PI, NFF, DFUEL, DFOIL, ACT, RF, NFUEL,
1N1, ENDEN, VBAR, SIGABS, VOL, SIGACT, RELACT, ACTFAC, MAL, CALACT,
2ALF, DIF, VOLMAL, RO, RC, RI, FEDGE1, FEDGE2, CO, C1, NFM, VFOIL,
3ALFBAR, DDLSEZ
DIMENSION NSW(8), NSR(10), NFR(10), ACT(10,50), RF(20), ENDEN(10,5
1 0), VBAR(10,50), SIGABS(10,50), VOL(10,50), SIGACT(10,50),
2 RELACT(10,50), ACTFAC(10,50), MAL(10), CALACT(20), ALF(20),
3 DIF(20), VOLMAL(10,50), RO(20), RC(20), RI(20), FEDGE1(20),
4 FEDGE2(20), CO(20), C1(20), DDLSEZ(20), FRACT1(20), FRACT2(20)
DIMENSION TERM(3,2)
A = FEDGE1(J)
B = FEDGE2(J)
IF (R1-A) 10,1,2
1 TERM(1,1) = 0.
  TERM(2,1) = 0.
  TERM(3,1) = VFOIL/2.
  GO TO 3
2 R1B = (R1**2)-(B**2)
  B1GR1 = ((R1**2) + (A*B))/(R1*(A+B))
  R1A = (R1**2) - (A**2)
  TERM(1,1) = -(R1**2)*ACOSF(B1GR1)
  TERM(2,1) = ( 0.5)*SQRTF(-R1A*R1B)
  TERM(3,1) = ((DFOIL/2. )**2)*ASINF
1                                     ((R1A+R1B)/((A**2)-(B**2)))
3 IF (R2-B) 5,4,10
4 TERM(1,2) = 0.
  TERM(2,2) = 0.
  TERM(3,2) = VFOIL/2.
  GO TO 6
5 R2B = (R2**2) - (B**2)
  R2A = (R2**2) - (A**2)
  B1GR2 = ((R2**2) + (A*B))/(R2*(A+B))
  TERM(1,2) = (R2**2)*ACOSF(B1GR2)
  TERM(2,2) = (-0.5)*SQRTF(-R2A*R2B)
  TERM(3,2) = -((DFOIL/2. )**2)*ASINF
1                                     ((R2A+R2B)/((A**2)-(B**2)))
6 VAL = 0.
  DO 7 I=1,3
  DO 7 J=1,2
7 VAL = VAL + TERM(I,J)
  RETURN
10 PRINT 11, J, R1, R2
11 FORMAT(57H1WHILE IN SUBROUTINE (INTEGR), FOR INTEGRATION OVER FOIL
1 ,I3, 9H BETWEEN , 1PE12.5, 5H AND , 1PE12.5, / 66H AN INTEGRA
2TION LIMIT FALLING OUTSIDE THE FOIL WAS ENCOUNTERED. )
  CALL EXIT
END

```





898.1	RUN 46
630.5	RUN 46
1038.7	RUN 46
1050.9	RUN 46
977.9	RUN 46
998.3	RUN 46
1056.0	RUN 46
1088.6	RUN 46
1054.2	RUN 46
1030.7	RUN 46
1067.3	RUN 46
1047.6	RUN 46
1073.1	RUN 46
1067.3	RUN 46
1033.7	RUN 46
1009.9	RUN 46
1070.7	RUN 46
1067.2	RUN 46
1069.9	RUN 46
0253A2B1 CORE...RUN 46...SERIES II THERMOS DATA...MOD SUBREGION SET 2	
-1 1 1	
0 END OF RUN.	

APPENDIX F  
 APPROXIMATE METHOD FOR CALCULATING  
 THE EFFECT OF ADDED THERMAL ABSORBERS

The steps taken in the planning of the experiments discussed here are recorded in this appendix for the convenience of future workers. The method is approximate but gave satisfactory results. The notation of Chap. II is used.

The availability of a THERMOS calculation for a cell of the lattice to be studied is presumed. Cross sections, concentrations, and dimensions used in the calculation should be chosen carefully, as the results are needed for the final data analysis, as well as the approximate calculations described here. The values of  $f$  and  $\eta$  are obtained from the THERMOS results.

Reasonable estimates of  $\epsilon$ ,  $\delta_{25}$ , and  $p$  are next calculated or obtained from results of previous measurements, and the value of  $k_{\infty}$  is obtained from Eq. (2.7).

For the calculation of  $V_3^0$ , the volume of absorber that must be added to a unit cell of the lattice to obtain a zero buckling value, the following approximations suffice:

$$\epsilon^0 = \epsilon, \quad (\text{F.1})$$

$$\eta^0 = \eta, \quad (\text{F.2})$$

$$p^0 = p, \quad (\text{F.3})$$

$$1 + \delta_{25}^0 = 1 + \delta_{25}. \quad (\text{F.4})$$

(Of course, a correction factor may be included here if desired, perhaps based on the results given in Table 5.8.) Then, we have:

$$k_{\infty} = \frac{f}{f^0}, \quad (\text{F.5})$$

$$f^0 = [\epsilon\eta p(1+\delta_{25})]^{-1}, \quad (\text{F.6})$$

$$f^0 = [1+A_1^0+A_2^0+A_3^0]^{-1} = \left[\frac{1}{f} + A_3^0\right]^{-1}. \quad (\text{F.7})$$



The assumption made in writing Eq. (F.7) is that the  $A_i$  terms for the cladding and moderator are the same in the unmodified and modified lattices. Table 5.3 shows that this is a good approximation for the lattices studied here.

From Eqs. (F.6) and (F.7), we obtain:

$$\frac{\bar{n}_3}{\bar{n}_o} \frac{\bar{v}_3 \bar{\Sigma}_3}{\bar{v}_o \bar{\Sigma}_o} \frac{V_3^o}{V_o} = \epsilon \eta p (1 + \delta_{25}) - \frac{1}{f}. \quad (\text{F.8})$$

For the ratio of  $\bar{v}_o \bar{\Sigma}_o$  and  $\bar{v}_3 \bar{\Sigma}_3$ , the ratio of the macroscopic cross sections (based on the 2200 m/sec microscopic cross section) is a sufficiently good estimate, if all absorbers are  $1/v$  absorbers or are nearly so. (See Ref. BR 1 for a discussion of this point for the lattices studied at M. I. T.,)  $V_o$  and  $V_3^o$  are the volume of fuel and absorber, respectively, in a unit cell. If the fuel rods have radius  $D$  and absorber rods of radius  $d$  are to be used, then it may be convenient to replace the  $V_3^o/V_o$  term with  $md^2/D^2$ , where  $m$  is the number of absorber rods per unit cell which will bring the buckling value of the lattice to zero.

For present purposes, the neutron density ratio in Eq. (F.8) is written:

$$\frac{\bar{n}_3}{\bar{n}_o} = \frac{\bar{n}_3}{n_{\text{mod}}} \frac{n_{\text{mod}}}{\bar{n}_o}. \quad (\text{F.9})$$

Here,  $n_{\text{mod}}$  is the thermal neutron density in the moderator far from fuel and absorber rods. A good estimate of  $n_{\text{mod}}/\bar{n}_o$  is obtained from the THERMOS calculation for the unmodified lattice. The ratio  $\bar{n}_3/n_{\text{mod}}$  must be calculated, either by a THERMOS calculation, or from a simpler calculation. Possibilities for the latter include the use of diffusion theory for the moderator, combined with the method of successive generations (SI 1, ST 1) or the self-absorption factors of Royston (RO 3) for the rod. Equation (F.8) may now be solved for  $V_3^o$ , or for  $m$ , whichever is desired.

For the lattices studied here, the material buckling,  $B_m^2$ , was approximately linearly related to the volume of added absorber,  $V_3$ , for values of  $B_m^2$  between zero and the value for the unmodified lattice,  $B_{\text{lat}}^2$ . If an estimate of the value of  $B_{\text{lat}}^2$  is available, a straight line may be plotted through the points  $(0, V_3^o)$  and  $(B_{\text{lat}}^2, 0)$  on a graph of  $B_m^2$

against  $V_3$ , to give an approximation of the material buckling value that will be obtained for a given value of  $V_3$ . This result may be derived from Eq. (4.30) under the assumption that the value of  $\bar{n}_3/\bar{n}_0$  is constant, and that the term  $\frac{1}{2}(\tau B_{lat}^2)^2$  is small compared to unity, where  $\tau$  is the Fermi age for the unmodified lattice.



APPENDIX G  
SIMULTANEOUS EXPERIMENTAL DETERMINATION OF  
DIFFUSION AREA AND FERMI AGE

Use of the experimental data to obtain values of the diffusion area,  $L^2$ , and the Fermi age,  $\tau$ , for the unmodified lattices is discussed in Sec. 2.6.2. In this appendix, an iterative least squares method for the simultaneous determination of both quantities is presented. The data available here do not lend themselves well to such a determination, for reasons discussed below as well as in Sec. 2.6.2. The method is included here chiefly for the use of future workers who may have data better suited to it.

The method proposed involves calculating the change in both  $L^2$  and  $\tau$  caused by the addition of absorber, and leaving as unknowns the values of these two parameters for the unmodified lattice. The diffusion area,  $L^2$ , is given by Eq. (4.16):

$$L^2 = \frac{\bar{D}}{\bar{\Sigma}_a}, \quad (\text{G.1})$$

where  $\bar{D}$  is the average diffusion coefficient for the lattice, and  $\bar{\Sigma}_a$  is the average macroscopic absorption cross section. If the tilde ( $\sim$ ) is used to indicate parameters relating to the assembly modified by the added absorber, the value of  $L^2$  for a modified lattice is given by the equation:

$$\tilde{L}^2 = \left[ \frac{\tilde{\Sigma}_a}{\bar{\Sigma}_a} \frac{\tilde{D}}{\bar{D}} \right] L^2. \quad (\text{G.2})$$

Under some circumstances, as for instance when a small amount of absorber material is added homogeneously to the moderator, it may be permissible to assume that the diffusion coefficient is unchanged by the added absorber; that is,

$$\tilde{D} = \bar{D}. \quad (\text{G.3})$$

The change in the Fermi age caused by the addition of thermal neutron absorbers is usually so small that it may be neglected (see,

for example, Ref. CO 1). If such an assumption may be made, we have:

$$\tilde{\tau} = \tau . \quad (G.4)$$

Assume that measurements have been made on a given lattice at  $n$  different absorber concentrations, as well as in the lattice without added absorber. Then a critical equation (such as Eq. (2.30) or Eq. (2.31)) can be written  $n+1$  times, with measured values of  $k_\infty$  and  $B_m^2$ ; if Eq. (G.2) is used for  $L^2$ , with calculated values of the bracketed term, the values of  $L^2$  and  $\tau$  for the unmodified lattice may be left as unknowns. If only one modified lattice is investigated, the values of  $L^2$  and  $\tau$  are specified; if more than one is investigated, then the system is overspecified, and a least squares analysis can be used to determine the "best" values of  $L^2$  and  $\tau$  for the unmodified lattice. A suitable iterative least squares analysis will be described next.

Consider  $n+1$  sets of values  $(F_i, x_i, y_i)$ , assumed to be related by an equation of the form:

$$F_i = L^2 x_i + \tau y_i . \quad (G.5)$$

Equations (2.30) and (2.31) may be written in this form if the term  $e^{\tau B_m^2}$  in Eq. (2.31) is replaced by its power series expansion, truncated after the third term. (Further terms may usually be neglected safely.) The equations are:

$$k_\infty - 1 - L^2 \tau B_m^4 = L^2 B_m^2 + \tau B_m^2 , \quad (G.6)$$

$$k_\infty - 1 - L^2 \tau B_m^4 - \frac{1}{2} \tau^2 (1 + L^2 B_m^2) B_m^4 = L^2 B_m^2 + \tau B_m^2 . \quad (G.7)$$

Then  $y_i$  in Eq. (G.5) is equal to the material buckling of assembly  $i$ , and  $x_i$  is equal to the quantity

$$B_m^2 \left[ \frac{\Sigma_a}{\Sigma_a} \frac{\bar{D}}{D} \right] \quad (G.8)$$

for assembly  $i$ . The value of  $F_i$  is either  $(k_\infty - 1 - \tau L^2 B_m^4)$  or  $(k_\infty - 1 - \tau L^2 B_m^4 - \frac{1}{2} \tau^2 (1 + L^2 B_m^2) B_m^4)$ , depending on which model is used to correlate the data. With the available measured data for each of the  $n+1$  assemblies  $(k_\infty, B_m^2)$ , calculated values of the diffusion coefficient and average absorption cross section, and reasonable estimates of  $L^2$



and  $\tau$ , the  $n+1$  values of  $F_i$ ,  $x_i$ , and  $y_i$  may be calculated. The best values of  $L^2$  and  $\tau$  for use in Eq. (G.5), in the least squares sense, may then be written as follows:

$$L^2 = \frac{\begin{vmatrix} \sum x_i F_i & \sum x_i y_i \\ \sum y_i F_i & \sum y_i^2 \end{vmatrix}}{\begin{vmatrix} \sum x_i^2 & \sum x_i y_i \\ \sum x_i y_i & \sum y_i^2 \end{vmatrix}}, \quad (\text{G.9})$$

$$\tau = \frac{\begin{vmatrix} \sum x_i^2 & \sum x_i F_i \\ \sum x_i y_i & \sum y_i F_i \end{vmatrix}}{\begin{vmatrix} \sum x_i^2 & \sum x_i y_i \\ \sum x_i y_i & \sum y_i^2 \end{vmatrix}}. \quad (\text{G.10})$$

All summations are from 1 to  $n+1$ .

The values of  $L^2$  and  $\tau$  determined will, in general, be different from the values used to calculate the  $F_i$ . New values of the  $F_i$  may be calculated, using the values of  $L^2$  and  $\tau$  just obtained, and the process repeated. This may be continued until the values of the  $F_i$  are stationary. The values of  $L^2$  and  $\tau$  obtained from Eqs. (G.9) and (G.10) will then be the "best values" appropriate for use in Eq. (2.30) or Eq. (2.31), depending on whether the  $F_i$  were calculated from the left-hand side of Eq. (G.6) or (G.7).

The method just described is best suited to an experiment in which a number of assemblies with buckling values lower than that of the unmodified lattice, but far from zero, are investigated. An assembly with zero material buckling contributes no information about the age or diffusion area of the unmodified lattice, since in this case, both  $x_i$  and  $y_i$  have the value zero. For reasons given in Sec. 2.6.2, most of the assemblies studied had material buckling values which were too small to be of use here (see Table 5.1); accordingly, no further discussion will be given.

## APPENDIX H

## REFERENCES

- AN 1 Argonne National Laboratory, "Reactor Physics Constants," ANL-5800 (July, 1958).
- AN 2 Anderson, C. A. and T. J. Thompson, "Measurement of Neutron Energy Spectra with the Massachusetts Institute of Technology Fast Chopper," Trans. Am. Nucl. Soc., 5, No. 1, 39 (1962).
- AR 1 Armour Research Foundation of Illinois Institute of Technology, "Investigation of the Physical and Chemical Properties of KANIGEN Nickel Coatings," Project No. B 599, Reports 1, 2 (Chicago: February, 1955).
- BE 1 Bennett, R. A., "Note on the Resonance Integrals of Natural Copper,  $\text{Cu}^{63}$  and  $\text{Cu}^{65}$ ," Physics Research Quarterly Report, October, November, December, 1960, HW-68389 (January, 1961).
- BL 1 Bliss, H. E., "Measurements of the Fast Effect in Heavy Water, Partially Enriched Uranium Lattices," M. S. Thesis, M. I. T. Nucl. Eng. Dept. (May, 1964).
- BL 2 Bliss, H. E., Sc. D. Thesis, M. I. T. Nucl. Eng. Dept. (forthcoming).
- BO 1 Bondorenko, I. I. et al., "Average Number and Spectrum of Prompt Neutrons in Fast Neutron Induced Fission," Proceedings of the Second International Conference on the Peaceful Uses of Atomic Energy, 15, 353 (1958).
- BR 1 Brown, P. S., T. J. Thompson, I. Kaplan, and A. E. Profio, "Measurements of the Spatial and Energy Distribution of Thermal Neutrons in Uranium, Heavy Water Lattices," NYO-10205, MITNE-17 (August, 1962).
- BU 1 Burnett, T. W. T. and T. G. Williamson, "Measurement of the Infinite Multiplication Factor in a Natural Uranium, Light-Water Lattice," Nuclear Sci. Eng., 21, 201 (1965).
- CO 1 Cohen, E. R. et al., "Exponential Experiments on  $\text{D}_2\text{O}$  Uranium Lattices," Proceedings of the International Conference on the Peaceful Uses of Atomic Energy, 5, 268 (1955).
- CR 1 Crandall, J. L., "Efficacy of Experimental Physics Studies on Heavy Water Lattices," Heavy Water Lattices: Second Panel Report, Report of a Panel Held in Vienna, 18-22 February 1963, Technical Report Series No. 20, p. 503 (Vienna: IAEA, September, 1963).
- CR 2 Crandall, J. L., Private communication, May 5, 1964.
- CR 3 Crandall, J. L., "Status of the United States Effort in  $\text{D}_2\text{O}$  Reactor Physics," DP-787 (September, 1962).



- DA 1 D'Ardenne, W. H., T. J. Thompson, D. D. Lanning, and I. Kaplan, "Studies of Epithermal Neutrons in Uranium, Heavy Water Lattices," MIT-2344-2, MITNE-53, August, 1964 (in press).
- DO 1 Donahue, D. J., R. A. Bennett and D. D. Lanning, "The Absorption Cross Section of Copper for Thermal Neutrons," Nuclear Sci. Eng., 7, 184 (1960).
- DO 2 Donahue, D. J., D. D. Lanning, R. A. Bennett, and R. E. Heineman, "Determination of  $k_{\infty}$  from Critical Experiments with the PCTR," Nuclear Sci. Eng., 4, 297 (1958).
- DU 1 Dunklee, A. E. and W. B. Rogers, "Measurement of Migration Area and Anisotropy in a Mockup of the EL-4 Lattice," DP-919 (November, 1964).
- EN 1 Engelder, T. C., N. L. Snidow, D. M. Roberts, and G. T. Fairburn, "Measurement of  $k_{\infty}$  and Other Lattice Parameters by the Small Lattice Experiment Technique," Spectral Shift Control Reactor Basic Physics Program, BAW-1283 (November, 1963).
- GA 1 Galanin, A. D., Thermal Reactor Theory (New York: Pergamon Press, 1960).
- GL 1 Glasstone, S. and M. C. Edlund, The Elements of Nuclear Reactor Theory, (Princeton, New Jersey: D. Van Nostrand Company, Inc., 1952).
- GO 1 Gosnell, J., Sc.D. Thesis, M. I. T. Nucl. Eng. Dept. (forthcoming).
- HA 1 Harrington, J., "Measurement of the Material Buckling of a Lattice of Slightly Enriched Uranium Rods in Heavy Water," M. S. Thesis, M. I. T. Nucl. Eng. Dept. (July, 1963).
- HA 2 Harrington, J., M. I. T. Heavy Water Lattice Project internal memoranda of 8/26/1963 and 12/18/1964.
- HE 1 Thompson, T. J., I. Kaplan and A. E. Profio, "Heavy Water Lattice Project Annual Report," NYO-9658 (September, 1961).
- HE 2 Kaplan, I., A. E. Profio, and T. J. Thompson, "Heavy Water Lattice Project Annual Report," NYO-10208, MITNE-26 (September, 1962).
- HE 3 Kaplan, I., D. D. Lanning, and T. J. Thompson, "Heavy Water Lattice Project Annual Report," NYO-10212, MITNE-46 (September, 1963).
- HE 4 Lanning, D. D., I. Kaplan, and F. M. Clikeman, "Heavy Water Lattice Project Annual Report," MIT-2344-3, MITNE-60 (September, 1964).
- HE 5 Thompson, T. J., I. Kaplan, F. M. Clikeman, and M. J. Driscoll, "Heavy Water Lattice Project Annual Report," MIT-2344-4, MITNE-65 (September, 1965).
- HE 6 "Heavy Water Lattice Project Annual Report," September, 1966 (forthcoming).



- HE 7 Heavy Water Lattices: Second Panel Report, Report of a Panel Held in Vienna, 18-22 February 1963, Technical Report Series No. 20 (Vienna: IAEA, September, 1963).
- HE 8 Hellman, S. P., "Measurements of  $\delta_{28}$  and  $\rho_{28}$  in a 2.5-Inch Triangular Lattice of 0.75-Inch Metallic Uranium Rods (0.947 wt% U<sup>235</sup>) in a Heavy Water Moderator," M. S. Thesis, M. I. T. Nucl. Eng. Dept. (September, 1965).
- HE 9 Heinemann, R. E., "Role of Exponential and PCTR Experiments at Hanford in the Design of Large Power Reactors," Proceedings of the Symposium on Exponential and Critical Experiments, Amsterdam, September 2-6, 1963, Vol. I, p. 65 (Vienna: IAEA, February, 1964).
- HE 10 Heinemann, R. E. et al., "Experience in the Use of the Physical Constants Testing Reactor," Proceedings of the Second International Conference on the Peaceful Uses of Atomic Energy, 12, 650 (1958).
- HO 1 Honeck, H. C., "The Distribution of Thermal Neutrons in Space and Energy in Reactor Lattices. Part I: Theory," Nuclear Sci. Eng., 8, 193 (1960).  
Honeck, H. C. and I. Kaplan, "The Distribution of Thermal Neutrons in Space and Energy in Reactor Lattices. Part II: Comparison of Theory and Experiment," Nuclear Sci. Eng., 8, 203 (1960).
- HO 2 Honeck, H. C., "THERMOS, A Thermalization Transport Theory Code for Reactor Lattice Calculations," BNL-5826 (September, 1961).
- HO 3 Honeck, H. C., "Some Methods for Improving the Cylindrical Reflecting Boundary Condition in Cell Calculations of the Thermal Neutron Flux," Trans. Am. Nucl. Soc., 5, No. 2,350 (1962).
- HO 4 Honeck, H. C., "An Incoherent Thermal Scattering Model for Heavy Water," Trans. Am. Nucl. Soc., 5, No. 1, 47 (1962).
- HU 1 Hughes, D. J. and R. B. Schwartz, "Neutron Cross Sections," BNL-325 (Second edition, July, 1958).
- HU 2 Hurley, T. J. and G. F. O'Neill, "Measured Nuclear Parameters for Natural Uranium Lattices in D<sub>2</sub>O," Trans. Am. Nucl. Soc., 4, No. 2, 295 (1961).
- KA 1 Kaplan, I., "Measurements of Reactor Parameters in Subcritical and Critical Assemblies: A Review," NYO-10,207, MITNE-25 (August, 1962).  
Kaplan, I., "Measurements of Reactor Parameters in Subcritical and Critical Assemblies," Advances in Nuclear Science and Technology, edited by E. J. Henley and H. Kouts, Vol. II, p. 139 (New York: Academic Press, Inc., 1964).
- KO 1 Kouts, H. and R. Sher, "Experimental Studies of Slightly Enriched Uranium, Water Moderated Lattices, Part 1. 0.600-Inch-Diameter Rods," BNL-486 (September, 1957).



- LE 1 Levine, M. M., K. E. Roach, D. B. Wehmayer, and P. F. Zweifel, "The Slowing Down of Neutrons by Deuterium," Nuclear Sci. Eng., 7, 14 (1960).
- MA 1 Malaviya, B. K., I. Kaplan, T. J. Thompson, and D. D. Lanning, "Studies of Reactivity and Related Parameters in Slightly Enriched Uranium Heavy Water Lattices," MIT-2344-1, MITNE-49 (May, 1964).
- MA 2 Mansfield, W. K. and J. M. Kim, "Exponential Experiments with Water and Natural Uranium Lattices," Proceedings of the Symposium on Exponential and Critical Experiments, Amsterdam, September 2-6, 1963, Vol. I, p. 457 (Vienna: IAEA, February, 1964).
- MU 1 Mummery, P. W., "The Experimental Basis of Lattice Calculations," Proceedings of the International Conference on Peaceful Uses of Atomic Energy, 5, 282 (1955).
- NE 1 Nelkin, M. S., "The Scattering of Slow Neutrons by Water," Phys. Rev., 119, 791 (1960).
- PA 1 Palmedo, P. F., I. Kaplan, and T. J. Thompson, "Measurements of the Material Bucklings of Lattices of Natural Uranium Rods in D<sub>2</sub>O," NYO-9660, MITNE-13 (January, 1962).
- PE 1 Peak, J., I. Kaplan, and T. J. Thompson, "Theory and Use of Small Subcritical Assemblies for the Measurement of Reactor Parameters," NYO-10204, MITNE-16 (April 1962).
- PE 2 Persson, R., E. Blomsjö, E. Andersen, O. Aspelund, and J. Döderlein, "Exponential Experiments on Heavy Water Natural Uranium Metal and Oxide Lattices," Proceedings of the Second International Conference on the Peaceful Uses of Atomic Energy, 12, 364 (1958).
- PR 1 Price, W. J., Nuclear Radiation Detection (New York: McGraw-Hill Book Company, Inc., 1958).
- RI 1 Riesch, G., "Measurement of the Multiplication Factor  $k_{\infty}$  of a Light Water-UO<sub>2</sub> Reactor Lattice," Nukleonik, 5, 3, p. 104 (1963).
- RO 1 Robertson, C. G., "Measurements of Neutron Utilization for Lattices of Slightly Enriched Uranium Rods," M. S. Thesis, M. I. T. Nucl. Eng. Dept. (June, 1965).
- RO 2 Rogers, W. B., V. D. Vandervelde, and N. P. Baumann, "Buckling Measurements by Successive Substitution in a Subcritical Assembly," Trans. Am. Nucl. Soc., 8, No. 2, 449 (1965).
- RO 3 Royston, R. J., "The Absorption of Neutrons by a Small, Strongly Absorbing Rod," AERE-T/M-117 (1954).
- SA 1 Safford, G. J. et al., "Fission Parameters for U<sup>235</sup>," Nucleonics, 17, No. 11, 134 (November, 1959).
- SA 2 Salah, S. and T. F. Parkinson, "Space-Dependent Spectrum Measurements in Heavy-Water-Moderated Lattices," Trans. Am. Nucl. Soc., 8, No. 1, 300 (1965).



- SA 3 de Saussure, G., L. W. Weston, R. Gwin, J. E. Russell, and R. W. Hockenbury, "Measurement of the  $U^{235}$  Neutron Capture-to-Fission Ratio,  $\alpha$ , for Incident Neutron Energies from 3.25 eV to 1.8 keV," Nuclear Sci. Eng., 23, 45 (1965).
- SI 1 Simms, R., I. Kaplan, T. J. Thompson, and D. D. Lanning, "Analytical and Experimental Investigations of the Behavior of Thermal Neutrons in Lattices of Uranium Metal Rods in Heavy Water," NYO-10211, MITNE-33 (October, 1963).
- SI 2 Simms, R., M. I. T. Heavy Water Lattice Program internal memorandum of 9/26/1963.
- SI 3 Simms, R., M. I. T. Heavy Water Lattice Program internal memorandum of 8/14/1962.
- ST 1 Stuart, G. and R. Woodruff, "Method of Successive Generations," Nuclear Sci. Eng., 3, 331 (1958).
- SU 1 Suich, J. E., "Calculation of Neutron Absorption Ratios in  $D_2O$ -Moderated Mixed Lattices," Trans. Am. Nucl. Soc., 7, No. 1, 32 (1964).
- WE 1 Weinberg, A. M. and E. P. Wigner, The Physical Theory of Neutron Chain Reactors, (Chicago: University of Chicago Press, 1958).
- WE 2 Weitzberg, A., I. Kaplan, and T. J. Thompson, "Measurements of Neutron Capture in  $U^{238}$  Lattices of Uranium Rods in Heavy Water," NYO-9659, MITNE-11 (January, 1962).
- WE 3 Westcott, C. H., "Effective Cross Section Values for Well-Moderated Thermal Reactor Spectra," CRRP-960 (Third edition corrected, November, 1960).
- WO 1 Wolberg, J. R., T. J. Thompson, and I. Kaplan, "A Study of the Fast Fission Effect in Lattices of Uranium Rods in Heavy Water," NYO-9661, MITNE-15 (February, 1962).
- WO 2 Worthing, A. G. and J. Geffner, Treatment of Experimental Data, (New York: John Wiley and Sons, Inc., 1943).



## BIOGRAPHICAL NOTE

## PERSONAL

Born: June 21, 1939; Boston, Massachusetts

Married: May 3, 1963, to Diethild Müller Harrington

## CITIZENSHIP

U.S.A.

## LANGUAGES

English, German

## EDUCATION

Massachusetts Institute of Technology (1957 - Present)

Received S.B. in Economics, Politics, and Science in June, 1961;

Received M.S. in Nuclear Engineering in September, 1963;

Anticipate Sc.D. in Nuclear Engineering in June, 1966.

(Minor field: numerical analysis and operations research;

Language: scientific German)

## HONORARY AND PROFESSIONAL SOCIETIES

Society of the Sigma Xi

American Nuclear Society

## PUBLICATIONS

Bliss, H.E., D.D. Lanning, J. Harrington, I. Kaplan, B.K. Malaviya, T.J. Thompson, "Studies of Subcritical Lattices with Distributed Neutron Absorber by Means of the Pulsed-Neutron Source Technique", Trans. Am. Nucl. Soc., 8, 533, November, 1965.

Harrington, J., D.D. Lanning, I. Kaplan, T.J. Thompson, "Use of Neutron Absorbers for the Experimental Determination of Lattice Parameters in Subcritical Assemblies". MIT-2344-6, MITNE 69, February, 1966.